Thermodynamik der deformierbaren Festkörper unter Einfluss des Elektromagnetismus und die numerische Berechnung multiphysikalischer Prozesse

Dr.-Ing. Bilen Emek Abali
ORCID: 0000-0002-8735-6071

Habilitationsschrift
an der Fakultät V
Verkehrs- und Maschinensysteme
der Technischen Universität Berlin

Lehrgebiet
Mechanik

Vorsitzende des Habilitationsausschusses:
Prof. Dr.-Ing. Utz von Wagner
Gutachter*innen:
Prof. Dr. rer. nat. Wolfgang H. Müller
Prof. Dr.-Ing. habil. Dr. h. c. mult. Holm Altenbach

Eröffnung des Habilitationsverfahrens: 18.04.2018
Tag des Habilitationskolloquiums: 10.07.2019
Fakultätsratsbeschluss über die Zuerkennung der Lehrbefähigung: 10.07.2019

Berlin 2019

Thermodynamics of deformable solids under electromagnetic interaction and computation of multiphysics applications

Dr.-Eng. Bilen Emek Abali
ORCID: 0000-0002-8735-6071

Habilitationthesis
at the Faculty V
Mechanical Engineering and Transport Systems
Technische Universität Berlin

Subject area
Mechanics

Berlin 2019

Vorwort

Wachsende Anforderungen an die Gewinnung, den Transport und auch an die Speicherung elektromagnetischer Energie erfordern neuartige technische Strukturen mit komplexen Materialien. Die zugehörigen physikalischen Prozesse führen zu gekoppelten mechanischen, thermischen und elektromagnetischen Belastungen. Experimente dieser gekoppelten Prozesse sind nur beschränkt möglich bzw. überhaupt nicht realisierbar, sodass numerische Berechnungen unabdingbar werden. Um akkurate Modellierungen und numerische Analysen von gekoppelten Systemen zu realisieren, brauchen wir die folgenden „Zutaten":

- Gleichungen, die das System beschreiben,
- Gleichungen, die das Materialverhalten abbilden,
- Experimente, die die notwendigen Konstanten bestimmen,
- Programme zur Herstellung der Modelle des Systems,
- numerische Lösungsmethoden der Gleichungen,
- Programme zur Darstellung der Ergebnisse.

Einige kommerzielle Programme wie Comsol, Ansys, Abaqus versuchen dem Anwender alle notwendigen Tools zur Vorbereitung, Modellierung und Darstellung bei Ingenieuranwendungen zur Verfügung zu stellen. Die Anwendungen sind allerdings vordefiniert und die Implementierung einer neuen Methode ist oft unmöglich, da der Quellcode nicht verfügbar ist, um das kommerzielle Programm vor Piratentum zu schützen.

Aufgrund der raschen technologischen Entwicklung besitzt heutzutage jeder Ingenieur eine „Workstation" als persönlichen Rechner. Zusätzlich arbeiten immer mehr Informatiker an Projekten mit *GNU Public* Lizenzen, bei denen die Quellcodes offen sind. Die Informatiker erhöhen die Sichtbarkeit ihrer Algorithmen und GNU Public schützt den Code, so dass er nicht verkauft werden darf. Diese zwei voneinander unabhängigen Entwicklungen haben es ermöglicht, Konsortien zu generieren, welche Codes und quelloffene Softwares für die fundamentale Forschung schreiben. Die Wissenschaftler können damit ihre eigenen Theorien abbilden, diese mit wenig Aufwand implementieren und sogar an ihrem Rechner lösen. In dieser Arbeit wird genau dieser Weg beschritten, wobei die Theorie entwickelt und implementiert wird, und durch Anwendungsbeispiele ihre Stärke sowie Grenzen aufgezeigt werden.

Der erste Teil der Arbeit besteht aus einer detaillierten Zusammenfassung der Theorie des Elektromagnetismus deformierbarer Festkörper. Insbesondere aufgrund der verschiedenen Darstellungen des Elektromagnetismus in der Literatur ist eine klare Erklärung der benutzten Theorie notwendig. Darüber hinaus sind die elektromagnetischen Felder nicht intuitiv verständlich, da sie von den menschlichen Sinnesorganen nicht direkt wahrgenommen werden, wie etwa das Gewicht einer Masse. Wir benutzen alle ein „Smartphone" oder Bluetooth-Geräte, obwohl die vielfältigen elektromagnetischen Felder nur indirekt in ihrer Wirkung fühlbar sind. Somit ist eine einwandfreie Motivation der Gleichungen zur Berechnung dieser nicht intuitiv begreifbaren Felder nicht nur hilfreich sondern auch der Schlüssel zu einer allgemeingültigen Theorie. Zusätzlich zur Theorie des Elektromagnetismus ist die Theorie der deformierbaren Körper im Detail darzustellen, da über die Modellierung der Interaktion zwischen Mechanik und Elektromagnetismus bislang noch kein Konsens besteht.

Im zweiten Teil dieser Arbeit werden bereits publizierte Arbeiten präsentiert,[1,2,3,4] und zwar zu den folgenden Themen:

- die elastoplastische Verformung der Festkörper
- über die Thermodynamik der Festkörper
- Elektromagnetismus der polarisierten, starren Körper
- Modellierung der thermoelektrischen Kopplung bei deformierbaren Körpern
- Modellierung der Funktionswerkstoffe zur Minimierung der Koronaentladung
- Ermüdungsmodellierung der Durchkontaktierung in einer Leiterplatte unter elektrischer Belastung
- Theorie und Anwendung piezoelektrischer und pyroelektrischer Materialien.

[1] B. E. Abali (2017a). *Computational Reality, Solving Nonlinear and Coupled Problems in Continuum Mechanics*. Bd. 55. Advanced Structured Materials. Springer. ISBN: 978-981-10-2443-6

[2] T. I. Zohdi und B. E. Abali (2018). „Modeling of power transmission and stress grading for corona protection". In: *Computational Mechanics* 62.3, S. 411–420. ISSN: 0178-7675

[3] B. E. Abali (2017b). „Computational study for reliability improvement of a circuit board". In: *Mechanics of Advanced Materials and Modern Processes* 3.1, S. 1–11. ISSN: 2198-7874

[4] B. E. Abali und F. A. Reich (2017). „Thermodynamically consistent derivation and computation of electro-thermo-mechanical systems for solid bodies". In: *Computer Methods in Applied Mechanics and Engineering* 319, S. 567–595. ISSN: 0045-7825

Die Erstellung dieser wissenschaftlichen Arbeiten ist durch die Unterstützung mehrerer Personen möglich geworden. Ich bedanke mich recht herzlich bei meinen Kollegen[5]: Tarek I. Zohdi, Felix A. Reich, Holm Altenbach, Christoph Baumann, Wolfgang H. Müller, Panayiotis Papadopoulos, Ingo Müller, Ömer Savaş, Alejandro Queiruga, Francesco dell'Isola, Christina Völlmecke, Maria Kashtalyan, Sebastian Glane, Paul Lofink, Dimitri V. Georgievskii, Ralf Wille, Martin Schneider-Ramelow, Olaf Wittler und Hans Walter für die Zusammenarbeit über die Jahre. Die dauerhafte Vervollständigung meines Lebens von meiner Familie: Elisabeth Kindler-Abali, G. Ipek Abali, Lale Abalı und A. Ertan Abalı hat mir ermöglicht, auch diese Arbeit abzuschließen.

Bilen Emek Abali
Dezember 2017, Berlin

[5]ohne Wertung der Reihenfolge der Namen.

Zusammenfassung

Die mathematische Beschreibung und zugehörige Simulation deformierbarer Festkörper unter mechanischer, thermischer und elektromagnetischer Belastung werden dargestellt. Ein solches multiphysikalisches System wird durch Bilanzgleichungen im Verbund mit konstitutiven Gleichungen berechenbar. Die Bilanzgleichungen inklusive Elektromagnetismus werden diskutiert und motiviert. Die konstitutiven Gleichungen zur Modellierung des Materialverhaltens werden mit Hilfe thermodynamischer Prinzipien hergeleitet. Diese Gleichungen ergeben ein gekoppeltes, nichtlineares Differentialgleichungssystem, welches nur noch numerisch berechnet werden kann. Eine Implementierung zur Lösung aller Ingenieursanwendungen wird durch Benutzung mehrerer quelloffener Pakete ermöglicht. Damit werden für diverse Prozesse numerische Berechnungen präsentiert, um die Anwendbarkeit der vorgestellten Methode darzulegen.

Abstract

Theory and corresponding computational simulations of solid bodies deforming due to the combined action of mechanical, thermal, and electromagnetic loading are presented. The governing equations of such a multiphysics simulation are obtained by balance equations completed by constitutive equations. The balance equations involving the electromagnetic interaction as well as the constitutive equations are motivated whereby many coupling phenomena are shown, discussed, and derived by using thermodynamics. The governing equations build a nonlinear and coupled set of differential equations, which can only be solved numerically. Engineering examples are implemented and computed by using open-source packages and softwares. Several processes are simulated showing the strength of the developed approach.

Inhaltsverzeichnis

Seite

I Zusammenfassung der Theorie des Elektromagnetismus der deformierbaren Festkörper 1

Kapitel I Einleitung **3**

Kapitel II Theorie der Thermomechanik und des Elektromagnetismus für Festkörper **9**
1 Bilanzgleichungen der Thermomechanik ohne Elektromagnetismus . . 10
2 Elektromagnetismus im starren Körper im isothermen Zustand 15
3 Beschreibung der Thermomechanik mit Elektromagnetismus 19

Kapitel III Numerische Berechnung der thermomechanisch-elektromagnetischen Systeme **25**
1 Raum- und Zeitdiskretisierung 26
2 Variationelle Formulierung 28

Kapitel IV Diskussion und thematische Abgrenzung der Veröffentlichungen **31**

II Veröffentlichungen 39

Kapitel I Associated plasticity **41**
1 Isotropic hardening 45
2 Kinematic hardening 50

Kapitel II Thermoviscoelasticity **61**

Kapitel III Polarized materials **75**
1 Capacitor simulation 89
2 Transformer simulation 97
3 Proximity and skin effects 105

Kapitel IV Thermoelectric coupling **113**

Kapitel V Modeling of power transmission and stress grading for corona protection **131**
1 Introduction 131
2 Field equations for 1D model problem 133

2.1 Current flow . . . 133
2.2 Temperature evolution . . . 135
2.3 Algorithm . . . 135
3 Direct numerical FEM calculations . . . 136
4 Material properties . . . 139
4.1 Determining the effective material parameters . . . 140
4.2 Nonlinearity due to the material parameters . . . 142
5 Results and comparison . . . 142
6 Conclusion . . . 147

Kapitel VI Computational study for reliability improvement of a circuit board **153**
1 Introduction . . . 154
2 Methods . . . 155
2.1 Constitutive equations . . . 158
2.2 Weak form . . . 164
2.3 Lifetime prediction . . . 166
3 Results and discussion . . . 167
4 Conclusions . . . 174

Kapitel VII Thermodynamically consistent derivation and computation of electro-thermo-mechanical systems for solid bodies **179**
1 Introduction . . . 180
2 Governing equations . . . 181
2.1 Electromagnetic stress and supply . . . 183
2.2 Balance equations with the electromagnetic interaction . . . 184
2.3 Field equations . . . 187
3 Constitutive equations . . . 189
3.1 At equilibrium . . . 190
3.2 At non-equilibrium . . . 192
4 Computational approach . . . 196
5 Applications . . . 203
5.1 Piezoelectric transducer and pyroelectric energy harvester . . . 204
5.2 Magnetostriction on an inductor . . . 210
5.3 Sensor based on magnetoelectric coupling . . . 213
6 Conclusion . . . 216

Teil I.

Zusammenfassung der Theorie des Elektromagnetismus der deformierbaren Festkörper

Kapitel I

Einleitung

Ingenieurwissenschaftliche Systeme beinhalten Komponenten, die unter mechanischen, thermischen und elektromagnetischen Belastungen arbeiten können. Eine mechanische Belastung ist einfach zu verstehen; z. B. kann jeder die Deformation eines Kunststofflöffels per Hand verursachen. Mit einer thermischen Belastung kommt man (hoffentlich selten) in Berührung; beim Kochen z. B. benutzt man nicht die Hände, um den heißen Kochtopf zu heben. Die Belastung eines Smartphones durch elektromagnetische Felder ist im Alltag nicht zu spüren, da die menschlichen Sinnesorgane dazu ungeeignet sind.

Alle diese Phänomene, Mechanik, Thermodynamik und Elektromagnetismus, treten gemeinsam auf. Elektrisch geladene Teilchen besitzen Masse. Das massebehaftete Material ist deformierbar. Eine Deformation erzeugt Wärme, welche die Temperatur verändert. Somit ist grundsätzlich zu berücksichtigen, dass die Natur bei diesen Vorgängen keine Trennung kennt. Immerhin ist aus experimentellen Erkenntnissen zu schließen, dass ein Bauteil in einem spezifischen System unter einem Typ dieser Ereignisse am meisten leidet und die anderen dann vernachlässigt werden können. In einem typischen Ingenieurstudiengang werden diese Vorgänge sogar in separaten Vorlesungen untersucht. In allen großen und bekannten Universitäten gibt es voneinander unabhängige Lehrmodule, die Mechanik, Thermodynamik und Elektromagnetismus als unabhängige Phänomene begreifen.

Dieses etablierte Konzept hat Gründe. Aus didaktischer Sicht ist die Trennung der physikalischen Vorgänge notwendig, um den Wissenstransfer in kleineren Blöcken umzusetzen. Zusätzlich ist die Lehre der Mechanik viel älter als die des Elektromagnetismus. Somit war die Lehre der Mechanik – im Grunde genommen genau so wie heute an der Hochschule – als eigenständiges Fachgebiet bereits etabliert, bevor Hans Christian Ørsted die Verbindung zwischen Elektrizität und Magnetisierung empirisch

festgestellt hat. Dazu hatte er in seiner Berliner Zeit eine grundlegende Arbeit verfasst (siehe Oersted, 1820), und seitdem wurden Elektrizität und Magnetisierung nicht mehr als unabhängig voneinander betrachtet. Schon mit den Arbeiten von André Marie Ampère und Carl Friedrich Gauß (siehe Ampere, 1825 und Gauß, 1833) wurde die Interaktion zwischen "unsichtbarem" Elektromagnetismus und "sichtbarer" Materie detektiert. Die Interaktion hat sogar zu Missverständnissen geführt. Lange Zeit haben die Wissenschaftler vermutet, dass ein unmessbares, "fiktives" Material, genannt Äther, existiert, in dem die elektromagnetischen Felder sich – analog zu akustischen Wellen in einem "echtem" Material – verbreiten. Heutzutage wissen wir, dass es kein Äther gibt und elektromagnetische Wellen sich sogar im Vakuum verbreiten.

Die Interaktion zwischen Elektromagnetismus und mechanischen Phänomenen kann über ein Kraftkonzept dargestellt werden. Die Berechnung dieser sogenannten Lorentz Kraft basiert auf Maxwell, 1865, Heaviside, 1889, Lorentz, 1937. Es besteht Konsenz, dass eine elektromagnetische Kraft existiert. Jedoch wissen wir heute immer noch nicht, ob sie durch den mathematischen Ausdruck in Form der Lorentz Kraft gegeben ist. Basierend auf dem elektromagnetischen Kraftkonzept werden Elektromotoren gebaut, die wir (ohne Übertreibung) in allen Geräten mit einer Batterie oder Strom aus der Steckdose benutzen. Die Interaktion zwischen Elektromagnetismus und Mechanik ist vielfältiger als die genannte Lorentz Kraft. 1880 haben die Brüder Pierre und Paul-Jacques Curie eine weitere Interaktion zwischen Elektromagnetismus und Mechanik entdeckt. Die sogenannte Piezoelektrizität ist die Deformation des Materials unter elektrischer Spannung. So eine Interaktion ist darin begründet, dass die elektrischen Kräfte die Atome in einer Kristallstruktur bewegen und somit mechanische Spannung hervorrufen. Die Begründung ist in der Längenskala der Kristallstruktur gegeben und schon in den Arbeiten von Woldemar Voigt vor Ende des 19. Jahrhunderts untersucht worden (siehe Voigt, 1895). Aufgrund des Fortschrittes in der Chemie können neuerdings synthetische Materialien mit der für Piezoelektrizität erforderlichen Struktur hergestellt werden. Dieses materialspezifische Phänomen wird heutzutage unter anderem in Sensoren benutzt.

Die Lehre der Thermodynamik ist auf viel kompliziertere Art und Weise entstanden. Schon im 17. Jahrhundert haben Robert Boyle, Edmé Mariotte und dann später Louis Gay-Lussac und William Thomson (Lord Kelvin) die Grundlagen der Thermodynamik im klassischen Sinne geschaffen, die mehrmals diskutiert und komplett verändert wurden. Laurent Antoine Lavoisier, 1789 hat z.B die sogenannte kalorische Wärmetheorie eingeführt. Diese Theorie konnte durch die Gedankenexperimente von Robert Julius Mayer, James Prescott Joule, Hermann Ludwig Ferdinand Helmholtz falsizifiert werden und wurde dann durch den sogenannten ersten Hauptsatz der Thermodynamik ersetzt. Dieses Konzept wurde in Gibbs, 1873 benutzt, auf welchem

jeder Grundkurs zur Thermodynamik an einer Universität basiert. Die Interaktion zwischen Thermodynamik und Mechanik war stets offensichtlich. Jedes Material wird unter gewisser Deformation warm. Aber die systematische Einführung relevanter Größen und notwendiger Grundgleichungen hat erst mit Carl Eckart 1940 begonnen (siehe Eckart, 1940a, Eckart, 1940b, Eckart, 1940c). Diese Methode wird Thermodynamik der irreversiblen Prozesse genannt. Sie benutzt die sogenannte GIBBSsche Gleichung und baut darauf auf. Genau dieser Punkt wurde als Schwachstelle angesehen, so dass Wissenschaftler mehrere erweiterte Methoden eingeführt haben. Heutzutage gibt es zahlreiche thermodynamische Theorien, welche eine Interaktion zwischen Mechanik, Thermodynamik und Elektromagnetismus zu modellieren gestatten. Die meistbenutzten sind:

- die Nicht-Gleichgewichts-Thermodynamik (Gyarmati, 1970; Groot und Mazur, 1984),
- die MÜLLERsche rationale Thermodynamik (siehe I. Müller, 1985; Jou, Casas-Vazquez und Lebon, 1999; Hutter, Ven und Ursescu, 2006),
- das COLEMAN–NOLL Verfahren (siehe Eringen und Maugin, 1990; Kovetz, 2000).

In der vorgelegten Arbeit werden wir die Grundgleichungen motivieren, die ein physikalisch-technisches System vollständig beschreiben. Dazu benötigen wir Bilanzgleichungen und konstitutive Gleichungen. Die Bilanzgleichungen gelten für alle Systeme und auch für alle Materialien. Man kann sie als Axiome bezeichnen und versuchen zu motivieren, aber eigentlich nicht wirklich herleiten. Immerhin wissen wir heutzutage, dass die Bilanzgleichungen eine sehr genaue Modellierung der Realität gestatten, sodass wir von ihrer Richtigkeit überzeugt sind. Die konstitutiven Gleichungen sind vom tatsächlichen System abhängig. Die Tatsache, welches Material und auch welche Längenskala benutzt werden, verändert die Genauigkeit der Darstellung einer konstitutiven Gleichung. Deswegen ist eine strukturierte Herleitung dieser konstitutiven Gleichungen mit einer thermodynamischen Methode ein wichtiger Beitrag in dieser Arbeit. Unterschiedliche Aspekte der obengenannten Methoden der Thermodynamik werden Schritt für Schritt angewandt, um die gekoppelten Differentialgleichungen eines thermo-mechano-elektromagnetischen Systems zu gewinnen.

Durch die technologischen Fortschritte Mikroelektronik besitzen Ingenieure sogar private Rechner mit mehreren Prozessoren über 2 GHz Taktung. Diese Kapazitäten sind mehr als ausreichend, um gekoppelte Systeme numerisch zu lösen. Diese Idee hat auch Informatiker angeregt, für Ingenieure Programme vorzufertigen, mit denen physikalische Probleme numerisch gelöst werden können. Eine wichtige Realisierung

ist SciPy,[6] das auf die Python-Programmiersprache basiert. Mit Benutzung der SciPy Pakete wurde 2003 das FEniCS Projekt[7] durch Teilnahme mehrerer Forschungsinstitute initiiert. Das FEniCS Projekt schreibt quelloffene Pakete, mit deren Benutzung die Ingenieure ein System partieller Differentialgleichungen mit der Methode der finiten Elemente numerisch lösen können. Diese Programmumgebung ist von großem Vorteil, da sonst jede einzelne Gruppe ihren eigenen Forschungscode schreiben müsste. Mit der Benutzung von FEniCS kann nun jeder Wissenschaftler bei relativ geringem Aufwand ein System lösen. Dieses System kann neuartige Gleichungen beinhalten. Bei einem kommerziellen Programm, welches auch mittels der finiten Elementmethode ähnliche Systeme lösen kann, ist eine Implementierung neuartiger Gleichungen entweder nicht erlaubt oder mit großen Hürden verbunden, um den Quellcode des Programms zu schützen. Deshalb ist dies sehr ineffizient. In der vorgestellten Arbeit beschreiben, implementieren und lösen wir ingenieurwissenschaftliche Probleme aus der Mechanik, der Thermodynamik und des Elektromagnetismus. Alle Codes sind quelloffen und in der Arbeit inkludiert oder die Quellen werden referenziert.[8]

In diesem ersten Teil werden die Gleichungen zur Beschreibung eines Systems motiviert, diskutiert und hergeleitet. Der erste Teil dient zur Zusammenfassung der im zweiten Teil folgenden publizierten Arbeiten. Der zweite Teil ist didaktisch-aufbauend zusammengestellt.

1. Zuerst wird die klassische Plastizität erklärt und die sogenannten Prandtl–Reuss Gleichungen für ein isotherm-angenommenes System hergeleitet. Dabei werden die verschiedenen Verfestigungsmodellierungen erwähnt und eine Implementierung für die kinematische Verfestigung im Fall eines einachsigen Zugtests vorgestellt. Dieser Teil stammt aus Abali, 2017a, Sect. 1.6.

2. Nun wird die Dissipation modelliert und die Annahme der Isothermie in Frage gestellt. Die Thermodynamik der viskoelastischen Körper unter großer Deformation wird detailliert erklärt. Dazu wird die Lagrangesche Darstellung angewandt, und schlussendlich wird wieder ein einachsiger Zugtest mit einer linearen viskoelastischen Materialgleichung implementiert. Für diesen Fall ist nämlich die Temperatursteigerung so gering, dass man die Annahme der Isothermie wirklich anwenden darf. Es wird ein explizites Beispiel präsentiert, bei dem die Naturereignisse für gewisse Fälle getrennt modelliert werden können. Dieser Teil ist aus Abali, 2017a, Sect. 2.4.

3. Der Elektromagnetismus wird eingeführt, wobei die Maxwell Gleichungen aus den Bilanzgleichungen motiviert werden. Diese Methode ist nützlich, um

[6] https://www.scipy.org/
[7] https://fenicsproject.org/
[8] http://lkm.tu-berlin.de/ComputationalReality

die nicht-intuitiven elektromagnetischen Felder einführen und auf eine Art "verständlicher" machen zu können. Starrer Körper und isothermer Zustand werden angenommen. Dazu werden mehrere Beispiele gelöst, die wichtige Wechselwirkungen der elektromagnetischen Felder untereinander darstellen. Dieser Teil ergibt sich aus Abali, 2017a, Sect. 3.2.

4. Ein deformierter Körper unter thermischer Belastung wird mit Elektromagnetismus gekoppelt. Die Herleitung der konstitutiven Gleichungen mit der Thermodynamik führen auf die sogenannte thermoelektrische Kopplung, die oft Peltier–Seebeck Effekt genannt wird und eine Wechselwirkung zwischen Wärmefluss und elektrischem Strom darstellt. Dieses Phänomen wird für eine dynamische Energieumwandlung benutzt, so dass aus der dissipierten Joulesschen Wärme ein Teil als elektrischer Strom zurückgewonnen wird. Dieser Teil stammt aus Abali, 2017a, Sect. 3.3.

5. Die Interaktion zwischen Thermodynamik und Elektromagnetismus ist bei der Koronaentladung von großer Bedeutung. Dazu wird eine technisch-relevante Anwendung aus der Industrie modelliert und ausgewertet, um die Auswahl der benutzten Funktionswerkstoffe zu erleichtern. Das Ziel ist die Minimierung der Koronaentladung durch effiziente Simulationen. Die größten Energieverluste bei der Energieübertragung sind wegen der Koronaentladungen bei Hochspannungsleitungen. Dieser Teil ist aus Zohdi und Abali, 2018.

6. Elektronische Bauteile besitzen eine Leiterplatte mit verschiedenen Komponenten, die zueinander elektrische Signale über Kupferleitungen auf der Leiterplatte schicken. Die dabei entstandene Joulesche Wärme erzeugt thermische Spannungen, die plastische Deformation und Ermüdung verursachen. Die Ermüdung einer Kupferleitung auf einer Leiterplatte ist modelliert und ausgewertet. Die Lebensdauer der elektronischen Bauteile sind durch das Versagen der Ermüdung begrenzt. Dieser Teil ergibt sich aus Abali, 2017b.

7. Die materialspezifischen Kopplungen wie Piezoelektrizität, Pyroelektrizität und thermische Ausdehnung werden in Sensoren und Aktuatoren benutzt. Eine vollständige theoretische Einführung der notwendigen Gleichungen mittels der thermodynamischen Ansätze führen auf gekoppelte und nichtlineare Feldgleichungen. Solche multiphysikalischen Systeme werden diskutiert, Anwendungen werden modelliert und simuliert. Dieser Teil stammt aus Abali und Reich, 2017.

Kapitel II

Theorie der Thermomechanik und des Elektromagnetismus für Festkörper

In der Kontinuumsmechanik wird ein Festkörper Kontinuumskörper genannt, für den wir die Verschiebung, die Temperatur, das elektrische Feld und die magnetische Flussdichte suchen. Diese Größen sind messbar und werden durch Erfüllung der Bilanzgleichungen berechnet. Deswegen ist zuerst die Aufstellung der Bilanzgleichungen notwendig. Dies wird in dieser Arbeit unter folgenden Annahmen erreicht:

- Der Körper besteht aus massebehafteten Partikeln. Deshalb wird er als ein materielles System behandelt.
- Die zu berechnenden Größen sind analytische Funktionen.
- Die Deformation kann in einen Referenzzustand projiziert werden, wobei dieser Zustand sich nicht verändert.

Die erste Annahme beruht auf der Idee, dass das Rechengebiet zur Berechnung ein zur Masse abgeschlossenes Gebiet darstellt. Mit anderen Worten: die Anzahl der Partikel bleibt vom Anfang bis Ende der Deformation gleich. Die Partikel bewegen sich, aber sie verlassen den Kontinuumskörper nicht, er besitzt die gleiche Gesamtmasse. Diese Annahme ist wichtig zur Erstellung der Bilanzgleichungen in globaler Form – wir beginnen mit dieser Annahme.

Die zweite Annahme ist gleichwertig mit der Vermutung, dass die Felder keine Unstetigkeiten besitzen. Anders ausgedrückt gibt es keine singulären Flächen, d. h. das Material besitzt keine Inklusionen oder Risse. Somit sind die Felder so oft ableitbar wie nötig. In mathematischer Sprache gehören alle Felder zur C^∞ und werden analytische Funktionen genannt. Es ist wichtig zu beachten, dass nur die Zielgrößen

keine Unstetigkeiten besitzen. Wenn sich zwei verschiedene Materialien in Kontakt befinden, zeigen die Materialgleichungen Sprünge, da die Materialparameter eine sprunghafte Veränderung beim Übergang von einem zum anderen Material aufweisen.

Die dritte Annahme ist wichtig für die Festkörper und stellt eine große Einschränkung durch mögliche Deformation dar. Dies ist eigentlich der Unterschied zu Fluiden, bei denen die Deformation nicht zu dem gleichen Referenzzustand mit einer mathematischen Abbildung zurückgeführt werden kann. Bei einem Festkörper stellen wir uns die Menge der Teilchen in einer strukturierten Anordnung vor. Dies wird als die Anfangskonfiguration identifiziert. Die Partikel bewegen sich zu der Endkonfiguration. Zwischen dieser Konfigurationen kann eine mathematische Relation gefunden werden, die injektiv ist, d. h. die Partikel bewegen sich nicht ineinander. Diese Eigenschaft lässt uns einen Körper Festkörper nennen. Die Anfangskonfiguration ist gewählt als Referenzzustand, in dem das Material keine Deformation besitzt. Wir wissen die Anfangsbedingungen für einen gewissen Prozess. Die Endkonfiguration ist nicht bekannt, und das Ziel ist die Berechnung dieser aktuellen Konfiguration. Durch die oben genannten Annahmen werden wir Bilanzgleichungen auf materiellen Flächen und Volumen in der aktuellen Konfiguration einführen und sie dann in die Anfangskonfiguration abbilden.

Der Kontinuumsmechanik übliche Notation wird benutzt.[9] Alle Gleichungen werden im kartesischen Koordinatensystem dargestellt. Da wir nur Tensoren benutzen, gilt eine Gleichung im kartesischen Koordinatensystem auch in allen Koordinatensystemen, zu denen eine zulässige Koordinatentransformation definiert werden kann. Die EINSTEINsche Summationkonvention über die wiederholten Indizes wird immer angewandt. Die Indizes gehen von 1 bis 3 im drei-dimensionalen Raum.

1. Bilanzgleichungen der Thermomechanik ohne Elektromagnetismus

Die Theorie der Thermomechanik ohne Elektromagnetismus erzielt die Berechnung der Verschiebung u_i in m(eter) und der Temperatur T in K(elvin) für alle Partikel des Festkörpers. Ein Partikel im Festkörper kann mit einem Punkt im Kontinuumskörper identifiziert werden. In der Thermomechanik ohne Elektromagnetismus sind Masse, Impuls und Energie Erhaltungsgrößen. Eine Erhaltungsgröße bedeutet, dass die Bilanzgleichung dieser Größe keine Produktion beinhaltet. Wir schreiben die Bilanzgleichungen in der aktuellen Konfiguration für den Kontinuumskörper $\mathcal{B}$ mit der

[9] Die Notation ist angelehnt an Truesdell und Toupin, 1960.

Berandung $\partial\mathcal{B}$ wie folgt:

$$\begin{aligned}\left(\int_{\mathcal{B}} \rho \,\mathrm{d}v\right)^{\bullet} &= 0 \ , \\ \left(\int_{\mathcal{B}} \rho v_i \,\mathrm{d}v\right)^{\bullet} &= \int_{\partial\mathcal{B}} \sigma_{ji} n_j \,\mathrm{d}a + \int_{\mathcal{B}} \rho f_i \,\mathrm{d}v \ , \\ \left(\int_{\mathcal{B}} \rho e \,\mathrm{d}v\right)^{\bullet} &= \int_{\partial\mathcal{B}} F_j n_j \,\mathrm{d}a + \int_{\mathcal{B}} \rho s \,\mathrm{d}v \ ,\end{aligned} \tag{II.1}$$

wobei die zeitlichen Änderungen der Masse, des Impulses und der Energie durch die Flüsse über die Ränder und durch die Zufuhrterme ausgeglichen sind. Masse, Impuls und Energie gehören zu den massebehafteten Partikeln, sodass wir sie über eine Integration der Masse $\mathrm{d}m = \rho \,\mathrm{d}v$ mit der Massendichte ρ definieren. Somit entsteht die Geschwindigkeit v_i als Impuls pro Masse. Die Verschiebung u_i ist die gesuchte Größe in der Mechanik. Die Rate der Verschiebung ist die Geschwindigkeit $v_i = u_i^{\bullet}$. In analoger Weise gibt es die spezifische Energie e welche die gesamte Energie pro Masse ist. Die gesamte Energie ist gegeben durch die sogenannte kinetische Energie und die innere Energie, wie folgt:

$$e = u + \frac{1}{2}\boldsymbol{v}^2 \ , \tag{II.2}$$

wobei wir in dieser Arbeit annehmen werden, dass die spezifische innere Energie u nicht von den Raten der gesuchten Größen abhängt. Diese Annahme führt zurück auf die Theorie in Caratheodory, 1909, welche in Pauli, 1973 sogar als der 1. Hauptsatz der Thermodynamik genannt wird. Eine Erweiterung dieser Annahme ist möglich (siehe Jou, Casas-Vazquez und Lebon, 1999), immerhin nehmen wir in dieser Arbeit an, dass die innere Energie von der Verschiebung und Temperatur abhängt, aber nicht von deren Raten. Die Flüsse σ_{ji} und F_j werden durch die sogenannten konstitutiven Gleichungen definiert. Die Zufuhrterme f_i und s werden auch definiert und gegebenenfalls vorgegeben. Durch Einsetzen der Massenbilanz in die Impuls- und Energiebilanzen, sowie durch Benutzen des Gaussschen Satzes an den Randtermen ergeben sich die lokalen Impuls- und Energiebilanzen wie folgt:

$$\rho v_i^{\bullet} - \frac{\partial \sigma_{ji}}{\partial x_j} - \rho f_i = 0 \ , \quad \rho e^{\bullet} - \frac{\partial F_j}{\partial x_j} - \rho s = 0 \ . \tag{II.3}$$

Nun wird die Definition aus Gl. (II.2) mittels der lokalen Impulsbilanz umgeschrieben:

$$\begin{aligned} e^{\bullet} &= \left(u + \frac{1}{2} v_i v_i\right)^{\bullet} = u^{\bullet} + v_i^{\bullet} v_i \ , \\ \rho e^{\bullet} &= \rho u^{\bullet} + v_i \left(\frac{\partial \sigma_{ji}}{\partial x_j} + \rho f_i\right) \ . \end{aligned} \tag{II.4}$$

Somit erreichen wir die Bilanzgleichung der inneren Energie:

$$\begin{aligned} \rho u^{\bullet} + v_i \frac{\partial \sigma_{ji}}{\partial x_j} - \frac{\partial F_j}{\partial x_j} + v_i \rho f_i - \rho s = 0 \ , \\ \rho u^{\bullet} - \frac{\partial}{\partial x_j}\big(F_j - \sigma_{ji} v_i\big) - \rho(s - f_i v_i) = \sigma_{ji} \frac{\partial v_i}{\partial x_j} \ , \end{aligned} \tag{II.5}$$

wobei der Flussterm:

$$-q_j = F_j - \sigma_{ji} v_i \ , \tag{II.6}$$

auch Wärmefluss genannt wird und der Zufuhrterm:

$$r = s - f_i v_i \ , \tag{II.7}$$

auch unter dem Namen Radiation oder Strahlung[10] bekannt ist. Das Minuszeichen vor dem Wärmefluss ist Konvention. Am Ende des 19. Jahrhunderts wurde die Thermodynamik zur Entwicklung von Dampfmaschinen genutzt. Dabei wurde die Wärmeenergie durch Kohleverbrennung in mechanische Arbeit umgewandelt. Die in das System eingeführte Wärmeenergie und die aus dem System gewonnene mechanische Energie sind als positive Größen deklariert. Somit ist ein Minuszeichen vor dem Wärmefluss nötig, sodass die Änderung der Energie im System einen positiven Wert hat. Dies sieht man noch besser, wenn wir aus der lokalen Bilanzgleichung der inneren Energie:

$$\rho u^{\bullet} + \frac{\partial q_j}{\partial x_j} - \rho r = \sigma_{ji} \frac{\partial v_i}{\partial x_j} \ , \tag{II.8}$$

die globale Bilanzgleichung nach der Anwendung der Massenbilanz und des Gaussschen Satzes schreiben,

$$\left(\int_{\mathcal{B}} \rho u \, \mathrm{d}v \right)^{\bullet} = - \int_{\partial \mathcal{B}} q_j n_j \, \mathrm{d}a + \int_{\mathcal{B}} \rho r \, \mathrm{d}v + \int_{\mathcal{B}} \sigma_{ji} \frac{\partial v_i}{\partial x_j} \, \mathrm{d}v \ . \tag{II.9}$$

Die Flächennormale n_i auf der Oberfläche $\partial\mathcal{B}$ zeigt aus dem Körper $\mathcal{B}$ hinaus, sodass das Minuszeichen nötig ist, um einen Zuwachs der inneren Energie, d. h. eine positive Rate auf der linken Seite bei einem positiven Wärmefluss zu gewährleisten. In der Bilanz der inneren Energie ist ein Produktionterm:

$$\sigma_{ji} \frac{\partial v_i}{\partial x_j} \tag{II.10}$$

zu sehen. Dieser Term wird oft innere Reibung genannt. Deshalb ist die innere Energie keine Erhaltungsgröße.

[10] Hier ist nicht die elektromagnetische Strahlung genannt, sondern eine radiale Erhitzung durch eine Punktquelle. Der Zufuhrterm wirkt volumetrisch und ein typisches Beispiel für diesen Term ist die Erhitzung in einem Mikrowellenofen oder durch einen Laserstrahl.

Bilanzgleichungen der Masse, des Impulses und der inneren Energie sind in der aktuellen Konfiguration geschrieben. Die Transformation auf die Anfangskonfiguration geschieht mithilfe der Tensorrechnung. Zwischen zwei benachbarten Partikeln wird ein infinitesimaler Vektor in der aktuellen Konfiguration $\mathrm{d}x_i$ und in der Anfangskonfiguration $\mathrm{d}X_i$ gestreckt, wobei die Transformation zwischen beiden:

$$\mathrm{d}x_i = \frac{\partial x_i}{\partial X_j}\,\mathrm{d}X_j \ , \quad F_{ij} = \frac{\partial x_i}{\partial X_j} \ , \tag{II.11}$$

mit dem sogenannten Deformationsgradienten F_{ij} gegeben ist. Die Transformation dieses Linienelements kann nun benutzt werden, um die Transformationsformeln der Flächen und Volumenelemente zu ermitteln:

$$\mathrm{d}v = J\,\mathrm{d}V \ , \quad n_j\,\mathrm{d}a = N_k(\boldsymbol{F}^{-1})_{kj}J\,\mathrm{d}A \ . \tag{II.12}$$

Nach nochmaliger Benutzung des Gaussschen Satzes über die Berandung in der Anfangskonfiguration und mittels der Lokalisierung werden die Bilanzgleichungen in der Anfangskonfiguration:

$$\rho_0 = \rho J \ , \quad \rho_0 v_i^{\bullet} - \frac{\partial P_{ki}}{\partial X_k} - \rho_0 f_i = 0 \ , \quad \rho_0 u^{\bullet} + \frac{\partial Q_k}{\partial X_k} - \rho_0 r = J\sigma_{ji}\frac{\partial v_i}{\partial x_j} \ , \tag{II.13}$$

mit

$$P_{ki} = \sigma_{ji}(\boldsymbol{F}^{-1})_{kj}J \ , \quad Q_k = q_j(\boldsymbol{F}^{-1})_{kj}J \ , \tag{II.14}$$

generiert. Es ist von Vorteil, wenn die Produktion der inneren Energie:

$$J\sigma_{ji}\frac{\partial v_i}{\partial x_j} = S_{ij}E_{ij}^{\bullet} \tag{II.15}$$

umgeschrieben wird. Die zweite Piola–Kirchhoff Spannung S_{ij} wird durch die Thermodynamik definiert, sodass die erste Piola–Kirchhoff Spannung $P_{ij} = F_{jl}S_{il}$ für die Impulsbilanz benutzt werden kann. Die Green–Lagrange Dehnung,

$$E_{ij} = \frac{1}{2}\big(C_{ij} - \delta_{ij}\big) \ , \tag{II.16}$$

ist gegeben mit dem Cauchy–Green Deformationstensor $C_{ij} = F_{ki}F_{kj}$.

Nun ist es möglich, die Gibbssche Gleichung zu motivieren. Alle unbekannten Größen, nämlich die spezifische Energie u, die Spannung S_{ij}, der Wärmefluss Q_i können in zwei Teile in den unterschiedlichen Zuständen getrennt werden: im Gleichgewicht und im Nicht-Gleichgewicht. Dann wird die oben erwähnte Annahme getroffen, dass die spezifische Energie nur einen Anteil im Gleichgewicht hat: $u = u|_{\mathrm{GG}}$. Dies kann mit

einem Potential modelliert werden. Für den Fall der spezifischen Energie ist es:

$$u = \int \mathrm{d}u \ . \tag{II.17}$$

Das Potential $\mathrm{d}u$ wird totales Differential genannt und besitzt ein erstes Integral in Gleichung (II.17). Diese Integralform hat die direkte Konsequenz, dass nur die Randbedingungen entscheidend sind. Für einen Prozess vom Zustand 1 zum Zustand 2 sind nur die Werte im Zustand 1 und 2 notwendig, um dieses Integral auszuwerten. Diese Eigenschaft wird manchmal der 1. Hauptsatz der Thermodynamik genannt (siehe Pauli, 1973). Diese Integralform ist nur im Gleichgewicht gültig, wo die Raten der Größen keine Rolle spielen. Angefangen mit Caratheodory, 1909 wird die Divergenz des Wärmeflusses im Gleichgewicht,

$$-\left.\frac{\partial Q_i}{\partial X_i}\right|_{\mathrm{GG}} = Q^{\bullet}|_{\mathrm{GG}} \ , \quad \frac{1}{T} Q^{\bullet}|_{\mathrm{GG}} = \rho_0 \eta^{\bullet} \ , \tag{II.18}$$

mit der spezifischen Entropierate $\eta^{\bullet}$ vorgegeben. Dabei ist die Entropie im Gleichgewicht auch mit einem Potential $\mathrm{d}\eta$ zu modellieren, sodass $\eta = \int \mathrm{d}\eta$ gilt. Die Spannung wird in einen reversiblen und dissipativen Teil getrennt:

$$S_{ij} = {}^{\mathrm{e}}S_{ij} + {}^{\mathrm{d}}S_{ij} \ , \tag{II.19}$$

wobei der reversible Teil ${}^{\mathrm{e}}S_{ij}$ im Gleichgewicht gültig ist und mit einem Potential angegeben wird. Nun wird aus der Bilanzgleichung der inneren Energie im Gleichgewicht:

$$\rho_0 \, \mathrm{d}u - \rho_0 T \, \mathrm{d}\eta = {}^{\mathrm{e}}S_{ij} \, \mathrm{d}E_{ij} \ , \tag{II.20}$$

die Gibbssche Gleichung:

$$\mathrm{d}u = T \, \mathrm{d}\eta + v \, {}^{\mathrm{e}}S_{ij} \, \mathrm{d}E_{ij} \ , \tag{II.21}$$

mit dem spezifischen Volumen $v = 1/\rho_0$ hergeleitet (für eine alternative Herleitung dieser Relation, siehe I. Müller, 1985, Chap. 8). Durch die üblichen Argumentationen aus Nye, 1967 entstehen:

$$\begin{aligned} \mathrm{d}\eta &= \frac{c}{T} \, \mathrm{d}T + C_{ijkl} \alpha_{kl} v \, \mathrm{d}E_{ij} \ , \\ \mathrm{d} \, {}^{\mathrm{e}}S_{ij} &= -C_{ijkl} \alpha_{kl} \, \mathrm{d}T + C_{ijkl} \, \mathrm{d}E_{kl} \ . \end{aligned} \tag{II.22}$$

Dabei sind die spezifische Wärmekapazität c in $\mathrm{J}/(\mathrm{kg\,K})$, der Steifigkeitstensor C_{ijkl} in $\mathrm{N/m^2}$ sowie die thermischen Ausdehnungskoeffizienten α_{ij} in $1/\mathrm{K}$ aus den Experimenten zu bestimmen. Alle diesen Materialparameter können von der Temperatur T und Dehnung E_{ij} abhängen. Für den Fall der Materialkonstanten können wir von der Anfangskonfiguration mit $T = T_{\mathrm{ref.}}$ und $E_{ij} = 0$ ohne Spannung und Entropie bis

zur aktuellen Konfiguration integrieren:

$$\begin{aligned} \eta &= c \ln\left(\frac{T}{T_{\text{ref.}}}\right) + C_{ijkl}\alpha_{kl} v E_{ij} \ , \\ {}^{\text{e}}S_{ij} &= -C_{ijkl}\alpha_{kl}(T - T_{\text{ref.}}) + C_{ijkl}E_{kl} \ . \end{aligned} \tag{II.23}$$

Dies ist ein Spezialfall; wir benutzen weiterhin den allgemeinen Fall in Gleichung (II.22) und schreiben die GIBBSsche Gleichung somit um. Nach Umschreiben und Einsetzen in die Bilanz der inneren Energie entsteht die Bilanz der Entropie:

$$\rho_0 \eta^{\bullet} + \frac{\partial}{\partial X_i}\left(\frac{Q_i}{T}\right) - \rho_0 \frac{r}{T} = \frac{1}{T}\, {}^{\text{d}}S_{ij} E^{\bullet}_{ij} - \frac{1}{T^2} Q_i \frac{\partial T}{\partial X_i} \ . \tag{II.24}$$

Diese Bilanzgleichung hat einen Produktionterm, sodass die Entropie auch keine Erhaltungsgröße ist. Die Entropieproduktion:

$$\Sigma = \frac{1}{T}\, {}^{\text{d}}S_{ij} E^{\bullet}_{ij} - \frac{1}{T^2} Q_i \frac{\partial T}{\partial X_i} \ , \tag{II.25}$$

muss null oder positiv sein: $\Sigma \geq 0$. Diese Restriktion ist der 2. Hauptsatz der Thermodynamik (siehe Eckart, 1940a). Aus dieser Bedingung werden mit den üblichen Argumenten die Materialgleichungen für ${}^{\text{d}}S_{ij}$ und Q_i in Abhängigkeit der Dehnungsrate $E^{\bullet}_{ij}$ und Temperaturgradienten $\partial T / \partial X_i$ erstellt. Für ein lineares Materialmodell sind sie

$$\begin{aligned} {}^{\text{d}}S_{ij} &= \frac{\mu_1 - \mu_2}{3} E^{\bullet}_{kk} \delta_{ij} + \mu_2 E^{\bullet}_{ij} \ , \\ Q_i &= -\kappa \frac{\partial T}{\partial X_i} \ , \end{aligned} \tag{II.26}$$

wobei die erste KELVIN Modell und die zweite FOURIER Modell genannt werden.

Die Bilanz- und Materialgleichungen für einen viskoelastischen Festkörper wurden diskutiert, motiviert und hergeleitet. Die Gleichungen sind gekoppelt und nichtlinear. Die ganze Herleitung ist unter der Annahme gemacht, dass die massebehafteten Partikel keine elektrische Ladung haben.

2. Elektromagnetismus im starren Körper im isothermen Zustand

Die elektrische Ladung ist eine fundamentale Größe und die Bewegung der Ladung erzeugt die folgenden – messbaren – elektromagnetischen Felder: das elektrische Feld E_i in V(olt)/m und die magnetische Flussdichte B_i in T(esla). Um die elektroma-

gnetischen Felder zu berechnen, werden die MAXWELL Gleichungen benutzt, die von Maxwell, 1892 eingeführt und dann mehrmals verbessert wurden (siehe Janssen und Mecklenburg, 2006). Es gibt unterschiedliche Möglichkeiten, diese Gleichungen einzuführen (siehe Chu, Haus und Penfield Jr, 1966, Sect. II; Pao und Hutter, 1975). Wir folgen I. Müller, 1985, Chap. 9 zur Motivation der MAXWELL Gleichungen aus den Bilanzgleichungen und benutzen die AMPERE–LORENTZ Konvention in GIORGI Einheiten.[11]

Analog zum vorherigen Teil fangen wir mit dem FARADAY Gesetz an:

$$\left(\int_{\mathcal{S}} B_i \, \mathrm{d}a_i \right)^{\cdot} = - \int_{\partial \mathcal{S}} \mathcal{E}_i \, \mathrm{d}\ell_i \ , \tag{II.27}$$

welches als eine Bilanzgleichung auf einer materiellen Fläche in der aktuellen Konfiguration angesehen werden kann. Es ist wichtig zu beachten, dass die materielle Fläche $\mathcal{S}$ und die materielle Linie (die Berandung) $\partial\mathcal{S}$ zu dem deformierten Körper gehören. Deshalb sind auch Felder auf dem bewegten Körper eingeführt. Die magnetische Flussdichte auf dem deformierten Körper $\mathcal{B}_i$ ist identisch zu der magnetischen Flussdichte im festen Laborsystem B_i. Das elektrische Feld im deformierten Körper $\mathcal{E}_i$ und das elektrische Feld im festen Laborsystem E_i stehen in folgender Relation:

$$E_i = \mathcal{E}_i - \epsilon_{ijk} v_j B_k \ . \tag{II.28}$$

Nach mehreren Schritten werden aus dem FARADAY Gesetz folgende Gleichungen erreicht:

$$\frac{\partial B_i}{\partial x_i} = 0 \ , \quad \frac{\partial B_i}{\partial t} + \epsilon_{ijk} \frac{\partial E_k}{\partial x_j} = 0 \ , \tag{II.29}$$

diese sind zwei der vier MAXWELL Gleichungen. Eine Lösung dieser Gleichungen ist mit diesem Ansatz möglich:

$$E_i = -\frac{\partial \phi}{\partial x_i} - \frac{\partial A_i}{\partial t} \ , \quad B_i = \epsilon_{ijk} \frac{\partial A_k}{\partial x_j} \ . \tag{II.30}$$

Die eingeführten Größen werden elektrisches Potential ϕ in V und magnetisches Potential A_i in T m genannt.[12] Das Ziel ist die Bestimmung dieser Potentiale, aus der die fundamentalen Größen, und zwar E_i und B_i Felder, berechnet werden. Um sie zu berechnen, sind Feldgleichungen notwendig, die aus der Bilanz der elektrischen Ladung gewonnen werden. Da jedes geladene Partikel eine Masse besitzt, kann die

[11] Meter, Kilogramm, Sekunde, Volt, Ampere, Coulomb

[12] Statt der elektromagnetischen Felder E_i und B_i mit insgesamt 6 Komponenten, werden die elektromagnetischen Potentiale ϕ und A_i mit 4 Komponenten eingeführt. Deshalb sind die Lösungen von den elektromagnetischen Feldern nicht eindeutig. Es fehlen 2 skalare Funktionen, und zwar die Rate des elektrischen Potentials und die Divergenz des magnetischen Potentials. Die Wahl dieser Größen wird elektromagnetische Eichung genannt. In dieser Arbeit nutzen wir die LORENZ Eichung.

Massenbilanz auf eine Ladungsbilanz umgeschrieben werden:

$$\left(\int_{\mathcal{B}} \rho z \, \mathrm{d}v \right)^{\bullet} = 0 \ , \tag{II.31}$$

wobei z die spezifische Ladung in C/kg ist. Dabei ist das Gebiet $\mathcal{B}$ aus den geladenen Partikeln entstanden. Deshalb folgen wir der Ladung und nicht der Masse, sodass die Rate des infinitesimalen Volumenelements:

$$(\,\mathrm{d}v)^{\bullet} = \frac{\partial v_i^{\mathrm{e}}}{\partial x_i} \, \mathrm{d}v \ , \tag{II.32}$$

durch die Geschwindigkeit des elektrisch geladenen Partikels v_i^{e} gegeben wird. Somit erreicht man die Bilanz der elektrischen Ladung:

$$\frac{\partial \rho z}{\partial t} + \frac{\partial \rho z v_i^{\mathrm{e}}}{\partial x_i} = 0 \ , \tag{II.33}$$

wobei $J_i = \rho z v_i^{\mathrm{e}}$ elektrischer Strom heißt. Daraus werden die weiteren Maxwell Gleichungen in mehreren Schritten erreicht:

$$\rho z = \frac{\partial D_i}{\partial x_i} \ , \quad -\frac{\partial D_i}{\partial t} + \epsilon_{ijk} \frac{\partial H_k}{\partial x_j} = J_i \ , \tag{II.34}$$

die zur Lösung der elektromagnetischen Potentiale eingesetzt werden. Dazu sollen die neu eingeführten Größen definiert werden: das Ladungspotential D_i in C/m^2 und das Strompotential H_i in A/m. Die universelle – für alle Materialien gültige – Definition dieser Größen wird durch Maxwell–Lorentz Ätherrelationen gegeben:

$$D_i = \varepsilon_0 E_i \ , \quad H_i = \frac{1}{\mu_0} B_i. \tag{II.35}$$

Die universellen Konstanten

$$\varepsilon_0 = 8{,}85 \cdot 10^{-12} \, \mathrm{A\,s/(V\,m)} \ , \quad \mu_0 = 12{,}6 \cdot 10^{-7} \, \mathrm{V\,s/(A\,m)} \ , \tag{II.36}$$

geben die Verbreitungsgeschwindigkeit der elektromagnetischen Wellen im Vakuum (die Lichtgeschwindigkeit) $c = (\varepsilon_0 \mu_0)^{-2}$ an.

Im Material gibt es 2 Ladungstypen. Die Ladungen im Molekül sind gebunden, deren Bewegung ist in einer atomischen Längenskala. Die Valenzelektronen befinden sich in der sogenannten Elektronenwolke und bewegen sich in makroskopischen Abständen. Deswegen werden die Effekte unterschiedlicher Längenskalen auch separat untersucht. Diesbezüglich werden Ladungspotential und Strompotential aufgeteilt:

$$D_i = \mathfrak{D}_i - P_i \ , \quad H_i = \mathfrak{H}_i + \mathcal{M}_i \ . \tag{II.37}$$

Die Potentiale $\mathfrak{D}_i$ und $\mathfrak{H}_i$ bestehen aufgrund der freien Ladungen. Die sogenannte elektrischen und magnetischen Polarisierungen P_i und $\mathcal{M}_i$ bestehen aufgrund der gebundenen Ladungen. Da für die totalen Potentiale D_i und H_i die MAXWELL–LORENTZ Ätherrelationen in einem Inertialsystem gelten, sind konstitutive Gleichungen für die freien Ladungs- und Strompotentiale $\mathfrak{D}_i$ und $\mathfrak{H}_i$ oder für die elektrischen und magnetischen Polarisierungen P_i und $\mathcal{M}_i$ notwendig. Durch die Separation der Potentiale wird der elektrische Strom wie folgt aufgeteilt:

$$J_i = J_i^{\text{fr.}} + \frac{\partial P_i}{\partial t} + \varepsilon_{ijk}\frac{\partial \mathcal{M}_k}{\partial x_j} \ , \tag{II.38}$$

wobei der totale freie Strom durch:

$$J_i^{\text{fr.}} = \mathcal{J}_i^{\text{fr.}} + \rho z^{\text{fr.}} v_i \ , \quad \rho z^{\text{fr.}} = \frac{\partial \mathfrak{D}_i}{\partial x_i} \ , \tag{II.39}$$

gegeben ist. Für den (effektiven, elektrischen, freien) Strom $\mathcal{J}_i^{\text{fr.}}$ ist eine konstitutive Gleichung zu definieren.

Das elektrische Potential ϕ wird durch Lösen der Ladungsbilanz:

$$\begin{aligned} \frac{\partial \rho z}{\partial t} + \frac{\partial J_i}{\partial x_i} &= 0 \ , \\ \frac{\partial^2 \mathfrak{D}_i}{\partial t \partial x_i} + \frac{\partial}{\partial x_i}\Big(J_i^{\text{fr.}} + \frac{\partial P_i}{\partial t} + \varepsilon_{ijk}\frac{\partial \mathcal{M}_k}{\partial x_j}\Big) &= 0 \ , \end{aligned} \tag{II.40}$$

nach dem Einsetzen der oben aufgeführten Identitäten bestimmt. Zur Berechnung des magnetischen Potentials A_i wird aus der MAXWELL Gleichung:

$$-\frac{\partial D_i}{\partial t} + \varepsilon_{ijk}\frac{\partial H_k}{\partial x_j} = J_i \ , \tag{II.41}$$

durch Benutzung der LORENZ Eichung:

$$\frac{\partial \phi}{\partial t} + c^2 \frac{\partial A_i}{\partial x_i} = 0 \ , \tag{II.42}$$

die folgende Gleichung erstellt:

$$\varepsilon_0 \frac{\partial^2 A_i}{\partial t^2} - \frac{1}{\mu_0}\frac{\partial^2 A_i}{\partial x_j \partial x_j} = J_i^{\text{fr.}} + \frac{\partial P_i}{\partial t} + \epsilon_{ijk}\frac{\partial \mathcal{M}_k}{\partial x_j} \ . \tag{II.43}$$

Die Feldgleichungen (VII.39), (VII.41) sind gekoppelt, d. h. sie müssen gleichzeitig gelöst werden. Bevor wir sie lösen können, sind die konstitutiven Gleichungen zu definieren.

Für den starren Körper im isothermen Zustand sind die konstitutiven Gleichungen als Spezialfall aus der Herleitung im allgemeineren Fall (siehe folgendes Kapitel) abzuleiten. Die lineare konstitutive Gleichung für den Strom:

$$\mathcal{J}_i^{\text{fr.}} = \varsigma \mathcal{E}_i \ , \tag{II.44}$$

wird OHMsches Gesetz genannt. Lineare konstitutiven Gleichungen zur elektrischen Polarisierung:

$$P_i = \varepsilon_0 \chi^{\text{el.}} E_i \ , \tag{II.45}$$

und zur magnetischen Polarisierung:

$$\mathcal{M}_i = \frac{\chi^{\text{mag.}}}{\mu_0 \bar{\mu}^{\text{mag.}}} B_i \ , \tag{II.46}$$

werden durch die Materialkonstanten ς, $\chi^{\text{el.}}$, $\chi^{\text{mag.}}$, $\mu^{\text{mag.}}$ vollständig definiert, sodass die Gleichungen (VII.39), (VII.41) abgeschlossen sind.

3. Beschreibung der Thermomechanik mit Elektromagnetismus

Über die Kopplung zwischen Thermomechanik und Elektromagnetismus besteht kein Konsens. Dies beruht auf zwei voneinander unabhängigen Schwierigkeiten. Die erste besteht in der Definition der korrekten Abbildung der elektromagnetischen Felder von der aktuellen Konfiguration auf die Anfangskonfiguration. Ein wichtiger Beitrag über die Transformation dieser Felder ist durch die Relativitätstheorie entstanden. Diese Theorie basiert auf der sogenannten LORENTZ Transformation, deren Form für Punktladungen bekannt ist. Für langsame (relativ zur Lichtgeschwindigkeit) Prozesse ist die LORENTZ Transformation identisch zur GALILEI Transformation, die in der nicht-relativistischen Mechanik benutzt wird. Die Impulsbilanz ist forminvariant unter GALILEI Transformationen.[13] Die elektromagnetischen Felder werden durch die LORENTZ Transformation in Viererschreibweise (siehe W. H. Müller, 2014, Sect. 13.12) transformiert. Diese Erklärung für starre Körper wird nicht bestritten. Aber wenn wir die gleiche Argumentationskette für die deformierten Körper anwenden möchten und den Deformationsgradienten als die zulässige Transformation zwischen den Konfigurationen einführen, besteht kein Konsens, wie die Transformation für die Viererschreibweise (zur Beschreibung der Transformation der elektromagnetischen Felder) aussehen soll. Wir werden diesen Punkt übergehen und die bekannten Transformationen der elektromagnetischen Felder durch die LORENTZ

[13] Oft wird dies zur Definition eines Inertialsystems verwendet. Somit findet die GALILEI Transformation zwischen zwei Inertialsystemen statt, wobei in jedem Inertialsystem die Form der Impulsbilanz gleich bleibt.

Transformation benutzen. Dabei werden wir die Terme mit der Geschwindigkeit per Lichtgeschwindigkeit mit null approximieren und gleichzeitig die geometrischen Nichtlinearitäten vernachlässigen.[14]

Die zweite Schwierigkeit besteht darin, dass die Definition der elektromagnetischen Kraftdichte $\mathcal{F}_i$ umstritten ist. Diese Kraftdichte herrscht aufgrund der elektromagnetischen Felder und verursacht eine Änderung der mechanischen Impulsdichte ρv_i. Somit wird die Interaktion zwischen mechanischen und elektromagnetischen Feldern ermöglicht. Die Impulsbilanz ist nun:

$$\rho \frac{\mathrm{d}v_i}{\mathrm{d}t} - \frac{\partial \sigma_{ji}}{\partial x_j} - \rho f_i = \mathcal{F}_i \ , \tag{II.47}$$

wobei die elektromagnetische Kraftdichte ein Produktionsterm ist. Deshalb ist der mechanische Teil vom Impuls ρv_i keine Erhaltungsgröße. In analoger Weise kann man eine Gleichung für die elektromagnetische Kraftdichte schreiben:

$$\frac{\partial \mathcal{G}_i}{\partial t} = \frac{\partial m_{ji}}{\partial x_j} - \mathcal{F}_i \ , \tag{II.48}$$

die (aufgrund der Einheiten) mit elektromagnetischer Spannung m_{ij} und elektromagnetischem Impuls $\mathcal{G}_i$ angegeben ist. Die Rate des elektromagnetischen Impulses ist durch die partielle Ableitung gegeben, da der elektromagnetische Impuls kein Material benötigt, um sich auszubreiten. Deshalb entfällt der konvektive Teil.

Mit der Definition des elektromagnetischen Impulses wird begonnen. Dann werden elektromagnetische Spannung und Kraftdichte aus Gleichung (II.48) durch die Benutzung der Maxwell Gleichungen und Maxwell–Lorentz Ätherrelationen herausgefunden. Diese Methode gibt konsistente Ergebnisse und wird in der Literatur sehr oft benutzt (siehe Lorentz, 1904, Eq. (15); Jones, 1964, Chap. 1; Groot und Mazur, 1984, Chap. XIV; Griffiths, 1999, Chap. 8; Low, 2004, Sect. 3.3). Die Definitionen der Spannung und Kraftdichte sind nicht eindeutig, wobei dieses nicht kritisch sind, da die Cauchy Spannung σ_{ij} auch durch die Definitionen verändert. Diese Methode erlaubt, dass wir die ganze Wahl auf die Definition des elektromagnetischen Impulses subsumieren. Genau die Frage der Wahl des elektromagnetischen Impulses ist in der Literatur umstritten (siehe Obukhov, 2008; Mansuripur, 2010; Griffiths, 2012; aber auch die Arbeiten von Barnett, 2010 und Pfeifer u. a., 2007). Es gibt 3 berühmte Ansätze – genannt nach John Henry Poynting, Hermann Minkowski und Max Abraham:

$$\mathcal{G}_i^{\mathrm{P}} = (\boldsymbol{D} \times \boldsymbol{B})_i \ , \quad \mathcal{G}_i^{\mathrm{M}} = (\boldsymbol{\mathfrak{D}} \times \boldsymbol{B})_i \ , \quad \mathcal{G}_i^{\mathrm{A}} = \frac{1}{c^2}(\boldsymbol{E} \times \boldsymbol{\mathfrak{H}})_i \ . \tag{II.49}$$

[14] Mathematisch bedeutet dies die Approximation $F_{ij} = \delta_{ij} + \dfrac{\partial u_i}{\partial X_j} \approx \delta_{ij}$ unter der Annahme, dass die Verschiebungsgradienten relativ zu geometrischen Größen sehr klein sind.

Alle diese Vorschläge sind durch klare Gedankenexperimente motiviert und experimentell bestätigt worden (siehe Brevik, 1979 und Kemp und Grzegorczyk, 2011 für verschiedene Experimente zu elektromagnetischen Impulsen). Eine Sammlung mehrerer anerkannter Vorschläge sind in Bobbio, 2000, Sect. 4.4, Sect. 8.7 zu finden; verschiedene Simulationen mit einer Validierung durch Experimente werden in Bethune-Waddell und Chau, 2015 präsentiert.

Angelehnt an experimentelle Nachweise für den Minkowskischen elektromagnetischen Impuls in Verma, Chaudhary und Singh, 2017 wählen wir $\mathcal{G}_i^{\mathrm{M}}$ für diese Arbeit aus. Umgeschrieben mittels der relevanten Beziehungen vom vorherigen Kapitel:

$$\mathcal{G}_i^{\mathrm{M}} = \epsilon_{ijk}\mathfrak{D}_j B_k = \epsilon_{ijk}(D_j + P_j)B_k = \mathcal{G}_i^{\mathrm{P}} + (\boldsymbol{P} \times \boldsymbol{B})_i \ , \tag{II.50}$$

erkennen wir einen wichtigen Zusammenhang. Der Poynting Impuls und der Minkowski Impuls sind für den Fall ohne Polarisierung identisch. Mit der Wahl des Minkowksi Impulses und durch mehrmalige Benutzung der Maxwell Gleichungen werden die elektromagnetische Spannung und Kraftdichte erreicht:

$$\begin{aligned} m_{ji} &= -\frac{1}{2}\delta_{ij}(H_k B_k + D_k E_k) + H_i B_j + D_j E_i \ , \\ \mathcal{F}_i &= \rho z E_i + \epsilon_{ijk} J_j B_k - \epsilon_{ijk}\frac{\partial P_j}{\partial t} B_k - \epsilon_{ijk} P_j \frac{\partial B_k}{\partial t} \ . \end{aligned} \tag{II.51}$$

Die elektromagnetische Spannung in Gleichung (II.51)$_1$ wird Maxwell Spannung genannt. Ohne Polarisierung entsteht die Kraftdichte aus den ersten zwei Termen in Gleichung (II.51)$_2$ – nur die ersten zwei Terme werden Lorentz Kraft genannt.

Nun gibt es die Impulsbilanz in Gleichung (II.47), die mit der elektromagnetischen Kraftdichte in Gleichung (II.51)$_2$ vervollständigt ist. Eine analoge Strategie wie in Kapitel 1 wird angewandt, um die Bilanz der inneren Energie zu ermitteln. Die detaillierte Formulierung in Abali, 2017a, Sect. 3.5 erklärt die Schritte, wobei die Reihenfolge der Schritte entscheidend ist. Mit der Benutzung der Impulsbilanz sowie der Maxwell Gleichungen und Maxwell–Lorentz Relationen wird die Bilanzgleichung der kinetischen Energie gefunden. Dann wird mit der Bilanzgleichung der totalen Energie angefangen und daraus die Bilanzgleichung der kinetischen Energie abgezogen. Somit erhält man die Bilanzgleichung der inneren Energie:

$$\frac{\partial \rho u}{\partial t} - \frac{\partial}{\partial X_j}\big(- v_j \rho u - q_j\big) - \rho r = \Gamma \ , \tag{II.52}$$

mit dem Produktionsterm:

$$\Gamma = \big(\sigma_{ji} - P_j E_i + \mathcal{M}_i B_j\big)\frac{\partial v_i}{\partial X_j} + \mathcal{E}_i \mathcal{J}_i^{\mathrm{fr.}} - P_i \frac{\mathrm{d}E_i}{\mathrm{d}t} + B_i \frac{\mathrm{d}\mathcal{M}_i}{\mathrm{d}t} \ . \tag{II.53}$$

Dabei haben wir die geometrischen Nichtlinearitäten vernachlässigt. Die Erstellung dieser Bilanzgleichung ist neuartig[15] und zum ersten Mal in Abali, 2017a, Sect. 3.5 erschienen. Insbesondere für die thermodynamische Modellierung der konstitutiven Gleichungen ist die Bilanzgleichung der inneren Energie von großer Bedeutung. Wir haben dabei nur die Gleichungen benutzt, die universell sind. Somit ist die Bilanz der inneren Energie für alle Materialien und Prozesse gültig.

Bei der Definition des Wärmeflusses in Analogie mit Gleichung (II.6) wird die folgende Relation benutzt:

$$-q_j = -v_j(e^{\mathrm{p}\cdot} + e^{\mathrm{f}\cdot}) + F_j + \big(\boldsymbol{E} \times \boldsymbol{\mathfrak{H}}\big)_j - \big(\sigma_{ji} - P_j E_i + \mathcal{M}_i B_j\big) v_i \ , \tag{II.54}$$

mit

$$e^{\mathrm{p}\cdot} = -B_i \mathcal{M}_i + P_j E_j \ , \quad e^{\mathrm{f}\cdot} = \frac{1}{2}\big(D_j E_j + \frac{1}{2} B_i H_i\big) \ . \tag{II.55}$$

Insbesondere die elektromagnetische Strahlung (Radiation) $\boldsymbol{E} \times \boldsymbol{\mathfrak{H}}$ führt zu Missverständnissen in der Literatur.[16] Die entscheidende Frage ist nämlich die Messung der Temperatur. Die Annahme der Einbeziehung der elektromagnetischen Strahlung im Wärmefluss bedeutet, dass wir die Temperatur durch die elektromagnetische Strahlung messen. In der Tat kann ein sogenannter Quantum-Sensor[17] in einer Wärmebildkamera die Temperatur durch die Strahlung messen. Es ist durchaus möglich, dass wir die elektromagnetische Strahlung in Gleichung (II.54) nicht einbeziehen. Dies würde bedeuten, dass die Temperatur durch einen pyroelektrischen Sensor in einer Wärmebildkamera gemessen würde. Wir benutzen in dieser Arbeit die erste Wahl, sodass die Formulierung $-q_i$ statt $-q_i + (\boldsymbol{E} \times \boldsymbol{\mathfrak{H}})_i$ angewandt wird.

Wie in Kapitel 1 führen wir nun Größen im Gleichgewicht ein. Für den Wärmefluss wird wieder die (spezifische) Entropie η benutzt. Für die unbekannten σ_{ij}, P_i, $\mathcal{M}_i$ wird eine Separation vorgeschlagen:

$$\sigma_{ji} = {}^{\mathrm{r}}\sigma_{ji} + {}^{\mathrm{d}}\sigma_{ji} \ , \quad P_i = {}^{\mathrm{r}}P_i + {}^{\mathrm{d}}P_i \ , \quad \mathcal{M}_i = {}^{\mathrm{r}}\mathcal{M}_i + {}^{\mathrm{d}}\mathcal{M}_i \ . \tag{II.56}$$

Alle reversiblen Teile η, ${}^{\mathrm{r}}\sigma_{ij}$, ${}^{\mathrm{r}}P_i$, ${}^{\mathrm{r}}\mathcal{M}_i$ sind mit der analogen Methode wie in Kapitel 1 zu finden. Erstens wird aus der Bilanz der inneren Energie die GIBBSsche Gleichung:

$$\mathrm{d}u = T\,\mathrm{d}\eta + v\,{}^{\mathrm{r}}\sigma_{ji}\,\mathrm{d}\varepsilon_{ij} - v\,{}^{\mathrm{r}}P_i\,\mathrm{d}E_i + v B_i\,\mathrm{d}\,{}^{\mathrm{r}}\mathcal{M}_i \ , \tag{II.57}$$

im Fall des Gleichgewichts erreicht. Die Annahme in Gleichung (II.17) gibt an, dass die spezifische innere Energie eine Funktion abhängig von $\{\eta, \varepsilon_{ij}, {}^{\mathrm{r}}P_i, {}^{\mathrm{r}}\mathcal{M}_i\}$ ist. Dies ist

[15] Die Idee der Umformulierung beruht auf der Arbeit von Groot und Mazur, 1984, Chap. XIV, Sect. 2, in welcher die ABRAHAM elektromagnetische Impulsdichte, $\mathcal{G}_i^{\mathrm{A}}$, benutzt wurde.

[16] Dieser wichtiger Punkt wurde in I. Müller, 1985, §9.9.4 angesprochen.

[17] Der sogenannte Bolometer wurde 1878 von Samuel P. Langley konzipiert.

konzeptionell schwierig, da wir η und ${}^{\mathrm{r}}\mathcal{M}_i$ noch nicht in Abhängigkeit der Zielgrößen T, u_i, ϕ, A_i definiert haben. Die Lösung wird durch Einführung einer sogenannten freien Energie:

$$\psi = u - T\eta - B_i v\, {}^{\mathrm{r}}\mathcal{M}_i \ , \tag{II.58}$$

erstellt, weil

$$\begin{aligned} \mathrm{d}\psi = {} & \mathrm{d}u - \eta\,\mathrm{d}T - T\,\mathrm{d}\eta - B_i v\,\mathrm{d}\,{}^{\mathrm{r}}\mathcal{M}_i - {}^{\mathrm{r}}\mathcal{M}_i v\,\mathrm{d}B_i = \\ = {} & -\eta\,\mathrm{d}T + {}^{\mathrm{r}}\sigma_{ji} v\,\mathrm{d}\varepsilon_{ij} - {}^{\mathrm{r}}P_i v\,\mathrm{d}E_i - {}^{\mathrm{r}}\mathcal{M}_i v\,\mathrm{d}B_i \ , \end{aligned} \tag{II.59}$$

nun auf eine Abhängigkeit $\psi = \psi(T, \varepsilon_{ij}, E_i, B_i)$ zeigt. Der sogenannte Zustandsraum $\{T, \varepsilon_{ij}, E_i, B_i\}$ besteht aus den Größen, die durch die Zielgrößen T, u_i, ϕ, A_i gegeben sind. Wieder durch die bekannten Argumentationen erreichen wir die folgenden Differentialrelationen:

$$\begin{aligned} \mathrm{d}\eta &= \frac{c}{T}\,\mathrm{d}T + vC_{ijkl}\alpha_{kl}\,\mathrm{d}\varepsilon_{ij} - v\tilde{T}_{ijk}\alpha_{kl}\,\mathrm{d}E_i - v\tilde{S}_{ijk}\alpha_{kl}\,\mathrm{d}B_i \ , \\ \mathrm{d}\,{}^{\mathrm{r}}\sigma_{ij} &= -C_{ijkl}\alpha_{kl}\,\mathrm{d}T + C_{ijkl}\,\mathrm{d}\varepsilon_{kl} - \tilde{T}_{kij}\,\mathrm{d}E_k + \tilde{S}_{kji}\,\mathrm{d}B_k \ , \\ \mathrm{d}\,{}^{\mathrm{r}}P_i &= -\tilde{T}_{ijk}\alpha_{kl}\,\mathrm{d}T + \tilde{T}_{ijk}\,\mathrm{d}\varepsilon_{jk} + \varepsilon_0\chi^{\mathrm{el.}}_{ij}\,\mathrm{d}E_j + \tilde{R}_{ji}\,\mathrm{d}B_j \ , \\ \mathrm{d}\,{}^{\mathrm{r}}\mathcal{M}_i &= -\tilde{S}_{ijk}\alpha_{kl}\,\mathrm{d}T + \tilde{S}_{ijk}\,\mathrm{d}\varepsilon_{jk} + \tilde{R}_{ij}\,\mathrm{d}E_j + \mu_0^{-1}\chi^{\mathrm{mag.}}_{ij}\,\mathrm{d}B_j \ . \end{aligned} \tag{II.60}$$

Alle Größen sind messbare Funktionen der Zustandsgrößen. Experimentell werden die spezifische Wärmekapazität c, der Steifigkeitstensor C_{ijkl}, die thermischen Ausdehnungskoeffizienten α_{ij}, der piezoelektrische[18] Tensor $\tilde{T}_{ijk}$, der piezomagnetische Tensor $\tilde{S}_{ijk}$, die elektrische Suszeptibilität $\chi^{\mathrm{el.}}_{ij}$, die magnetische Suszeptibilität $\chi^{\mathrm{mag.}}_{ij}$ und die magnetoelektrische Kopplung $\tilde{R}_{ij}$ bestimmt. Falls alle diese Materialparameter bekannt sind, werden die konstitutiven Gleichungen durch Integration von $\mathrm{d}\eta$, $\mathrm{d}\,{}^{\mathrm{r}}\sigma_{ij}$, $\mathrm{d}\,{}^{\mathrm{r}}P_i$, $\mathrm{d}\,{}^{\mathrm{r}}\mathcal{M}_i$ erreicht. Somit ist $\mathrm{d}u$ in Gleichung (II.57) vollständig definiert und wird in die innere Energiebilanz in Gleichung (II.52) eingesetzt, sodass daraus die Entropiebilanz nach Umschreibung erreicht wird:

$$\rho_0\frac{\partial\eta}{\partial t} + \frac{\partial\Phi_j}{\partial X_j} - \rho_0\frac{r}{T} = \Sigma \ , \tag{II.61}$$

mit dem Flussterm Φ_i und dem Produktionsterm Σ wie folgt:

$$\begin{aligned} \Phi_j &= \frac{q_j}{T} \ , \\ \Sigma &= -\frac{q_j}{T^2}\frac{\partial T}{\partial X_j} + \frac{1}{T}\big({}^{\mathrm{d}}\sigma_{ji} - P_j E_i + \mathcal{M}_i B_j\big)\frac{\partial v_i}{\partial X_j} + \\ &\quad + \frac{1}{T}\mathcal{E}_i\mathcal{J}^{\mathrm{fr.}}_i - \frac{1}{T}\,{}^{\mathrm{d}}P_i\frac{\partial E_i}{\partial t} + \frac{1}{T}B_i\frac{\partial\,{}^{\mathrm{d}}\mathcal{M}_i}{\partial t} \ . \end{aligned} \tag{II.62}$$

Die dissipativen Polarisierungen ${}^{\mathrm{d}}P_i$ und ${}^{\mathrm{d}}\mathcal{M}_i$ erzeugen die experimentell bekannten Hystereseverluste bei zyklischen Ladungen. Zur Modellierung der Kopplungen der

[18] Oft werden in der Literatur die piezoelektrischen Koeffizienten $\tilde{d}_{ijk}$ gegeben, wobei $\tilde{T}_{mij} = C_{ijkl}\tilde{d}_{mkl}$ gilt.

piezo- und pyroelektrischen Materialien werden die dissipativen Polarisierungen vernachlässigt:

$$ {}^{\mathrm{d}}P_i = 0 \ , \quad {}^{\mathrm{d}}\mathcal{M}_i = 0 \Rightarrow P_i = {}^{\mathrm{r}}P_i \ , \quad \mathcal{M}_i = {}^{\mathrm{r}}\mathcal{M}_i \ . \tag{II.63} $$

Die konstitutiven Gleichungen zu den Größen q_i, ${}^{\mathrm{d}}\sigma_{ij}$, $\mathcal{J}_i^{\mathrm{fr.}}$ werden durch den 2. Hauptsatz der Thermodynamik $\Sigma \geq 0$ unter Benutzung von Darstellungstheoremen gefunden. Für den Fall der reinen Elastizität lauten die Gleichungen wie folgt:

$$ q_i = -\kappa \frac{\partial T}{\partial X_i} + \varsigma \pi T \mathcal{E}_i \ , \quad \mathcal{J}_i^{\mathrm{fr.}} = \varsigma \pi \frac{\partial T}{\partial X_i} + \varsigma \mathcal{E}_i \ , \quad {}^{\mathrm{d}}\sigma_{ji} = P_j E_i - \mathcal{M}_i B_j \ , \tag{II.64} $$

wobei die positive Wärmeleitfähigkeit κ, die positive elektrische Leitfähigkeit ς und die thermoelektrische Kopplung π experimentell bestimmt werden sollen. Alle diesen Größen können von den Temperaturgradienten und dem elektrischen Feld abhängig sein. Falls κ und ς Konstante und $\pi = 0$ sind, werden die Gleichungen $(\text{II.64})_{1,2}$ FOURIERsches Gesetz und OHMsches Gesetz genannt.

Kapitel III

Numerische Berechnung der thermomechanisch-elektromagnetischen Systeme

Ein physikalischer Prozess aus der Thermomechanik ist in Kapitel 1 beschrieben worden. Die Zielgrößen sind die Verschiebung u_i und die Temperatur T als Funktionen im Ort X_i und in der Zeit t. Die Ortskoordinaten zeigen auf die Anfangspositionen der massenbehafteten Partikel. Es gibt für jede Zielgröße eine partielle Differentialgleichung, die aus Bilanzgleichungen stammt. Diese sogenannten Feldgleichungen für Thermomechanik sind:

$$\begin{aligned} \rho_0 \ddot{u}_i - P_{ji,j} - \rho_0 f_i &= 0 \ , \\ \rho_0 \dot{\eta} + \left(\frac{Q_i}{T}\right)_{,i} - \rho_0 \frac{r}{T} &= \frac{1}{T}\, {}^{\mathrm{d}}S_{ij} \dot{E}_{ij} - \frac{1}{T^2} Q_i T_{,i} \ , \end{aligned} \tag{III.1}$$

wobei die Kommanotation für die Ortsableitung $(\cdot)_{,i} = \partial(\cdot)/\partial X_i$ eingeführt wurde. Diese Gleichungen in der LAGRANGEschen Darstellung berechnen die geometrischen Nichtlinearitäten akkurat. Darüber hinaus sind die Zeitableitungen $(\dot{})$, $(\ddot{})$ identisch mit den partiellen Zeitableitungen. Die erste Gleichung ist zur Berechnung der Verschiebung u_i und die zweite Gleichung ist zur Berechnung der Temperatur T geeignet. Wir nennen sie die primitiven Variablen $\boldsymbol{p} = \{u_i, T\}$. Das Ziel ist die Berechnung der primitiven Variablen. Alle konstitutiven Gleichungen sind im letzten Kapitel thermodynamisch hergeleitet und sie beinhalten die primitiven Variablen (und deren Raum- und Zeitableitungen). Somit bestehen die oberen Gleichungen (III.1) nur aus den primitiven Variablen – diese partiellen Differentialgleichungen werden auch Feldgleichungen genannt. Da beide Feldgleichungen beide primitiven Variablen beinhalten, stellt dies ein gekoppeltes Gleichungssystem dar. Deshalb müssen wir beide Feldgleichungen gleichzeitig lösen. Durch die numerische Berechnung approximieren wir u_i und T. Die Genauigkeit dieser Lösung hängt von der Approximation ab. In der Zeit und im Raum werden unterschiedliche Methoden

benutzt, um die Funktionen zu approximieren.

Der thermomechanische Prozess mit der elektromagnetischen Interaktion ist in Kapitel 3 eingeführt. Dabei handelt es sich um das elektrische Potential ϕ und das magnetische Potential A_i als zusätzliche primitive Variablen. Wichtige Annahmen sind getroffen und Vereinfachungen gemacht worden. Erstens wird der MINKOWSKI Impuls angenommen. Als Konsequenz ist die dissipative Spannung aus der Thermodynamik wie in Gleichung (II.64)$_3$ herausgekommen. Zweitens wird die geometrische Nichtlinearität vernachlässigt, sodass die Kommanotation zur Ortsableitung als eine Ableitung nach x_i oder nach X_i angesehen werden kann. Somit ist die Transformation der elektromagnetischen Felder bekannt und wir erhalten diese Feldgleichungen:

$$\begin{aligned}
\frac{\partial \mathfrak{D}_{i,i}}{\partial t} + \left(\jmath_i^{\text{fr.}} + v_i \mathfrak{D}_{j,j} + \epsilon_{ijk} \mathcal{M}_{k,j} \right)_{,i} &= 0 \ , \\
\varepsilon_0 \frac{\partial^2 A_i}{\partial t^2} - \frac{1}{\mu_0} \frac{\partial^2 A_i}{\partial X_j \partial X_j} &= \jmath_i^{\text{fr.}} + v_i \mathfrak{D}_{j,j} + \frac{\partial P_i}{\partial t} + \epsilon_{ijk} \mathcal{M}_{k,j} \ , \\
\rho_0 \frac{\partial^2 u_i}{\partial t^2} + \epsilon_{ijk} \frac{\partial \mathfrak{D}_j B_k}{\partial t} - (\sigma_{ji} + m_{ji})_{,j} - \rho_0 f_i &= 0 \ , \\
\rho_0 \frac{\partial \eta}{\partial t} + \Phi_{j,j} - \rho_0 \frac{r}{T} &= \Sigma \ ,
\end{aligned} \tag{III.2}$$

wobei die erste Gleichung für das elektrische Potential ϕ, die zweite Gleichung für das magnetische Potential A_i, die dritte Gleichung für die Verschiebung u_i, und die vierte Gleichung für die Temperatur T, benutzt werden. Die Gleichungen sind gekoppelt und nichtlinear. Deswegen müssen die primitiven Variablen $\boldsymbol{p} = \{\phi, A_i, u_i, T\}$ gleichzeitig gelöst werden. Wir werden eine neuartige Methode zur Lösung der primitiven Variablen vorschlagen und implementieren. Diese Methode ermöglicht[19] eine akkurate Lösung zahlreicher technisch-relevanter Anwendungen.

1. Raum- und Zeitdiskretisierung

Das Ziel ist die Berechnung der Zielgrößen $\boldsymbol{p} = \{\phi, A_i, u_i, T\}$ im Raum und in der Zeit. Diese sogenannten primitiven Variablen $\boldsymbol{p}$ sind glatte Funktionen (unendlich oft stetig differenzierbar). Zur numerischen Berechnung der primitiven Variablen werden sie im Raum und in der Zeit als diskrete und hinreichend glatte Funktionen approximiert. Für die Zeitdiskretisierung werten wir die Zeit in diskreten Zeitschritten

[19] Zusätzlich sind die Feldgleichugen so gewählt, dass keine numerischen Probleme bei der Benutzung von Standard-Methoden auftreten.

$t = \{0, \Delta t, 2\Delta t, 3\Delta t, \dots\}$ aus. Somit können wir für jede partielle Zeitableitung:

$$\frac{\partial \boldsymbol{p}}{\partial t} = \frac{\boldsymbol{p} - \boldsymbol{p}^0}{\Delta t} \ , \tag{III.3}$$

einführen, wobei $\boldsymbol{p}$ die unbekannte (zu berechnende) Variable in der aktuellen Zeit t und $\boldsymbol{p}^0$ die vor einem Zeitschritt $t - \Delta t$ berechnete Variable symbolisieren. Diese finite Differenzenmethode (FDM) wird auch Euler-Rückwärts-Methode genannt und ist stabil für reelle Zahlen, da die Ableitung in der aktuellen Zeit approximiert wird. Für die Raumdiskretisierung wird die finite Elementenmethode (FEM) benutzt, sodass wir die Werte an diskreten Raumpunkten berechnen. Diese Raumpunkte werden Knoten genannt und sind vor der Berechnung durch Vernetzung festzusetzen. Mit den Werten an K Knoten kann nun die Funktion approximiert werden:

$$\boldsymbol{p} = \sum_K \boldsymbol{p}^K \beta^K \ , \tag{III.4}$$

wobei $\boldsymbol{p}^K$ die Werte an den Knoten und $\beta^K = \beta^K(X_i)$ die Formfunktionen jeweiliger Knoten in dem Rechengebiet Ω bedeuten. Die Formfunktionen sind so definiert, dass sie den Wert 1 für den entsprechenden Knoten und 0 für alle anderen Knoten bekommen:

$$\beta^K(X_i^L) = \begin{cases} 1 \text{ falls } K = L \\ 0 \text{ falls } K \neq L \end{cases} \ . \tag{III.5}$$

Somit ist die Formfunktion mit einem lokalen Träger definiert, der nur in einem finiten Element gegeben wird. Zwischen den Knoten kann die Formfunktion irgendeine Polynomfunktion sein. Wir werden lineare Formfunktionen für alle primitiven Variablen benutzen. Die Entwicklung der Funktion in Gleichung (III.4) ist im Allgemeinen als eine Reihenentwicklung bekannt, wobei die diskreten Funktionen β^K einen mathematisch abstrakten Hilbert Raum spannen (siehe Hilbert, 1902). Zusätzlich sind die Formfunktionen differenzierbar, sodass der Raum Hilbertscher Sobolev Raum genannt wird (siehe Courant und Hilbert, 1966). Wir werden 8 primitive Variablen:

$$\boldsymbol{p} = \{\phi, A_1, A_2, A_3, u_1, u_2, u_3, T\} \ , \tag{III.6}$$

im dreidimensionalen (physikalischen) Raum durch den (abstrakten) Hilbertschen Sobolev Raum:

$$\mathcal{V} = \left\{\boldsymbol{p} \in [\mathcal{H}^3(\Omega)]^8 : \boldsymbol{p}|_{\partial\Omega} = \text{geg.}\right\} \ , \tag{III.7}$$

approximieren. Anhand des Galerkin Ansatzes sind auch die Testfunktionen durch den gleichen Raum zu entwickeln:

$$\hat{\mathcal{V}} = \left\{\delta\boldsymbol{p} \in [\mathcal{H}^n(\Omega)]^8 : \delta\boldsymbol{p}|_{\partial\Omega} = \text{geg.}\right\} \ . \tag{III.8}$$

Wie in der FEM üblich, werden wir die Testfunktionen an der Berandung mit gegebener Lösung null setzen. Für eine mögliche Implementierung solcher Formfunktionen siehe Oden, 1972; Zienkiewicz und Taylor, 1991; Wriggers, 2008; Zohdi, 2015.

2. Variationelle Formulierung

Die primitiven Variablen werden durch Erfüllung der Gleichungen (VII.70) berechnet. Wir können alle diese Feldgleichungen als Residuen umschreiben, wobei die rechte Seite von der linken Seite subtrahiert wird. Für alle Raumkoordinaten und Zeitpunkte sollen Residuen gleich null sein, mit anderen Worten werden sie punktweise erfüllt. In diesem Fall sind die primitiven Variablen korrekt. Wir werden nun diese Forderung lockern, indem die Residuen mit einer Testfunktion multipliziert und über ein Rechengebiet Ω integriert werden. Nun wird die Forderung erneuert, dass die Residuen global erfüllt werden. Diese aus Gleichung (VII.70) erstellten Integralformen werden "gewichtete Residuen" genannt, wobei die Testfunktionen noch nicht definiert sind. In der Tat ist die Lösung von der gewählten Testfunktion abhängig. Falls wir die Erfüllung der Integralformen für beliebige Testfunktionen fordern, müssen dann die Feldgleichungen auch punktweise erfüllt werden. Somit erreichen wir die variationelle Formulierung, in der die Variation der Testfunktionen im Inneren des Rechengebiets beliebig zugelassen wird. Für die FEM werden wir den Galerkin Ansatz anwenden und die Testfunktionen vom gleichen Raum wie die primitiven Variablen wählen. Die Integralformen werden in die gleiche Einheit (der Energie) gebracht:

$$
\begin{aligned}
\int_\Omega \left(\mathfrak{D}_{i,i} - \mathfrak{D}^0_{i.i} + \Delta t \Big(\jmath_i^{\text{fr.}} + \frac{(u_i - u_i^0)}{\Delta t} \mathfrak{D}_{j,j} + \epsilon_{ijk} \mathcal{M}_{k,j} \Big)_{,i} \right) \delta\phi \, \mathrm{d}V = 0 \ , \\
\int_\Omega \left(\varepsilon_0 \frac{A_i - 2A_i^0 + A_i^{00}}{\Delta t \Delta t} - \frac{1}{\mu_0} \frac{\partial^2 A_i}{\partial X_j \partial X_j} - \jmath_i^{\text{fr.}} - \frac{(u_i - u_i^0)}{\Delta t} \mathfrak{D}_{j,j} - \right. \\
\left. - \frac{P_i - P_i^0}{\Delta t} - \epsilon_{ijk} \mathcal{M}_{k,j} \right) \delta A_i \, \mathrm{d}V = 0 \ , \qquad \text{(III.9)} \\
\int_\Omega \left(\rho_0 \frac{u_i - 2u_i^0 + u_i^{00}}{\Delta t \Delta t} + \epsilon_{ijk} \frac{\partial \mathfrak{D}_j B_k}{\partial t} - (\sigma_{ji} + m_{ji})_{,j} - \rho_0 f_i \right) \delta u_i \, \mathrm{d}V = 0 \ , \\
\int_\Omega \left(\rho_0 (\eta - \eta^0) + \Delta t \Phi_{j,j} - \Delta t \rho_0 \frac{r}{T} - \Delta t \Sigma \right) \delta T \, \mathrm{d}V = 0 \ .
\end{aligned}
$$

In dem definierten Raum (siehe Gleichungen (III.7), (III.8)) ist die Polynomordnung der Formfunktion gleich eins, d. h. die Verschiebung, die Temperatur und die elektromagnetischen Potentiale dürfen nur einmal räumlich abgeleitet werden. In den konstitutiven Gleichungen sind oft erste Ableitungen vorhanden, sodass dies zu einem Ausdruck führt, in dem eine doppelt abgeleitete primitive Variable mit einer einfach abgeleiteten Testfunktion multipliziert wird. Entweder soll die Formfunktion verändert werden, sodass die Bedingung der doppelten Differenzierbarkeit erfüllt wird; oder diese Bedingung soll "geschwächt" werden, welche die übliche Methode in der FEM ist. Somit wird eine partielle Integration mit dem Gaussschen Satz an allen Termen angewandt, in denen die genannte Art der Multiplikation vorkommt. Dabei entstehen an den Übergängen (engl. *interface*) $\partial\Omega^I$ Terme, die mit der Benutzung der Bilanzgleichungen an den singulären Flächen ersetzt wurden. Am Ende erhalten

wir die sogenannte schwache Form:

$$\text{Form} = \mathrm{F}_\phi + \mathrm{F}_{\boldsymbol{A}} + \mathrm{F}_{\boldsymbol{u}} + \mathrm{F}_T \ , \tag{III.10}$$

mit den folgenden Formen:

$$\begin{aligned}
\mathrm{F}_\phi &= \int_\Omega \big(-(\mathfrak{D}_i - \mathfrak{D}_i^0)\delta\phi_{,i} - \Delta t \mathcal{J}_i^{\mathrm{fr.}} \delta\phi_{,i} - (u_i - u_i^0)\mathfrak{D}_{j,j}\delta\phi_{,i} - \\
&\quad - \Delta t \epsilon_{ijk} \mathcal{M}_{k,j} \delta\phi_{,i} \big) \,\mathrm{d}V + \int_{\partial\Omega^I} N_i \Delta t \epsilon_{ijk} [\![\mathcal{M}_{k,j}]\!] \delta\phi \,\mathrm{d}A \ , \\
\mathrm{F}_{\boldsymbol{A}} &= \int_\Omega \Big(\varepsilon_0 \frac{A_i - 2A_i^0 + A_i^{00}}{\Delta t \Delta t} \delta A_i + \frac{1}{\mu_0} A_{i,j} \delta A_{i,j} - \mathcal{J}_i^{\mathrm{fr.}} \delta A_i - \\
&\quad - \frac{u_i - u_i^0}{\Delta t} \mathfrak{D}_{j,j} \delta A_i - \frac{P_i - P_i^0}{\Delta t} \delta A_i + \epsilon_{ijk} \mathcal{M}_k \delta A_{i,j} \Big) \,\mathrm{d}V \ , \\
\mathrm{F}_{\boldsymbol{u}} &= \int_\Omega \left(\rho_0 \frac{u_i - 2u_i^0 + u_i^{00}}{\Delta t \Delta t} \delta u_i + \epsilon_{ijk} \frac{\mathfrak{D}_j B_k - \mathfrak{D}_j^0 B_k^0}{\Delta t} \delta u_i - \bar{\sigma}_{ji,j} \delta u_i + \right. \\
&\quad \left. + \tau_{ji} \delta u_{i,j} - \rho_0 f_i \delta u_i \right) \mathrm{d}V + \int_{\partial\Omega^I} N_j [\![\bar{\sigma}_{ji}]\!] \delta u_i \,\mathrm{d}A \ , \\
\mathrm{F}_T &= \int_\Omega \left(\rho_0 (\eta - \eta^0) \delta T - \Delta t \Phi_i \delta T_{,i} - \Delta t \rho_0 \frac{r}{T} \delta T - \Delta t \Sigma \delta T \right) \mathrm{d}V + \\
&\quad + \int_{\partial\Omega^I} \Delta t [\![\Phi_i]\!] N_i \delta T \,\mathrm{d}A \ .
\end{aligned} \tag{III.11}$$

Die numerische Implementierung dieser schwachen Form ist mittels der quelloffenen Software und Pakete möglich. Alle Simulationen sind mit einem modernen Laptop (ausgestattet mit Ubuntu[20] Betriebssystem) durchgeführt. Die Vorbereitung eines Modells ist in Salome[21] erstellt (siehe die Anweisungen in Abali, 2017a, Anhang A.3). Die numerischen Berechnungen sind durch einen erstellten Code in Python[22] mit den Paketen aus FEniCS Projekt[23] durchgeführt worden. Alle erstellten Codes sind frei verfügbar (lizenziert mit Gnu GPL, 2007) und publiziert.[24]

Die schwache Form ist nichtlinear und kann erst nach einer Linearisierung gelöst werden. In dieser Arbeit wird eine abstrakte Linearisierung[25] implementiert, wobei sie direkt in der partiellen Differentialgleichungen angewandt wird. Die sogenannte Newtonsche Methode wird durch Umformulierung der schwachen Form vor der Matrizenbildung eingeführt. Dies hat den Vorteil, dass die Formulierung auch eine hohe

[20] https://www.ubuntu.com/
[21] http://www.salome-platform.org/
[22] https://www.python.org/
[23] https://fenicsproject.org/
[24] Einige Codes sind direkt in dieser Arbeit zu finden, für den Rest siehe http://www.lkm.tu-berlin.de/ComputationalReality
[25] Die Methode ist angelehnt an Logg, Mardal und Wells, 2012, Part I, §2.2.3

Nichtlinearität besitzen kann; die Methode bleibt gleich. Für die Linearisierung ist eine Ableitung der Integralform notwendig. Dies wird symbolisch[26] gemacht, sodass der Nutzer eigentlich nur die schwache Form einträgt; die numerische Implementierung macht den Rest automatisch.

[26]Mit den Paketen aus SyFi im FEniCS Projekt (siehe Alnaes und Mardal, 2010; Alnaes und Mardal, 2012).

Kapitel IV

Diskussion und thematische Abgrenzung der Veröffentlichungen

In Teil II sind insgesamt 7 publizierte Arbeiten in einer didaktisch-aufbauenden Systematik zu finden. Die 1., 2., 3. und 4. Arbeit sind Teile aus dem Buch[27] (in dem sogenannten *post-print* Format):
B. E. Abali (2017a). *Computational Reality, Solving Nonlinear and Coupled Problems in Continuum Mechanics*. Bd. 55. Advanced Structured Materials. Springer. ISBN: 978-981-10-2443-6

In der 1. Arbeit wird die Plastizität motiviert, die Gleichungen hergeleitet und eine Implementierung im FEniCS Projekt vollständig gezeigt. Die klassische Plastizität, genannt Prandtl–Reuss Plastizität, ist der wichtige Baustein für die Mechanik der irreversiblen Deformationen. Der Körper deformiert sich elastisch und plastisch zur gleichen Zeit. Zusätzlich sind diese Vorgänge von unterschiedlichem Charakter, sodass eine mathematische Unterscheidung und korrekte Beschreibung dieses – experimentell mehrmals bestätigten – Phänomens anspruchsvoll ist. Deshalb ist die Theorie und Anwendung der klassischen Plastizität, obwohl seit langer Zeit bekannt, in den herkömmlichen Büchern selten zu sehen. In der 1. Arbeit wird nur die Mechanik betrachtet und die Thermodynamik außer Acht gelassen.

Die 2. Arbeit beschäftigt sich mit der theoretischen Thermodynamik, wobei die konstitutiven Gleichungen – oft Materialgleichungen genannt – aus den Grundprinzipien der Thermodynamik Schritt für Schritt hergeleitet werden. Aus didaktischen Gründen wird ein viskoelastischer Körper angenommen, sodass die herausfordernde Argumentation der Thermodynamik verständlich demonstriert wird. Die Herleitung der Materialgleichungen sind vollständig durchgeführt und eine Implementierung

[27] https://doi.org/10.1007/978-981-10-2444-3

im FEniCS Projekt wurde aufgezeigt. In der 2. Arbeit ist die Thermomechanik der Kontinuumskörper ohne Elektromagnetismus erklärt.

In der 3. Arbeit wird die moderne Theorie des Elektromagnetismus eingeführt. Aus didaktischen Gründen wird ein starrer Körper und isothermes System vorausgesetzt. Zur Vorbereitung auf die Thermodynamik werden die nicht-intuitiven elektromagnetischen Felder durch die sogenannte moderne Theorie eingeführt und die in der Literatur unterschiedlich vorkommenden Bezeichnungen detailliert erklärt. Mehrere Beispiele aus der technischen Elektrotechnik, nämlich ein Kondensator, einen Stromwandler (Transformator) und den Proximity-Koppelstrom, sind mittels des FEniCS Projektes implementiert und diskutiert. Die konstitutiven Gleichungen sind für starre Körper und isotherme Systeme bekannt, in der 3. Arbeit werden sie ohne Herleitung angewandt.

Die 4. Arbeit bringt die Thermomechanik und den Elektromagnetismus zusammen. Eine thermodynamische Herleitung der konstitutiven Gleichungen für den deformierten (nicht polarisierten) Körper mit der elektromagnetischen Interaktion wird eingeführt und vollständig durchgeführt. Dabei entstehen wichtige Kopplungen zwischen den Feldern, z. B. der thermoelektrische Effekt. Dieser sogenannte Peltier–Seebeck Effekt wird in dynamischer Energieumwandlung benutzt. Die Implementierung eines Beispiels ist durch das FEniCS Projekt verwirklicht. In der 4. Arbeit werden die thermodynamische Begründung der thermoelektrischen Kopplung und eine nueartige Implementierung vorgestellt.

Die 5. Arbeit ist das Paper[28] im *post-print* Format, veröffentlicht als:
T. I. Zohdi und B. E. Abali (2018). „Modeling of power transmission and stress grading for corona protection“. In: *Computational Mechanics* 62.3, S. 411–420. ISSN: 0178-7675

In dieser Arbeit wird eine technisch-relevante Anwendung modelliert, bei der die Kopplung der Thermodynamik mit dem Elektromagnetismus von großer Bedeutung ist. Die Koronaentladung entsteht bei der Energieumwandlung und Energieübertragung. Sie ist Energieverlust und gefährdet die unmittelbare Umgebung. Deshalb werden die benutzten Funktionswerkstoffe optimiert. Eine Simulation dieses Phänomens – insbesondere der entstandenen Temperatur während der Entladung – erfordert eine akkurate Modellierung der Interaktion zwischen der Thermodynamik und dem Elektromagnetismus. Ein reduziertes, effizientes Modell zur Berechnung der Temperatur bei der Koronaentladung wird vorgeschlagen; die Genauigkeit

[28] https://doi.org/10.1007/s00466-017-1504-2

dieses Modells ist mittels der detaillierten Modellierung mit vollständiger Kopplung überprüft worden.

Die 6. Arbeit ist das Paper[29] im *post-print* Format, veröffentlicht als:
B. E. Abali (2017b). „Computational study for reliability improvement of a circuit board“. In: *Mechanics of Advanced Materials and Modern Processes* 3.1, S. 1–11. ISSN: 2198-7874

In dieser Arbeit wird eine technisch-relevante Anwendung in der Elektronik modelliert, in der die Kopplung zwischen der Thermomechanik und dem Elektromagnetismus zum Ausfall des Bauteils führt. Eine Leiterplatte in einem elektronischen Gerät ist mit den Schaltwegen modelliert. Der elektrische Strom zur Signalübertragung zwischen den Komponenten auf der Leiterplatte erzeugt Wärme, die eine Deformation der Bauteile mit unterschiedlichen Materialien verursacht. Somit ist eine thermische Spannung generiert, die typischerweise plastische Deformationen erzeugt. Diese wiederum führt zur Ermüdung und zum Ausfall der elektronischen Bauteile. Die Ermüdung des Bauteils wird durch die plastische Deformation begründet. Die multiphysikalische Simulation in dieser Arbeit erlaubt eine Analyse solch einer Leiterplatte und gegebenenfalls eine Optimierung der Geometrie zur Verlängerung der Lebensdauer.

Die 7. Arbeit ist das Paper[30] im *post-print* Format, veröffentlicht als:
B. E. Abali und F. A. Reich (2017). „Thermodynamically consistent derivation and computation of electro-thermo-mechanical systems for solid bodies“. In: *Computer Methods in Applied Mechanics and Engineering* 319, S. 567–595. ISSN: 0045-7825

In dieser Arbeit wird die Theorie des Elektromagnetismus im deformierten Körper auf die polarisierten Materialien erweitert. Somit sind Kopplungen wie Piezoelektrizität, Pyroelektrizität vorhanden. Diese Interaktion ist eine Konsequenz der Kristallstruktur, sodass die Kopplung materialspezifisch ist. Heutzutage werden solche Materialien synthetisch produziert und in Sensoren und Aktuatoren benutzt. Die thermodynamische Herleitung der konstitutiven Gleichungen generiert die notwendigen Kopplungsterme mit zahlreichen Materialparametern. Für lineare Materialmodelle sind diese Parameter in der Literatur zu finden. In dieser Arbeit wird nicht nur die vollständige Theorie aufgebaut, sondern auch die numerische Implementierung vorgestellt. Mehrere Simulationen werden durchgeführt.

[29] https://doi.org/10.1186/s40759-017-0024-2
[30] https://doi.org/10.1016/j.cma.2017.03.016

Literatur

Abali, B. E. (2017a). *Computational Reality, Solving Nonlinear and Coupled Problems in Continuum Mechanics*. Bd. 55. Advanced Structured Materials. Springer. ISBN: 978-981-10-2443-6.

Abali, B. E. (2017b). „Computational study for reliability improvement of a circuit board“. In: *Mechanics of Advanced Materials and Modern Processes* 3.1, S. 1–11. ISSN: 2198-7874.

Abali, B. E. und Reich, F. A. (2017). „Thermodynamically consistent derivation and computation of electro-thermo-mechanical systems for solid bodies“. In: *Computer Methods in Applied Mechanics and Engineering* 319, S. 567–595. ISSN: 0045-7825.

Alnaes, M. S. und Mardal, K. A. (2010). „On the Efficiency of Symbolic Computations Combined With Code Generation for Finite Element Methods“. In: *ACM Transactions on Mathematical Software* 37.1.

Alnaes, M. S. und Mardal, K. A. (2012). „Automated solution of differential equations by the finite element method, the FEniCS book“. In: *Automated Solution of Differential Equations by the Finite Element Method*. Hrsg. von A. Logg, K.-A. Mardal und G. N. Wells. Bd. 84. Lecture Notes in Computational Science and Engineering. Springer. Kap. 15 Syfi and sfc: symbolic finite elements and form compilation.

Ampere, M. (1825). „Memoir on a new electro-dynamic experiment, on its application to the formula representing the mutual action of the two elements of voltaic conductors, and on some new results deduced from that formula“. In: *Philosophical Magazine Series 1* 66.331, S. 373–387.

Barnett, S. M. (2010). „Resolution of the Abraham–Minkowski dilemma“. In: *Physical Review Letters* 104.7, S. 070401.

Bethune-Waddell, M. und Chau, K. J. (2015). „Simulations of radiation pressure experiments narrow down the energy and momentum of light in matter“. In: *Reports on Progress in Physics* 78.12, S. 122401.

Bobbio, S. (2000). „Electrodynamics of materials“. In: *Forces, Stresses, and Energies in Solids and Fluids, Academic Press (Orlando, Florida)*.

Brevik, I. (1979). „Experiments in phenomenological electrodynamics and the electromagnetic energy-momentum tensor“. In: *Physics Reports* 52.3, S. 133–201.

Caratheodory, C. (1909). „Untersuchungen über die Grundlagen der Thermodynamik“. In: *Mathematische Annalen* 67.3, S. 355–386.

Chu, L. J., Haus, H. A. und Penfield Jr, P. (1966). „The force density in polarizable and magnetizable fluids“. In: *Proceedings of the IEEE* 54.7, S. 920–935.

Courant, R. und Hilbert, D. (1966). „Methods of mathematical physics Vol. 2“. In: *New York: Interscience Publication, third printing* 2.

Eckart, C. (1940a). „The thermodynamics of irreversible processes. I. The simple fluid“. In: *Physical Review* 58.3, S. 267–269.

Eckart, C. (1940b). „The thermodynamics of irreversible processes. II. Fluid mixtures“. In: *Physical Review* 58.3, S. 269–275.

Eckart, C. (1940c). „The thermodynamics of irreversible processes. III. Relativistic theory of the simple fluid“. In: *Physical Review* 58.10, S. 919–924.

Eringen, A. und Maugin, G. (1990). *Electrodynamics of continua. Vol. 1: Foundations and solid media. Vol. 2: Fluids and complex media*. Springer-Verlag, New York.

Gauß, C. F. (1833). „Die Intensität der erdmagnetischen Kraft, zurückgeführt auf absolutes Maaß“. In: *Annalen der Physik* 104.6, S. 241–273.

Gibbs, J. W. (1873). „A method of geometrical representation of the thermodynamic properties of substances by means of surfaces“. In: *Trans. Connecticut Acad. Art. Sci., New Haven* 2, S. 382–404.

Gnu GPL (2007). *Gnu Gpl—the GNU General Public License*. http://www.gnu.org/copyleft/gpl.html.

Griffiths, D. J. (2012). „Resource letter EM-1: electromagnetic momentum“. In: *American Journal of Physics* 80.1, S. 7–18.

Griffiths, D. J. (1999). *Introduction to electrodynamics*. 3. Aufl. Prentice-Hall, New Jersey.

Groot, S. R. de und Mazur, P. (1984). *Non-equilibrium thermodynamics*. Dover Publications, New York.

Gyarmati, I. (1970). *Non-equilibrium thermodynamics*. Hrsg. von I. Szabo, E. Gyarmati und W. F. Heinz. Springer, Berlin.

Heaviside, O. (1889). „On the electromagnetic effects due to the motion of electrification through a dielectric“. In: *The London, Edinburgh, and Dublin Philosophical Magazine and Journal of Science* 27.167, S. 324–339.

Hilbert, D. (1902). „The Foundations of Geometry (Transl. by Townsend, E. J.)“ In: *The Open Court Publishing Co.*

Hutter, K., Ven, A. A. und Ursescu, A. (2006). *Electromagnetic Field Matter Interactions in Thermoelasic Solids and Viscous Fluids*. Bd. 710. Springer, Berlin Heidelberg.

Janssen, M. und Mecklenburg, M. (2006). „From classical to relativistic mechanics: Electromagnetic models of the electron“. In: *Interactions*. Hrsg. von L. J. Hendricks V.F. Jorgensen K. Bd. 251. Boston Studies in the Philosophy of Science. Springer, Dordrecht, S. 65–134.

Jones, D. S. (1964). *The Theory of Electromagnetism*. Pergamon Press, New York, S. 1–99. ISBN: 978-0-08-013686-8.

Jou, D., Casas-Vazquez, J. und Lebon, G. (1999). „Extended irreversible thermodynamics revisited (1988-98)“. In: *Reports on Progress in Physics* 62.7, S. 1035–1142.

Kemp, B. A. und Grzegorczyk, T. M. (2011). „The observable pressure of light in dielectric fluids“. In: *Optics letters* 36.4, S. 493–495.

Kovetz, A. (2000). *Electromagnetic theory*. Oxford University Press Oxford.

Lavoisier, L. A. (1789). *Traité élémentaire de chimie*.

Logg, A., Mardal, K. A. und Wells, G. N. (2012). *Automated solution of differential equations by the finite element method, the FEniCS book*. Bd. 84. Lecture Notes in Computational Science and Engineering. Springer. ISBN: 978-3-642-23098-1.

Lorentz, H. A. (1904). „Zittungsverlagen akad. van Wettenschappen 1, 74 (nov. 26, 1892); Versuch einer Theorie der elektrischen und optischen Erscheinungen in bewegten Körpern, 1895“. In: *(Engl. version) Proceedings Academic Science, Amsterdam* 6, S. 809.

Lorentz, H. A. (1937). „Versuch einer Theorie der electrischen und optischen Erscheinungen in bewegten Körpern, 1895“. In: *Collected Papers*. Springer, S. 1–138.

Low, F. E. (2004). *Classical field theory: electromagnetism and gravitation*. Wiley-Vch Verlag, Weinheim.

Mansuripur, M. (2010). „Resolution of the Abraham–Minkowski controversy“. In: *Optics Communications* 283.10, S. 1997–2005.

Maxwell, J. C. (1865). „A dynamical theory of the electromagnetic field“. In: *Philosophical transactions of the Royal Society of London* 155, S. 459–512.

Maxwell, J. C. (1892). *A Treatise on Electricity and Magnetism*. Clarendon Press, Oxford.

Müller, I. (1985). *Thermodynamics*. Pitman Publishing, London.

Müller, W. H. (2014). *An excursion to continuum mechanics*. Springer.

Nye, J. F. (1967). *Physical properties of crystals: their representation by tensors and matrices*. Oxford at Clarendon Press.

Obukhov, Y. N. (2008). „Electromagnetic energy and momentum in moving media“. In: *Annalen der Physik* 17.9-10, S. 830–851.

Oden, J. T. (1972). „Finite Elements of Nonlinear continua“. In:

Oersted, H. C. (1820). „Electricity and magnetic needles“. In: *Philosophy* 16.4, S. 273–276.

Pao, Y.-H. und Hutter, K. (1975). „Electrodynamics for moving elastic solids and viscous fluids“. In: *Proceedings of the IEEE* 63.7, S. 1011–1021.

Pauli, W. (1973). *Pauli lectures on Physics, vol.3, Thermodynamics and the kinetic theory of gases*. Dover (2000) repub. of MIT Press, Cambridge, Massachusetts.

Pfeifer, R. N., Nieminen, T. A., Heckenberg, N. R. und Rubinsztein-Dunlop, H. (2007). „Colloquium: Momentum of an electromagnetic wave in dielectric media“. In: *Reviews of Modern Physics* 79.4, S. 1197.

Truesdell, C. und Toupin, R. A. (1960). *Principles of classical mechanics and field theory, Handbuch der Physik Vol. III/1 (Ed. by Flügge, S.)* Hrsg. von S. Flügge. Springer, Berlin Heidelberg.

Verma, G., Chaudhary, K. und Singh, K. P. (2017). „Nanomechanical effects of light unveil photons momentum in medium“. In: *Scientific Reports* 7.1, S. 42554.

Voigt, W. (1895). „Piezo-und Pyroelectricität, dielectrische Influenz und Electrostriction bei Krystallen ohne Symmetriecentrum“. In: *Annalen der Physik* 291.8, S. 701–731.

Wriggers, P. (2008). *Nonlinear finite element methods*. Springer Science & Business Media.

Zienkiewicz, O. und Taylor, R. (1991). *The Finite Element Method. Vols. I and II*.

Zohdi, T. I. und Abali, B. E. (2018). „Modeling of power transmission and stress grading for corona protection“. In: *Computational Mechanics* 62.3, S. 411–420. ISSN: 0178-7675.

Zohdi, T. I. (2015). *A Finite Element Primer for Beginners: The Basics*. Springer.

Teil II.

Veröffentlichungen

Kapitel I

Associated plasticity

The post-print version of the published manuscript:
Section 1.6 in Abali, B. E. (2017). Computational Reality: Solving Nonlinear and Coupled Problems in Continuum Mechanics (Advanced Structured Materials Vol. 55). Springer Nature Singapore.

The final publication is available at Springer via
https://doi.org/10.1007/978-981-10-2444-3

Particles in their initial positions, X_i, move and displace as a consequence of a mechanical loading. This displacement, u_i, for every particle, X_i, at the current time, t, is a function in space and time, $u_i = u_i(X_j, t)$. We compute the displacement with the balance of linear momentum augmented by the constitutive equation. The balance of linear momentum possesses stress. The constitutive equation relates stress to displacements over strains. This connection is a mathematical equation, every stress value is related to a unique strain value. For example zero stress is related to zero strain. If we compute a loading and unloading scenario—stress increases and then decreases—the particles move under loading and move back to their initial positions after unloading. Before loading, at zero stress, no deformation occurs (zero strain). After loading and unloading, at zero stress, zero strain has to occur again. In other words, the process is reversible and the displacements are recoverable.

In the so-called *elastic* behavior, the displacement vanishes after unloading. The process is reversible and for several cases it is admissible. For engineering materials like steel, copper, magnesium, and aluminum, the admissible strains are less than $0.2\% = 0.002$. Above this threshold a *plastic* deformation starts occurring such that after unloading some of the displacements remain in the continuum body. The process is not reversible; some of displacements are recovered, not all. During this plastic deformation the material behavior changes, too. We need different material models for elasticity and plasticity. Hence, we need to distinguish between elastic and plastic *regimes*.

We start with elasticity. As discussed in Section[31] 1.4, stress tensor consists of volumetric and deviatoric parts. We can motivate this decomposition for small strains by using another argumentation. Consider a cubic body expressed in Cartesian coordinates with its origin in one corner. Lengths of its sizes are simply identical to unit vectors of the coordinate system. The volume reads

$$V = X_1 X_2 X_3 = 1 \ . \tag{I.1}$$

Suppose that its length changes due to a mechanical loading. The displacement, u_1, u_2, u_3 along X_1, X_2, X_3, respectively, can be used to calculate the volumetric change:

$$\begin{gathered} V + \Delta V = (X_1 + u_1)(X_2 + u_2)(X_3 + u_3) = \\ = X_1 X_2 X_3 + X_1 X_2 u_3 + X_1 u_2 X_3 + X_1 u_2 u_3 + u_1 X_2 X_3 + u_1 u_2 X_3 + u_1 u_2 u_3 \ . \end{gathered} \tag{I.2}$$

By multiplying the latter by $V/X_1 X_2 X_3 = 1$ and then neglecting the nonlinear terms, viz.,

$$\begin{gathered} \frac{u_2 u_3}{X_2 X_3} = \varepsilon_{22}\varepsilon_{33} \leq 0.002^2 \approx 0 \ , \quad \frac{u_1 u_2}{X_1 X_2} = \varepsilon_{11}\varepsilon_{22} \leq 0.002^2 \approx 0 \ , \\ \frac{u_1 u_2 u_3}{X_1 X_2 X_3} = \varepsilon_{11}\varepsilon_{22}\varepsilon_{33} \leq 0.002^3 \approx 0 \ , \end{gathered} \tag{I.3}$$

since small strains (smaller than 0.002) occur in the elastic regime, we obtain

$$\begin{gathered} V + \Delta V = V + \frac{u_3}{X_3} V + \frac{u_2}{X_2} V + \frac{u_1}{X_1} V \\ \frac{\Delta V}{V} = \frac{u_3}{X_3} + \frac{u_2}{X_2} + \frac{u_1}{X_1} = \varepsilon_{kk} \ . \end{gathered} \tag{I.4}$$

We can use a simplified notation:

$$\varepsilon_{kk} = 3e \ , \tag{I.5}$$

where the parameter e is simply the measure of the volumetric change (dilation) in Cartesian coordinates. The deviatoric strains are responsible for a distortion without dilation

$$\varepsilon_{|ij|} = \varepsilon_{ij} - e\delta_{ij} \ . \tag{I.6}$$

Employing Hooke's law for isotropic materials, we obtain the linear relation between the symmetric Cauchy stress and symmetric strain:

$$\sigma_{ij} = c_1 e \delta_{ij} + c_2 \varepsilon_{|ij|} = \lambda \delta_{ij} \varepsilon_{kk} + 2\mu \varepsilon_{ij} \ . \tag{I.7}$$

This tensor equation of rank two has to hold in its lower ranks, too. We can reduce

[31] As appeared in Abali, 2017.

the rank by contracting indices, for a Cartesian coordinate system we multiply by the KRONECKER delta:[32]

$$\delta_{ij}\sigma_{ij} = \sigma_{ii} = \lambda\delta_{ii}3e + 2\mu\varepsilon_{ii} = \lambda 9e + 2\mu 3e \ , \tag{I.8}$$

and introduce a simplified notation:

$$\sigma_{ii} = 3s \Rightarrow s = (3\lambda + 2\mu)e \ . \tag{I.9}$$

Another bulk quantity, s, for stress has been used, the deviatoric part reads

$$\sigma_{|ij|} = \sigma_{ij} - s\delta_{ij} \ . \tag{I.10}$$

Finally, we observe a simple relation

$$\begin{aligned} \sigma_{ij} &= \lambda\delta_{ij}\varepsilon_{kk} + 2\mu\varepsilon_{ij} \ , \\ \sigma_{|ij|} + s\delta_{ij} &= \lambda\delta^{ij}3e + 2\mu\big(\varepsilon_{|ij|} + e\delta_{ij}\big) \ , \\ \sigma_{|ij|} + (3\lambda + 2\mu)e\delta_{ij} &= \lambda\delta_{ij}3e + 2\mu e\delta_{ij} + 2\mu\varepsilon_{|ij|} \ , \\ \sigma_{|ij|} &= 2\mu\varepsilon_{|ij|} \ . \end{aligned} \tag{I.11}$$

In other words, under the assumption of small strains, deviatoric and volumetric parts can be (additively) decomposed and related to each other separately. Indeed, we have seen this decomposition already by using the energy concept, however, herein we present the same result without using the notion of energy. The assumption of small strains in the elastic regime is adequate for engineering materials like steel, aluminum, magnesium, and copper.

By excessing the yield stress, σ_{Y}, body starts to flow with the velocity, $v_i = v_i(X_j, t)$, of particles X_i. Since velocity is the rate of displacement, we obtain

$$\frac{\partial v_{(i}}{\partial X^{j)}} = \frac{\partial^2 u_{(i}}{\partial X^{j)}\partial t} = \frac{\partial^2 u_{(i}}{\partial t \partial X^{j)}} = \frac{\partial \varepsilon_{ij}}{\partial t} = \dot{\varepsilon}_{ij} \ , \tag{I.12}$$

where $\dot{\varepsilon}_{ij}$ is the strain rate. The strain rate or equally the symmetric part of velocity gradient causes a viscous flow. If a *yield condition* is fulfilled such velocities occur. Hence this type of deformation is elasto-plastic and the flow of continuum body can be expressed by strain rate. In a simple tensile test, a loading above the yield stress causes a plastic deformation, which remains in the body after unloading. Thus, we can simply measure the elastic and plastic elongations. By dividing the elastic and plastic elongations by the length of the beam, we obtain elastic and plastic strains.[33] In order

[32] We lower the rank by contracting indices. In order to contract two indices we multiply by the metric tensor. KRONECKER delta is also the metric tensor in Cartesian coordinates.

[33] This consideration has been used in Prandtl, 1924 and Reuss, 1930, therefore, the associated plasticity is also called PRANDTL-REUSS plasticity, see Müller, 2014, Chap. 11. The PRANDTL-REUSS plasticity is named for Ludwig Prandtl and András Reuß (Endre Reuss).

to model the plastic behavior we need the strain rate or symmetric velocity gradients. According to the VON MISES yield criterion, the second invariant[34] of deviatoric part of the stress tensor should be greater than an experimentally determined quantity. We know from a tensile test that the material starts deforming plastically above the yield stress, σ_{Y}. This scalar value is representing the threshold of the plasticity. In a tensile test the stress tensor attains the yield stress in one component as the materials starts yielding

$$\sigma_{ij} = \begin{pmatrix} \sigma_{\mathrm{Y}} & 0 & 0 \\ 0 & 0 & 0 \\ 0 & 0 & 0 \end{pmatrix} \ . \tag{I.13}$$

Since we want to use the VON MISES yield criterion, we calculate the second invariant:

$$\sigma_{|ij|} = \sigma_{ij} - s\delta_{ij} = \begin{pmatrix} \frac{2}{3}\sigma_{\mathrm{Y}} & 0 & 0 \\ 0 & -\frac{1}{3}\sigma_{\mathrm{Y}} & 0 \\ 0 & 0 & -\frac{1}{3}\sigma_{\mathrm{Y}} \end{pmatrix} \ , \tag{I.14}$$

and relate it to the yield stress:

$$\begin{aligned} \sigma_{|ij|}\sigma_{|ij|} &= \frac{6}{9}\sigma_{\mathrm{Y}}^2 \ , \\ \sigma_{\mathrm{Y}} &= \sqrt{\frac{3}{2}\sigma_{|ij|}\sigma_{|ij|}} \ , \end{aligned} \tag{I.15}$$

which is the yield criterion. The value of σ_{Y} is specific to the material. For any deformation we can calculate

$$\sigma_{\mathrm{eq}} = \sqrt{\frac{3}{2}\sigma_{|ij|}\sigma_{|ij|}} \ , \tag{I.16}$$

and compare it to the yield stress obtained from the tensile test. When the plasticity starts, $\sigma_{\mathrm{eq}} = \sigma_{\mathrm{Y}}$, the yield criterion is fulfilled.

As a consequence of mechanical loading, a deformation occurs. Upon unloading, plastic part of the deformation remains in the body whereas the elastic part is recovered. Since we express the deformation by using the strain tensor, a simple approach of modeling such a behavior reads

$$\varepsilon_{ij} = {}^{\mathrm{e}}\varepsilon_{ij} + {}^{\mathrm{p}}\varepsilon_{ij} \ , \tag{I.17}$$

where ${}^{\mathrm{e}}\varepsilon_{ij}$ denotes the elastic part of the strain tensor and ${}^{\mathrm{p}}\varepsilon_{ij}$ the plastic part. This additive decomposition of strain tensor is a phenomenological fact. For many engineering materials with small deformations and small strains the approach gives

[34] There are three invariants in three-dimensional space of the stress tensor. The first invariant of stress is the bulk quantity $s = \sigma_{ii}$, the second invariant is $\sigma_{ij}\sigma_{ij}$ and the third invariant is, $\sigma_{ij}\sigma_{jk}\sigma_{ki}$.

accurate results. For the elastic part of strains we have applied HOOKE's law:

$$\sigma_{ij} = C_{ijkl}\,{}^{\mathrm{e}}\varepsilon_{ij} = C_{ijkl}\big(\varepsilon_{kl} - {}^{\mathrm{p}}\varepsilon_{kl}\big) \ . \tag{I.18}$$

The plasticity is given by strain rate. Hence, the latter equation is rewritten

$$\dot{\sigma}_{ij} = C_{ijkl}\big(\dot{\varepsilon}_{kl} - {}^{\mathrm{p}}\dot{\varepsilon}_{kl}\big) \ , \tag{I.19}$$

since the stiffness tensor is constant in time. We need a constitutive relation for ${}^{\mathrm{p}}\dot{\varepsilon}_{ij}$. In a former section we have utilized a scalar function, stored energy, in order to define the stress as in Eq.[31] (1.91). Stored energy has a first integral, i.e., it is a potential. The same concept is used for plasticity and we assume that a flow potential f exists, leading to

$${}^{\mathrm{p}}\dot{\varepsilon}_{ij} = \dot{\Lambda}\frac{\partial f}{\partial \sigma_{ij}} \ , \tag{I.20}$$

where we need a (positive) multiplier $\dot{\Lambda}$ since the plastic strain cannot be expressed with a first integral. In other words, the evolution of plastic strain is important, we cannot use the start and end states for calculating plastic strain. Therefore, a flow potential, f, fails to define the plastic strain and we need a multiplier. Both will be defined in the following by using the yield criterion. This approach is called *associated plasticity* in the literature.

1. Isotropic hardening

We start by defining the flow potential, f. For many engineering materials, the VON MISES yield criterion is used in order to generate a function resulting in 0 in case of plasticity:

$$\begin{aligned} f &= \frac{1}{3}\sigma_{\mathrm{eq}}^2 - \frac{1}{3}k^2 \ , \\ f &= \frac{1}{2}\sigma_{|ij|}\sigma_{|ij|} - \frac{1}{3}k^2 \ . \end{aligned} \tag{I.21}$$

The value of k changes with respect to the plastic deformation. Consider a tensile test, the value of $k = \sigma_{\mathrm{Y}}$ in the elastic regime. Obviously, the flow potential is negative, $f < 0$. The axial force increases such that the equivalent stress approaches the yield stress and f goes to zero. At the moment, when the yield criterion is fulfilled, f vanishes and plasticity starts. If the force increases further, we would have a positive f if the value of k remains as $k = \sigma_{\mathrm{Y}}$. However, the value of k increases as the plasticity is occurring such that $f = 0$ as long as a plastic deformation is performed.

The flow potential is zero in the plastic regime and negative in the elastic regime:

$$f \leq 0 \ , \quad f \leq \begin{cases} = 0 & \text{plastic regime} \\ < 0 & \text{elastic regime} \end{cases} \ . \tag{I.22}$$

Of course, we need to model k depending on the plastic deformation. For simplicity, consider a linear function in the plastic strain:

$$k = \sigma_{\mathrm{Y}} + h \, {}^{\mathrm{p}}\varepsilon_{\mathrm{eq}} \ , \tag{I.23}$$

where ${}^{\mathrm{p}}\varepsilon_{\mathrm{eq}}$ denotes the equivalent plastic strain. This approach[35] is obviously the simplest case. Many engineering materials show such a simple *hardening* behavior. An explanation of this behavior is based on arising dislocations in case of plastic yielding, where the high density of dislocations slows down the plastic flow. From a phenomenological point of view, we observe in a tensile experiment a behavior as in Eq. (I.23) and model it by determining the material constants σ_{Y} and h without considering a microscopic reasoning. Since we determine the parameters from a tensile test we need to use the VON MISES equivalent stress and strain.

For example an AISI steel 1010 has the *initial* yield stress $\sigma_{\mathrm{Y}} = 305\,\mathrm{MPa}$. This value remains constant. For the elastic regime the flow potential is below zero, $f < 0$, since the equivalent stress is smaller than $k = \sigma_{\mathrm{Y}}$. When the loading causes an equivalent stress higher than σ_{Y}, the value of k increases such that $f = 0$ during the plasticity.[36] As we have seen in Eq. (I.23), k depends on the plastic strain and is independent on the stress. The flow potential depends on k and stress,

$$f = f(k, \sigma_{ij}) \ . \tag{I.24}$$

During plastic deformation $f = 0$ and moreover f remains zero:

$$\begin{aligned} f^{\bullet} &= 0 \ , \\ f^{\bullet} &= \frac{\partial f}{\partial \sigma_{ij}} \dot{\sigma_{ij}} + \frac{\partial f}{\partial k} k^{\bullet} = 0 \ . \end{aligned} \tag{I.25}$$

By using Eq. (I.21) we obtain

$$\frac{\partial f}{\partial \sigma_{ij}} = \frac{\partial f}{\partial \sigma_{|kl|}} \frac{\partial \sigma_{|kl|}}{\partial \sigma_{ij}} = \sigma_{|kl|} \big(\delta_{ki} \delta_{lj} - \frac{1}{3} \delta_{kl} \delta_{ni} \delta_{nj} \big) = \sigma_{|ij|} - \frac{1}{3} \delta_{ij} \sigma_{|kk|} = \sigma_{|ij|} \ , \tag{I.26}$$

[35] See Odqvist, 1933

[36] This approach gives the so-called KARUSH-KUHN-TUCKER conditions:

$$\Lambda^{\bullet} \geq 0 \ , \quad f \leq 0 \ , \quad \Lambda^{\bullet} f = 0 \ ,$$

since in the elastic regime $f < 0$ and $\Lambda^{\bullet} = 0$ whereas in the plastic regime $f = 0$ and $\Lambda^{\bullet} > 0$. We will not make much use of these relations, they are mostly used in conditional optimization.

as well as

$$\frac{\partial f}{\partial k} = -\frac{2}{3}k \ , \tag{I.27}$$

thus the condition in Eq. (I.25) results in

$$f^{\bullet} = 0 = \sigma_{|ij|}\sigma^{\bullet}_{ij} - \frac{2}{3}kk^{\bullet} \ . \tag{I.28}$$

The latter can be rewritten in terms of the rate of k as follows

$$k^{\bullet} = \frac{3\sigma_{|ij|}\sigma^{\bullet}_{ij}}{2k} \ . \tag{I.29}$$

By combining the latter with the rate of k obtained from the linear isotropic hardening model in Eq. (I.23),

$$k^{\bullet} = h\,{}^{\mathrm{p}}\varepsilon^{\bullet}_{\mathrm{eq}} \ , \tag{I.30}$$

we acquire the so-called *evolution equation* for plastic equivalent strain:

$$\begin{aligned} k^{\bullet} = h\,{}^{\mathrm{p}}\varepsilon^{\bullet}_{\mathrm{eq}} &= \frac{3\sigma_{|ij|}\sigma^{\bullet}_{ij}}{2k} \ , \\ {}^{\mathrm{p}}\varepsilon^{\bullet}_{\mathrm{eq}} &= \frac{3\sigma_{|ij|}\sigma^{\bullet}_{ij}}{2kh} \ . \end{aligned} \tag{I.31}$$

The evolution equation describes the change of plastic equivalent strain. The plastic strain accumulates in the continuum body due to the evolution equation

$${}^{\mathrm{p}}\varepsilon_{\mathrm{eq}} = \int {}^{\mathrm{p}}\varepsilon^{\bullet}_{\mathrm{eq}}\,\mathrm{d}t \ . \tag{I.32}$$

The plastic strain lacks a first integral, we cannot write $\int \mathrm{d}\,{}^{\mathrm{p}}\varepsilon_{\mathrm{eq}}$. Therefore, we need an evolution equation also for the three-dimensional case. In order to obtain ${}^{\mathrm{p}}\varepsilon^{\bullet}_{ij}$ we start by inserting Eq. (I.19):

$${}^{\mathrm{p}}\varepsilon^{\bullet}_{\mathrm{eq}} = \frac{3\sigma_{|ij|}C_{ijkl}\left(\varepsilon^{\bullet}_{kl} - {}^{\mathrm{p}}\varepsilon^{\bullet}_{kl}\right)}{2kh} \ , \tag{I.33}$$

and continue by utilizing Eq.(I.20) with Eq. (I.26):

$$\begin{aligned} {}^{\mathrm{p}}\varepsilon^{\bullet}_{ij} &= \Lambda^{\bullet}\frac{\partial f}{\partial \sigma_{ij}} = \Lambda^{\bullet}\sigma_{|ij|} \ , \\ {}^{\mathrm{p}}\varepsilon^{\bullet}_{\mathrm{eq}} &= \frac{3\sigma_{|ij|}C_{ijkl}\left(\varepsilon^{\bullet}_{kl} - \Lambda^{\bullet}\sigma_{|kl|}\right)}{2kh} \ . \end{aligned} \tag{I.34}$$

During plasticity, $f = 0$, we postulate that the power calculated by the equivalent stress and strain equals to the power calculated by the three-dimensional stress and strain states:

$$\sigma_{\mathrm{eq}}\,{}^{\mathrm{p}}\varepsilon^{\bullet}_{\mathrm{eq}} = \sigma_{ij}\,{}^{\mathrm{p}}\varepsilon^{\bullet}_{ij} \ . \tag{I.35}$$

The plastic flow of a solid is equal to a viscous flow of a fluid. In a viscous flow the shear deformation results in an incompressible flow without volumetric change. This phenomenon occurs in the plastic flow, too

$$ {}^{\mathrm{p}}\varepsilon_{kk} = 0 \Rightarrow {}^{\mathrm{p}}\dot{\varepsilon}_{kk} = 0 \ , \tag{I.36} $$

thus, there is only a deviatoric (traceless) plastic strain rate, ${}^{\mathrm{p}}\dot{\varepsilon}_{|ij|} = {}^{\mathrm{p}}\dot{\varepsilon}_{ij}$. The aforementioned postulate leads to

$$ \begin{gathered} \sigma_{\mathrm{eq}}\, {}^{\mathrm{p}}\dot{\varepsilon}_{\mathrm{eq}} = \sigma_{|ij|}\, {}^{\mathrm{p}}\dot{\varepsilon}_{|ij|} \ , \\ \sigma_{\mathrm{eq}} = \sqrt{\frac{3}{2}\sigma_{|ij|}\sigma_{|ij|}} \Rightarrow {}^{\mathrm{p}}\dot{\varepsilon}_{\mathrm{eq}} = \sqrt{\frac{2}{3}\, {}^{\mathrm{p}}\dot{\varepsilon}_{|ij|}\, {}^{\mathrm{p}}\dot{\varepsilon}_{|ij|}} \ . \end{gathered} \tag{I.37} $$

Now, the postulate can be rewritten

$$ {}^{\mathrm{p}}\dot{\varepsilon}_{\mathrm{eq}} = \frac{1}{\sigma_{\mathrm{eq}}}\sigma_{|ij|}\, {}^{\mathrm{p}}\dot{\varepsilon}_{|ij|} \ . \tag{I.38} $$

Moreover, during plasticity, from Eq. (I.21) we acquire

$$ f = 0 \Rightarrow k = \sqrt{\frac{2}{3}\sigma_{|ij|}\sigma_{|ij|}} = \sigma_{\mathrm{eq}} \ . \tag{I.39} $$

By using the latter and Eq. $(\mathrm{I.34})_1$ we obtain

$$ {}^{\mathrm{p}}\dot{\varepsilon}_{\mathrm{eq}} = \frac{1}{k}\sigma_{|ij|}\, {}^{\mathrm{p}}\dot{\varepsilon}_{|ij|} = \frac{1}{k}\sigma_{|ij|}\dot{\Lambda}\sigma_{|ij|} = \frac{1}{k}\dot{\Lambda}\frac{2}{3}k^2 = \frac{2}{3}\dot{\Lambda}k \ . \tag{I.40} $$

Finally, we can explicitly define $\dot{\Lambda}$ by combining Eq. $(\mathrm{I.34})_2$ with the latter

$$ \begin{gathered} \dot{\Lambda} = \frac{9\sigma_{|ij|}C_{ijkl}\left(\dot{\varepsilon}_{kl} - \dot{\Lambda}\sigma_{|kl|}\right)}{4k^2h} \ , \\ \dot{\Lambda}\left(1 + \frac{9}{4k^2h}\sigma_{|ij|}C_{ijkl}\sigma_{|kl|}\right) = \frac{9}{4k^2h}\sigma_{|ij|}C_{ijkl}\dot{\varepsilon}_{kl} \ , \\ \dot{\Lambda} = \frac{\sigma_{|ij|}C_{ijkl}\dot{\varepsilon}_{kl}}{\frac{4}{9}k^2h + \sigma_{|ij|}C_{ijkl}\sigma_{|kl|}} \ . \end{gathered} \tag{I.41} $$

We have reached the material model of the plastic multiplier in case of the linear hardening. We recall Eq. $(\mathrm{I.34})_1$:

$$ {}^{\mathrm{p}}\dot{\varepsilon}_{ij} = \dot{\Lambda}\sigma_{|ij|} \ , \tag{I.42} $$

such that the evolution of the plastic strain can be computed by means of the additional parameter, h, from the used linear hardening model. This parameter shall be obtained by a tensile testing. We aim at defining a constitutive equation for stress,

which reads

$$\overset{\bullet}{\sigma}_{ij} = C_{ijkl}\left(\overset{\bullet}{\varepsilon}_{kl} - \overset{\text{P}}{\varepsilon}_{kl}^{\bullet}\right) = \left(C_{ijmn} - C_{ijkl}\sigma_{|kl|}\frac{\sigma_{|op|}C_{opmn}}{\frac{4}{9}k^2h + \sigma_{|ij|}C_{ijkl}\sigma_{|kl|}}\right)\overset{\bullet}{\varepsilon}_{mn} \ . \tag{I.43}$$

In order to allow plasticity to occur above the yield stress, we can define a conditional parameter:

$$\langle\gamma\rangle = \begin{cases} 1 & \text{if } k \geq \sigma_{\text{Y}} \\ 0 & \text{otherwise} \end{cases} \ , \tag{I.44}$$

where the conditional parameter is written with MACAULAY brackets[37] $\langle\cdot\rangle$. This parameter is used as follows

$$\overset{\bullet}{\sigma}_{ij} = \left(C_{ijmn} - \langle\gamma\rangle\frac{C_{ijkl}\sigma_{|kl|}\sigma_{|op|}C_{opmn}}{\frac{4}{9}k^2h + \sigma_{|ij|}C_{ijkl}\sigma_{|kl|}}\right)\overset{\bullet}{\varepsilon}_{mn} \ . \tag{I.45}$$

Formally, the parameter γ can be computed after having computed the displacement field (and thus stress). This approach is computationally costly, therefore, we will employ it regarding the displacement field from the last time step. By choosing appropriately small time steps, the computation will be accurate.

From the point of algorithmic ease the MACAULAY brackets can be implemented in an unusual way:

$$He(a) = \frac{1}{|a|}\left(\frac{a + |a|}{2}\right) = \begin{cases} 1 & \text{if } a > 0 \\ 0 & \text{otherwise} \end{cases} \ . \tag{I.46}$$

This step-function is known as the HEAVISIDE function.[38] Especially in signal processing and system control and dynamics, by using the time instead of a, HEAVISIDE function is used frequently. We can use the same idea for the MACAULAY brackets and implement it in this way:

$$\langle\gamma\rangle = He(k - \sigma_{\text{Y}}) = \frac{1}{|k - \sigma_{\text{Y}}|}\left(\frac{k - \sigma_{\text{Y}} + |k - \sigma_{\text{Y}}|}{2}\right) \ . \tag{I.47}$$

In the code below we use a boolean query for obtaining $\langle\gamma\rangle$, it is quicker than the HEAVISIDE function.

Since we apply the displacement field from the last time step for obtaining $\langle\gamma\rangle$, the behavior of plastic flow is characterized with a time lag, which converges to reality by choosing small time steps. During plasticity the deformation is partly elastic and partly plastic. The plastic deformation is a viscous flow and we can imagine

[37] They are named for William Herrick Macaulay.
[38] It is named after Oliver Heaviside.

this phenomenon as a consequence of the velocity gradient. Elastic deformation is modeled by using the displacement gradient (strain). Displacement and velocity are coupled; but they are independent.[39] Therefore, elasticity and plasticity are coupled and independent phenomena.

2. Kinematic hardening

In the associated plasticity an isotropic hardening rule has some limitations. The yield stress, k, increases in all directions (isotropic), hence, it can only be used for a monotonic loading. For the case of a cyclic loading the BAUSCHINGER effect[40] can be modeled by amending the hardening rule. The so-called *kinematic* hardening uses a *back stress*, β_{ij}, which results in a dependence on loading in the hardening model. Instead of the aforementioned flow potential with linear isotropic hardening:

$$f = \frac{1}{2}\sigma_{|ij|}\sigma_{|ij|} - \frac{1}{3}(\sigma_{\mathrm{Y}} + h\,{}^{\mathrm{p}}\varepsilon_{\mathrm{eq}})^2 \ , \tag{I.48}$$

we use a flow potential[41] in this form:

$$f = \frac{1}{2}(\sigma_{|ij|} - \beta_{ij})(\sigma_{|ij|} - \beta_{ij}) - \frac{1}{3}\sigma_{\mathrm{Y}}^2 \ . \tag{I.49}$$

We aim at modeling the back stress, β_{ij}, in an adequate way. By starting with zero back stress, we can model the back stress by using an evolution equation for its rate, $\beta^{\bullet}_{ij}$. We search for a model of the rate of back stress. The simplest model[42] is a linear relation:

$$\beta^{\bullet}_{ij} = c\,{}^{\mathrm{p}}\varepsilon^{\bullet}_{ij} \ , \tag{I.50}$$

where the material parameter c has to be determined instead of h in isotropic hardening. Starting from the latter relation for back stress, a theoretical treatise[43] results in

$$\beta^{\bullet}_{ij} = (\sigma_{ij} - \beta_{ij})\Gamma^{\bullet} \ , \quad \Gamma^{\bullet} \geq 0 \ , \tag{I.51}$$

where we have introduced $\Gamma^{\bullet}$, which has to be obtained in a way that Eq. (I.50) holds. We redo the same steps as in isotropic hardening. The flow potential in Eq. (I.49)

[39] Formally, a sinusoidal displacement, $u = a\sin(bt)$, and thus the velocity, $v = a\,b\cos(bt)$, are independent, $\int u\,v\,\mathrm{d}t = 0$, since sinus and cosinus are orthogonal. This independence means that a variation in one does not change the other. A velocity in the current time causes a displacement in a *future* time, therefore, they are affecting each other in the subsequent times, however, independent at the current time.

[40] This effect has been discussed in Bauschinger, 1886 for the first time and therefore it is named after Johann Bauschinger.

[41] See Melan, 1938

[42] See Prager, 1955

[43] See Shield and Ziegler, 1958

is a function of stress and back stress, $f = f(\sigma_{ij}, \beta_{ij})$. While a plastic yielding is occurring,

$$f^{\bullet} = 0 = \frac{\partial f}{\partial \sigma_{ij}} \sigma^{\bullet}_{ij} + \frac{\partial f}{\partial \beta_{ij}} \beta^{\bullet}_{ij} = \big(\sigma_{|ij|} - \beta_{ij}\big)\sigma^{\bullet}_{|ij|} - \big(\sigma_{|ij|} - \beta_{ij}\big)\beta^{\bullet}_{ij} \ , \tag{I.52}$$

we obtain the following relation by using Eq. (I.51):

$$\begin{aligned} \big(\sigma_{|ij|} - \beta_{ij}\big)\sigma^{\bullet}_{|ij|} &= \big(\sigma_{|ij|} - \beta_{ij}\big)\beta^{\bullet}_{ij} \ , \\ \big(\sigma_{|ij|} - \beta_{ij}\big)\sigma^{\bullet}_{|ij|} &= \big(\sigma_{|ij|} - \beta_{ij}\big)\big(\sigma_{ij} - \beta_{ij}\big)\Gamma^{\bullet} \ , \\ \Gamma^{\bullet} &= \frac{\big(\sigma_{|ij|} - \beta_{ij}\big)\sigma^{\bullet}_{|ij|}}{\big(\sigma_{|ij|} - \beta_{ij}\big)\big(\sigma_{ij} - \beta_{ij}\big)} \ . \end{aligned} \tag{I.53}$$

Equation (I.50) states a traceless (deviatoric) back stress, $\beta_{ij} = \beta_{|ij|}$, since ${}^{\mathrm{p}}\varepsilon^{\bullet}_{ii} = 0$. Moreover, during plasticity, $f = 0$, we insert Eq. (I.49) into the latter and find

$$\Gamma^{\bullet} = \frac{\big(\sigma_{|ij|} - \beta_{ij}\big)\sigma^{\bullet}_{ij}}{\big(\sigma_{|ij|} - \beta_{ij}\big)\big(\sigma_{|ij|} - \beta_{ij}\big)} = \frac{\big(\sigma_{|ij|} - \beta_{ij}\big)\sigma^{\bullet}_{ij}}{\frac{2}{3}\sigma^{2}_{\mathrm{Y}}} \ . \tag{I.54}$$

The starting assumption with the flow potential for kinematic hardening,

$${}^{\mathrm{p}}\varepsilon^{\bullet}_{ij} = \Lambda^{\bullet}\frac{\partial f}{\partial \sigma_{ij}} = \Lambda^{\bullet}\big(\sigma_{|ij|} - \beta_{ij}\big) \ , \tag{I.55}$$

allows us to obtain from Eq. (I.50) with Eq. (I.51) the evolution of back stress:

$$\beta^{\bullet}_{ij} = c\Lambda^{\bullet}\big(\sigma_{|ij|} - \beta_{ij}\big) = \big(\sigma_{|ij|} - \beta_{ij}\big)\Gamma^{\bullet} \ , \tag{I.56}$$

for arbitrary σ_{ij} and β_{ij} values. Hence, it reads

$$c\Lambda^{\bullet} = \Gamma^{\bullet} \ , \quad \Lambda^{\bullet} = \frac{\big(\sigma_{|ij|} - \beta_{ij}\big)\sigma^{\bullet}_{ij}}{\frac{2}{3}c\sigma^{2}_{\mathrm{Y}}} \ . \tag{I.57}$$

In order to eliminate the rate of stress, we use again HOOKE's law,

$$\Lambda^{\bullet} = \frac{\big(\sigma_{|ij|} - \beta_{ij}\big)C_{ijkl}\big(\varepsilon^{\bullet}_{kl} - {}^{\mathrm{p}}\varepsilon^{\bullet}_{kl}\big)}{\frac{2}{3}c\sigma^{2}_{\mathrm{Y}}} \ , \quad {}^{\mathrm{p}}\varepsilon^{\bullet}_{kl} = \Lambda^{\bullet}\big(\sigma_{|kl|} - \beta_{kl}\big) \ , \tag{I.58}$$

and acquire

$$\begin{aligned} \Lambda^{\bullet}\left(1 + \frac{\big(\sigma_{|ij|} - \beta_{ij}\big)C_{ijkl}\big(\sigma_{|kl|} - \beta_{kl}\big)}{\frac{2}{3}c\sigma^{2}_{\mathrm{Y}}}\right) &= \frac{\big(\sigma_{|ij|} - \beta_{ij}\big)C_{ijkl}\varepsilon^{\bullet}_{kl}}{\frac{2}{3}c\sigma^{2}_{\mathrm{Y}}} \ , \\ \Lambda^{\bullet} &= \frac{\big(\sigma_{|ij|} - \beta_{ij}\big)C_{ijkl}\varepsilon^{\bullet}_{kl}}{\frac{2}{3}c\sigma^{2}_{\mathrm{Y}} + \big(\sigma_{|ij|} - \beta_{ij}\big)C_{ijkl}\big(\sigma_{|kl|} - \beta_{kl}\big)} \ . \end{aligned} \tag{I.59}$$

Often $c = 2/3h$ is chosen for a better correspondence to the isotropic hardening. In this case we obtain the constitutive equation for kinematic hardening:

$$\overset{\bullet}{\sigma}_{ij} = C_{ijmn}\big(\overset{\bullet}{\varepsilon}_{mn} - \overset{\bullet}{{}^{\mathrm{p}}\varepsilon}_{mn}\big) = C_{ijmn}\big(\overset{\bullet}{\varepsilon}_{mn} - \overset{\bullet}{\Lambda}(\sigma_{|mn|} - \beta_{mn})\big) \ , \tag{I.60}$$

by using the conditional parameter $\langle\gamma\rangle$ from Eq. (I.47) the constitutive equation can be rewritten

$$\overset{\bullet}{\sigma}_{ij} = \left(C_{ijmn} - \langle\gamma\rangle \frac{C_{ijkl}\big(\sigma_{|kl|} - \beta_{kl}\big)\big(\sigma_{|op|} - \beta_{op}\big)C_{opmn}}{\frac{4}{9}\sigma_{\mathrm{Y}}^2 h + \big(\sigma_{|ij|} - \beta_{ij}\big)C_{ijkl}\big(\sigma_{|kl|} - \beta_{kl}\big)}\right)\overset{\bullet}{\varepsilon}_{mn} \ . \tag{I.61}$$

The latter equation is the counterpart of Eq. (I.45) with the isotropic hardening. For the case of the isotropic hardening the yield stress, k, evolves with the plastic strain; whereas for the case of the kinematic hardening, the back stress, β_{ij}, evolves with the plastic strain.

In order to implement the constitutive equation, time discretization is used in the LAGRANGEan frame

$$\begin{aligned} \overset{\bullet}{\sigma}_{ij} &= \frac{\partial\sigma_{ij}}{\partial t} = \frac{\sigma_{ij} - \sigma_{ij}^0}{\Delta t} \ , \\ \sigma_{ij} &= \sigma_{ij}^0 + \Delta t\overset{\bullet}{\sigma}_{ij} \ . \end{aligned} \tag{I.62}$$

By considering linearized strains for small deformation the variational form becomes

$$\mathrm{Form} = \int_{\mathcal{B}_0}\left(\rho_0\frac{u_i - 2u_i^0 + u_i^{00}}{\Delta t\Delta t}\delta u_i + \sigma_{ji}\delta u_{i,j} - \rho_0 f_i\delta u_i\right)\mathrm{d}V - \int_{\partial\mathcal{B}_0^{\mathrm{N}}}\hat{t}_i\delta u_i\,\mathrm{d}A \ , \tag{I.63}$$

where stress in Eq. (I.62) is complemented with Eq. (I.45) or Eq. (I.61). Unfortunately, we need to know σ_{ij} in Eq. (I.45) or Eq. (I.61) for computing the current stress, σ_{ij}. The correct way of programming relies on an iterative schema,[44] which is computationally costly. Therefore, we use the value of stress from the last time step and approximate the rate of stress, for example, for kinematic hardening we acquire

$$\begin{aligned} \overset{\bullet}{\sigma}_{ij} &= \left(C_{ijmn} - \langle\gamma\rangle \frac{C_{ijkl}\big(\sigma_{|kl|}^0 - \beta_{kl}^0\big)\big(\sigma_{|op|}^0 - \beta_{op}^0\big)C_{opmn}}{\frac{4}{9}\sigma_{\mathrm{Y}}^2 h + \big(\sigma_{|ij|}^0 - \beta_{ij}^0\big)C_{ijkl}\big(\sigma_{|kl|}^0 - \beta_{kl}^0\big)}\right)\overset{\bullet}{\varepsilon}_{mn} \ , \\ \beta_{ij} &= \beta_{ij}^0 + \Delta t\overset{\bullet}{\beta}_{ij} \ , \quad \overset{\bullet}{\beta}_{ij} = \frac{(\sigma_{|kl|}^0 - \beta_{kl}^0)\overset{\bullet}{\sigma}_{kl}}{\frac{2}{3}\sigma_{\mathrm{Y}}^2}\big(\sigma_{|ij|}^0 - \beta_{ij}^0\big) \ . \end{aligned} \tag{I.64}$$

For small time increments the numerical solution is accurate and the computational time is reasonable.

Consider a one-axial tensile testing where a quadratic beam is under a mechanical

[44] See Simo and Hughes, 2006, Chap. 3

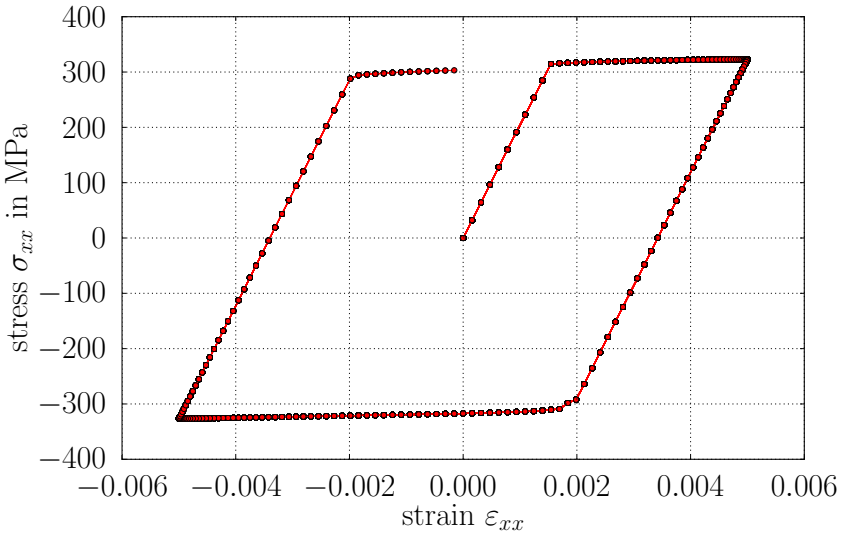

Figure I.1.: Hysteresis plot for a tensile test simulation of plasticity with kinematic hardening.

loading. The machine is controlled by displacement. Suppose that a cyclic loading is set. We give below the code for the kinematic hardening and the hysteresis plot can be seen in Fig. I.1. The computation is in three-dimensions as seen in Figs. I.2. HOOKE's law incorporates the transverse strain, although the loading is only axial. The plasticity model affects the material behavior only during the plasticity, which is decided by using two conditions: $f = 0$ and $f^{\bullet} = 0$. Both of them are computed with a boolean query in each time step. The second condition enables an elastic response as a consequence of unloading. The code is given below.

```
"""Computational reality 06, plasticity"""
__author__ = "B. Emek Abali"
__license__ = "GNU GPL Version 3.0 or later"
#This code underlies the GNU General Public License, http://
    ↪ www.gnu.org/licenses/gpl-3.0.en.html

from fenics import *
import numpy
set_log_level(ERROR)
xlength =100. #[mm]
ylength =10. #[mm]
zlength =10. #[mm]
mesh = BoxMesh(Point(0, 0, 0), Point(xlength, ylength, zlength),
    ↪ 10, 3, 3)
Coeff = FunctionSpace(mesh,'P',1)
Space = VectorFunctionSpace(mesh,'P',1)
Tensor = TensorFunctionSpace(mesh,'P',1)
```

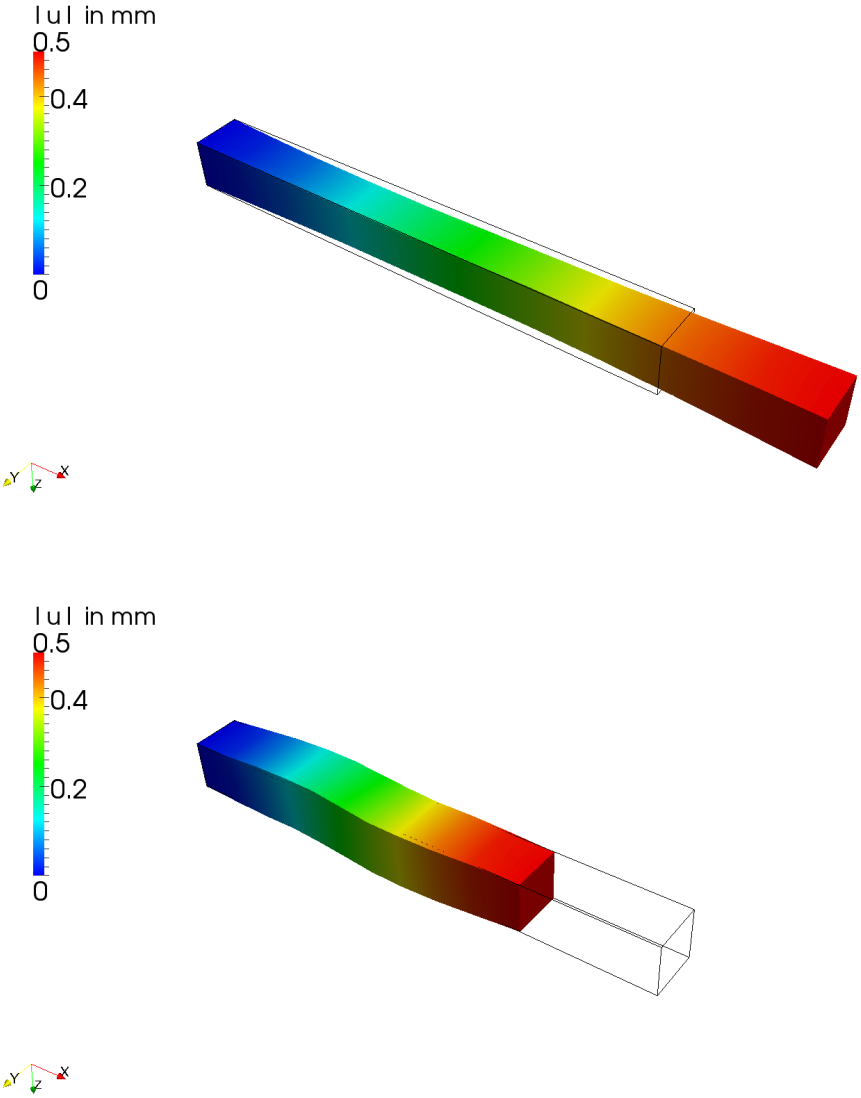

Figure I.2.: Deformation is presented by using a scale factor of 50. Top: After 1/4 cycle. Bottom: After 3/4 cycle. The initial geometry is outlined.

```
16 delu = TestFunction(Space)
17 du = TrialFunction(Space)
18 u = Function(Space)
19 u0 = Function(Space)
20 u00 = Function(Space)
21
22 cells = CellFunction('size_t', mesh)
23 facets = FacetFunction('size_t', mesh)
24 dA = Measure('ds', domain=mesh, subdomain_data=facets)
25 dV = Measure('dx', domain=mesh, subdomain_data=cells)
```

```
26
27 print 'initializing ,time'
28 t=0.0
29 t_end = 10.0
30 dt = 0.05
31
32 #Defining boundary conditions
33 left = CompiledSubDomain('near(x[0],0) && on_boundary')
34 right = CompiledSubDomain('near(x[0],l) && on_boundary',l=xlength)
35
36 boundaries = FacetFunction('uint',mesh)
37 boundaries.set_all(0)
38 # a cyclic displacement on the right end
39 displ = Expression(('0.5*sin(2.*pi*f*time)','0.0','0.0'),f=0.1,
    ↪ time=0)
40 bc1 = DirichletBC(Space,displ,right)
41 bc2 = DirichletBC(Space,(0.0,0.0,0.0),left)
42 bc = [bc1,bc2]
43
44 #Setting up the material parameters in tonne, seconds, Newton,
    ↪ milimeter
45 rho0 = 8.3E-9 #tonne/mm^3
46 nu, E = 0.3, 200000.0 # [-], [MPa]
47 h=0.01*E
48 lambada=E*nu/(1.0+nu)/(1.0-2.0*nu)
49 mu=E/(2.0+2.0*nu)
50 #Y=Function(Coeff)
51 sigmaY=Constant(300.0) # [MPa]
52 # index notation
53 i,j,k,l,m,n,o,p = indices(8)
54 delta= Identity(3)
55 eps= as_tensor(1.0/2.0*(u[i].dx(j)+u[j].dx(i)),(i,j))
56 eps0= as_tensor(1.0/2.0*(u0[i].dx(j)+u0[j].dx(i)),(i,j))
57 epsDot=as_tensor((eps[i,j]-eps0[i,j])/dt,(i,j))
58 gamma=Function(Coeff)
59
60 C = as_tensor(lambada*delta[i,j]*delta[k,l]\
61 +mu*delta[i,k]*delta[j,l]+mu*delta[i,l]*delta[j,k],(i,j,k,l))
62
63 sigma0 = Function(Tensor)
64 dev_sigma0 = as_tensor(sigma0[i,j]-1./3.*sigma0[k,k]*delta[i,j],(i
    ↪ ,j))
65 beta0=Function(Tensor)
66
67 sigmaDot = as_tensor( (C[i,j,m,n]-gamma*C[i,j,k,l]*(dev_sigma0[k,l
    ↪ ]\
68 -beta0[k,l])*(dev_sigma0[o,p]-beta0[o,p])*C[o,p,m,n]/(4./9.*sigmaY
```

```
    ↪ **2*h\
+(dev_sigma0[i,j]-beta0[i,j])*C[i,j,k,l]*(dev_sigma0[k,l]\
-beta0[k,l]) ) )*epsDot[m,n], (i,j) )

sigma = as_tensor(sigma0[i,j]+dt*sigmaDot[i,j],(i,j))
dev_sigma = as_tensor(sigma[i,j]-1./3.*sigma[k,k]*delta[i,j],(i,j)
    ↪ )

betaDot = as_tensor( gamma*(dev_sigma0[k,l]-beta0[k,l])*sigmaDot[k
    ↪ ,l]\
/(2.0/3.0*sigmaY**2)*(dev_sigma0[i,j]-beta0[i,j]),(i,j))

beta=as_tensor(beta0[i,j]+dt*betaDot[i,j],(i,j))

f= Constant((0.,0.,0.))

Form = (rho0*(u[i]-2.*u0[i]+u00[i])/(dt*dt)*delu[i] \
     + sigma[j,i]*delu[i].dx(j) \
     - rho0*f[i]*delu[i] )*dV
Gain = derivative(Form,u,du)

#Plotting stress vs. strain curves
import matplotlib as mpl
mpl.use('Agg')
import matplotlib.pyplot as pylab
pylab.rc('text', usetex=True )
pylab.rc('font', family='serif', serif='cm', size=30 )
pylab.rc('legend', fontsize=30)
pylab.rc(('xtick.major','ytick.major'), pad=15)

#pylab.ion()
fig = pylab.figure(1, figsize=(12,8))
fig.clf()
pylab.subplots_adjust(bottom=0.18)
pylab.subplots_adjust(left=0.16)
pylab.xlabel(r'strain $\varepsilon_{xx}$')
pylab.ylabel(r'stress $\sigma_{xx}$ in MPa')
pylab.grid(True)

stress_plot = []
strain_plot = []
temp_array= []
time= []
uinit = Expression(('0.0','0.0','0.0'))
u0.interpolate(uinit)
u00.assign(u0)
file_u = File ('/calcul/CR06/displacements.pvd')
```

```
113
114 while t <= t_end :
115     displ.time = t
116     print 'time: ', t
117     solve(Form==0, u, bc, J=Gain, \
118         solver_parameters={"newton_solver":{"linear_solver": "
                ↪ mumps", "relative_tolerance": 1e-3} }, \
119         form_compiler_parameters={"cpp_optimize": True, "
                ↪ representation": "quadrature", "quadrature_degree":
                ↪ 2}  )
120
121     sigma_ = project(sigma,Tensor, solver_type="mumps",\
122         form_compiler_parameters={"cpp_optimize": True, "
                ↪ representation": "quadrature", "quadrature_degree":
                ↪ 2}  )
123     strain_plot.append(u(xlength,ylength/2.,zlength/2.)[0]/xlength
            ↪ )
124     stress_plot.append(sigma_(xlength/2.,ylength/2.,zlength/2.)
            ↪ [0])
125     file_u << (u,t)
126     sigma0.assign(sigma_)
127     beta_ = project(beta,Tensor, solver_type="mumps",\
128         form_compiler_parameters={"cpp_optimize": True, "
                ↪ representation": "quadrature", "quadrature_degree":
                ↪ 2}  )
129     beta0.assign(beta_)
130     flow_ = project(1./2.*(dev_sigma0[i,j]-beta0[i,j])*(dev_sigma0
            ↪ [i,j]-beta0[i,j]) -1./3.*sigmaY**2, Coeff)
131     flow_bool = flow_.vector().array() >= 0.
132     direction_ = project((dev_sigma0[i,j]-beta0[i,j])*epsDot[i,j],
            ↪  Coeff, solver_type="mumps",\
133         form_compiler_parameters={"cpp_optimize": True, "
                ↪ representation": "quadrature", "quadrature_degree":
                ↪ 2}  )
134     direction_bool=1./2.*(numpy.sign(direction_.vector().array())
            ↪ +1.)
135     gamma.vector()[:] = numpy.array(flow_bool*direction_bool,dtype
            ↪ =int)
136
137     u00.assign(u0)
138     u0.assign(u)
139     t = t + dt
140
141     pylab.plot(strain_plot,stress_plot,color='red',marker='o',
            ↪ markersize=5)
142     #pylab.draw()
143
```

```
144     pylab.savefig('/calcul/CR06/CompReal06_plast_tensile.pdf')
```

To-do

We have implemented the kinematic hardening law such that the stress-strain hysteresis curve is enclosed in a cyclic loading.

- Try to implement the isotropic hardening and compare the hysteresis curves.
- What is the so-called BAUSCHINGER effect? Which hardening law is more realistic?
- Depends the plasticity modeling on the loading rate? How is the response of the material subject to a quicker loading?

References

Abali, B. E. (2017). *Computational Reality, Solving Nonlinear and Coupled Problems in Continuum Mechanics*. Vol. 55. Advanced Structured Materials. Springer. ISBN: 978-981-10-2443-6.

Bauschinger, J. (1886). „Über die Veränderung der Elastizitätsgrenze und der Festigkeit des Eisens und Stahls durch Strecken und Quetschen, durch Erwärmen und Abkühlen und durch oftmals wiederholte Beanspruchung.“ In: *Mitteilungen des mechanisch-technischen Laboratoriums der Königlich Technischen Hochschule München* 13, p. 1.

Melan, E. (1938). „Zur Plastizität des räumlichen Kontinuums.“ In: *Archive of Applied Mechanics* 9.2, pp. 116–126.

Müller, W. H. (2014). *An excursion to continuum mechanics*. Springer.

Odqvist, F. K. G. (1933). „Die Verfestigung von flußeisenähnlichen Körpern. ein Beitrag zur Plastizitätstheorie.“ In: *ZAMM-Journal of Applied Mathematics and Mechanics/Zeitschrift für Angewandte Mathematik und Mechanik* 13.5, pp. 360–363.

Prager, W. (1955). „The theory of plasticity: A survey of recent achievements.“ In: *Proceedings of the Institution of Mechanical Engineers* 169.1, pp. 41–57.

Prandtl, L. (1924). „Spannungsverteilung in plastischen Körpern.“ In: *Proceedings of the 1st international Congress on applied mechanics, Delft*, pp. 43–54.

Reuss, A. (1930). „Berücksichtigung der elastischen Formänderung in der Plastizitätstheorie.“ In: *ZAMM-Journal of Applied Mathematics and Mechanics/Zeitschrift für Angewandte Mathematik und Mechanik* 10.3, pp. 266–274.

Shield, R. T. and Ziegler, H. (1958). „On Prager's hardening rule.“ In: *Zeitschrift für angewandte Mathematik und Physik ZAMP* 9.3, pp. 260–276.

Simo, J. C. and Hughes, T. J. (2006). *Computational inelasticity*. Vol. 7. Springer Science & Business Media.

Kapitel II

Thermoviscoelasticity

The post-print version of the published manuscript:
Section 2.4 in Abali, B. E. (2017). Computational Reality: Solving Nonlinear and Coupled Problems in Continuum Mechanics (Advanced Structured Materials Vol. 55). Springer Nature Singapore.

The final publication is available at Springer via https://doi.org/10.1007/978-981-10-2444-3

By considering the principles of thermodynamics in a EULERian frame, we have derived all of the necessary constitutive equations for a viscous fluid in the last section. For fluids we use an open system. In this section we will derive the constitutive equations for a deformable solid in a LAGRANGEan (reference) frame expressed in Cartesian coordinates. A material system is utilized for solids. As the reference frame we choose the initial frame, where the positions (coordinates) of particles are known. We start first by transforming the balance equations from the current frame to the initial frame. The following identities in a Cartesian coordinate system:

$$\mathrm{d}v = J\,\mathrm{d}V \ , \quad n_j\,\mathrm{d}a = (\boldsymbol{F}^{-1})_{kj} J N_k\,\mathrm{d}A \ , \tag{II.1}$$

have been derived in Section[45] 1.4 for arbitrary coordinate systems. The balance equations of mass, momentum, and internal energy in the current frame for a material system:[46]

$$\begin{aligned}
\left(\int_{\mathcal{B}} \rho\,\mathrm{d}v\right)^{\cdot} &= 0 \ , \\
\left(\int_{\mathcal{B}} \rho v_i\,\mathrm{d}v\right)^{\cdot} &= \int_{\partial\mathcal{B}} \sigma_{ji} n_j\,\mathrm{d}a + \int_{\mathcal{B}} \rho f_i\,\mathrm{d}v \ , \\
\left(\int_{\mathcal{B}} \rho u\,\mathrm{d}v\right)^{\cdot} &= -\int_{\partial\mathcal{B}} q_j n_j\,\mathrm{d}a + \int_{\mathcal{B}} \left(\rho r + \sigma_{ji}\frac{\partial v_i}{\partial x_j}\right)\mathrm{d}v \ ,
\end{aligned} \tag{II.2}$$

[45] As appeared in Abali, 2017.

[46] A material system is a closed system possessing the same particles over time. In a material system no (mass) convection is allowed.

are transformed into the initial frame

$$\begin{aligned}
\left(\int_{\mathcal{B}_0} \rho J \,\mathrm{d}V\right)^{\cdot} &= 0 \ , \\
\left(\int_{\mathcal{B}_0} \rho v_i J \,\mathrm{d}V\right)^{\cdot} &= \int_{\partial\mathcal{B}_0} \sigma_{ji} (\boldsymbol{F}^{-1})_{kj} J N_k \,\mathrm{d}A + \int_{\mathcal{B}_0} \rho f_i J \,\mathrm{d}V \ , \\
\left(\int_{\mathcal{B}_0} \rho u J \,\mathrm{d}V\right)^{\cdot} &= -\int_{\partial\mathcal{B}_0} q_j (\boldsymbol{F}^{-1})_{kj} J N_k \,\mathrm{d}A + \int_{\mathcal{B}_0} \left(\rho r + \sigma_{ji} \frac{\partial v_i}{\partial x_j}\right) J \,\mathrm{d}V \ .
\end{aligned} \tag{II.3}$$

Initial frame is constant in time, $(\,\mathrm{d}V)^{\cdot} = 0$, thus, the balance of mass in the initial frame reads

$$\rho_0 = \rho J \ . \tag{II.4}$$

The mass density in the initial state, ρ_0, is of course constant in time, $\rho_0^{\cdot} = 0$. By introducing fluxes in the initial frame:

$$P_{ki} = \sigma_{ji} (\boldsymbol{F}^{-1})_{kj} J \ , \quad Q_k = q_j (\boldsymbol{F}^{-1})_{kj} J \ , \tag{II.5}$$

and inserting the mass balance into the momentum balance and internal energy balance, we acquire

$$\begin{aligned}
\int_{\mathcal{B}_0} \rho_0 v_i^{\cdot} \,\mathrm{d}V &= \int_{\partial\mathcal{B}_0} P_{ki} \,\mathrm{d}A + \int_{\mathcal{B}_0} \rho f_i J \,\mathrm{d}V \ , \\
\int_{\mathcal{B}_0} \rho_0 u^{\cdot} \,\mathrm{d}V &= -\int_{\partial\mathcal{B}_0} Q_k N_k \,\mathrm{d}A + \int_{\mathcal{B}_0} \left(\rho_0 r + J \sigma_{ji} \frac{\partial v_i}{\partial x_j}\right) \mathrm{d}V \ .
\end{aligned} \tag{II.6}$$

After utilizing Gauss's law on the boundary integrals, we write the balance equations in their local forms:

$$\rho_0 v_i^{\cdot} - \frac{\partial P_{ki}}{\partial X_k} - \rho_0 f_i = 0 \ , \quad \rho_0 u^{\cdot} + \frac{\partial Q_k}{\partial X_k} - \rho_0 r = J \sigma_{ji} \frac{\partial v_i}{\partial x_j} \ . \tag{II.7}$$

We have written the production terms on the right-hand side. Since the formulation is in the initial frame, the partial derivative with respect to x_i needs to be reformulated as a differentiation in X_i. The velocity gradient in the current frame reads

$$\frac{\partial v_i}{\partial x_j} = \frac{\partial v_i}{\partial X_k} \frac{\partial X_k}{\partial x_j} = \frac{\partial v_i}{\partial X_k} (\boldsymbol{F}^{-1})_{kj} \ , \tag{II.8}$$

hence, we obtain

$$J \sigma_{ji} \frac{\partial v_i}{\partial x_j} = J \sigma_{ji} \frac{\partial v_i}{\partial X_k} (\boldsymbol{F}^{-1})_{kj} = P_{ki} \frac{\partial v_i}{\partial X_k} \ . \tag{II.9}$$

The second Piola-Kirchhoff stress tensor:

$$S_{ij} = (\boldsymbol{F}^{-1})_{jk} P_{ik} = (\boldsymbol{F}^{-1})_{jk} \sigma_{lk} (\boldsymbol{F}^{-1})_{il} J \ , \tag{II.10}$$

is more beneficial by obtaining constitutive equations. From the latter the nominal stress becomes:

$$P_{ij} = F_{jl} S_{il} \ . \tag{II.11}$$

We further rewrite the production term. By starting with the right CAUCHY-GREEN deformation tensor, $C_{ij} = F_{ki} F_{kj}$, and its corresponding GREEN-LAGRANGE strain tensor, $2E_{ij} = (C_{ij} - \delta_{ij})$, we obtain

$$\begin{aligned} C_{ij} = F_{ki} F_{kj} = F_{kj} F_{ki} = C_{ji} \ , \\ 2\dot{E}_{ij} = \dot{C}_{ij} = 2\dot{F}_{k(i} F_{kj)} \ . \end{aligned} \tag{II.12}$$

In the initial frame we have the following identity:

$$\frac{\partial v_j}{\partial X_i} = \frac{\partial^2 x_j}{\partial X_i \partial t} = \frac{\partial^2 x_j}{\partial t \partial X_i} = \dot{F}_{ji} \ , \tag{II.13}$$

since $x_i = x_i(t, X_j)$. By using the aforementioned relations we acquire the following version of the production term:

$$P_{ij} \frac{\partial v_j}{\partial X_i} = F_{jl} S_{il} \frac{\partial v_j}{\partial X_i} = F_{jl} S_{il} \dot{F}_{ji} = F_{j(l} S_{il} \dot{F}_{ji)} = S_{il} \dot{E}_{il} \ , \tag{II.14}$$

for a symmetric stress tensor, $S_{ij} = S_{ji}$. In case of non-polar materials, the CAUCHY stress tensor is symmetric, leading to the symmetric second PIOLA-KIRCHHOFF stress tensor given in Eq. (II.10). For non-polar materials the balance of internal energy in the initial frame reads

$$\rho_0 \dot{u} + \frac{\partial Q_k}{\partial X_k} - \rho_0 r = S_{ij} \dot{E}_{ij} \ . \tag{II.15}$$

At equilibrium the balance of internal energy is

$$\rho_0 \dot{u} - \rho_0 T \dot{\eta} = {}^{\mathrm{e}}S_{ij} \dot{E}_{ij} \ , \tag{II.16}$$

since the internal energy is fully recoverable and the stress tensor is decomposed into an elastic (reversible) term, ${}^{\mathrm{e}}S_{ij}$, and into a dissipative (irreversible) term, ${}^{\mathrm{d}}S_{ij}$, such that

$$S_{ij} = {}^{\mathrm{e}}S_{ij} + {}^{\mathrm{d}}S_{ij} \ . \tag{II.17}$$

We need constitutive equations for the specific entropy, η, for the heat flux, Q_i, and for the elastic and dissipative stress tensors, ${}^{\mathrm{e}}S_{ij}$, ${}^{\mathrm{d}}S_{ij}$. By using the 1st law of thermodynamics we can rewrite the rate of internal energy as a differential form:

$$\mathrm{d}u = T \, \mathrm{d}\eta + {}^{\mathrm{e}}S_{ij} v \, \mathrm{d}E_{ij} \ , \tag{II.18}$$

where the specific volume, $v = 1/\rho_0$, is a known quantity. The latter differential form is often introduced as GIBBS's equation.[47]

[47] For an alternative derivation of GIBBS's equation we refer to Müller, 1985, Chap. 8.

In Eq. (II.18) the internal energy is given as a function of η and E_{ij}. Having a function of the strains is adequate since the strains are given by the primitive variables (displacement). However, we have just introduced a variable called entropy, η, we lack a definition for it. We simply want to exchange the dependency from entropy to the temperature, which is one of the primitive variables. We transform[48] the differential form in Eq. (II.18) by introducing a free energy:

$$\psi = u - T\eta \ , \tag{II.19}$$

into the following form:

$$\mathrm{d}\psi = \mathrm{d}u - \eta\,\mathrm{d}T - T\,\mathrm{d}\eta = -\eta\,\mathrm{d}T + {}^{\mathrm{e}}S_{ij}v\,\mathrm{d}E_{ij} \ . \tag{II.20}$$

This differential form implies an energy depending on the temperature and strain,

$$\psi = \psi(T, E_{ij}) \ , \tag{II.21}$$

such that

$$-\eta = \frac{\partial\psi}{\partial T} \ , \quad {}^{\mathrm{e}}S_{ij}v = \frac{\partial\psi}{\partial E_{ij}} \ . \tag{II.22}$$

The temperature and strain are called the primary or state variables. Since the energy depends on the primary variables, its derivatives depend on the same set of variables, too. So the derived, dual, or conjugate variables, η, ${}^{\mathrm{e}}S_{ij}$, depend on the primary variables

$$\begin{aligned} \mathrm{d}\eta &= A\,\mathrm{d}T + \bar{p}_{ij}\,\mathrm{d}E_{ij} \ , \\ \mathrm{d}\,{}^{\mathrm{e}}S_{ij} &= p_{ij}\,\mathrm{d}T + C_{ijkl}\,\mathrm{d}E_{kl} \ . \end{aligned} \tag{II.23}$$

We can readily apply the Maxwell symmetry condition (reciprocal relation):

$$\bar{p}_{ij} = \frac{\partial\eta}{\partial E_{ij}} = -\frac{\partial^2\psi}{\partial E_{ij}\partial T} = -\frac{\partial^2\psi}{\partial T\partial E_{ij}} = -\frac{\partial\,{}^{\mathrm{e}}S_{ij}v}{\partial T} = -v\frac{\partial\,{}^{\mathrm{e}}S_{ij}}{\partial T} = -vp_{ij} \ . \tag{II.24}$$

The specific volume is a given function in space for heterogeneous materials or a constant value for homogeneous materials. It is coupled to the temperature through constitutive equations, however, it is independent on T so we have taken it out in the differentiation with respect to the temperature. The dual variables read

$$\begin{aligned} \mathrm{d}\eta &= A\,\mathrm{d}T - p_{ij}v\,\mathrm{d}E_{ij} \ , \\ \mathrm{d}\,{}^{\mathrm{e}}S_{ij} &= p_{ij}\,\mathrm{d}T + C_{ijkl}\,\mathrm{d}E_{kl} \ . \end{aligned} \tag{II.25}$$

As in the previous section $A = c/T$, where the specific heat capacity, c, is measured by varying the temperature and recording the change of heat by fixed strains, $\mathrm{d}E_{ij} = 0$. In other words, all of the boundaries are clamped and the temperature is varied. The *stiffness tensor* C_{ijkl} is measured on a constant temperature, $\mathrm{d}T = 0$,

[48] Mathematicians call this transformation a Legendre transformation named after Adrien-Marie Legendre.

by varying the strains $\mathrm{d}E_{ij}$ and recording the stress changes $\mathrm{d}\,{}^{\mathrm{e}}S_{ij}$. Since C_{ijkl} consists of many coefficients we also need to establish various measurements. One of such measurements is the prominent tensile test. Throughout the experiment, the temperature is fixed such that the components of C_{ijkl} are valid for a specific temperature. One needs to redo the experiments in different temperatures for determining components as a function in T. The thermal pressure p_{ij} is the pressure occurring due to temperature variation by fixed strains, $\mathrm{d}E_{ij} = 0$. The body tries to expand or shrink and applies a pressure on the clamped boundaries holding the strains fixed.

The values for the thermal pressure are difficult to find in the literature. Therefore, we introduce the coefficients of thermal expansion, α_{ij}, which are measured by varying the temperature and measuring the strain change

$$\mathrm{d}E_{ij} = \alpha_{ij}\,\mathrm{d}T \ , \tag{II.26}$$

for a specific stress. Since such a measurement is realized by fixed stress, $\mathrm{d}\,{}^{\mathrm{e}}S_{ij} = 0$, we can observe from Eq. (II.25)$_2$

$$\begin{aligned} 0 = p_{ij}\,\mathrm{d}T + C_{ijkl}\,\mathrm{d}E_{kl} \ , \quad p_{ij}\,\mathrm{d}T = -C_{ijkl}\alpha_{kl}\,\mathrm{d}T \\ \Rightarrow p_{ij} = -C_{ijkl}\alpha_{kl} \ . \end{aligned} \tag{II.27}$$

Now, the dual variables become

$$\begin{aligned} \mathrm{d}\eta &= \frac{c}{T}\,\mathrm{d}T + C_{ijkl}\alpha_{kl}v\,\mathrm{d}E_{ij} \ , \\ \mathrm{d}\,{}^{\mathrm{e}}S_{ij} &= -C_{ijkl}\alpha_{kl}\,\mathrm{d}T + C_{ijkl}\,\mathrm{d}E_{kl} \ . \end{aligned} \tag{II.28}$$

For non-polar materials the stress tensor is symmetric, we assume that the elastic part is also symmetric, ${}^{\mathrm{e}}S_{ij} = {}^{\mathrm{e}}S_{ji}$. We restrict the formalism for linear materials such that the stiffness tensor, C_{ijkl}, the coefficients of thermal expansion, α_{ij}, and the specific heat capacity, c, are constants and we acquire the dual variables by integrating from the reference state, $T = T_{\mathrm{ref.}}$, $E_{ij} = 0$, to the current state

$$\begin{aligned} \eta &= c\ln\left(\frac{T}{T_{\mathrm{ref.}}}\right) + C_{ijkl}\alpha_{kl}vE_{ij} \ , \\ {}^{\mathrm{e}}S_{ij} &= -C_{ijkl}\alpha_{kl}(T - T_{\mathrm{ref.}}) + C_{ijkl}E_{kl} \ . \end{aligned} \tag{II.29}$$

Often, thermal strains are introduced

$${}^{\mathrm{th}}E_{kl} = \alpha_{kl}(T - T_{\mathrm{ref.}}) \ , \tag{II.30}$$

such that the elastic stress is written as

$${}^{\mathrm{e}}S_{ij} = C_{ijkl}\big(E_{kl} - {}^{\mathrm{th}}E_{kl}\big) \ . \tag{II.31}$$

Finally, we have determined the GIBBS equation:

$$\begin{aligned} \mathrm{d}u &= T\,\mathrm{d}\eta + {}^{\mathrm{e}}S_{ij} v\,\mathrm{d}E_{ij} = \\ &= c\,\mathrm{d}T + TC_{ijkl}\alpha_{kl} v\,\mathrm{d}E_{ij} + C_{ijkl}\big(E_{kl} - \alpha_{kl}(T - T_{\mathrm{ref.}})\big) v\,\mathrm{d}E_{ij} = \\ &= c\,\mathrm{d}T + vC_{ijkl}\alpha_{kl}T_{\mathrm{ref.}}\,\mathrm{d}E_{ij} + vC_{ijkl}E_{kl}\,\mathrm{d}E_{ij}\ , \end{aligned} \tag{II.32}$$

solely depending on the temperature and displacement (over the known relation between strain and displacement). For a linear thermoelastic isotropic body, the material parameters reduce to

$$C_{ijkl} = \lambda\delta_{ij}\delta_{kl} + \mu\delta_{ik}\delta_{jl} + \mu\delta_{il}\delta_{jk}\ , \quad \alpha_{ij} = \alpha\delta_{ij}\ , \tag{II.33}$$

thus, the internal energy rate reads

$$u^{\bullet} = cT^{\bullet} + v(3\lambda + 2\mu)\alpha T_{\mathrm{ref.}}\dot{E}_{ii} + v(\lambda\delta_{ij}E_{kk} + 2\mu E_{ij})\dot{E}_{ij}\ . \tag{II.34}$$

For deriving the heat flux, Q_i, and the dissipative stress, ${}^{\mathrm{d}}S_{ij}$, we start with Eq. (II.18) in the following form:

$$\rho_0 u^{\bullet} = \rho_0 T\eta^{\bullet} + \big(S_{ij} - {}^{\mathrm{d}}S_{ij}\big)\dot{E}_{ij}\ , \tag{II.35}$$

and insert it into Eq. (II.15) in order to acquire the balance of entropy in the reference frame:

$$\begin{aligned} \rho_0\eta^{\bullet} + \frac{\partial}{\partial X_i}\Big(\frac{Q_i}{T}\Big) - \rho_0\frac{r}{T} &= \frac{1}{T}\,{}^{\mathrm{d}}S_{ij}\dot{E}_{ij} + Q_i\frac{\partial}{\partial X_i}\Big(\frac{1}{T}\Big)\ , \\ \rho_0\eta^{\bullet} + \frac{\partial}{\partial X_i}\Big(\frac{Q_i}{T}\Big) - \rho_0\frac{r}{T} &= \frac{1}{T}\,{}^{\mathrm{d}}S_{ij}\dot{E}_{ij} - \frac{1}{T^2}Q_i\frac{\partial T}{\partial X_i}\ . \end{aligned} \tag{II.36}$$

The right-hand side is the production term and it has to be positive according to the 2nd law of thermodynamics:

$$\Sigma = \frac{1}{T}\,{}^{\mathrm{d}}S_{ij}\dot{E}_{ij} - \frac{1}{T^2}Q_i G_i \geq 0\ , \tag{II.37}$$

where again for simplicity we have used the following notation:

$$G_i = \frac{\partial T}{\partial X_i}\ . \tag{II.38}$$

The stress tensor is symmetric for non-polar materials; we have employed a symmetric reversible term, the dissipative term has to be symmetric, too. A symmetric tensor of rank two can be decomposed into a spherical (volumetric) term and a deviatoric term. Multiplication of a volumetric with a deviatoric term vanishes such that the entropy production reads

$$\Sigma = \frac{1}{3T}\,{}^{\mathrm{d}}S_{ii}\dot{E}_{jj} + \frac{1}{T}\,{}^{\mathrm{d}}S_{|ij|}\dot{E}_{|ij|} - \frac{1}{T^2}Q_i G_i \geq 0\ . \tag{II.39}$$

By introducing thermodynamical fluxes:

$$\mathcal{F}^{\alpha} = \Big\{ Q_i \ , \quad {}^{\mathrm{d}}S_{ii} \ , \quad {}^{\mathrm{d}}S_{|ij|} \Big\} \ , \tag{II.40}$$

and thermodynamical forces:

$$\mathcal{K}^{\alpha} = \Big\{ -\frac{G_i}{T^2} \ , \quad \frac{1}{3T} E^{\bullet}_{jj} \ , \quad \frac{1}{T} E^{\bullet}_{|ij|} \Big\} \ , \tag{II.41}$$

we can rewrite the 2$^{\mathrm{nd}}$ law:

$$\Sigma = \mathcal{F}^{\alpha} \cdot \mathcal{K}^{\alpha} \ , \quad \alpha = 1, 2, 3 \ . \tag{II.42}$$

All of thermodynamical fluxes are of different type (tensors of different ranks). According to the Curie principle thermodynamical fluxes depend only on their corresponding thermodynamical forces of the same rank such that we obtain

$$\mathcal{F}^1 = \mathcal{F}^1(\mathcal{K}^1) \ , \quad \mathcal{F}^2 = \mathcal{F}^2(\mathcal{K}^2) \ , \quad \mathcal{F}^3 = \mathcal{F}^3(\mathcal{K}^3) \ . \tag{II.43}$$

We can readily propose linear constitutive equations:

$${}^{\mathrm{d}}S_{ii} = \mu_1 E^{\bullet}_{ii} \ , \quad {}^{\mathrm{d}}S_{|ij|} = \mu_2 E^{\bullet}_{|ij|} \ , \quad Q_i = -\kappa G_i \ , \tag{II.44}$$

where μ_1, μ_2, and κ are all positive constants such that $\Sigma \geq 0$. The viscous part of the stress reads

$$\begin{aligned} {}^{\mathrm{d}}S_{ij} = \frac{1}{3} {}^{\mathrm{d}}S_{kk}\delta_{ij} + {}^{\mathrm{d}}S_{|ij|} = \frac{\mu_1}{3} E^{\bullet}_{kk}\delta_{ij} + \mu_2 \Big(E^{\bullet}_{ij} - \frac{1}{3} E^{\bullet}_{kk}\delta_{ij} \Big) = \\ = \frac{\mu_1 - \mu_2}{3} E^{\bullet}_{kk}\delta_{ij} + \mu_2 E^{\bullet}_{ij} \ . \end{aligned} \tag{II.45}$$

Then by using the obtained elastic stress we acquire a linear thermoviscoelastic material model:

$$S_{ij} = C_{ijkl}\big(E_{kl} - \alpha_{ij}(T - T_{\mathrm{ref.}})\big) + \frac{\mu_1 - \mu_2}{3} E^{\bullet}_{kk}\delta_{ij} + \mu_2 E^{\bullet}_{ij} \ . \tag{II.46}$$

For a constant κ the constitutive equation:

$$Q_i = -\kappa \frac{\partial T}{\partial X_i} \ , \tag{II.47}$$

is called Fourier's law in the Lagrangean frame.

In order to compute the displacement and temperature in a linear thermoviscoelastic

body, we employ the balance of momentum and the balance of entropy:

$$\begin{aligned} \rho_0 u_i^{\bullet\bullet} - \frac{\partial P_{ji}}{\partial X_j} - \rho_0 f_i = 0 \ , \\ \rho_0 \eta^{\bullet} + \frac{\partial}{\partial X_i}\Big(\frac{Q_i}{T}\Big) - \rho_0 \frac{r}{T} = \frac{1}{T}\,{}^{\mathrm{d}}S_{ij} E_{ij}^{\bullet} - \frac{1}{T^2} Q_i \frac{\partial T}{\partial X_i} \ . \end{aligned} \tag{II.48}$$

The primitive variables are displacement, u_i, and temperature, T. Hence we multiply the balance of linear momentum with δu_i and integrate over the continuum body for generating a form in the unit of energy. By multiplying the balance of entropy with δT and integrating over the body, we obtain a form in the unit of power. After discretizing in time, we can multiply the equation with Δt in order to acquire both forms in the unit of energy. Having forms in the same unit, we can sum them up. Furthermore, we apply Gauss's law in order to weaken the forms and acquire

$$\begin{aligned} \text{Form} = \int_{\mathcal{B}_0} \Bigg(\rho_0 \frac{u_i - 2u_i^0 + u_i^{00}}{\Delta t \Delta t} \delta u_i + P_{ji} \delta u_{i,j} - \rho_0 f_i \delta u_i + \\ + \frac{\rho_0}{T}(\eta - \eta^0)\delta T - \Delta t \frac{1}{T} Q_i \delta T_{,i} - \Delta t \frac{\rho_0 r}{T} \delta T - \frac{1}{T}\,{}^{\mathrm{d}}S_{ij}(E_{ij} - E_{ij}^0)\delta T + \\ + \Delta t \frac{1}{T^2} Q_i T_{,i} \delta T \Bigg) \,\mathrm{d}V + \int_{\partial \mathcal{B}_0} \Big(\Delta t \frac{1}{T} \hat{Q} \delta T - \hat{t}_i \delta u_i \Big) \,\mathrm{d}A \ , \end{aligned} \tag{II.49}$$

where the comma notation has been used for a partial space derivative in X_i. We summarize the necessary relations:

$$\begin{aligned} F_{ij} = \frac{\partial u_i}{\partial X_j} + \delta_{ij} \ , \quad C_{ij} = F_{ki} F_{kj} \ , \quad E_{ij} = \frac{1}{2}(C_{ij} - \delta_{ij}) \ , \\ {}^{\mathrm{e}}S_{ij} = -C_{ijkl}\alpha_{kl}(T - T_{\mathrm{ref.}}) + C_{ijkl} E_{kl} \ , \quad \eta = c \ln\Big(\frac{T}{T_{\mathrm{ref.}}}\Big) + C_{ijkl}\alpha_{kl} v E_{ij} \ , \\ {}^{\mathrm{d}}S_{ij} = \frac{\mu_1 - \mu_2}{3} E_{kk}^{\bullet} \delta_{ij} + \mu_2 E_{ij}^{\bullet} \ , \quad Q_i = -\kappa \frac{\partial T}{\partial X_i} \ , \\ S_{ij} = {}^{\mathrm{e}}S_{ij} + {}^{\mathrm{d}}S_{ij} \ , \quad P_{ij} = F_{jl} S_{il} \ . \end{aligned} \tag{II.50}$$

For an isotropic body the stiffness tensor and coefficients of thermal expansion are

$$C_{ijkl} = \lambda \delta_{ij}\delta_{kl} + \mu \delta_{ik}\delta_{jl} + \mu \delta_{il}\delta_{jk} \ , \quad \alpha_{ij} = \alpha \delta_{ij} \ . \tag{II.51}$$

Therefore, in case of an isotropic body we need seven material parameters, viz., λ, μ, α, μ_1, μ_2, κ, and c.

In a tensile testing we normally assume that the process is isothermal. By computing the reality where heat is produced due to the entropy production, we can validate this engineering assumption. The geometry is a beam along X_1 and we use a Robin

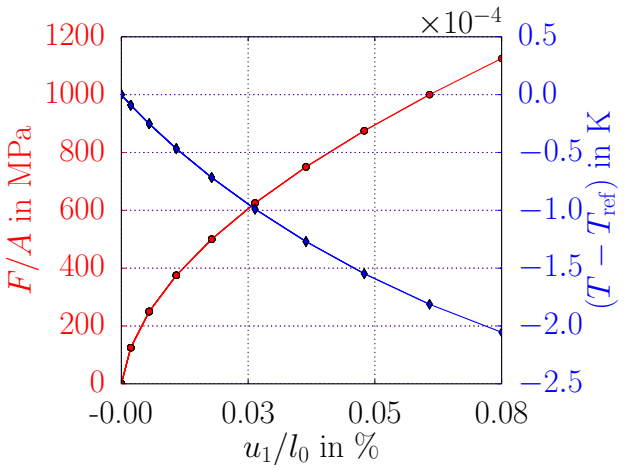

Figure II.1.: Tensile testing and temperature change due to the deformation.

boundary condition for the heat flux over all boundaries:

$$\hat{Q} = h(T - T_{\text{amb}}) \ . \tag{II.52}$$

On the left side we hold the beam fixed and on the right side we pull with the force given by the traction vector $\hat{t}_i = (800t, 0, 0)\,\text{MPa}$ linearly in time, t. The traction (force per area) is the controlled parameter, i.e., the machine is steered by the force. The tip displacement is measured, it is an observed quantity. Conveniently we plot stress vs. strain, where the stress (on the right tip) is the (axial) traction and the (normal axial) strain, E_{11}, is the displacement divided by the initial length. The traction vector, $\hat{t} = N_j P_{ji}$, is given by the nominal or engineering stress, P_{ji}. The strain, E_{ij}, is called the engineering strain; we have introduced it as the Green-Lagrange strain measure.

We apply a mechanical load and measure the temperature in the middle of the beam as well as the stress and strain on the tip. In Fig. II.1 the temperature change can be seen, it is clearly negligible. This is good news, because we measure the elasticity components, λ, ν for isotropic materials by using a tensile testing and assume that the temperature remains constant. The code for the computation is given below.

```
"""Computational Reality 13, thermoviscoelasticity"""
__author__ = "B. Emek Abali"
__license__  = "GNU GPL Version 3.0 or later"
#This code underlies the GNU General Public License, http://
    ↪ www.gnu.org/licenses/gpl-3.0.en.html

from fenics import *
import numpy
set_log_level(ERROR)
```

```
#units: mm, 1000 kg=ton, s, MPa, mJ, K
delta = Identity(3)
f = Constant((0.0, 0.0, -9810.))
r = 0.
Tref = 293.15 #in K
Tamb=Tref

# Material data of P265GH (St 45.8) from VDI Waermeatlas, at 293.15 K
rho0 = 7850.0E-9 #in kg / mm^3
kappa = 57.0 #in mJ / (s mm K)
capacity = 430.0E6 #in mJ / (ton K)
alpha = 12.2E-6 #in 1/K at 373.15 K
EModul = 211.E+3 #in MPa
nu = 0.28
h = 10.E-3 #in mJ / (s m^2 K)
mu1 = 1.E+6 #in MPa / s
mu2 = 3.E+6 #in MPa / s

tMax = 5.0
Dt = 0.5
t = 0.0

xMin, xMax, xElements = 0.0, 100.0, 10
yMin, yMax, yElements = -10., +10., 10
zMin, zMax, zElements = +10., -10., 10
mesh = BoxMesh(Point(xMin,yMin,zMin), Point(xMax,yMax,zMax), xElements,yElements,zElements)
N = FacetNormal(mesh)
length = abs(xMax-xMin)

T_Space = FunctionSpace(mesh, 'P', 1)
u_Space = VectorFunctionSpace(mesh, 'P', 1)
Space = MixedFunctionSpace([T_Space, u_Space])

cells = CellFunction('size_t', mesh)
facets = FacetFunction('size_t', mesh)
dA = Measure('ds', domain=mesh, subdomain_data=facets)
dV = Measure('dx', domain=mesh, subdomain_data=cells)

left = CompiledSubDomain('near(x[0],l) && on_boundary',l=xMin)
right = CompiledSubDomain('near(x[0],l) && on_boundary',l=xMax)
back = CompiledSubDomain('near(x[1],l) && on_boundary',l=yMin)
front = CompiledSubDomain('near(x[1],l) && on_boundary',l=yMax)
bottom = CompiledSubDomain('near(x[2],l) && on_boundary',l=zMin)
top = CompiledSubDomain('near(x[2],l) && on_boundary',l=zMax)

```

```
facets.set_all(0)
right.mark(facets, 1)
tHat = Expression(('A*t','0.','0.'), A=250., t=0.)
bc = [DirichletBC(Space.sub(1), Constant((0.0, 0.0, 0.0)), left),\
DirichletBC(Space.sub(1).sub(1), Constant(0.0), right),\
DirichletBC(Space.sub(1).sub(2), Constant(0.0), right)]

dunkn = TrialFunction(Space)
test = TestFunction(Space)
delT, delu = split(test)

unkn = Function(Space)
unkn0 = Function(Space)
unkn00 = Function(Space)

unkn_init = Expression(('T_ini','0','0','0'),T_ini=Tref)
unkn = interpolate(unkn_init,Space)
unkn0.assign(unkn)
unkn00.assign(unkn0)

T, u = split(unkn)
T0, u0 = split(unkn0)
T00, u00 = split(unkn0)

i, j, k, l = indices(4)
delta = Identity(3)
F = as_tensor(u[i].dx(j)+delta[i,j], (i,j))
F0 = as_tensor(u0[i].dx(j)+delta[i,j], (i,j))
C = as_tensor(F[k,i]*F[k,j], (i,j))
C0 = as_tensor(F0[k,i]*F0[k,j], (i,j))
E = as_tensor(1./2.*(C[i,j]-delta[i,j]), (i,j))
E0 = as_tensor(1./2.*(C0[i,j]-delta[i,j]), (i,j))
lambada = EModul * nu / (1. + nu) / (1. - 2. * nu)
mu = 0.5 * EModul / (1. + nu)
C_ = as_tensor(lambada*delta[i,j]*delta[k,l]+mu*delta[i,k]*delta[j
    ↪ ,l]+mu*delta[i,l]*delta[j,k], (i,j,k,l))
alp = as_tensor(alpha*delta[i,j], (i,j))
eStress = as_tensor(-C_[i,j,k,l]*alp[k,l]*(T-Tref) + C_[i,j,k,l]*E
    ↪ [k,l], (i,j))
dStress = as_tensor((mu1-mu2)/3.*(E-E0)[k,k]/Dt*delta[i,j] + mu2*(
    ↪ E-E0)[i,j]/Dt, (i,j))
S = as_tensor(eStress[i,j]+dStress[i,j], (i,j))
P = as_tensor(F[j,l]*S[i,l], (i,j))
eta = as_tensor( capacity*ln(T/Tref) + C_[i,j,k,l]*alp[k,l]*1./
    ↪ rho0*E[i,j] , ())
eta0 = as_tensor( capacity*ln(T0/Tref) + C_[i,j,k,l]*alp[k,l]*1./
    ↪ rho0*E0[i,j] , ())
```

```
96  Q = as_tensor(-kappa*T.dx(i), (i,))
97
98  Form = (rho0*(u-2.*u0+u00)[i]/Dt/Dt*delu[i] + P[j,i]*delu[i].dx(j)
        ↪  - rho0*f[i]*delu[i]  + rho0/T*(eta-eta0)*delT - Dt/T*Q[i]*
        ↪ delT.dx(i) - Dt*rho0*r/T*delT - 1./T*dStress[i,j]*(E-E0)[i,j
        ↪ ]*delT + Dt/T**2*Q[i]*T.dx(i)*delT )*dV + Dt/T*h*(T-Tamb)*
        ↪ delT*(dA(0)+dA(1)) - tHat[i]*delu[i]*dA(1)
99
100 Gain = derivative(Form, unkn, dunkn)
101
102 import matplotlib as mpl
103 mpl.use('Agg')
104 import matplotlib.pyplot as pylab
105 pylab.rc('text', usetex=True )
106 pylab.rc('font', family='serif', serif='cm', size=30 )
107 pylab.rc('legend', fontsize=30)
108 pylab.rc(('xtick.major','ytick.major'), pad=15)
109 pylab.subplots_adjust(top=0.90)
110 pylab.subplots_adjust(bottom=0.17)
111 pylab.subplots_adjust(left=0.20)
112 pylab.subplots_adjust(right=0.8)
113
114 fig = pylab.figure(1, figsize=(14,10))
115 ax1 = fig.add_subplot(111)
116 ax1.grid(True, axis='x')
117 ax1.set_xlabel('$u_1/l_0$ in $\%$')
118 ax1.set_ylabel('$F/A$ in MPa', color='r')
119 ax1.tick_params(axis='y', colors='r')
120 ax1.grid(True, axis='y', color='r')
121 ax2 = ax1.twinx()
122 ax2.set_ylabel('$(T-T_\mathrm{ref})$ in K', color='b')
123 ax2.tick_params(axis='y', colors='b')
124 ax2.grid(True, axis='y', color='b')
125 ax2.ticklabel_format(style='sci', axis='y', scilimits=(-2,2))
126
127 pwd='/calcul/CR13/'
128 file_u = File(pwd+'displ.pvd')
129 file_T = File(pwd+'temp.pvd')
130 strain,stress,temp =[],[],[]
131
132 while t < tMax:
133     print 'time: ',t
134     tHat.t = t
135     solve(Form==0, unkn, bc, J=Gain, \
136         solver_parameters={"newton_solver":{"linear_solver": "
            ↪ mumps", "relative_tolerance": 1e-5} }, \
137         form_compiler_parameters={"cpp_optimize": True, "
```

```
            ↪ representation": "quadrature", "quadrature_degree":
            ↪ 2}  )
138
139     file_T << (unkn.split()[0], t)
140     file_u << (unkn.split()[1], t)
141
142     strain.append(unkn.split()[1](xMax,0.,0.)[0]/length*100.)
143     stress.append(tHat(xMax,0.,0.)[0])
144     temp.append(unkn.split()[0](xMax/2.,0.,0.)-Tref)
145     ax1.plot(strain,stress, 'o-', color='r')
146     ticks = numpy.linspace(numpy.array(strain).min(), numpy.array(
            ↪ strain).max(), 4)
147     ax1.set_xticks(ticks)
148     ax1.set_xticklabels(['%1.2f' % i_ticks for i_ticks in ticks])
149     ax2.plot(strain,temp, 'd-', color='b')
150     fig.savefig(pwd+'CompReal13_tensiletest.pdf')
151     unkn00.assign(unkn0)
152     unkn0.assign(unkn)
153     t += Dt
```

To-do

We have employed the 1st and 2nd laws of thermodynamics, obtained constitutive (material) equations, and computed a coupled thermoviscoelastic problem. In a tensile testing the temperature change is negligible.

- Which term is responsible for the temperature change?
- Implement the code for a thermoelastic problem by setting $\mu_1 = \mu_2 = 0$, thus, ${}^{\mathrm{d}}S_{ij} = 0$. Solve a laser welding application as in Section[45] 2.1 and determine the deformations.
- Try to implement a bimetal and apply a thermal loading. Guess and inspect the occurring deformation.

References

Abali, B. E. (2017). *Computational Reality, Solving Nonlinear and Coupled Problems in Continuum Mechanics*. Vol. 55. Advanced Structured Materials. Springer. ISBN: 978-981-10-2443-6.

Müller, I. (1985). *Thermodynamics*. Pitman Publishing, London.

Kapitel III

Polarized materials

The post-print version of the published manuscript:
Section 3.2 in Abali, B. E. (2017). Computational Reality: Solving Nonlinear and Coupled Problems in Continuum Mechanics (Advanced Structured Materials Vol. 55). Springer Nature Singapore.

The final publication is available at Springer via https://doi.org/10.1007/978-981-10-2444-3

As a material specific property, the continuum body can be electrically or magnetically *polarized* subject to electromagnetic fields. The electric or magnetic polarization indicates a change in the electric charge distribution in the body. Suppose that the electric charge is homogeneously distributed. Under the influence of electromagnetic fields, charged particles deviate from their homogeneous distribution and the continuum body becomes polarized. Before we discuss this phenomenon deeply, we reinvent the Maxwell equations and then bring in the ideas of polarization.

We start with a balance equation on a material surface,[49] $\mathcal{S}$, known as Faraday's law:[50]

$$\left(\int_{\mathcal{S}} B_i \, \mathrm{d}a_i \right)^{\cdot} = - \int_{\partial \mathcal{S}} \mathcal{E}_i \, \mathrm{d}\ell_i \ , \tag{III.1}$$

where the magnetic flux area density, B_i, in a material surface, $\mathcal{S}$, is balanced with the electromotive intensity, $\mathcal{E}_i$, acting on the boundary of the surface, $\partial\mathcal{S}$. We recall that $\mathcal{B}_i = B_i$. Hence, Faraday's law is defined on a material surface co-moving with the continuum body. This equation has to hold for any surface, for example in case

[49] A material surface is a material system without convection terms where the domain is a surface instead of a volume leading to an area density instead of a volume density.

[50] It is named after Michael Faraday.

of a closed surface without boundaries, $\partial\bar{\mathcal{S}} = \{\}$, it still holds

$$\left(\oint_{\bar{\mathcal{S}}} B_i \, \mathrm{d}a_i \right)^{\bullet} = 0 \ . \tag{III.2}$$

This closed surface can be visualized like a closed hull over a body, $\bar{\mathcal{S}} = \partial\mathcal{B}$, such that $\partial\partial\mathcal{B} = \{\}$. By integrating in time we obtain an integration constant to be determined by the known initial condition. We may set the initial magnetic flux as zero. By starting with zero magnetic flux area density, $B_i(t = 0, x_j) = 0$, the integration constant vanishes

$$\int_{\partial\mathcal{B}} B_i \, \mathrm{d}a_i = 0 \ . \tag{III.3}$$

Since the surface is closed we can apply Gauss's law and obtain

$$\frac{\partial B_i}{\partial x_i} = 0 \ . \tag{III.4}$$

The latter equation is one of Maxwell's equations and it holds universally.[51] Now we want to obtain a local form from Eq. (III.1). First we use product rule and Stokes's law on the line integral

$$\int_{\mathcal{S}} B_i^{\bullet} \, \mathrm{d}a_i + \int_{\mathcal{S}} B_i (\, \mathrm{d}a_i)^{\bullet} = - \int_{\mathcal{S}} \mathrm{curl}(\boldsymbol{\mathcal{E}})_i \, \mathrm{d}a_i \ . \tag{III.5}$$

Since the domain is on a material surface, x_i denotes the current position of massive particles such that $x_i^{\bullet} = v_i$ of matter. Thus, we can use the identities in Eqs.[52] (1.120), (1.121) as follows

$$(\, \mathrm{d}v)^{\bullet} = (J \, \mathrm{d}V)^{\bullet} = J^{\bullet} \, \mathrm{d}V = \frac{J^{\bullet}}{J} \, \mathrm{d}v \ , \quad (\, \mathrm{d}v)^{\bullet} = \frac{\partial v_i}{\partial x_i} \, \mathrm{d}v \Rightarrow J^{\bullet} = J \frac{\partial v_i}{\partial x_i} \ , \tag{III.6}$$

and

$$(\, \mathrm{d}a_i)^{\bullet} = \left(J (\boldsymbol{F}^{-1})_{ji} \, \mathrm{d}A_j \right)^{\bullet} = \left(J \frac{\partial v_k}{\partial x_k} (\boldsymbol{F}^{-1})_{ji} + J (\boldsymbol{F}^{-1})^{\bullet}_{ji} \right) \mathrm{d}A_j \ . \tag{III.7}$$

Moreover, we know $F_{ij} (\boldsymbol{F}^{-1})_{jk} = \delta_{ik}$ such that the following identity:

$$\begin{aligned} \left(F_{ij} (\boldsymbol{F}^{-1})_{jk} \right)^{\bullet} &= 0 \ , \\ F_{ij} (\boldsymbol{F}^{-1})^{\bullet}_{jk} &= - F^{\bullet}_{ij} (\boldsymbol{F}^{-1})_{jk} \ , \\ (\boldsymbol{F}^{-1})^{\bullet}_{jk} &= - F^{\bullet}_{il} (\boldsymbol{F}^{-1})_{lk} (\boldsymbol{F}^{-1})_{ji} \ , \end{aligned} \tag{III.8}$$

[51] A relation holds universally, if it is free of any dependence on the underlying material. In other words, a universal relation holds for all materials and even in the case of no material—vacuum.

[52] As appeared in Abali, 2017.

can be used in order to acquire

$$\begin{aligned}(\,\mathrm{d}a_i)^{\bullet} &= J\frac{\partial v_k}{\partial x_k}(\boldsymbol{F}^{-1})_{ji}\,\mathrm{d}A_j - JF^{\bullet}_{nl}(\boldsymbol{F}^{-1})_{li}(\boldsymbol{F}^{-1})_{jn}\,\mathrm{d}A_j = \\ &= \frac{\partial v_k}{\partial x_k}\,\mathrm{d}a_i - F^{\bullet}_{nl}(\boldsymbol{F}^{-1})_{li}\,\mathrm{d}a_n = \left(\frac{\partial v_k}{\partial x_k}\delta_{ji} - \frac{\partial v_j}{\partial x_i}\right)\mathrm{d}a_j\ ,\end{aligned} \tag{III.9}$$

since

$$F^{\bullet}_{nl}(\boldsymbol{F}^{-1})_{li} = \left(\frac{\partial x_n}{\partial X_l}\right)^{\bullet}\frac{\partial X_l}{\partial x_i} = \frac{\partial v_n}{\partial X_l}\frac{\partial X_l}{\partial x_i} = \frac{\partial v_n}{\partial x_i}\ . \tag{III.10}$$

Therefore, we obtain the following local form for FARADAY's law:

$$\begin{aligned}B^{\bullet}_j + B_i\left(\frac{\partial v_k}{\partial x_k}\delta_{ji} - \frac{\partial v_j}{\partial x_i}\right) &= -\operatorname{curl}(\boldsymbol{\mathfrak{E}})_j\ , \\ \frac{\partial B_j}{\partial t} + \frac{\partial B_j}{\partial x_k}v_k + B_j\frac{\partial v_k}{\partial x_k} - B_i\frac{\partial v_j}{\partial x_i} + \operatorname{curl}(\boldsymbol{\mathfrak{E}})_j &= 0\ , \\ \frac{\partial B_j}{\partial t} + \frac{\partial B_j v_k}{\partial x_k} - B_i\frac{\partial v_j}{\partial x_i} + \operatorname{curl}(\boldsymbol{\mathfrak{E}})_j &= 0\ .\end{aligned} \tag{III.11}$$

Since $\epsilon_{ijk}\epsilon_{klm} = \delta_{il}\delta_{jm} - \delta_{im}\delta_{jl}$, we can insert the following relation:

$$\begin{aligned}\operatorname{curl}(\boldsymbol{v}\times\boldsymbol{B})_i = \epsilon_{ijk}\frac{\partial(\boldsymbol{v}\times\boldsymbol{B})_k}{\partial x_j} = \epsilon_{ijk}\epsilon_{klm}\frac{\partial v_l B_m}{\partial x_j} = \frac{\partial v_i B_j}{\partial x_j} - \frac{\partial v_j B_i}{\partial x_j}\ , \\ \frac{\partial v_j B_i}{\partial x_j} = \frac{\partial v_i B_j}{\partial x_j} - \operatorname{curl}(\boldsymbol{v}\times\boldsymbol{B})_i\ ,\end{aligned} \tag{III.12}$$

into the latter to obtain

$$\begin{aligned}\frac{\partial B_j}{\partial t} + \frac{\partial v_j B_i}{\partial x_i} - \operatorname{curl}(\boldsymbol{v}\times\boldsymbol{B})_j - B_i\frac{\partial v_j}{\partial x_i} + \operatorname{curl}(\boldsymbol{\mathfrak{E}})_j &= 0\ , \\ \frac{\partial B_j}{\partial t} + v_j\frac{\partial B_i}{\partial x_i} + \operatorname{curl}\left(\boldsymbol{\mathfrak{E}} - \boldsymbol{v}\times\boldsymbol{B}\right)_j &= 0\ .\end{aligned} \tag{III.13}$$

By using Eq.[52] (3.11) and inserting one of MAXWELL's equations in Eq. (III.4) we express the latter in the laboratory frame

$$\begin{aligned}\frac{\partial B_j}{\partial t} + \operatorname{curl}\left(\boldsymbol{E}\right)_j &= 0\ , \\ \frac{\partial B_i}{\partial t} + \epsilon_{ijk}\frac{\partial E_k}{\partial x_j} &= 0\ .\end{aligned} \tag{III.14}$$

This equation is another one of MAXWELL's equations holding universally. We have declared E_i and B_i as the primitive variables. Two of MAXWELL's equations, namely

Eqs. (III.4) and (III.14), can be solved by using the following trial functions:

$$E_i = -\frac{\partial \phi}{\partial x_i} - \frac{\partial A_i}{\partial t} \ , \quad B_i = \epsilon_{ijk} \frac{\partial A_k}{\partial x_j} \ , \tag{III.15}$$

where we introduce the so-called *electric* and *magnetic potentials*, ϕ and A_i, as functions in space and time:

$$\phi = \phi(x_i, t) \ , \quad A_i = A_i(x_j, t) \ . \tag{III.16}$$

The electric potentials are the new primitive variables instead of E_i and B_i. It is important to recall that we introduce the electric and magnetic potentials as one possible solution of Eqs. (III.4) and (III.14). We just propose these *ansatz* functions[53] and insert them into Eqs. (III.4) and (III.14) in order to ensure that they satisfy the aforementioned MAXWELL's equations, see Appendix[52] A.6 on p. 305.

There is one drawback in the proposed solution of Eqs. (III.4) and (III.14). Instead of E_i and B_i, i.e., six components in 3D space, we search now for ϕ, A_i, i.e., only fours components in 3D space. Hence we loose information given by two scalar functions. Concretely, we lack information of $\partial\phi/\partial t$ and $\partial A_i/\partial x_i$, which is called the *gauge freedom*.[54] We can choose $\partial\phi/\partial t$ and $\partial A_i/\partial x_i$ arbitrarily and Eqs. (III.15) still satisfy Eqs. (III.4) and (III.14). We have already seen one of the consequences of this free choice of $\partial\phi/\partial t$ in the last section. The electric potential has been set up instantaneously and remained the same. We need to deliver this missing information for an accurate consistent formulation. The most common choice is GAUSS's gauge:[55]

$$\frac{\partial \phi}{\partial t} = 0 \ , \quad \frac{\partial A_i}{\partial x_i} = 0 \ . \tag{III.17}$$

Since the choice is free, the latter is definitely admissible and the simplest choice at all. Another choice is called LORENZ's gauge:[56]

$$\frac{\partial \phi}{\partial t} = -c^2 \frac{\partial A_i}{\partial x_i} \ , \tag{III.18}$$

which will lead to some useful simplifications in the formulation and will be used herein. For the moment it is hard to see, how this choice shall simplify the formulation.

We need governing equations for solving electric potentials, ϕ, A_i, in space and time.

[53] The German word *ansatz* has the equal meaning of a trial function. We simply find out by trial the functions satisfying differential equations.

[54] For the motivation of the gauge freedom see Appendix[52] A.6 on p. 305.

[55] This gauge is named after Carl Friedrich Gauß.

[56] The gauge is named for Ludvig Valentin Lorenz.

These equations follow from the balance of electric charge:

$$\begin{gathered}\frac{\partial \rho z}{\partial t}+\frac{\partial J_i}{\partial x_i}=0\ , \quad J_i=\jmath_i+\rho z v_i\ , \\ z\Big(\frac{\partial \rho}{\partial t}+\rho\frac{\partial v_i}{\partial x_i}+v_i\frac{\partial \rho}{\partial x_i}\Big)+\rho\frac{\partial z}{\partial t}+\rho v_i\frac{\partial z}{\partial x_i}+\frac{\partial \jmath_i}{\partial x_i}=0\ , \\ z\Big(\rho^{\bullet}+\rho\frac{\partial v_i}{\partial x_i}\Big)+\rho z^{\bullet}+\frac{\partial \jmath_i}{\partial x_i}=0\ .\end{gathered} \tag{III.19}$$

By employing the balance of mass we obtain the balance of electric charge:

$$\rho z^{\bullet}+\frac{\partial \jmath_i}{\partial x_i}=0\ . \tag{III.20}$$

This local form of a balance equation can be written in a global form for an arbitrary (fixed) domain, Ω, of an open system, which is unbounded to the matter

$$\begin{gathered}\int_\Omega\left(\rho z^{\bullet}+\frac{\partial \jmath_i}{\partial x_i}\right)\mathrm{d}v=0\ , \\ \int_\Omega \rho z^{\bullet}\,\mathrm{d}v=-\int_{\partial\Omega}\jmath_i\,\mathrm{d}a_i\ , \\ \Big(\int_\Omega \rho z\,\mathrm{d}v\Big)^{\bullet}=-\int_{\partial\Omega}\rho z v_i\,\mathrm{d}a_i-\int_{\partial\Omega}\jmath_i\,\mathrm{d}a_i\ ,\end{gathered} \tag{III.21}$$

where we have used Gauss's law and then the balance of mass for an open system as introduced in Eq.[52] (1.261) on p. 86. By taking Eq.[52] (3.5) on p. 169 into account, the balance of electric charge in a fixed domain (control volume) reads

$$\Big(\int_\Omega \rho z\,\mathrm{d}v\Big)^{\bullet}=-\int_{\partial\Omega}J_i\,\mathrm{d}a_i\ . \tag{III.22}$$

In an arbitrarily chosen control volume in space, we can compute the electric charge by using a so-called *charge potential*, D_i, representing the amount of charge escaping from the domain across its boundaries as follows

$$\int_\Omega \rho z\,\mathrm{d}v=\int_{\partial\Omega}D_i\,\mathrm{d}a_i\ . \tag{III.23}$$

Hence D_i describes in a way the displacement of electric charges. By using Gauss's law we obtain another Maxwell equation:

$$\rho z=\frac{\partial D_i}{\partial x_i}\ . \tag{III.24}$$

Moreover, we can now rewrite Eq. (III.22) and obtain a balance on an arbitrary sur-

face, S, instead of a volume,

$$\begin{aligned}\left(\int_{\partial\Omega} D_i \,\mathrm{d}a_i\right)^{\cdot} &= -\int_{\partial\Omega} J_i \,\mathrm{d}a_i \ , \\ \left(\int_{S} D_i \,\mathrm{d}a_i\right)^{\cdot} &= \int_{\partial S} H_i \,\mathrm{d}\ell_i - \int_{S} J_i \,\mathrm{d}a_i \ ,\end{aligned} \tag{III.25}$$

where H_i is called the *current potential*. It is of importance to clarify that a volume has an enclosed surface or hull. Hence the hull, $\partial\Omega$, has no boundaries. If we exchange the enclosed surface $\partial\Omega$ with an arbitrary surface S, we have to add a term on the boundary of the surface, ∂S, with its line element, $\mathrm{d}\ell_i$.[57] All quantities, D_i, H_i, and J_i, are measured in the laboratory frame. The arbitrary surface, S, may possess a velocity, w_i, then the local form becomes

$$\frac{\partial D_i}{\partial t} + w_i \frac{\partial D_j}{\partial x_j} - \operatorname{curl}(\boldsymbol{w} \times \boldsymbol{D})_i = \operatorname{curl}(\boldsymbol{H})_i - J_i \ , \tag{III.26}$$

by using the aforementioned transformation and identities between Eq. (III.6) and Eq. (III.13). As we want to use a fixed domain, $w_i = 0$, it reads

$$\begin{aligned}\frac{\partial D_i}{\partial t} &= \epsilon_{ijk} \frac{\partial H_k}{\partial x_j} - J_i \ , \\ -\frac{\partial D_i}{\partial t} &+ \epsilon_{ijk} \frac{\partial H_k}{\partial x_j} = J_i \ ,\end{aligned} \tag{III.27}$$

which is the final one of Maxwell's equations. From Eqs. (III.24) and (III.27) we can compute the primitive variables, ϕ, A_i, after closing up the governing equations by defining constitutive equations for D_i and H_i.

The Maxwell–Lorentz aether relations[58] define the necessary constitutive equations in free space[59]

$$D_i = \varepsilon_0 E_i \ , \quad H_i = \frac{1}{\mu_0} B_i \ , \tag{III.28}$$

where $\varepsilon_0 = 8.85 \cdot 10^{-12}\,\mathrm{A\,s/(V\,m)}$ and $\mu_0 = 12.6 \cdot 10^{-7}\,\mathrm{V\,s/(A\,m)}$ are universal con-

[57] The line element is directed along the positive surface boundary. The positive direction is such that we "walk along" the surface boundary and the surface is on our left-hand side.

[58] They are named after James Clerk Maxwell and Hendrik Antoon Lorentz.

[59] Free space is a technical definition used as a reference for electromagnetic fields, E_i, B_i. It can be visualized as a perfect vacuum without any medium such as massive particles that may transport the electromagnetic fields. Even in this free space the fields do propagate (with the speed of light, c).

stants.[60] Additionally, there is a paramount relation:

$$\varepsilon_0 \mu_0 = \frac{1}{c^2} \ , \tag{III.29}$$

where the speed of light in the free space, c, is also a universal constant. We can rewrite the MAXWELL-LORENTZ aether relations as follows

$$\frac{\partial D_i}{\partial E_j} = \delta_{ij} \varepsilon_0 \ , \quad \frac{\partial H_i}{\partial B_j} = \delta_{ij} \mu_0^{-1} \ . \tag{III.30}$$

They hold in free space. If we want to amend the formulation such that it holds in matter then we separate the electric charges, z, in two parts: Free and bound charges.

Basically the atomic structure is such that charged particles within core are bound and outer charged particles—valence electrons—may move between atoms and molecules. Therefore, there are charged particles that move *freely* in body and thus conduct an electric current. The displacement of free charges per mass, $z^{\mathrm{fr.}}$, is given by the free charge potential: $\mathfrak{D}_i$. The atomic position (energy level) of valence electrons determines how much energy is necessary to conduct electric current. At most there are 8 valence electrons: The first 2 are in s-band and the rest 6 are in p-band. The energy levels of s and p bands varies with the occupancy. Monovalent metals such as copper and silver have only one valence electron in the s-band with high energy such that only a small portion of energy succeeds to move them to neighboring atoms. Copper, silver, and gold are the best conductors.[61] In case of aluminum, s-band is full with two electrons and there is 1 electron in p-band. The energy level is lower than in monovalent metals. Therefore, aluminum is a good conductor, however, not as good as the monovalent metals.[62] If the s-band is full without any p-band electrons, then metal is divalent and the energy level is even lower. Hence we have to supply more energy to move the valence electrons. Iron (steel) and titanium have more resistivity than aluminum.[63] Valence electrons are moving freely and enable a *free conduction current* in matter.

There are also charges per mass, $z - z^{\mathrm{fr.}}$, which are *bound*. This quantity is rather difficult to visualize. Consider a massive particle consisting of many molecules. The molecules consisting of atoms possess many positively and negatively charged particles distributed in space. The center of positive charges and the center of negative charges coincide. We call this state *unpolarized*. As a consequence of an electric field, these bound charges shift a bit (less than the atomic radius) and so-called *dipoles* appear—the material is now *electrically polarized*. This atomic

[60] Universal constants hold for every material, even without matter (in free space).
[61] Electronic configurations: Copper (Cu) $3d^{10}4s^1$, silver (Ag) $4d^{10}5s^1$, gold (Au) $4f^{14}5d^{10}6s^1$.
[62] Electronic configuration: Aluminum (Al) $3s^2 3p^1$.
[63] Electronic configurations: Iron (Fe) $3d^6 4s^2$, titanium (Ti) $3d^2 4s^2$.

displacement creates a *polarization current*.

By convention the direction of the electric polarization is given from the center of negative charges to the center of positive charges, in the opposite direction of (positive) charge escape, D_i. Suppose the charge density is $q = \rho z$ in $\mathrm{C/m^3}$. If positive and negative charges in an atom moved apart a distance of d_i (pointing from $-q$ to $+q$), then the dipole moment $m_i = qd_i$ in $\mathrm{C/m^2}$ creates a polarized material. For a molecule with N atoms we can sum up all m_i and divide them by the number, N, in order to obtain an average value, $\langle m_i \rangle$. In the continuum scale the electric polarization, $P_i = \langle m_i \rangle N$, is a charge area density in $\mathrm{C/m^2}$ directing toward positive charges. Now the bound (positive) charges diverging from the domain can be given

$$\int_\Omega \rho(z - z^{\mathrm{fr.}})\,\mathrm{d}v = -\int_{\partial\Omega} P_i\,\mathrm{d}a_i \ , \tag{III.31}$$

since positive charges move from positive to negative, i.e., toward the opposite direction of P_i. By using Gauss's law we obtain

$$\rho(z - z^{\mathrm{fr.}}) = -\frac{\partial P_i}{\partial x_i} \ . \tag{III.32}$$

By inserting the latter into Eq. (III.24) we acquire

$$\begin{aligned} \frac{\partial D_i}{\partial x_i} - \rho z^{\mathrm{fr.}} &= -\frac{\partial P_i}{\partial x_i} \ , \\ \frac{\partial D_i}{\partial x_i} + \frac{\partial P_i}{\partial x_i} &= \rho z^{\mathrm{fr.}} \ , \end{aligned} \tag{III.33}$$

which is equal to

$$\frac{\partial \mathfrak{D}_i}{\partial x_i} = \rho z^{\mathrm{fr.}} \ , \tag{III.34}$$

with the free charge potential, $\mathfrak{D}_i = D_i + P_i$. We can now obtain a total charge potential:

$$D_i = \mathfrak{D}_i - P_i \ , \tag{III.35}$$

where $\mathfrak{D}_i$ denotes a charge potential due to free charges and P_i due to bound charges. The minus sign is because of the convention that the direction of the electric polarization is against the direction of the total charge potential. A moving electric charge creates an electric current. The freely moving electric current is much greater than the displacement current occurring due to the electric polarization. For a conductor, the electric polarization fails to be significant. Practically, an electric polarization occurs in an insulator.

Additional to the electric polarization the material possesses a *magnetic polarization*.

Consider again in the atomic scale the dipoles. According to RUTHERFORD-BOHR's atomic model[64] the electrons moving around the nucleus creates a current, j_i, in A/m^2 in the atomic scale. These dipole loops induce a moment, $m_i = \epsilon_{ijk} d_j j_k$ in A/m, due to the atomic current. This current is a *monopole* without positive and negative sides. The average value, $\langle m_i \rangle$, is measured as a magnetic polarization (or simply a magnetization) $M_i = \langle m_i \rangle N$. Magnetization in A/m is a current line density. In the macroscopic scale we comprehend the magnetization, M_i, as a property of bound charges. Unfortunately, if the bound charges creating an electric polarization have a circular motion they create $\boldsymbol{P} \times \boldsymbol{v}$ that we cannot distinguish from the magnetization, M_i, experimentally. Therefore, the sum:

$$\mathcal{M}_i = M_i + \epsilon_{ijk} P_j v_k \ , \tag{III.36}$$

is observed in an experiment and also used in modeling the magnetization.[65] Analogous to polarization we introduce the so-called total (free and bound) current potential:

$$H_i = \mathfrak{H}_i + \mathcal{M}_i \ , \tag{III.37}$$

with a plus sign since this time we have introduced the magnetic polarization in the direction of current, thus, it has the same sign as the current potential. Now by inserting Eqs. (III.35) and (III.37) into Eq. (III.27) we obtain

$$\begin{aligned} -\frac{\partial \mathfrak{D}_i}{\partial t} + \frac{\partial P_i}{\partial t} + \epsilon_{ijk} \frac{\partial \mathfrak{H}_k}{\partial x_j} + \epsilon_{ijk} \frac{\partial \mathcal{M}_k}{\partial x_j} = J_i \ , \\ -\frac{\partial \mathfrak{D}_i}{\partial t} + \epsilon_{ijk} \frac{\partial \mathfrak{H}_k}{\partial x_j} = J_i^{\text{fr.}} \ , \end{aligned} \tag{III.38}$$

with

$$J_i^{\text{fr.}} = J_i - \frac{\partial P_i}{\partial t} - \epsilon_{ijk} \frac{\partial \mathcal{M}_k}{\partial x_j} \ . \tag{III.39}$$

We can rewrite the latter for an interpretation of the total current, $\mathcal{J}_i$, as a sum of free current, $J_i^{\text{fr.}}$, and polarization current

$$J_i = J_i^{\text{fr.}} + \frac{\partial P_i}{\partial t} + \epsilon_{ijk} \frac{\partial \mathcal{M}_k}{\partial x_j} \ . \tag{III.40}$$

All currents are measured in the laboratory frame. We can introduce objective electric current for the total current, J_i, as well as for the free current, $J_i^{\text{fr.}}$, as follows

$$J_i = \mathcal{J}_i + \rho z v_i \ , \quad J_i^{\text{fr.}} = \mathcal{J}_i^{\text{fr.}} + \rho z^{\text{fr.}} v_i \ . \tag{III.41}$$

[64] This model fails to be correct since if electrons would rotate they would radiate electromagnetic waves. Since experimentally we cannot detect any radiation from atoms this visualization is false. Better models are proposed by using *quantum mechanics*. However, we keep up with *continuum mechanics*; for introducing magnetic polarization we use the nice visualization of RUTHERFORD-BOHR's model named for Ernest Rutherford and Niels Henrik David Bohr.

[65] The magnetization used for the modeling, $\mathcal{M}_i$, is an objective quantity.

For polarized materials the objective free current is given by Ohm's law:

$$\mathcal{J}_i^{\text{fr.}} = \varsigma \mathcal{E}_i \ , \tag{III.42}$$

we postpone its derivation to Section[52] 3.5 on p. 243. We shall define charge and current potentials, $\mathfrak{D}_i$ and $\mathfrak{H}_i$, respectively, as well as electric and magnetic polarizations, P_i and $\mathcal{M}_i$, respectively, in order to close Eqs. (III.34), $(\text{III.38})_2$.

There are two similar methods used in the literature for defining the necessary constitutive equations. The first method is based on defining the charge and current potentials from that the electric and magnetic polarizations follow. For a material with bound charges we need to define material equations for electric and current potentials, $\mathfrak{D}_i$ and $\mathfrak{H}_i$, respectively. Based on the Maxwell–Lorentz aether relations in Eqs. (III.30) we can motivate

$$\frac{\partial \mathfrak{D}_i}{\partial E_j} = \varepsilon_{ij}^{\text{el.}} \ , \quad \frac{\partial \mathfrak{H}_i}{\partial B_j} = (\boldsymbol{\mu}_{\text{mag.}}^{-1})_{ij} \ , \tag{III.43}$$

hence we obtain relations for $\mathfrak{D}_i$ and $\mathfrak{H}_i$ by measuring the *permittivity* tensor, $\varepsilon_{ij}^{\text{el.}}$, and the *permeability* tensor, $\mu_{ij}^{\text{mag.}}$. For so-called *simple* materials the electric potential depends only on the electric field and the current potential depends only on the magnetic flux:

$$\mathfrak{D}_i = \varepsilon_{ij}^{\text{el.}} E_j \ , \quad \mathfrak{H}_i = (\boldsymbol{\mu}_{\text{mag.}}^{-1})_{ij} B_j \ , \tag{III.44}$$

where the *dielectric permittivity*, $\varepsilon_{ij}^{\text{el.}}$, and the *magnetic permeability*, $\mu_{ij}^{\text{mag.}}$, consist of constant coefficients[66] (constant in E_i and B_i) for linear materials. For isotropic materials they are reduced to $\varepsilon_{ij}^{\text{el.}} = \varepsilon^{\text{el.}} \delta_{ij}$ and $\mu_{ij}^{\text{mag.}} = \mu^{\text{mag.}} \delta_{ij}$ such that we can now write

$$\begin{aligned} \mathfrak{D}_i &= \varepsilon^{\text{el.}} E_i = \varepsilon_0 \bar{\varepsilon}^{\text{el.}} E_i \ , \\ \mathfrak{H}_i &= \mu_{\text{mag.}}^{-1} B_i = (\mu_0 \bar{\mu}^{\text{mag.}})^{-1} B_i = \frac{1}{\mu_0 \bar{\mu}^{\text{mag.}}} B_i \ , \end{aligned} \tag{III.45}$$

by introducing the relative permittivity $\bar{\varepsilon}^{\text{el.}} = \varepsilon^{\text{el.}}/\varepsilon_0$ and the relative permeability $\bar{\mu}^{\text{mag.}} = \mu^{\text{mag.}}/\mu_0$ without unit. By measuring the permittivity and permeability we have defined the charge and current potentials. We deduce from them the electric and magnetic polarizations:

$$\begin{aligned} P_i &= \mathfrak{D}_i - D_i = \varepsilon_0 \bar{\varepsilon}^{\text{el.}} E_i - \varepsilon_0 E_i = \varepsilon_0 (\bar{\varepsilon}^{\text{el.}} - 1) E_i = \varepsilon_0 \chi^{\text{el.}} E_i \ , \\ \mathcal{M}_i &= -\mathfrak{H}_i + H_i = -\frac{1}{\mu_0 \bar{\mu}^{\text{mag.}}} B_i + \frac{1}{\mu_0} B_i = \frac{\bar{\mu}^{\text{mag.}} - 1}{\mu_0 \bar{\mu}^{\text{mag.}}} B_i = \frac{\chi^{\text{mag.}}}{\mu_0 \bar{\mu}^{\text{mag.}}} B_i \ , \end{aligned} \tag{III.46}$$

where $\chi^{\text{el.}} = \bar{\varepsilon}^{\text{el.}} - 1$ and $\chi^{\text{mag.}} = \bar{\mu}^{\text{mag.}} - 1$ are the electric and magnetic *susceptibilities*,

[66] The permittivity is measured in F(arad)/m $\hat{=}$ C/(V m) $\hat{=}$ A s/(V m) where F is named after Michael Faraday. The permeability is measured in H(enry)/m $\hat{=}$ Wb/(A m) $\hat{=}$ V s/(A m) where H is named for Joseph Henry.

respectively. Often they are found in the literature in the following form:

$$P_i = \varepsilon_0 \chi^{\text{el.}} E_i = \chi^{\text{el.}} D_i \ , \quad \mathcal{M}_i = \frac{\chi^{\text{mag.}}}{\mu_0 \bar{\mu}^{\text{mag.}}} B_i = \chi^{\text{mag.}} \mathfrak{H}_i \ . \tag{III.47}$$

We have two different options for describing the constitutive equations for polarized matter. The first option is to measure dielectric permittivity and magnetic permeability such that Eqs. (III.45) define the constitutive equations for the electric and current potentials. The second possibility relies upon measurements of electric and magnetic susceptibilities[67] and using Eqs. (III.46) as constitutive equations for the electric and magnetic polarizations. Both are correct since we have started with their relation as in Eqs. (III.35) (III.37). In both way we have related them to the primitive variables, ϕ, A_i, since E_i, B_i are given in terms of the electric and magnetic potentials in Eqs. (III.15). By having defined the polarization we have arrived at a constitutive equation for the free current, $J^{\text{fr.}}$, in Eq. (III.39). Hence the governing Eqs. (III.34), $(\text{III.38})_2$ are now closed and can be solved.

Our goal is to compute ϕ and A_i, thus, we need two weak forms. Although we skip a thorough discussion of the balance equations on singular surfaces, we will make much use of them especially in the weak forms of the electromagnetic potentials. A singular surface denotes an area over which a function undergoes a discontinuity. This singularity is simply a jump in the value of the function by crossing the singular surface. Consider two different materials attached together; their interface is a singular surface. A material specific quantity like a free charge potential, $\mathfrak{D}_i$, or free current potential, $\mathfrak{H}_i$, have jumps over the interface, since the permittivities and permeabilities are different for the two adjacent materials. Technically, interface is a singular surface without its own mass density. It is a fictitious surface, not a material surface.[68] Moreover, we neglect any effect of the surface charges on the interface.[69] Under these assumptions the balance equations on singular surfaces take the simple form:

$$\boldsymbol{n} \cdot \left[\!\left[\boldsymbol{\mathfrak{D}} \right]\!\right] = 0 \ , \quad \boldsymbol{n} \times \left[\!\left[\boldsymbol{\mathfrak{H}} \right]\!\right] = 0 \ , \tag{III.48}$$

where we have introduced squared brackets indicating a jump. Suppose the interface has material 1 and material 2 at both sides. The value of $\mathfrak{D}_i$ on the interface as

[67] There are various methods for measuring the susceptibilities, see for example Trainer, 2001 and Marcon and Ostanina, 2012.

[68] The interface is a fictitious surface without mass. If we have a thin layer between two different materials, we may declare it as a singular surface (surface has zero thickness) by neglecting the layers thickness. However, the singular would have then a mass. We consider herein singular surfaces without mass.

[69] In many applications the surface charges have no effect at all. In Section[52] 3.5 on p.243 we will simulate the piezoelectric effect under 100 V and have a small error less than 1 V by neglecting the surface charges, see for a detailed computation of surface charges in piezoelectic ceramics in Kim et al., 2012. For some applications concerning mass diffusion (electromigration) in mixtures, the surface charges may have a significant effect. In this book mixtures are out of scope.

a boundary of material 1 is different than the value on the interface as a boundary of material 2. In other words, $\mathfrak{D}_i^+$ indicates the value on the boundary of material 1, i.e., the interface adjacent to material 1. Analogously, $\mathfrak{D}_i^-$ is the value on the interface adjacent to material 2. At the same point on interface, the plane normal of the boundary belonging to material 1, n_i^+, is directed against the plane normal of the boundary of material 2, n_i^-, such that $n_i^+ = -n_i^-$. Then the balance equations read

$$\begin{aligned} n_i\big[\mathfrak{D}_i\big] &= n_i(\mathfrak{D}_i^+ - \mathfrak{D}_i^-) = n_i^+\mathfrak{D}_i^+ + n_i^-\mathfrak{D}_i^- = 0 \ , \\ \epsilon_{ijk} n_j\big[\mathfrak{H}_k\big] &= \epsilon_{ijk} n_j(\mathfrak{H}_k^+ - \mathfrak{H}_k^-) = \epsilon_{ijk}(n_j^+\mathfrak{H}_k^+ + n_j^-\mathfrak{H}_k^-) = 0 \ . \end{aligned} \tag{III.49}$$

In order to obtain a weak form for computing the electric potential, ϕ, we use the balance of electric charge:

$$\frac{\partial \rho z}{\partial t} + J_{i,i} = 0 \ , \tag{III.50}$$

again by starting to use the comma notation for partial derivatives in space. By inserting one of MAXWELL's equations in Eq. (III.24) and the total current as in Eq. (III.39) into the balance equation, we acquire the field equation for electric potential:

$$\frac{\partial D_{i,i}}{\partial t} + \left(J_i^{\text{fr.}} + \frac{\partial P_i}{\partial t} + \epsilon_{ijk}\mathcal{M}_{k,j} \right)_{,i} = 0 \ . \tag{III.51}$$

Within a domain where P_i is continuous we can interchange the order of space and time derivative such that the field equation reads

$$\frac{\partial \mathfrak{D}_{i,i}}{\partial t} + \left(J_i^{\text{fr.}} + \epsilon_{ijk}\mathcal{M}_{k,j} \right)_{,i} = 0 \ . \tag{III.52}$$

First we utilize the time discretization. Secondly, by multiplying with the test function, $\delta\phi$, and integrating over the domain where P_i and $\mathfrak{D}_i$ are continuous, we obtain a variational form. In order to have it in the unit of energy we multiply the form with Δt, which is constant in space. Thirdly, by integrating by parts we lower the continuity condition and generate the weak form:

$$\begin{aligned} \mathrm{F}_\phi = \int_{\Omega^*} \big(&- (\mathfrak{D}_i - \mathfrak{D}_i^0)\delta\phi_{,i} - \Delta t J_i^{\text{fr.}}\delta\phi_{,i} - \Delta t \epsilon_{ijk}\mathcal{M}_{k,j}\delta\phi_{,i} \big)\, \mathrm{d}v + \\ &+ \int_{\partial\Omega^*} n_i(\mathfrak{D}_i - \mathfrak{D}_i^0 + \Delta t J_i^{\text{fr.}} + \Delta t \epsilon_{ijk}\mathcal{M}_{k,j})\delta\phi \, \mathrm{d}a \ . \end{aligned} \tag{III.53}$$

Consider a domain, Ω, consisting of two materials, Ω_1 and Ω_2. A polarized material surrounded by air is an adequate example. We simply state that $\Omega = \Omega_1 \cup \Omega_2$ and $\partial\Omega^I = \partial\Omega_1 \cap \partial\Omega_2$, where the interaction boundary between the different materials, $\partial\Omega^I$, is a fictitious, singular surface. The primitive variables are continuous within the whole domain: The electric and magnetic potentials, ϕ, A_i, are continuous in Ω. Hence, the electric field, E_i, as well as the magnetic flux density, B_i, are continuous in Ω. However, this case fails to be true for constitutive equations. For example, $\mathcal{J}_i^{\text{fr.}}$ has a jump on the interface since the electrical conductivities within Ω_1 and Ω_2

differ. Analogously P_i and $\mathfrak{D}_i$ have discontinuities on the interface.

By discretizing in space we solve the integral form in each finite element and sum it up over the elements. If we observe two elements on both sides of the interface, i.e., one element is in Ω_1 and the other one is in Ω_2, then the summation over elements lead to two boundary integrals coming from each element with a plane normal pointing outward the domain Ω_1 or Ω_2. Hence we obtain a jump on the interface and attain the following weak form:

$$\begin{aligned} \mathrm{F}_\phi = \int_\Omega \big(&- (\mathfrak{D}_i - \mathfrak{D}_i^0)\delta\phi_{,i} - \Delta t J_i^{\mathrm{fr.}}\delta\phi_{,i} - \Delta t \epsilon_{ijk}\mathcal{M}_{k,j}\delta\phi_{,i}\big)\,\mathrm{d}v + \\ &+ \int_{\partial\Omega^I} n_i\big[\mathfrak{D}_i - \mathfrak{D}_i^0 + \Delta t J_i^{\mathrm{fr.}} + \Delta t \epsilon_{ijk}\mathcal{M}_{k,j}\big]\delta\phi\,\mathrm{d}a + \\ &+ \int_{\partial\Omega} n_i(\mathfrak{D}_i - \mathfrak{D}_i^0 + \Delta t J_i^{\mathrm{fr.}} + \Delta t \epsilon_{ijk}\mathcal{M}_{k,j})\delta\phi\,\mathrm{d}a\ . \end{aligned} \tag{III.54}$$

From the balance equation on singular surfaces we know that $n_i\big[\mathfrak{D}_i\big] = 0$. Therefore, the weak form for computing the electric potential reads

$$\begin{aligned} \mathrm{F}_\phi = \int_\Omega \big(&- (\mathfrak{D}_i - \mathfrak{D}_i^0)\delta\phi_{,i} - \Delta t J_i^{\mathrm{fr.}}\delta\phi_{,i} - \Delta t \epsilon_{ijk}\mathcal{M}_{k,j}\delta\phi_{,i}\big)\,\mathrm{d}v + \\ &+ \int_{\partial\Omega^I} \Big(n_i\Delta t\big[J_i^{\mathrm{fr.}}\big]\delta\phi + n_i\Delta t\epsilon_{ijk}\big[\mathcal{M}_{k,j}\big]\delta\phi\Big)\,\mathrm{d}a + \\ &+ \int_{\partial\Omega} n_i(\mathfrak{D}_i - \mathfrak{D}_i^0 + \Delta t J_i^{\mathrm{fr.}} + \Delta t \epsilon_{ijk}\mathcal{M}_{k,j})\delta\phi\,\mathrm{d}a\ . \end{aligned} \tag{III.55}$$

We will employ Dirichlet boundary conditions on $\partial\Omega$ such that $\delta\phi|_{\partial\Omega} = 0$ leads to the following weak form:

$$\begin{aligned} \mathrm{F}_\phi = \int_\Omega \big(&- (\mathfrak{D}_i - \mathfrak{D}_i^0)\delta\phi_{,i} - \Delta t J_i^{\mathrm{fr.}}\delta\phi_{,i} - \Delta t \epsilon_{ijk}\mathcal{M}_{k,j}\delta\phi_{,i}\big)\,\mathrm{d}v + \\ &+ \int_{\partial\Omega^I} \Big(n_i\Delta t\big[J_i^{\mathrm{fr.}}\big]\delta\phi + n_i\Delta t\epsilon_{ijk}\big[\mathcal{M}_{k,j}\big]\delta\phi\Big)\,\mathrm{d}a\ . \end{aligned} \tag{III.56}$$

For the magnetic potential, A_i, we will use Maxwell's Eq. (III.27), namely,

$$-\frac{\partial D_i}{\partial t} + \epsilon_{ijk}H_{k,j} = J_i\ , \tag{III.57}$$

after implementing Lorenz's gauge. This choice of the gauge is because of numerical reasons—Lorenz's gauge enables a simplification in the field equation. In order to see this simplification we employ the Maxwell-Lorentz aether relations

$$-\frac{\partial}{\partial t}(\varepsilon_0 E_i) + \epsilon_{ijk}\frac{\partial}{\partial x_j}\Big(\frac{1}{\mu_0}B_k\Big) = J_i\ . \tag{III.58}$$

After utilizing Eqs. (III.15) we obtain

$$\varepsilon_0 \frac{\partial}{\partial t}\Big(\frac{\partial \phi}{\partial x_i} + \frac{\partial A_i}{\partial t}\Big) + \frac{1}{\mu_0}\,\epsilon_{ijk}\epsilon_{kmn}\frac{\partial^2 A_n}{\partial x_j \partial x_m} = J_i \ . \tag{III.59}$$

Since $\epsilon_{ijk} = \epsilon_{kij}$ and additionally with the identity, $\epsilon_{kij}\epsilon_{kmn} = \delta_{im}\delta_{jn} - \delta_{in}\delta_{jm}$, holding in Cartesian coordinates, we acquire the following equation:

$$\begin{aligned} \varepsilon_0 \frac{\partial^2 \phi}{\partial t \partial x_i} + \varepsilon_0 \frac{\partial^2 A_i}{\partial t^2} + \frac{1}{\mu_0}\left(\frac{\partial^2 A_j}{\partial x_j \partial x_i} - \frac{\partial^2 A_i}{\partial x_j \partial x_j}\right) &= J_i \ , \\ \frac{\partial}{\partial x_i}\left(\varepsilon_0 \frac{\partial \phi}{\partial t} + \frac{1}{\mu_0}\frac{\partial A_j}{\partial x_j}\right) + \varepsilon_0 \frac{\partial^2 A_i}{\partial t^2} - \frac{1}{\mu_0}\frac{\partial^2 A_i}{\partial x_j \partial x_j} &= J_i \ , \end{aligned} \tag{III.60}$$

where Schwarz's theorem[70] has been used. The first term vanishes by applying Lorenz's gauge in Eq. (III.18). After inserting the total current from Eq. (III.39), the field equation for magnetic potential reads

$$\varepsilon_0 \frac{\partial^2 A_i}{\partial t^2} - \frac{1}{\mu_0}\frac{\partial^2 A_i}{\partial x_j \partial x_j} = J_i^{\text{fr.}} + \frac{\partial P_i}{\partial t} + \epsilon_{ijk}\mathcal{M}_{k,j} \ . \tag{III.61}$$

As usual, after discretizing in time we generate the weak form by multiplying with the test function and lower the differentiability by integrating by parts and acquire

$$\begin{aligned} \mathrm{F}_{\boldsymbol{A}} = \int_\Omega \Big(\varepsilon_0 \frac{A_i - 2A_i^0 + A_i^{00}}{\Delta t \Delta t}\delta A_i + \frac{1}{\mu_0} A_{i,j}\delta A_{i,j} - J_i^{\text{fr.}}\delta A_i - \\ - \frac{P_i - P_i^0}{\Delta t}\delta A_i + \epsilon_{ijk}\mathcal{M}_k \delta A_{i,j}\Big)\,\mathrm{d}v - \int_{\partial\Omega}\Big(\frac{1}{\mu_0}A_{i,j} + \epsilon_{ijk}\mathcal{M}_k\Big)\delta A_i n_j\,\mathrm{d}a \ . \end{aligned} \tag{III.62}$$

Again by summing up over the finite elements we find out (by recalling that μ_0 is a universal constant)

$$\begin{aligned} \mathrm{F}_{\boldsymbol{A}} = \int_\Omega \Big(\varepsilon_0 \frac{A_i - 2A_i^0 + A_i^{00}}{\Delta t \Delta t}\delta A_i + \frac{1}{\mu_0} A_{i,j}\delta A_{i,j} - J_i^{\text{fr.}}\delta A_i - \\ - \frac{P_i - P_i^0}{\Delta t}\delta A_i + \epsilon_{ijk}\mathcal{M}_k \delta A_{i,j}\Big)\,\mathrm{d}v - \int_{\partial\Omega^I}\left(\frac{1}{\mu_0}\big[A_{i,j}\big] + \epsilon_{ijk}\big[\mathcal{M}_k\big]\right)\delta A_i n_j\,\mathrm{d}a - \\ - \int_{\partial\Omega}\Big(\frac{1}{\mu_0}A_{i,j} + \epsilon_{ijk}\mathcal{M}_k\Big)\delta A_i n_j\,\mathrm{d}a \ . \end{aligned} \tag{III.63}$$

For the jump condition we use the following balance equation on singular surfaces:

$$\epsilon_{ijk} n_j \big[\mathfrak{H}_k\big] = 0 \ . \tag{III.64}$$

[70] The interchangeability of the order of variables in a differentiation is named after Hermann Amandus Schwarz.

By rewriting the latter we acquire

$$\begin{aligned} \epsilon_{ijk} n_j \big[H_k - \mathcal{M}_k\big] &= 0 \ , \\ \epsilon_{ijk} n_j \big[H_k\big] &= \epsilon_{ijk} n_j \big[\mathcal{M}_k\big] \ , \\ \epsilon_{ijk} n_j \frac{1}{\mu_0} \epsilon_{klm} \big[A_{m,l}\big] &= \epsilon_{ijk} n_j \big[\mathcal{M}_k\big] \ . \end{aligned} \tag{III.65}$$

Now by using the identity $\epsilon_{ijk}\epsilon_{klm} = \delta_{il}\delta_{jm} - \delta_{im}\delta_{jl}$ we obtain

$$\begin{aligned} n_j \frac{1}{\mu_0} \big[A_{j,i} - A_{i,j}\big] &= \epsilon_{ijk} n_j \big[\mathcal{M}_k\big] \ , \\ n_j \frac{1}{\mu_0} \big[A_{j,i}\big] &= n_j \frac{1}{\mu_0} \big[A_{i,j}\big] + \epsilon_{ijk} n_j \big[\mathcal{M}_k\big] \ . \end{aligned} \tag{III.66}$$

Therefore, the weak form for computing the magnetic potential reads

$$\begin{aligned} \mathrm{Form}_{\boldsymbol{A}} = \int_\Omega \Big(& \varepsilon_0 \frac{A_i - 2A_i^0 + A_i^{00}}{\Delta t \Delta t} \delta A_i + \frac{1}{\mu_0} A_{i,j} \delta A_{i,j} - J_i^{\mathrm{fr}\cdot} \delta A_i - \\ & - \frac{P_i - P_i^0}{\Delta t} \delta A_i + \epsilon_{ijk} \mathcal{M}_k \delta A_{i,j} \Big) \, \mathrm{d}v - \\ - \int_{\partial\Omega^I} & \frac{1}{\mu_0} \big[A_{j,i}\big] \delta A_i n_j \, \mathrm{d}a - \int_{\partial\Omega} \Big(\frac{1}{\mu_0} A_{i,j} + \epsilon_{ijk} \mathcal{M}_k \Big) \delta A_i n_j \, \mathrm{d}a \ . \end{aligned} \tag{III.67}$$

Since the primitive variables are continuous across the interface, the integral on $\partial\Omega^I$ vanishes. Moreover, we will use DIRICHLET boundary conditions on $\partial\Omega$ such that $\delta A_i|_{\partial\Omega} = 0$ leads to the weak form:

$$\begin{aligned} \mathrm{F}_{\boldsymbol{A}} = \int_\Omega \Big(& \varepsilon_0 \frac{A_i - 2A_i^0 + A_i^{00}}{\Delta t \Delta t} \delta A_i + \frac{1}{\mu_0} A_{i,j} \delta A_{i,j} - J_i^{\mathrm{fr}\cdot} \delta A_i - \\ & - \frac{P_i - P_i^0}{\Delta t} \delta A_i + \epsilon_{ijk} \mathcal{M}_k \delta A_{i,j} \Big) \, \mathrm{d}v \ . \end{aligned} \tag{III.68}$$

By using the weak form: $\mathrm{Form} = \mathrm{F}_\phi + \mathrm{F}_{\boldsymbol{A}}$ with F_ϕ as in Eq. (III.56) and $\mathrm{F}_{\boldsymbol{A}}$ as in Eq. (III.68), we compute three engineering examples: Capacitor, transformer, skin and proximity effects in a conductor.

1. Capacitor simulation

An electric insulator between two metal conductors is a capacitor. Since the insulator does not permit an electric current, any positive or negative charges brought on the conductors are held. In other words, the capacitor stores electric energy. The stored charges on the conductors can be used as a power supply by connecting them in a

circuit. This method is used in camera flashes where the capacitor is first charged by the battery and then the flash gets its power from the capacitor. If the current (power consumption) is high the battery starts to sag (shows a high latency and provides a lower energy output due to the resistance). Capacitors are much more accurate and reliable especially for high power consumptions, like a bright light for a short period of time as being the case in a camera flash.

Consider an insulator between two metal plates. As insulator we will use PTFE[71], metal plates are made of copper. The capacitor is surrounded by air. The geometry consists of three different parts, namely PTFE, copper, and air. For generating the geometry and meshing, i.e., for preprocessing we use Salome[72] and obtain the model in Fig. III.1. Air is an insulator, $\varsigma_{\text{air}} = 3 \cdot 10^{-15}$, and its susceptibilities are zero. In other

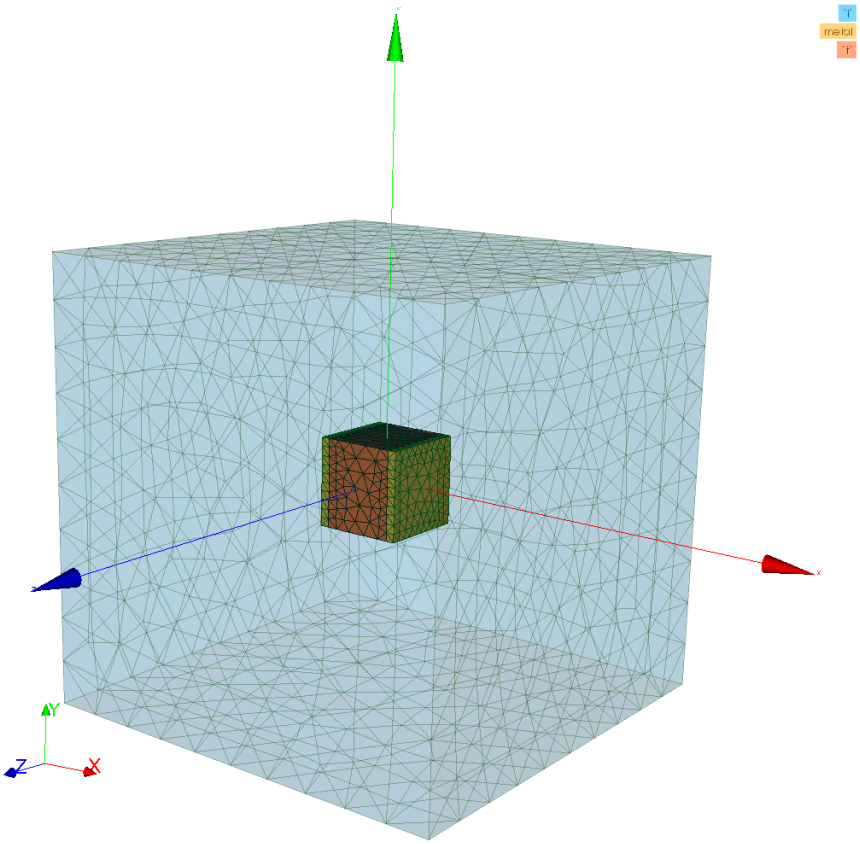

Figure III.1.: The geometry is a capacitor in air with an insulator out of PTFE with two copper plates on both sides.

words, air can be undertaken as a free space (vacuum) by means of electromagnetic

[71] PTFE stands for PolyTetraFluoroEthylene—its prominent brand-name is Teflon from DuPont in France.

[72] See Appendix[52] A.3 on p. 297 for instructions how to mark the surfaces for applying the boundary conditions and to mark the volumes for different parts.

interaction with the following permittivity and permeability:

$$\varepsilon_0 = 8.85 \cdot 10^{-12}\,\mathrm{A\,s/(V\,m)}\ , \quad \mu_0 = 12.6 \cdot 10^{-7}\,\mathrm{V\,s/(A\,m)}\ . \tag{III.69}$$

PTFE is an insulator and shows a strong electric polarization and a weak magnetic polarization:

$$\varsigma = 10^{-25}\,\mathrm{S/m}\ , \quad \chi^{\mathrm{el.}}_{\mathrm{PTFE}} = 1\ , \quad \chi^{\mathrm{mag.}}_{\mathrm{PTFE}} = 10^{-6}\ . \tag{III.70}$$

Copper (Cu) is a conductor, thus, it shows no electric polarization, $\chi^{\mathrm{el.}}_{\mathrm{Cu}} = 0$, but a weak magnetization:

$$\varsigma = 58.5^{6}\,\mathrm{S/m}\ , \quad \chi^{\mathrm{mag.}}_{\mathrm{Cu}} = -10^{-5}\ . \tag{III.71}$$

Since $\chi^{\mathrm{mag.}}_{\mathrm{Cu}} < 0$, copper is a diamagnetic material.

For computing the primitive variables, viz., electric potential ϕ and magnetic potential A_i, we exploit the weak form as given in Eqs. (III.56), (III.68). At both sides of the capacitor we set the electric potential such that the difference increases (linearly) over time. After 1 s there is 0.2 V difference between the plates. Since PTFE is an insulator no current flows, however, we can measure an electric field due to the electric polarization. In other words, bound charges shift and this displacement of charges known as *dielectric displacement* creates an electric field within the capacitor as well as in the surrounding air. Moreover, this field varies in time leading to a magnetic field. Both effects can be seen in Fig. III.2.

Electric field, E_i, and magnetic flux (area density), B_i, are orthogonal to each other. We show in Fig. III.2 the electric field on z-plane and the magnetic flux on y-plane. The magnetic flux is small, however, it exists. Its magnitude depends on the rate of voltage on the plates, we generate 0.2 V difference in 1 s. In other words, the polarization current during charging is very low. Since PTFE is an insulator, there occurs no conduction current and the polarization current gains importance. If the capacitor is fully charged and the circuit is cut off, then the electric field becomes stationary, polarization current and thus the magnetic flux vanish completely.

Far away from the capacitor—on the domain boundaries—electromagnetic fields vanish throughout the simulation, $\phi\big|_{\partial\Omega} = 0$, $A_i\big|_{\partial\Omega} = 0$, which is implemented as Dirichlet conditions. On interfaces between air and copper, PTFE and copper, air and PTFE; the conditions from the balance equations on singular surfaces are implemented as aforementioned by dedcing Eqs. (III.56), (III.68). The geometry for the computation can be found in Abali, 2013. Below, the code is given for the capacitor where standard finite element form functions are used and all primitive variables are computed at once in each iteration.

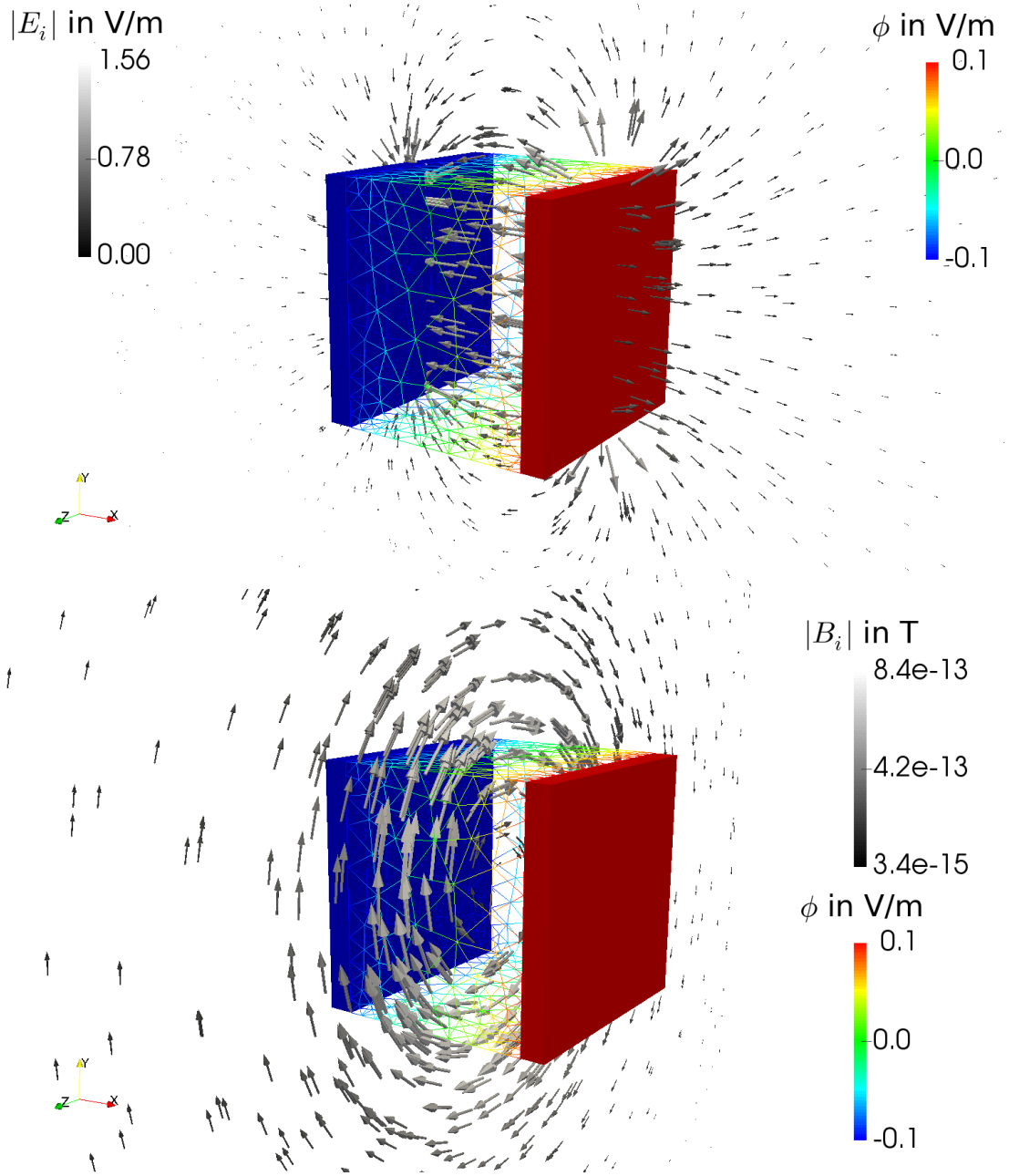

Figure III.2.: PTFE insulator is visualized as wireframe and the copper plates as surfaces. The capacitor is colored by ϕ. The polarization of the capacitor creates an electric field shown on the upper figure. It creates also a magnetic flux during charging presented on the lower figure. The E_i and B_i fields are visualized by arrows only on cut planes for the sake of a better visualization. The transient solution is presented at 1 s.

```
"""Computational reality 16, polarized material, simulation of a capacitor"""
__author__ = "B. Emek Abali"
__license__  = "GNU GPL Version 3.0 or later"
#This code underlies the GNU General Public License, http://www.gnu.org/licenses/gpl-3.0.en.html

from fenics import *
import numpy
set_log_level(ERROR)
'''
2D 1 "boundary_in"
2D 2 "boundary_out"
2D 3 "metal_air"
2D 4 "ptfe_air"
2D 5 "ptfe_metal"
2D 6 "boundary_air"
3D 1 "air"
3D 2 "metal"
3D 3 "ptfe"
'''
mesh = Mesh('geo/CR16_geo.xml')
cells = MeshFunction('size_t',mesh,'geo/CR16_geo_physical_region.xml')
facets = MeshFunction('size_t',mesh,'geo/CR16_geo_facet_region.xml')

def material_coefficient(target_mesh, cells_list, coeffs):
    coeff_func = Function(FunctionSpace(target_mesh, 'DG', 0))
    markers = numpy.asarray(cells_list.array(), dtype=numpy.int32)
    coeff_func.vector()[:] = numpy.choose(markers-1, coeffs)
    return coeff_func

n = FacetNormal(mesh)
#interface, area, volume elements
di = Measure('dS', domain=mesh, subdomain_data=facets)
da = Measure('ds', domain=mesh, subdomain_data=facets)
dv = Measure('dx', domain=mesh, subdomain_data=cells)

Scalar = FunctionSpace(mesh, 'P', 1)
Vector = VectorFunctionSpace(mesh, 'P', 1)
Tensor = TensorFunctionSpace(mesh, 'P', 1)
Space = MixedFunctionSpace([Scalar, Vector]) #phi, A

#units: m, kg, s, A, V, K
delta = Identity(3)
```

```
43 levicivita2 = as_matrix([ (0,1,-1) , (-1,0,1) , (1,-1,0) ])
44 levicivita3 = as_tensor([ ( (0,0,0),(0,0,1),(0,-1,0) ) , (
       ↪ (0,0,-1),(0,0,0),(1,0,0) ) , ( (0,1,0),(-1,0,0),(0,0,0) ) ])
45 epsilon = levicivita3
46
47 eps_0 = 8.85E-12 #in A s/(V m)
48 mu_0 = 12.6E-7 #in V s/(A m)
49
50 null=1E-20 #for numerical reasons it is not zero
51
52 #air
53 varsigma_air = 3E-15
54 chi_el_air = null
55 chi_ma_air = null
56 mu_r_ma_air = chi_ma_air + 1.
57
58 #metal (copper)
59 varsigma_cu = 58.5E+6 #in S/m or in 1/(Ohm m)
60 chi_el_cu = null
61 chi_ma_cu = -1E-5
62 mu_r_ma_cu = chi_ma_cu + 1.
63
64 #Teflon (ptfe) is an insulator
65 varsigma_ptfe = 1E-25 #in S/m or in 1/(Ohm m)
66 chi_el_ptfe = 1.0
67 chi_ma_ptfe = 1E-6
68 mu_r_ma_ptfe = chi_ma_ptfe + 1.
69
70 chi_el = material_coefficient(mesh, cells, [chi_el_air, chi_el_cu,
       ↪ chi_el_ptfe])
71 chi_ma = material_coefficient(mesh, cells, [chi_ma_air, chi_ma_cu,
       ↪ chi_ma_ptfe])
72 mu_r_ma = material_coefficient(mesh, cells, [mu_r_ma_air,
       ↪ mu_r_ma_cu, mu_r_ma_ptfe])
73 varsigma = material_coefficient(mesh, cells, [varsigma_air,
       ↪ varsigma_cu, varsigma_ptfe])
74
75 tMax = 1.0
76 Dt = 0.1
77 t = 0.0
78
79 capacitor_1 = Expression('0.1*time', time=0)
80 capacitor_2 = Expression('-0.1*time', time=0)
81 bc01=DirichletBC(Space.sub(0), capacitor_1, facets, 1)
82 bc02=DirichletBC(Space.sub(0), capacitor_2, facets, 2)
83 bc03=DirichletBC(Space.sub(0), Constant(0.), facets, 6)
84 bc04=DirichletBC(Space.sub(1), Constant((0.,0.,0.)), facets, 6)
```

```
85
86  bc = [bc01,bc02,bc03,bc04]
87
88  dunkn = TrialFunction(Space)
89  test = TestFunction(Space)
90  del_phi, del_A = split(test)
91
92  unkn = Function(Space)
93  unkn0 = Function(Space)
94  unkn00 = Function(Space)
95
96  unkn_init = Expression(('0.0', '0.0','0.0','0.0'))
97  unkn00 = interpolate(unkn_init,Space)
98  unkn0.assign(unkn00)
99  unkn.assign(unkn0)
100
101 phi, A = split(unkn)
102 phi0, A0 = split(unkn0)
103 phi00, A00 = split(unkn00)
104
105 i, j, k, l = indices(4)
106 delta = Identity(3)
107 E = as_tensor(-phi.dx(i)-(A-A0)[i]/Dt, (i,))
108 E0 = as_tensor(-phi0.dx(i)-(A0-A00)[i]/Dt, (i,))
109 B = as_tensor(epsilon[i,j,k]*A[k].dx(j), (i,))
110
111 D = eps_0*E
112 D0 = eps_0*E0
113 H = 1./mu_0*B
114 P = eps_0*chi_el*E
115 P0 = eps_0*chi_el*E0
116 mD = D + P
117 mD0 = D0 + P0
118 MM =1./mu_0/mu_r_ma*chi_ma*B
119 J_fr = varsigma*E
120
121 F_phi = ( -(mD-mD0)[i]*del_phi.dx(i) - Dt*J_fr[i]*del_phi.dx(i) -
      ↪ Dt*epsilon[i,j,k]*MM[k].dx(j)*del_phi.dx(i) )*(dv(1)+dv(2)+
      ↪ dv(3)) + ( n('+')[i]*Dt*(J_fr('+') - J_fr('-'))[i]*del_phi('
      ↪ +') + n('+')[i]*Dt*epsilon[i,j,k]*(MM('+')[k].dx(j) - MM('-'
      ↪ )[k].dx(j))*del_phi('+') )*(di(3)+di(4)+di(5))
122
123 F_A = (eps_0*(A-2.*A0+A00)[i]/Dt/Dt*del_A[i] + 1./mu_0*A[i].dx(j)*
      ↪ del_A[i].dx(j) -J_fr[i]*del_A[i] - (P-P0)[i]/Dt*del_A[i] +
      ↪ epsilon[i,j,k]*MM[k]*del_A[i].dx(j) )*(dv(1)+dv(2)+dv(3))
124
125 Form = F_phi + F_A
```

```
126 Gain = derivative(Form, unkn, dunkn)
127
128 pwd='/calcul/CR16_capacitor/'
129 file_phi_metal = File(pwd+'phi_metal.pvd')
130 file_phi_ptfe = File(pwd+'phi_ptfe.pvd')
131 file_E = File(pwd+'E.pvd')
132 file_B = File(pwd+'B.pvd')
133
134 mesh_metal = SubMesh(mesh,cells,2)
135 mesh_ptfe = SubMesh(mesh,cells,3)
136
137 VectorSpace_metal = FunctionSpace(mesh_metal, 'P', 1)
138 VectorSpace_ptfe = FunctionSpace(mesh_ptfe, 'P', 1)
139 phi_metal = Function(VectorSpace_metal, name='$\phi$')
140 phi_ptfe = Function(VectorSpace_ptfe, name='$\phi$')
141
142
143 while t < tMax:
144     t += Dt
145     print 'time: ',t
146     capacitor_1.time = t
147     capacitor_2.time = t
148     solve(Form==0, unkn, bc, J=Gain, \
149         solver_parameters={"newton_solver":{"linear_solver": "
            ↪ mumps", "relative_tolerance": 1e-5} }, \
150         form_compiler_parameters={"cpp_optimize": True, "
            ↪ representation": "quadrature", "quadrature_degree":
            ↪ 2}  )
151
152     phi_metal.assign(project(unkn.split(deepcopy=True)[0],
        ↪ VectorSpace_metal))
153     file_phi_metal << (phi_metal, t)
154     phi_ptfe.assign(project(unkn.split(deepcopy=True)[0],
        ↪ VectorSpace_ptfe))
155     file_phi_ptfe << (phi_ptfe, t)
156     file_B << (project(B,Vector),t)
157     file_E << (project(E,Vector),t)
158
159     unkn00.assign(unkn0)
160     unkn0.assign(unkn)
```

2. Transformer simulation

Every electronic device uses electricity. For example in a laptop the motherboard needs 12 V, however, the plug on the wall supplies 110-240 V depending on the country. For decreasing the voltage from the plug to the necessary voltage for the laptop, we need a transformer. The transformer consists of a core and two windings. The primary winding is connected to the input (to the plug on the wall) and the secondary winding is connected to the output (to the laptop). We model a simple transformer with a primary winding of 3 turns and a secondary winding of 2 turns, see Fig. III.3.

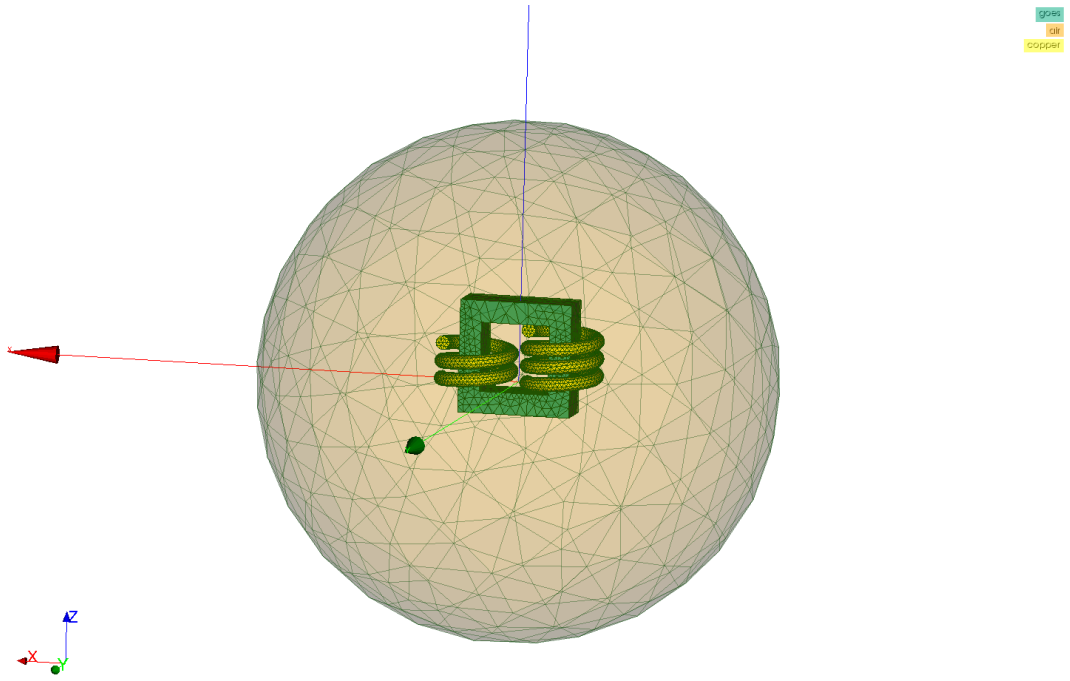

Figure III.3.: The geometry is a transformer in air. A ferromagnetic electric steel is used as the transformer core and it transports the magnetic flux from the primary to the secondary winding, without contacting the windings.

The windings and core are good conductors, however, they are not in contact. Since both windings are connected to different circuits, we have an input and an output voltages. The input voltage due to the alternating current (A.C.) varies harmonically in $\nu = 50\,\mathrm{Hz}$, and due to the coiled geometry of the winding, this induces a magnetic flux along the core. The core is chosen out of a ferromagnetic material with high permeability such that the magnetic flux is increased within the core. It generates a strong magnetic polarization directed along the core. Thus, the magnetic flux created

by the primary winding is increased and transported to the secondary winding. This flux induces a change in the electric potential on the secondary winding. As the input current in the primary winding is alternating, an induced A.C. is generated as the output.

If the magnetic core has no losses, then 3 turns input and 2 turns output would decrease the input voltage to 2/3. Of course the core material has some losses. Two different physical phenomena cause losses in the core. The first one is due to the magnetostriction, i.e., a deformation owing to the magnetic polarization. This effect causes a vibration in A.C. We assume rigid bodies in this section such that we ignore this effect in the simulation. The second aspect is mainly a characteristic of the chosen material. Modern transformers use a material called an *electric steel* with negligibly small losses. A small amount of silicon mixed into the steel is named as an electric steel. Moreover, the orientation of grains in the electric steel are directed along the core geometry. This choice reduces the loss further such that we assume that the material shows no hysteresis in A.C. In order to justify this assumption we consider a Grain Oriented Electric Steel (GOES) alloy with the experimental data as seen in Fig. III.4. The experimental data is provided in logarithmic base and shows that no

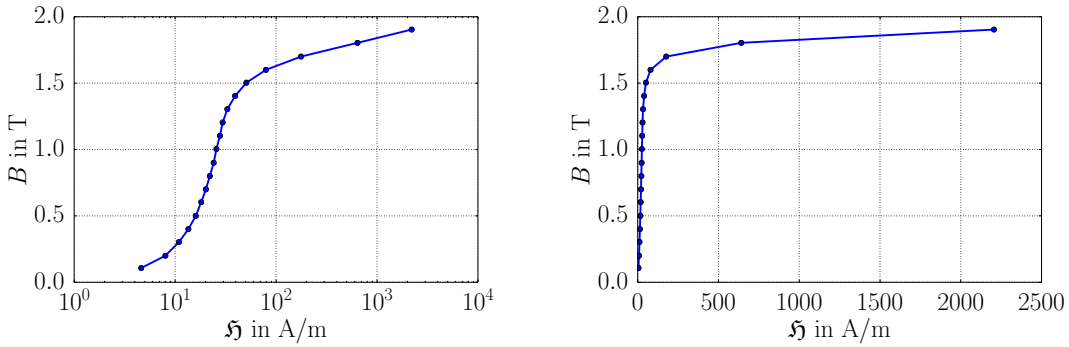

Figure III.4.: Permeability A.C. measurement of a Grain Oriented Electric Steel (GOES) alloy, in logarithmic base (left) and in non-logarithmic base (right). The experimental data is taken from Allegheny Technologies Incorporated, www.ATImetals.com

hysteresis occurs in A.C. In order to comprehend the data better, we plot it in normal (non-logarithmic) base. Obviously, the relation between B_i and $\mathfrak{H}_i$ is not linear in the whole range, in other words, the permeability is not a constant. However, by restricting to magnetic fluxes lower than 1.5 T we may assume a constant (relative) permeability:

$$\bar{\mu}^{\text{mag.}} = 20\,000 \ . \tag{III.72}$$

Copper and GOES alloy are conductors such that we implement Eqs. (III.56), (III.68) for computing the electric potentials. On the ends of the winding with 3 turns the electric potential is prescribed by DIRICHLET conditions:

$$\phi = A \sin(\nu 2\pi t) \ , \tag{III.73}$$

where $A = \pm 110\,\mathrm{V}$ at both ends and $\nu = 50\,\mathrm{Hz}$ such that we have a 220 V difference alternating with 50 Hz as usual in the home electricity in Europe. The core out of GOES alloy and the copper windings are embedded in air.[73] In reality there is a thin layer on the winding, a coating, suppressing a current in the plane normal direction. Hence, for a precise modeling, the current toward the interface normal is set to zero on the interface between air and winding. We employ Eqs. (III.56), (III.68) for computing the electromagnetic potentials leading to the magnetic flux due to the electric current in the primary winding. The winding made of copper possesses an electric conductivity as high as $\varsigma = 1/r = 58.5 \cdot 10^6$. However, this is not realistic. The winding is on a circuit with a resistance. Otherwise, the electric current would be so high that the production of heat due to the JOULE heating would melt the copper wire. For a 30 W transformer the resistance on the primary winding can be chosen as $R_1 = 100\,\Omega$. Since in the transformer we have 3 turns in the primary and 2 turns in the secondary winding we reduce from 220 V to $220/(3/2) \approx 150\,\mathrm{V}$. The current in A reads

$$I = \int \jmath_i \,\mathrm{d}a_i \ , \tag{III.74}$$

and the voltage is $V_1 = 220\,\mathrm{V}$ and $V_2 = 150\,\mathrm{V}$ in two windings. Since the power is the same in each winding:

$$P = I_1 V_1 = I_2 V_2 \ , \tag{III.75}$$

we can find out the adequate resistance on the secondary winding

$$\begin{aligned} V_1 = I_1 R_1 \ , \quad V_2 = I_2 R_2 \ , \\ \frac{R_1}{R_2} = \frac{V_1 I_2}{V_2 I_1} = \left(\frac{V_1}{V_2}\right)^2 = \left(\frac{3}{2}\right)^2 \ , \\ R_2 = \frac{R_1}{(3/2)^2} \approx 45\,\Omega \ . \end{aligned} \tag{III.76}$$

As the coils of radius, $r_\mathrm{c} = 0.004\,\mathrm{m}$, has a surface of $a = \pi r_\mathrm{c}^2/2$, the conductivity of windings, $\varsigma = 1/r$, read

$$\varsigma_1 = \frac{\ell_1}{R_1 a} \ , \quad \varsigma_2 = \frac{\ell_2}{R_2 a} \ , \tag{III.77}$$

where the length of each winding is $\ell_\mathrm{w} = 2\pi r_\mathrm{w}$ with the winding radius of $r_\mathrm{w} = 0.02\,\mathrm{m}$. The primary winding is then $\ell_1 = 3\ell_\mathrm{w}$ and the secondary winding is of length $\ell_2 = 2\ell_\mathrm{w}$. Since the resistance in the second winding is lower, the possible electric current is higher. The electric current in the first winding flows in a helix such that a magnetic flux is induced inside the coil, i.e., in the core in $-z$ direction. This flux creates a magnetic polarization in the core. The polarization is transferred over the core to the second winding. There the magnetic flux is in $+z$ direction and creates an electric current in the second winding in the opposite direction. In a power supply with A.C. the direction of current has no importance. We visualize the electric potentials in

[73] In reality, the transformer is housed in a polymer like epoxy, which is an insulator alike air. We just neglect the electric polarization occurring in the polymer housing.

the windings, the magnetic polarization within the core, and the magnetic flux in the whole space in Fig. III.5. The geometry for the computation is in Abali, 2013. The

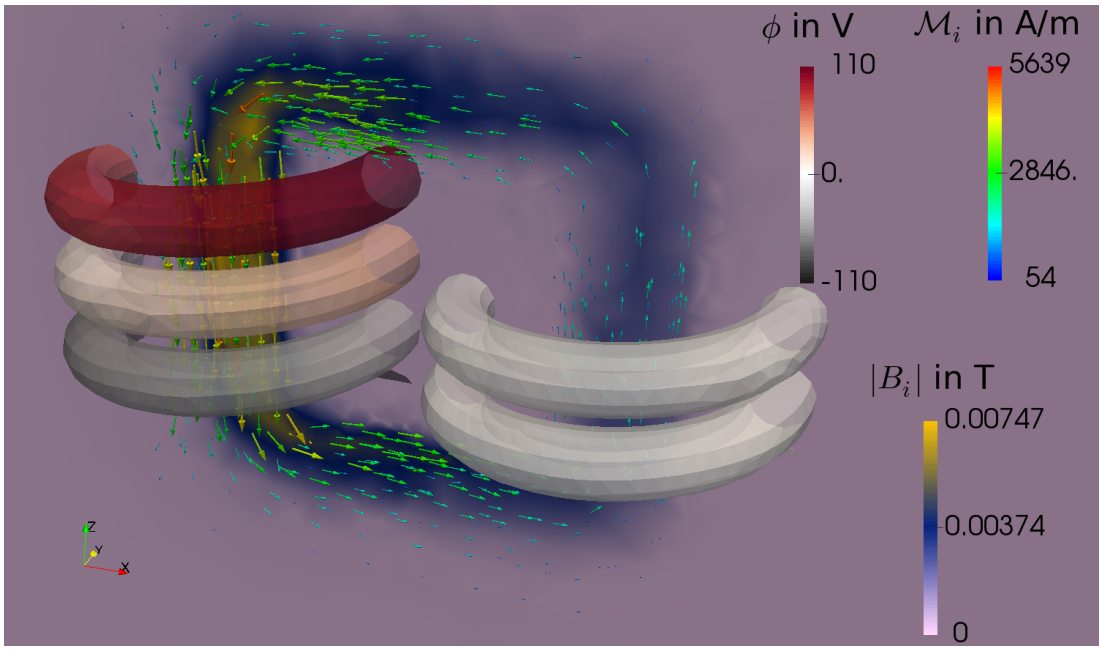

Figure III.5.: Three fields are visualized at $t = 0.05\,\mathrm{s}$. The core out of GOES alloy is magnetized, the magnetic polarization is visualized as arrows colored by the values of $\mathcal{M}_i$. The primary winding with 3 turns and the secondary winding with 2 turns are colored by the electric potential, ϕ. On a slice in y-plane, the magnitude of the magnetic flux density, B_i, is shown as colored. The magnetic flux is immensely increased inside the core, so the leaded magnetic field from the primary to the secondary coil induces an electric potential in the secondary coil. Since the current is alternating on the primary coil, the induced current is alternating, too.

code below is used for the transient simulation of electrodynamics in rigid bodies.

```
"""Computational reality 16, polarized material, simulation of a transformer"""
__author__ = "B. Emek Abali"
__license__  = "GNU GPL Version 3.0 or later"
#This code underlies the GNU General Public License, http://www.gnu.org/licenses/gpl-3.0.en.html

from fenics import *
import numpy
set_log_level(ERROR)
'''
2D 1 "copper_2_out"
2D 2 "copper_1_in"
2D 3 "copper_1_out"
2D 4 "air_goes"
2D 5 "copper1_air"
```

```
2D 6 "copper2_air"
2D 7 "air_boundary"
2D 8 "copper_2_in"
3D 1 "copper_1_with_3_turns"
3D 2 "copper_2_with_2_turns"
3D 3 "air"
3D 4 "goes"
'''
mesh = Mesh('geo/CR16_geo_trafo.xml')
cells = MeshFunction('size_t',mesh,'geo/
    ↪ CR16_geo_trafo_physical_region.xml')
facets = MeshFunction('size_t',mesh,'geo/
    ↪ CR16_geo_trafo_facet_region.xml')

def material_coefficient(target_mesh, cells_list, coeffs):
    coeff_func = Function(FunctionSpace(target_mesh, 'DG', 0))
    markers = numpy.asarray(cells_list.array(), dtype=numpy.int32)
    coeff_func.vector()[:] = numpy.choose(markers-1, coeffs)
    return coeff_func

n = FacetNormal(mesh)
#interface, area, volume elements
di = Measure('dS', domain=mesh, subdomain_data=facets)
da = Measure('ds', domain=mesh, subdomain_data=facets)
dv = Measure('dx', domain=mesh, subdomain_data=cells)

Scalar = FunctionSpace(mesh, 'P', 1)
Vector = VectorFunctionSpace(mesh, 'P', 1)
Tensor = TensorFunctionSpace(mesh, 'P', 1)
Space = MixedFunctionSpace([Scalar, Vector]) #phi, A

#units: m, kg, s, A, V, K
delta = Identity(3)
epsilon = as_tensor([ ( (0,0,0),(0,0,1),(0,-1,0) ) , ( (0,0,-1)
    ↪ ,(0,0,0),(1,0,0) ) , ( (0,1,0),(-1,0,0),(0,0,0) ) ])

eps_0 = 8.85E-12 #in A s/(V m)
mu_0 = 12.6E-7 #in V s/(A m)

null=1E-20 #for numerical reasons it is not zero

#Grain Oriented Electrical Steel (GOES) is a ferromagnetic
    ↪ material
varsigma_goes = 2.1E+6 #in S/m or in 1/(Ohm m)
chi_el_goes = null
mu_r_ma_goes = 20000. #approximately
chi_ma_goes = mu_r_ma_goes - 1.
```

```
58
59 #air
60 varsigma_air = 3E-15
61 chi_el_air = null
62 chi_ma_air = null
63 mu_r_ma_air = chi_ma_air + 1.
64
65 #metal (copper)
66 a = pi*0.004**2/2.
67 l_w = 2.*pi*0.02
68 #winding 1 with 3 turns
69 l_1 = 3.*l_w
70 R_1 = 100. #in Ohm or 1/S
71 V_1 = 220. #in V
72 I_1 = V_1/R_1
73 varsigma_cu_1 = l_1/(R_1*a) #in S/m
74 #winding 2 with 2 turns
75 l_2 = 2.*l_w
76 R_2 = 45.
77 varsigma_cu_2 = l_2/(R_2*a) #in S/m or in 1/(Ohm m)
78
79 chi_el_cu = null
80 chi_ma_cu = -1E-5
81 mu_r_ma_cu = chi_ma_cu + 1.
82
83 chi_el = material_coefficient(mesh, cells, [chi_el_cu, chi_el_cu,
       ↪ chi_el_air, chi_el_goes])
84 chi_ma = material_coefficient(mesh, cells, [chi_ma_cu, chi_ma_cu,
       ↪ chi_ma_air, chi_ma_goes])
85 mu_r_ma = material_coefficient(mesh, cells, [mu_r_ma_cu,
       ↪ mu_r_ma_cu, mu_r_ma_air, mu_r_ma_goes])
86 varsigma = material_coefficient(mesh, cells, [varsigma_cu_1,
       ↪ varsigma_cu_2, varsigma_air, varsigma_goes])
87
88 tMax = 0.02
89 Dt = tMax/20.
90 t = 0.0
91
92 bc01=DirichletBC(Space.sub(0), Constant(0.), facets, 7)
93 bc02=DirichletBC(Space.sub(1), Constant((0.,0.,0.)), facets, 7)
94 bc_cu_in = Expression('A*sin(nu*2.0*pi*time)',A=V_1/2.,nu=50.,time
       ↪ =0.)
95 bc_cu_out = Expression('A*sin(nu*2.0*pi*time)',A=-V_1/2.,nu=50.,
       ↪ time=0.)
96 bc03=DirichletBC(Space.sub(0), bc_cu_in, facets, 2)
97 bc04=DirichletBC(Space.sub(0), bc_cu_out, facets, 3)
98 bc = [bc01,bc02,bc03,bc04]
```

```
99
100 dunkn = TrialFunction(Space)
101 test = TestFunction(Space)
102 del_phi, del_A = split(test)
103
104 unkn = Function(Space)
105 unkn0 = Function(Space)
106 unkn00 = Function(Space)
107
108 unkn_init = Expression(('0.0', '0.0','0.0','0.0'))
109 unkn00 = interpolate(unkn_init,Space)
110 unkn0.assign(unkn00)
111 unkn.assign(unkn0)
112
113 phi, A = split(unkn)
114 phi0, A0 = split(unkn0)
115 phi00, A00 = split(unkn00)
116
117 i, j, k, l = indices(4)
118 delta = Identity(3)
119 E = as_tensor(-phi.dx(i)-(A-A0)[i]/Dt, (i,))
120 E0 = as_tensor(-phi0.dx(i)-(A0-A00)[i]/Dt, (i,))
121 B = as_tensor(epsilon[i,j,k]*A[k].dx(j), (i,))
122
123 D = eps_0*E
124 D0 = eps_0*E0
125 H = 1./mu_0*B
126 P = eps_0*chi_el*E
127 P0 = eps_0*chi_el*E0
128 mD = D + P
129 mD0 = D0 + P0
130 MM = 1./mu_0/mu_r_ma*chi_ma*B
131 J_fr = varsigma*E
132
133 F_phi = ( -(mD-mD0)[i]*del_phi.dx(i) - Dt*J_fr[i]*del_phi.dx(i) -
    ↪ Dt*epsilon[i,j,k]*MM[k].dx(j)*del_phi.dx(i) )*(dv(1)+dv(2)+
    ↪ dv(3)+dv(4)) + n('+')[i]*Dt*epsilon[i,j,k]*(MM('+')[k].dx(j)
    ↪ - MM('-')[k].dx(j))*del_phi('+')*(di(1)+di(4)+di(5)+di(6)+
    ↪ di(8))
134
135 F_A = (eps_0*(A-2.*A0+A00)[i]/Dt/Dt*del_A[i] + 1./mu_0*A[i].dx(j)*
    ↪ del_A[i].dx(j) -J_fr[i]*del_A[i] - (P-P0)[i]/Dt*del_A[i] +
    ↪ epsilon[i,j,k]*MM[k]*del_A[i].dx(j))*(dv(1)+dv(2)+dv(3)+dv
    ↪ (4))
136
137 Form = F_phi + F_A
138 Gain = derivative(Form, unkn, dunkn)
```

```
139
140 pwd='/calcul/CR16_transformer/'
141 file_phi = File(pwd+'phi.pvd')
142 file_M = File(pwd+'M.pvd')
143 file_B = File(pwd+'B.pvd')
144
145 mesh_1 = SubMesh(mesh,cells,1)
146 mesh_2 = SubMesh(mesh,cells,2)
147 mesh_3 = SubMesh(mesh,cells,3)
148 mesh_4 = SubMesh(mesh,cells,4)
149
150 phi_copper_1_ = Function(FunctionSpace(mesh_1, 'P', 1), name='$\
    ↪ phi$ in V')
151 phi_copper_2_ = Function(FunctionSpace(mesh_2, 'P', 1), name='$\
    ↪ phi$ in V')
152 MM_goes_ = Function(VectorFunctionSpace(mesh_4, 'P', 1), name='$|\
    ↪ mathcal{M}_i|$ in A/m')
153 B_ = Function(VectorFunctionSpace(mesh, 'P', 1), name='$|B_i|$ in
    ↪ T')
154
155
156 while t < tMax:
157     t += Dt
158     print 'time: ',t
159     bc_cu_in.time = t
160     bc_cu_out.time = t
161     solve(Form==0, unkn, bc, J=Gain, \
162         solver_parameters={"newton_solver":{"linear_solver": "
            ↪ mumps", "relative_tolerance": 1e-5} }, \
163         form_compiler_parameters={"cpp_optimize": True, "
            ↪ representation": "quadrature", "quadrature_degree":
            ↪ 2}  )
164
165     phi_copper_1_.assign(project(unkn.split(deepcopy=True)[0],
        ↪ FunctionSpace(mesh_1, 'P', 1)))
166     file_phi << (phi_copper_1_, t)
167     phi_copper_2_.assign(project(unkn.split(deepcopy=True)[0],
        ↪ FunctionSpace(mesh_2, 'P', 1)))
168     file_phi << (phi_copper_2_, t)
169     MM_goes_.assign(project(MM, VectorFunctionSpace(mesh_4, 'P',
        ↪ 1)))
170     file_M << (MM_goes_,t)
171     B_.assign(project(B, VectorFunctionSpace(mesh, 'P', 1)))
172     file_B << (B_,t)
173
174     unkn00.assign(unkn0)
175     unkn0.assign(unkn)
```

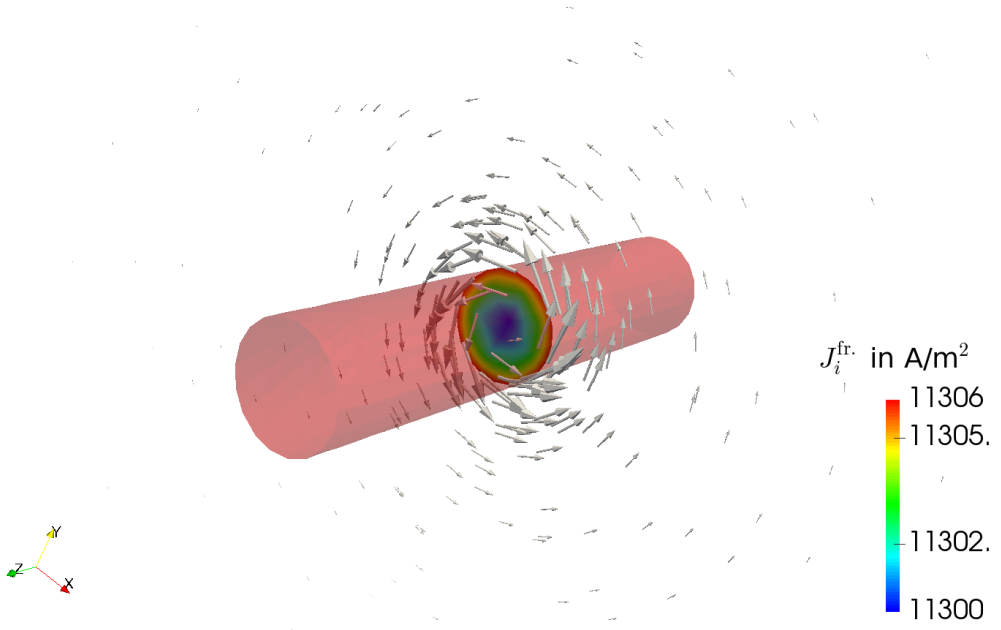

Figure III.6.: Skin effect at 500 kHz can be seen at 1/10 of the period. Colors denote to the magnitude of $J_i^{\text{fr.}}$ and arrows denote the direction of the magnetic flux density, B_i.

3. Proximity and skin effects

In a conductor, for example in a copper wire, the charge carriers are valence electrons. They conduct the charge and this transport is called the free objective electric current, $\mathcal{J}_i^{\text{fr.}}$. It depends on the electromotive intensity, $\mathcal{E}_i$, which is the electric field measured on the co-moving frame. In this section we assume the copper wire as a rigid body; all objective variables, $\mathcal{J}_i^{\text{fr.}}$, $\mathcal{E}_i$, $\mathcal{M}_i$, equal to their corresponding variables measured in the laboratory frame, $J_i^{\text{fr.}} = \mathcal{J}_i^{\text{fr.}}$, $E_i = \mathcal{E}_i$, $M_i = \mathcal{M}_i$.

An alternating electric current induces a magnetic field, which again induces a current in the wire itself. This induced current is swirling within the wire and is called Foucault or *eddy* current.[74] The eddy current is perpendicular to the cross-section of the wire and is directed along the current near the surface and against the current in the core of the wire. The net amount of current is greater on the outer shell than in the core of the wire. Even if we apply a constant electric potential over the cross-section, the current comes out as distributed. The effective conduction current (area density), $J_i^{\text{fr.}}$, is greater near surface than in core. In Fig. III.6 the so-called *skin effect* is visualized at 500 kHz. Skin effect occurs in an alternating current, A.C., since a current is induced due to the varying charge potential. Impedance is an effective resistance of the wire against A.C., thus, the skin effect increases the

[74] Eddy current was discovered firstly by Jean Bernard Léon Foucault.

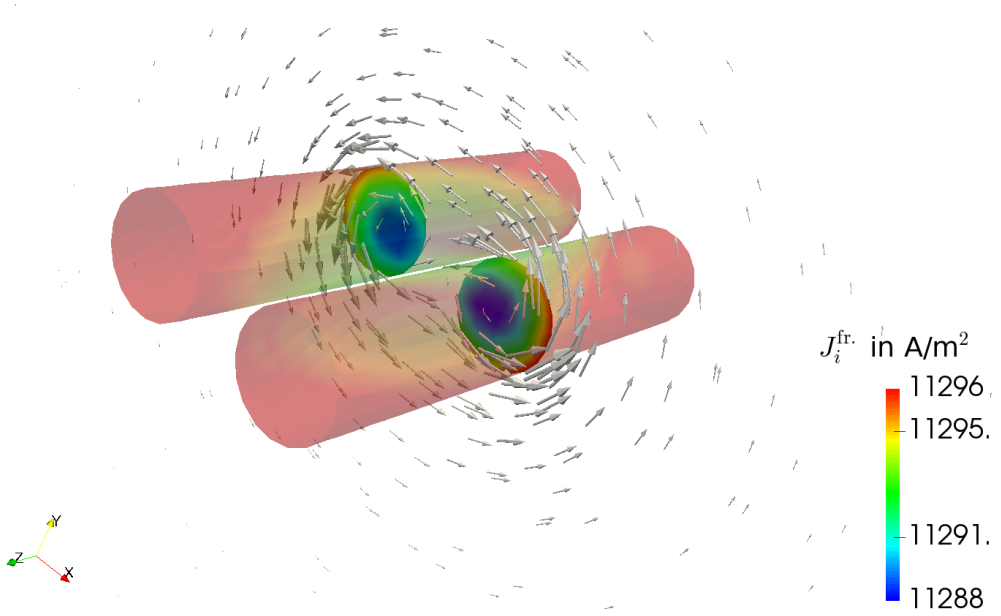

Figure III.7.: Proximity effect is seen at 1/10 of the period at 500 kHz. Colors denote to the magnitude of $J_i^{\text{fr.}}$ and arrows indicate B_i.

impedance of the wire more in the core than on the surface. The deviation of the impedance between surface and core increases with increasing frequency. Especially for digital cables carrying signals in MHz, the skin effect results in an effective current transported on the surface. Special finishing is used on the surface of high quality cables to maximize the purity of copper and increase the conductivity on the surface as much as possible.

By having two cables, the eddy currents of both play a role such that the current distribution on the cross-section changes, which is referred to as a *proximity effect*. The proximity effect is visualized in Fig. III.7. Especially for cables in high frequencies there are many different designs reducing the skin and proximity effects. The general idea is to use bundles twisted around each other such that the proximity effect is eliminated by the neighboring cables in every direction. These cables are called *litz wires*.[75] The geometries for the computations can be found in Abali, 2013 and the code used for computing the skin and proximity effects is given below.

```
1 """Computational reality 16, polarized material, skin and
    ↪ proximity effect"""
2 __author__ = "B. Emek Abali"
3 __license__ = "GNU GPL Version 3.0 or later"
4 #This code underlies the GNU General Public License, http://
    ↪ www.gnu.org/licenses/gpl-3.0.en.html
```

[75] *Der Litzendraht* in German means *stranded wire*.

```
5
6  from fenics import *
7  import numpy
8  set_log_level(ERROR)
9
10 '''
11 2D 1 "in"
12 2D 2 "out"
13 2D 3 "air_boundary"
14 2D 4 "air_copper"
15 3D 1 "air"
16 3D 2 "copper"
17 '''
18 mesh = Mesh('geo/CR16_geo_proximity_two_wires.xml')
19 cells = MeshFunction('size_t',mesh,'geo/
       ↪ CR16_geo_proximity_two_wires_physical_region.xml')
20 facets = MeshFunction('size_t',mesh,'geo/
       ↪ CR16_geo_proximity_two_wires_facet_region.xml')
21
22 def material_coefficient(target_mesh, cells_list, coeffs):
23     coeff_func = Function(FunctionSpace(target_mesh, 'DG', 0))
24     markers = numpy.asarray(cells_list.array(), dtype=numpy.int32)
25     coeff_func.vector()[:] = numpy.choose(markers-1, coeffs)
26     return coeff_func
27
28 n = FacetNormal(mesh)
29 #interface, area, volume elements
30 di = Measure('dS', domain=mesh, subdomain_data=facets)
31 da = Measure('ds', domain=mesh, subdomain_data=facets)
32 dv = Measure('dx', domain=mesh, subdomain_data=cells)
33
34 Scalar = FunctionSpace(mesh, 'P', 1)
35 Vector = VectorFunctionSpace(mesh, 'P', 1)
36 Tensor = TensorFunctionSpace(mesh, 'P', 1)
37 Space = MixedFunctionSpace([Scalar, Vector]) #phi, A
38
39 #units: m, kg, s, A, V, K
40 delta = Identity(3)
41 epsilon = as_tensor([ ( (0,0,0),(0,0,1),(0,-1,0) ) , ( (0,0,-1)
       ↪ ,(0,0,0),(1,0,0) ) , ( (0,1,0),(-1,0,0),(0,0,0) ) ])
42
43 eps_0 = 8.85E-12 #in A s/(V m)
44 mu_0 = 12.6E-7 #in V s/(A m)
45 null=1E-20 #for numerical reasons it is not zero
46
47 #air
48 varsigma_air = 3E-15
```

```
49 chi_el_air = null
50 chi_ma_air = null
51 mu_r_ma_air = chi_ma_air + 1.
52
53 #copper
54 rho_cu = 8960. #in kg / m^3
55 a = pi*0.01**2/2.
56 l = 0.1
57 R = 100.
58 varsigma_cu = l/(R*a) #in S/m or in 1/(Ohm m)
59 V = 220. #in V, I = V/R in A
60 chi_el_cu = null
61 chi_ma_cu = -1E-5
62 mu_r_ma_cu = chi_ma_cu + 1.
63
64 chi_el = material_coefficient(mesh, cells, [chi_el_air, chi_el_cu
       ↪ ])
65 chi_ma = material_coefficient(mesh, cells, [chi_ma_air, chi_ma_cu
       ↪ ])
66 mu_r_ma = material_coefficient(mesh, cells, [mu_r_ma_air,
       ↪ mu_r_ma_cu])
67 varsigma = material_coefficient(mesh, cells, [varsigma_air,
       ↪ varsigma_cu])
68
69 freq = 500000. #in Hz
70 tMax = 1./freq
71 Dt = tMax/20.
72 t = 0.0
73
74 bc01=DirichletBC(Space.sub(0), Constant(0.), facets, 3)
75 bc02=DirichletBC(Space.sub(1), Constant((0.,0.,0.)), facets, 3)
76 bc_in = Expression('A*sin(nu*2.0*pi*time)',A=V/2.,nu=freq,time=0.)
77 bc_out = Expression('A*sin(nu*2.0*pi*time)',A=-V/2.,nu=freq,time
       ↪ =0.)
78 bc03=DirichletBC(Space.sub(0), bc_in, facets, 1)
79 bc04=DirichletBC(Space.sub(0), bc_out, facets, 2)
80 bc = [bc01,bc02,bc03,bc04]
81
82 dunkn = TrialFunction(Space)
83 test = TestFunction(Space)
84 del_phi, del_A = split(test)
85
86 unkn = Function(Space)
87 unkn0 = Function(Space)
88 unkn00 = Function(Space)
89
90 unkn_init = Expression(('0.0', '0.0','0.0','0.0'))
```

```
91  unkn00 = interpolate(unkn_init,Space)
92  unkn0.assign(unkn00)
93  unkn.assign(unkn0)
94
95  phi, A = split(unkn)
96  phi0, A0 = split(unkn0)
97  phi00, A00 = split(unkn00)
98
99  i, j, k, l = indices(4)
100 delta = Identity(3)
101 E = as_tensor(-phi.dx(i)-(A-A0)[i]/Dt, (i,))
102 E0 = as_tensor(-phi0.dx(i)-(A0-A00)[i]/Dt, (i,))
103 B = as_tensor(epsilon[i,j,k]*A[k].dx(j), (i,))
104
105 D = eps_0*E
106 D0 = eps_0*E0
107 H = 1./mu_0*B
108 P = eps_0*chi_el*E
109 P0 = eps_0*chi_el*E0
110 mD = D + P
111 mD0 = D0 + P0
112 MM = 1./mu_0/mu_r_ma*chi_ma*B
113 J_fr = varsigma*E
114
115 F_phi = ( -(mD-mD0)[i]*del_phi.dx(i) - Dt*J_fr[i]*del_phi.dx(i) -
    ↪ Dt*epsilon[i,j,k]*MM[k].dx(j)*del_phi.dx(i) )*(dv(1)+dv(2))
    ↪ + ( n('+')[i]*Dt*(J_fr('+') - J_fr('-'))[i]*del_phi('+') + n
    ↪ ('+')[i]*Dt*epsilon[i,j,k]*(MM('+')[k].dx(j) - MM('-')[k].dx
    ↪ (j))*del_phi('+') )*di(4)
116
117 F_A = (eps_0*(A-2.*A0+A00)[i]/Dt/Dt*del_A[i] + 1./mu_0*A[i].dx(j)*
    ↪ del_A[i].dx(j) -J_fr[i]*del_A[i] - (P-P0)[i]/Dt*del_A[i] +
    ↪ epsilon[i,j,k]*MM[k]*del_A[i].dx(j))*(dv(1)+dv(2))
118
119 Form = F_phi + F_A
120 Gain = derivative(Form, unkn, dunkn)
121
122 pwd='/calcul/CR16_proximity_two_wires/'
123 file_phi = File(pwd+'phi.pvd')
124 file_z = File(pwd+'z.pvd')
125 file_B = File(pwd+'B.pvd')
126 file_J_fr = File(pwd+'J_fr.pvd')
127
128 mesh_1 = SubMesh(mesh,cells,1)
129 mesh_2 = SubMesh(mesh,cells,2)
130
131 phi_copper_ = Function(FunctionSpace(mesh_2, 'P', 1), name='$\phi$
```

```
    ↪  in V')
z_ = Function(FunctionSpace(mesh_2, 'P', 1), name='$z$ in C/kg')
B_ = Function(VectorFunctionSpace(mesh, 'P', 1), name='$|B_i|$ in
    ↪ T')
J_fr_ = Function(VectorFunctionSpace(mesh_2, 'P', 1), name='$J_i^\
    ↪ mathrm{fr.}$ in A/m$^2$')


while t < tMax:
    t += Dt
    print 'time: ',t
    bc_in.time = t
    bc_out.time = t
    tic()
    solve(Form==0, unkn, bc, J=Gain, \
        solver_parameters={"newton_solver":{"linear_solver": "
            ↪ mumps", "relative_tolerance": 1e-5} }, \
        form_compiler_parameters={"cpp_optimize": True, "
            ↪ representation": "quadrature", "quadrature_degree":
            ↪ 2}  )

    print 'finished in ',toc(),' seconds'
    phi_copper_.assign(project(unkn.split(deepcopy=True)[0],
        ↪ FunctionSpace(mesh_2, 'P', 1)))
    file_phi << (phi_copper_, t)
    B_.assign(project(B, VectorFunctionSpace(mesh, 'P', 1)))
    file_B << (B_,t)
    z_.assign(project(D[i].dx(i)/rho_cu, FunctionSpace(mesh_2, 'P'
        ↪ , 1)))
    file_z << (z_,t)
    J_fr_.assign(project(J_fr, VectorFunctionSpace(mesh_2, 'P', 1)
        ↪ ))
    file_J_fr << (J_fr_,t)

    unkn00.assign(unkn0)
    unkn0.assign(unkn)
```

To-do

The electric field, E_i, and the magnetic flux (area density), B_i, exist in material and in free space. They are always orthogonal to each other.

- Implement the code for capacitor and plot on the same cut plane E_i as well as B_i in order to see that they are orthogonal.

- Simulate a transformer with a different core.
- Use the code for a conducting wire and plot $D_{i,i} = \rho z$ in order to test the simplification of incompressible flow of electric charges utilized in the last section.
- In the literature there are formulations attacking MAXWELL's equations in a way to solve directly the fields E_i and B_i without using the electromagnetic potentials, ϕ, A_i. In this configuration the numerical implementation of appropriate elements is quite difficult. There are different proposals. One of them is implementing special elements for E_i and B_i. Search for NEDELEC elements and solutions of electromagnetic problems by using NEDELEC elements in FEniCS.
- Make a web based search for the capacitors. Learn how the capacitive touchscreen of a smartphone works.

References

Abali, B. E. (2013). *Supply code, Computational Reality, Technical University of Berlin, Institute of Mechanics, Chair of Continuum Mechanics and Material Theory*. http://www.lkm.tu-berlin.de/ComputationalReality/.

Abali, B. E. (2017). *Computational Reality, Solving Nonlinear and Coupled Problems in Continuum Mechanics*. Vol. 55. Advanced Structured Materials. Springer. ISBN: 978-981-10-2443-6.

Kim, S. M., Kim, H., Nam, Y., and Kim, S. (2012). „Effects of external surface charges on the enhanced piezoelectric potential of ZnO and AlN nanowires and nanotubes." In: *AIP Advances* 2.4, p. 042174.

Marcon, P. and Ostanina, K. (2012). „Overview of methods for magnetic susceptibility measurement." In: *PIERS Proceedings*, pp. 420–424.

Trainer, M. (2001). „Ferroelectricity: Measurement of the dielectric susceptibility of strontium titanate at low temperatures." In: *American Journal of Physics* 69.9, pp. 966–969.

Kapitel IV

Thermoelectric coupling

The post-print version of the published manuscript:
Section 3.3 in Abali, B. E. (2017). Computational Reality: Solving Nonlinear and Coupled Problems in Continuum Mechanics (Advanced Structured Materials Vol. 55). Springer Nature Singapore.

The final publication is available at Springer via https://doi.org/10.1007/978-981-10-2444-3

As we have seen in Section[76] 3.1 the continuum body heats up due to the heat produced during conducting an electric current. Formally, this production is JOULE's heating and written on the right hand side in the balance of internal energy. Since the temperature changes, the material shrinks or expands. In order to incorporate this effect into the computational reality, we have to use the balance of linear momentum with the electromagnetic interactions (with matter). We will motivate the balance equation and then derive the constitutive equations in a thermodynamically consistent way. In this section we employ the formulation for an *unpolarized* material, $z - z^{\text{fr.}} = 0$. Thus, electric and magnetic polarizations vanish

$$P_i = 0 \ , \quad \mathcal{M}_i = 0 \ . \tag{IV.1}$$

Total energy consists of the energy due to the *matter* and *field*. Matter denotes particles with mass and field means the electromagnetic fields due to particles with an electric charge. Of course materials like copper include molecules with mass and charge. However, mass and charge are treated separately, they are both assumed to exist independently. The thermodynamical formulation starts with the assertion that the total energy is conserved. In other words, a balance of total energy lacks a production term

$$\frac{\partial \rho e}{\partial t} - \frac{\partial}{\partial x_j}\big(- v_j \rho e + F_j\big) - \rho s = 0 \ , \tag{IV.2}$$

[76] As appeared in Abali, 2017.

where the specific total energy, e, its flux term, F_i, and its specific supply term, s, shall be defined. We postpone their derivation and proceed with the balance of momentum with the electromagnetic interactions:

$$\frac{\partial \rho v_i}{\partial t} - \frac{\partial}{\partial x_j}\big(- \rho v_i v_j + \sigma_{ji}\big) - \rho f_i = \mathcal{F}_i \ , \tag{IV.3}$$

where the additional force density, $\mathcal{F}_i$, is caused by the electromagnetic fields. A moving particle "feels" this additional force density—it is the LORENTZ force density for unpolarized systems:

$$\mathcal{F}_i = \rho z E_i + \epsilon_{ijk} J_j B_k \ , \tag{IV.4}$$

as given in Eq.[76] (3.12) with the help of the specific electric charge, z, the mass density, ρ, and the electric current, J_i. In case of electromagnetic interactions between matter and field, the momentum is not a conserved quantity and the LORENTZ force acts as a production. Now by using the balance of mass:

$$\frac{\partial \rho}{\partial t} + \frac{\partial \rho v_j}{\partial x_j} = 0 \ , \tag{IV.5}$$

and the so-called total time rate:[77]

$$\frac{\mathrm{d}}{\mathrm{d}t} = \frac{\partial}{\partial t} + v_j \frac{\partial}{\partial x_j} \ , \tag{IV.6}$$

we obtain from the balance of momentum

$$\rho \frac{\mathrm{d} v_i}{\mathrm{d}t} - \frac{\partial \sigma_{ji}}{\partial x_j} - \rho f_i = \mathcal{F}_i \ . \tag{IV.7}$$

By multiplying the latter with the velocity we acquire the balance of kinetic energy:

$$\begin{aligned} \rho \frac{\mathrm{d} v_i}{\mathrm{d}t} v_i - \frac{\partial \sigma_{ji}}{\partial x_j} v_i - \rho f_i v_i &= \mathcal{F}_i v_i \ , \\ \rho \frac{\mathrm{d}}{\mathrm{d}t}\Big(\frac{1}{2} v_i v_i\Big) - \frac{\partial \sigma_{ji} v_i}{\partial x_j} - \rho f_i v_i &= -\sigma_{ji} \frac{\partial v_i}{\partial x_j} + \mathcal{F}_i v_i \ . \end{aligned} \tag{IV.8}$$

The balance of mass is used once more in order to bring the balance of kinetic energy in the following form:

$$\frac{\partial}{\partial t}\Big(\rho \frac{1}{2} v_i v_i\Big) - \frac{\partial}{\partial x_j}\Big(- \rho v_j \frac{1}{2} v_i v_i + \sigma_{ji} v_i\Big) - \rho f_i v_i = -\sigma_{ji} \frac{\partial v_i}{\partial x_j} + \mathcal{F}_i v_i \ , \tag{IV.9}$$

where the right-hand side is the production term. Now by using

$$J_i = \mathcal{J}_i + \rho z v_i \ , \quad E_i = \mathcal{E}_i - \epsilon_{ijk} v_j B_k \ , \tag{IV.10}$$

[77] For a scalar and as a special case for the velocity the total time rate, $\frac{\mathrm{d}(\cdot)}{\mathrm{d}t}$, is equal to the objective time rate, $(\cdot)^{\bullet}$, for a fixed coordinate system, $w_i = 0$.

we can rewrite the final term in the production of kinetic energy,

$$\begin{aligned} \mathcal{F}_i v_i &= \big(\rho z E_i + \epsilon_{ijk} J_j B_k\big) v_i = \\ &= (J_i - \mathcal{J}_i) E_i + \epsilon_{ijk} v_i (\mathcal{J}_j + \rho z v_j) B_k = \\ &= J_i E_i - \mathcal{J}_j (E_j - \epsilon_{ijk} v_i B_k) = J_i E_i - \mathcal{J}_j (E_j + \epsilon_{jik} v_i B_k) = \\ &= J_i E_i - \mathcal{J}_j \mathcal{E}_j \ . \end{aligned} \tag{IV.11}$$

By employing Maxwell's Eq. (III.27)$_2$ and $\epsilon_{ijk} = -\epsilon_{ikj}$ we rewrite the latter,

$$\begin{aligned} \mathcal{F}_i v_i &= \bigg(- \frac{\partial D_i}{\partial t} + \epsilon_{ijk} \frac{\partial H_k}{\partial x_j} \bigg) E_i - \mathcal{J}_i \mathcal{E}_i = \\ &= - \frac{\partial D_i}{\partial t} E_i + \epsilon_{ijk} \frac{\partial H_k E_i}{\partial x_j} - \epsilon_{ijk} H_k \frac{\partial E_i}{\partial x_j} - \mathcal{J}_i \mathcal{E}_i = \\ &= - \frac{\partial D_i}{\partial t} E_i - \epsilon_{ikj} \frac{\partial H_k E_i}{\partial x_j} + H_k \epsilon_{kji} \frac{\partial E_i}{\partial x_j} - \mathcal{J}_i \mathcal{E}_i \ . \end{aligned} \tag{IV.12}$$

After inserting Maxwell's Eq. (III.14) and employing the Maxwell-Lorentz aether relations in Eqs. (III.28) we acquire

$$\begin{aligned} \mathcal{F}_i v_i &= - \frac{\partial D_i}{\partial t} E_i - \frac{\partial (\boldsymbol{E} \times \boldsymbol{H})_j}{\partial x_j} - H_k \frac{\partial B_k}{\partial t} - \mathcal{J}_i \mathcal{E}_i = \\ &= - \frac{1}{2} \frac{\partial \varepsilon_0 E_i E_i}{\partial t} - \frac{\partial (\boldsymbol{E} \times \boldsymbol{H})_j}{\partial x_j} - \frac{1}{\mu_0} B_k \frac{\partial B_k}{\partial t} - \mathcal{J}_i \mathcal{E}_i = \\ &= - \frac{1}{2} \frac{\partial}{\partial t} \Big(\varepsilon_0 E_i E_i + \frac{1}{\mu_0} B_k B_k \Big) - \frac{\partial (\boldsymbol{E} \times \boldsymbol{H})_j}{\partial x_j} - \mathcal{J}_i \mathcal{E}_i = \\ &= - \frac{\partial}{\partial t} \Big(\frac{1}{2} (D_i E_i + H_i B_i) \Big) - \frac{\partial (\boldsymbol{E} \times \boldsymbol{H})_j}{\partial x_j} - \mathcal{J}_i \mathcal{E}_i \ . \end{aligned} \tag{IV.13}$$

The latter is inserted into the balance of kinetic energy in Eq. (IV.9) and we obtain

$$\begin{aligned} \frac{\partial}{\partial t} \Big(\rho \frac{1}{2} v_i v_i + \frac{1}{2} (D_i E_i + H_i B_i) \Big) - \frac{\partial}{\partial x_j} \Big(- \rho v_j \frac{1}{2} v_i v_i - (\boldsymbol{E} \times \boldsymbol{H})_j + \sigma_{ji} v_i \Big) - \\ - \rho f_i v_i = - \sigma_{ji} \frac{\partial v_i}{\partial x_j} - \mathcal{J}_i \mathcal{E}_i \ . \end{aligned} \tag{IV.14}$$

The kinetic energy density has two components, $\rho e^{\text{kin.}} = \rho e^{\text{m.}} + e^{\text{f.}}$, one due to matter and one due to field:

$$\rho e^{\text{m.}} = \rho \frac{1}{2} v_i v_i \ , \quad e^{\text{f.}} = \frac{1}{2} (D_i E_i + H_i B_i) \ . \tag{IV.15}$$

For simplicity we rewrite the balance of kinetic energy as follows

$$\begin{aligned}\frac{\partial}{\partial t}\Big(\rho e^{\text{kin.}}\Big) - \frac{\partial}{\partial x_j}\Big(- v_j(\rho e^{\text{kin.}} - e^{\text{f.}}) - (\boldsymbol{E}\times\boldsymbol{H})_j + \sigma_{ji}v_i\Big) - \rho f_i v_i = \\ = -\sigma_{ji}\frac{\partial v_i}{\partial x_j} - \mathcal{J}_i\mathcal{E}_i \ .\end{aligned} \tag{IV.16}$$

Since $e^{\text{f.}}$ exists even in vacuum (without massive particles) we refrain from introducing a specific energy (energy per mass). The total energy is composed of the kinetic energy (of matter and field) and of internal energy:

$$e = e^{\text{kin.}} + u \ . \tag{IV.17}$$

Hence, we can subtract from the balance of total energy in Eq. (IV.2) the balance of kinetic energy in Eq. (IV.16),

$$\begin{aligned}\frac{\partial}{\partial t}\Big(\rho e - \rho e^{\text{kin.}}\Big) - \frac{\partial}{\partial x_j}\Big(- v_j(\rho e - \rho e^{\text{kin.}} + e^{\text{f.}}) + F_j + (\boldsymbol{E}\times\boldsymbol{H})_j - \sigma_{ji}v_i\Big) - \\ -\rho(s - f_i v_i) = \sigma_{ji}\frac{\partial v_i}{\partial x_j} + \mathcal{J}_i\mathcal{E}_i \ ,\end{aligned} \tag{IV.18}$$

and obtain the balance of internal energy:

$$\frac{\partial \rho u}{\partial t} - \frac{\partial}{\partial x_j}\big(- v_j u - q_j\big) - \rho r = \Gamma \ , \tag{IV.19}$$

with the so-called heat flux, q_i, supply term, r, and production term, Γ,

$$\begin{aligned}-q_j = -v_j e^{\text{f.}} + F_j + (\boldsymbol{E}\times\boldsymbol{H})_j - \sigma_{ji}v_i \ , \\ r = s - f_i v_i \ , \quad \Gamma = \sigma_{ji}\frac{\partial v_i}{\partial x_j} + \mathcal{J}_i\mathcal{E}_i \ .\end{aligned} \tag{IV.20}$$

Especially the heat flux can be chosen differently than herein. Flux of field, $(\boldsymbol{E}\times\boldsymbol{H})_j$, is the radiation transporting heat. A typical example is the heat of the Sun reaching the Earth through the free space. Since the radiation is a heat flux the above definition is possible. However, we could leave out the radiation from the heat flux and continue with a balance of internal energy where its flux is $-q_j + (\boldsymbol{E}\times\boldsymbol{H})_j$. The difference is how we measure the heat flux. If the measurement is done by including the radiation term then the definition used herein is appropriate. After using the balance of mass we obtain

$$\rho\frac{\mathrm{d}u}{\mathrm{d}t} + \frac{\partial q_j}{\partial x_j} - \rho r = \Gamma \ , \tag{IV.21}$$

as we can use the objective and total rates interchangeably for a scalar quantity,

$$\rho u^{\bullet} + \frac{\partial q_i}{\partial x_i} - \rho r = \Gamma = \sigma_{ji}\frac{\partial v_i}{\partial x_j} + \mathcal{J}_i\mathcal{E}_i \ . \tag{IV.22}$$

The primitive variables are $\{\phi, A_i, u_i, T\}$. For the electric potentials, ϕ, A_i, we will use the same equations as in the last section, after utilizing the LORENZ gauge we obtain

$$\frac{\partial \rho z}{\partial t} + \frac{\partial J_i}{\partial x_i} = 0 \ , \quad \varepsilon_0 \frac{\partial^2 A_i}{\partial t^2} - \frac{1}{\mu_0} \frac{\partial^2 A_i}{\partial x_j \partial x_j} = J_i \ , \tag{IV.23}$$

where the total current is

$$J_i = J_i^{\text{fr.}} + \frac{\partial P_i}{\partial t} + \epsilon_{ijk} \frac{\partial \mathcal{M}_k}{\partial x_j} \ , \quad J_i^{\text{fr.}} = \mathcal{J}_i^{\text{fr.}} + \rho z^{\text{fr.}} v_i \ . \tag{IV.24}$$

For the displacement, u_i, we will employ the balance of linear momentum:

$$\rho v_i^{\bullet} - \frac{\partial \sigma_{ji}}{\partial x_j} - \rho f_i = \mathcal{F}_i \ . \tag{IV.25}$$

For the temperature, T, we may utilize the balance of internal energy:

$$\rho u^{\bullet} + \frac{\partial q_i}{\partial x_i} - \rho r = \sigma_{ji} \frac{\partial v_i}{\partial x_j} + \mathcal{J}_i \mathcal{E}_i \ . \tag{IV.26}$$

In order to close these equations we need to determine the constitutive equations, $\mathcal{J}_i$, σ_{ij}, q_i. We start off with the balance of internal energy at the equilibrium state. We decompose the stress tensor into reversible and dissipative terms:

$$\sigma_{ij} = {}^{\text{r}}\sigma_{ij} + {}^{\text{d}}\sigma_{ij} \ , \quad {}^{\text{r}}\sigma_{ij} = -p\delta_{ij} + {}^{\text{e}}\sigma_{ij} \ , \tag{IV.27}$$

where ${}^{\text{e}}\sigma_{ij}$ denotes the elastic stress. We ignore the pressure, p, since its effect is negligibly small for solid bodies. The stress tensor is symmetric for non-polar materials

$$\sigma_{ji} \frac{\partial v_i}{\partial x_j} = \sigma_{ij} d_{ij} = \sigma_{ij} \varepsilon_{ij}^{\bullet} \ , \tag{IV.28}$$

where we have used that the rate of strains is equal to the symmetric part of the velocity gradient, for the sake of brevity we prove this identity in Appendix[76] A.4 on p. 301. We readily restricted the implementation to linearized strains, ε_{ij}, in other words, we assume that the displacements are so small that the deformation gradient is equal to the identity. In order to obtain the equilibrium state and the constitutive equations, we use the method introduced in Section[76] 2.3 on p. 126. For the mechanical equilibrium we utilize the decomposition of stress and identify the dissipative term with the irreversible process such that it has to vanish at equilibrium, ${}^{\text{d}}\sigma_{ij} = 0$. For the thermal equilibrium we introduce the entropy rate density, $\rho\eta^{\bullet}$, as the minus divergence of heat flux per temperature. Moreover, $r = 0$ for the thermal equilibrium. For the electromagnetic equilibrium $\mathcal{J}_i = 0$ holds such that the production term vanishes. The balance of internal energy at equilibrium reads

$$\rho u^{\bullet} - \rho T \eta^{\bullet} = {}^{\text{e}}\sigma_{ij} \varepsilon_{ij}^{\bullet} \ . \tag{IV.29}$$

By using the 1st law of thermodynamics we exchange the rates with differential forms and obtain Gibbs's equation:

$$\begin{aligned} \rho\,\mathrm{d}u &= \rho T\,\mathrm{d}\eta + {}^{\circ}\!\sigma_{ij}\,\mathrm{d}\varepsilon_{ij}\ , \\ \mathrm{d}u &= T\,\mathrm{d}\eta + {}^{\circ}\!\sigma_{ij} v\,\mathrm{d}\varepsilon_{ij}\ . \end{aligned} \tag{IV.30}$$

with the specific volume, $v = 1/\rho$. Obviously, the internal energy depends on the entropy and strain, $u = u(\eta, \varepsilon_{ij})$. In order to acquire a dependence on temperature instead on entropy, we introduce the specific free energy:

$$\begin{aligned} \psi = u - T\eta\ , \quad \mathrm{d}\psi &= \mathrm{d}u - \eta\,\mathrm{d}T - T\,\mathrm{d}\eta\ , \\ \mathrm{d}\psi &= -\eta\,\mathrm{d}T + {}^{\circ}\!\sigma_{ij} v\,\mathrm{d}\varepsilon_{ij}\ . \end{aligned} \tag{IV.31}$$

The specific free energy depends on the temperature and strain, $\psi = \psi(T, \varepsilon_{ij})$, as follows

$$\eta = -\frac{\partial \psi}{\partial T}\ , \quad {}^{\circ}\!\sigma_{ij} v = \frac{\partial \psi}{\partial \varepsilon_{ij}}\ . \tag{IV.32}$$

The dual variables, η and ${}^{\circ}\!\sigma_{ij}$, depend on the same set of state variables such that we obtain

$$\begin{aligned} \mathrm{d}\eta &= A\,\mathrm{d}T + \bar{p}_{ij}\,\mathrm{d}\varepsilon_{ij}\ , \\ \mathrm{d}\,{}^{\circ}\!\sigma_{ij} &= p_{ij}\,\mathrm{d}T + C_{ijkl}\,\mathrm{d}\varepsilon_{kl}\ , \end{aligned} \tag{IV.33}$$

where the coefficients depend on the state space, $A = A(T, \varepsilon_{ij})$, $\bar{p}_{ij} = \bar{p}_{ij}(T, \varepsilon_{ij})$, $p_{ij} = p_{ij}(T, \varepsilon_{ij})$, $C_{ijkl} = C_{ijkl}(T, \varepsilon_{ij})$. Instead of measuring entropy, the heat flux is measured, $\delta Q = T\,\mathrm{d}\eta = c\,\mathrm{d}T$, by a constant strain, $\mathrm{d}\varepsilon_{ij} = 0$. The specific heat capacity, $c = TA$, is determined by varying the temperature and measuring the heat flux. By holding the temperature constant, $\mathrm{d}T = 0$, at a specific temperature the stiffness tensor, C_{ijkl}, is determined by varying strain and measuring stress. We employ the Maxwell symmetry (reciprocal) relation:

$$\bar{p}_{ij} = \frac{\partial \eta}{\partial \varepsilon_{ij}} = -\frac{\partial^2 \psi}{\partial \varepsilon_{ij} \partial T} = -\frac{\partial^2 \psi}{\partial T \partial \varepsilon_{ij}} = -v \frac{\partial\, {}^{\circ}\!\sigma_{ij}}{\partial T} = -v p_{ij}\ , \tag{IV.34}$$

since the mass density and thus the specific volume depends on space and time but not on temperature. We obtain

$$\begin{aligned} \mathrm{d}\eta &= \frac{c}{T}\,\mathrm{d}T - p_{ij} v\,\mathrm{d}\varepsilon_{ij}\ , \\ \mathrm{d}\,{}^{\circ}\!\sigma_{ij} &= p_{ij}\,\mathrm{d}T + C_{ijkl}\,\mathrm{d}\varepsilon_{kl}\ . \end{aligned} \tag{IV.35}$$

The thermal pressure, p_{ij}, can be rewritten by introducing an experiment where temperature is varied and strain is measured, $\mathrm{d}\varepsilon_{ij} = \alpha_{ij}\,\mathrm{d}T$, in order to determine the thermal expansion coefficient, α_{ij}. Since this experiment is realized by holding

stress constant we have from Eq. (IV.35)$_2$

$$\begin{aligned} 0 = p_{ij}\,\mathrm{d}T + C_{ijkl}\,\mathrm{d}\varepsilon_{kl} = p_{ij}\,\mathrm{d}T + C_{ijkl}\alpha_{kl}\,\mathrm{d}T \\ \Rightarrow p_{ij} = -C_{ijkl}\alpha_{kl}\ . \end{aligned} \tag{IV.36}$$

We want to implement a linear material, i.e., all parameters, c, C_{ijkl}, and α_{ij} are constants, in other words, they do not depend on the state variables. In this case we simply integrate from a reference state, $T_{\text{ref.}}$, $\varepsilon_{ij} = 0$, without stress and entropy[78] to the actual state, T, ε_{ij}, and acquire the following constitutive equations:

$$\begin{aligned} \eta &= c\big(\ln(T) - \ln(T_{\text{ref.}})\big) + C_{ijkl}\alpha_{kl}v\varepsilon_{ij} = c\ln\Big(\frac{T}{T_{\text{ref.}}}\Big) + C_{ijkl}\alpha_{kl}v\varepsilon_{ij}\ , \\ {}^{\text{e}}\sigma_{ij} &= -C_{ijkl}\alpha_{kl}(T - T_{\text{ref.}}) + C_{ijkl}\varepsilon_{kl} = C_{ijkl}\big(\varepsilon_{kl} - \alpha_{kl}(T - T_{\text{ref.}})\big)\ . \end{aligned} \tag{IV.37}$$

Now the rate of internal energy density is determined completely

$$\rho u^{\bullet} = \rho T\eta^{\bullet} + {}^{\text{e}}\sigma_{ij}\varepsilon^{\bullet}_{ij}\ , \tag{IV.38}$$

so we can insert the latter into the balance of internal energy in Eq. (IV.26) and obtain

$$\rho T\eta^{\bullet} + \frac{\partial q_i}{\partial x_i} - \rho r = \mathcal{J}_i\mathcal{E}_i + {}^{\text{d}}\sigma_{ij}d_{ij}\ . \tag{IV.39}$$

In this section we set the dissipative stress zero by assuming that the material is only elastic. After a reformulation we obtain the balance of entropy for an unpolarized elastic material:

$$\rho\eta^{\bullet} + \frac{\partial}{\partial x_i}\Big(\frac{q_i}{T}\Big) - \frac{1}{T}\rho r = q_i\frac{\partial}{\partial x_i}\Big(\frac{1}{T}\Big) + \frac{1}{T}\mathcal{J}_i\mathcal{E}_i\ , \tag{IV.40}$$

with the entropy production:

$$\Sigma = q_i\frac{\partial}{\partial x_i}\Big(\frac{1}{T}\Big) + \frac{1}{T}\mathcal{J}_i\mathcal{E}_i = -\frac{q_i}{T^2}\frac{\partial T}{\partial x_i} + \frac{\mathcal{J}_i}{T}\mathcal{E}_i\ , \tag{IV.41}$$

which has to be positive according to the 2$^{\text{nd}}$ law of thermodynamics, $\Sigma \geq 0$. For notational simplicity we again use

$$G_i = \frac{\partial T}{\partial x_i}\ . \tag{IV.42}$$

[78] From a theoretical point of view this assumption is not satisfying. We shall consider $T = 0$ state as the zero state for entropy. At $T = T_{\text{ref.}}$ the entropy is then η_0 and it is unknown. Since we only employ the rate of entropy, the unknown value drops and in the end we reach the same formulation as presented herein. However, for strains the coefficient of thermal expansion, α_{ij}, has been measured by using a reference temperature, which is certainly not 0 K. In simulations we use $T_{\text{ref.}} = 300\,\text{K}$.

By introducing the thermodynamical fluxes:

$$\mathcal{F}^\alpha = \Big\{ -q_i \ , \quad \mathcal{J}_i \Big\} \ , \tag{IV.43}$$

and the thermodynamical forces:

$$\mathcal{K}^\alpha = \Big\{ \frac{G_i}{T^2} \ , \quad \frac{\mathcal{E}_i}{T} \Big\} \ , \tag{IV.44}$$

the 2nd law of thermodynamics reads

$$\Sigma = \mathcal{K}^\alpha \cdot \mathcal{F}^\alpha \geq 0 \ , \quad \alpha = 1, 2 \ , \tag{IV.45}$$

where over α the summation convention is applied. Since both thermodynamical forces are of the same type (tensor of rank one) both thermodynamical fluxes depend on both thermodynamical forces

$$\mathcal{F}^1 = \mathcal{F}^1(\mathcal{K}^1, \mathcal{K}^2) \ , \quad \mathcal{F}^2 = \mathcal{F}^2(\mathcal{K}^1, \mathcal{K}^2) \ . \tag{IV.46}$$

We propose the following relations:

$$-q_i = \lambda \frac{G_i}{T^2} + \gamma \frac{\mathcal{E}_i}{T} \ , \quad \mathcal{J}_i = \beta \frac{G_i}{T^2} + \theta \frac{\mathcal{E}_i}{T} \ . \tag{IV.47}$$

Since the 2nd law has to hold for any process

$$\begin{gathered} -q_i \frac{G_i}{T^2} + \mathcal{J}_i \frac{\mathcal{E}_i}{T} \geq 0 \ , \\ \lambda \frac{G_i G_i}{T^4} + (\gamma + \beta) \frac{G_i \mathcal{E}_i}{T^3} + \theta \frac{\mathcal{E}_i \mathcal{E}_i}{T^2} \geq 0 \ , \end{gathered} \tag{IV.48}$$

and since $T > 0$ we conclude

$$\lambda \geq 0 \ , \quad \gamma + \beta = 0 \ , \quad \theta \geq 0 \ . \tag{IV.49}$$

The first and third relations are obvious, since $G_i G_i \geq 0$ and $\mathcal{E}_i \mathcal{E}_i \geq 0$ for any process. The second relation comes from the fact that $G_i \mathcal{E}_i$ can be positive or negative for different processes. In order to satisfy the 2nd law for any process, we have to restrict $\gamma = -\beta$ such that the second relation vanishes. This restriction is referred to as Onsager's reciprocal relation.[79] By renaming $\kappa = \lambda / T^2$, $\pi = \beta / (T^2 \varsigma)$, and $\varsigma = \theta / T$ we obtain

$$q_i = -\kappa \frac{\partial T}{\partial x_i} + \varsigma \pi T \mathcal{E}_i \ , \quad \mathcal{J}_i = \varsigma \pi \frac{\partial T}{\partial x_i} + \varsigma \mathcal{E}_i \ . \tag{IV.50}$$

[79] In the literature the Onsager relation is motivated by microscopic calculations. Herein we reach the same conclusion by using thermodynamics. Onsager's relations are named after Lars Onsager.

The simplest case occurs if the heat conduction parameter, κ, the electrical conductivity, ς, and the thermoelectric coupling, π, are all constant. The thermoelectric coupling is in V/K and measured by varying temperature and measuring electric field in a conductor. By having $\pi = 0$ we reach the usual FOURIER's and OHM's laws; and realize that these material models are thermodynamically sound relations for materials without thermoelectric coupling. In reality every conductor possesses a thermoelectric coupling. For every conductor even a small temperature gradient induces an electric current. This phenomenon in one conductor is called the THOMSON effect[80] and the same process between two different conductors is called the SEEBECK effect.[81] Basically this effect is used in thermocouples measuring the temperature. Moreover, we can have a heat conduction (thus entropy transport) without temperature difference but just due to an electric field. This process is called the PELTIER effect.[82]

Consider a conductor clamped on one side, which is held fixed at a reference temperature, $T_{\text{ref.}}$. The geometry is simply a beam surrounded by air, we only model the beam. In order to measure the temperature at the free end we connect the conductor to a circuit and measure the potential difference in both ends. This is basically how a thermocouple works and for such a simulation we need weak forms for computing the electric (scalar) potential, ϕ, the magnetic (vector) potential, A_i, the displacement, u_i, and the temperature, T. Since we want to compute the deformation, the LAGRANGEan frame is more appropriate. For the sake of simplicity we neglect the geometrical (and also material) nonlinearities such that the transformation of the balance equations from the current to the reference frame becomes an ease. As the reference frame we choose the initial frame, X_i. Since the geometric nonlinearities are ignored, the mass balance simplifies to $\rho = \rho_0$. Moreover, the volume element in the initial and current frame will be equal, $\mathrm{d}v = \mathrm{d}V$.

For the weak form of electric potential, ϕ, we use the following balance of electric charge in Eq. (IV.23)$_1$ in the initial frame:

$$\frac{\partial \rho_0 z}{\partial t} + J_{i,i} = 0 \ , \quad J_{i,i} = \frac{\partial J_i}{\partial X_i} \ , \tag{IV.51}$$

without geometric nonlinearities. The latter is very similar to Eq. (III.22) such that we follow the same steps and obtain Eq. (III.56). Since we have assumed that $P_i = 0$ and $\mathcal{M}_i = 0$, the weak form in the initial frame for small displacements reads

$$\mathrm{F}_\phi = \int_{\mathcal{B}_0} \big(-(D_i - D_i^0)\delta\phi_{,i} - \Delta t J_i \delta\phi_{,i} \big) \, \mathrm{d}V + \int_{\partial\mathcal{B}_0} N_i \Delta t J_i \delta\phi \, \mathrm{d}A \ , \tag{IV.52}$$

[80] It is called for William Thomson (Lord Kelvin).
[81] It is named after Thomas Johann Seebeck.
[82] This effect is named after Jean Charles Athanase Peltier.

in the unit of energy. The interface between beam and air is simply the boundary satisfying the balance laws on singular surfaces. Air is not modeled, its electric conduction is taken as zero. Zero polarization leads to $J_i^{\text{fr.}} \equiv J_i$ and the electric current is given by

$$J_i = \jmath_i + \rho z v_i \ , \quad \rho z = D_{i,i} \ , \tag{IV.53}$$

where $\jmath_i$ is defined in Eq. (IV.50)$_2$. For computing the magnetic potential, A_i, we start with Eq. (IV.23)$_2$ and transform it from the current to the initial frame by neglecting geometric nonlinearities and acquire

$$\varepsilon_0 \frac{\partial^2 A_i}{\partial t^2} - \frac{1}{\mu_0} A_{i,jj} = J_i \ , \quad A_{i,jj} = \frac{\partial^2 A_i}{\partial X_j \partial X_j} \ . \tag{IV.54}$$

Its weak form is Eq. (III.68). Since polarization is omitted, there remains

$$\mathrm{F}_{\boldsymbol{A}} = \int_{\mathcal{B}_0} \left(\varepsilon_0 \frac{A_i - 2A_i^0 + A_i^{00}}{\Delta t \Delta t} \delta A_i + \frac{1}{\mu_0} A_{i,j} \delta A_{i,j} - J_i \delta A_i \right) \mathrm{d}V \ , \tag{IV.55}$$

in the unit of energy, where $J_i^{\text{fr.}} \equiv J_i$. In the initial frame the velocity equals to the partial derivative of displacement in time, thus,

$$v_i = \frac{\partial u_i}{\partial t} = \frac{u_i - u_i^0}{\Delta t} \ . \tag{IV.56}$$

In order to compute the displacement we use the balance of linear momentum in the initial frame by neglecting geometric nonlinearities:

$$\rho_0 \frac{\partial^2 u_i}{\partial t^2} - \frac{\partial \sigma_{ji}}{\partial X_j} - \rho_0 f_i - \mathcal{F}_i = 0 \ , \quad \mathcal{F}_i = \frac{\partial D_j}{\partial X_j} E_i + \epsilon_{ijk} J_j B_k \ . \tag{IV.57}$$

Hence, we obtain the following weak form in the unit of energy:

$$\begin{aligned} \mathrm{F}_{\boldsymbol{u}} = \int_\Omega \Bigg(& \rho_0 \frac{u_i - 2u_i^0 + u_i^{00}}{\Delta t \Delta t} \delta u_i + \sigma_{ji} \delta u_{i,j} - \rho_0 f_i \delta u_i - \\ & - \mathcal{F}_i \delta u_i \Bigg) \mathrm{d}V - \int_{\partial\Omega} \hat{t}_i \delta u_i \, \mathrm{d}A \ . \end{aligned} \tag{IV.58}$$

The boundaries will vanish for the clamped end by using DIRICHLET conditions and also for the other boundaries by assuming free boundaries, $\hat{t}_i = n_j \sigma_{ji} = 0$. For computing temperature we utilize the balance of entropy in Eqs. (IV.40), (IV.41) in the initial frame without geometric nonlinearities:

$$\begin{aligned} \rho_0 \frac{\partial \eta}{\partial t} + \frac{\partial}{\partial X_i} \left(\frac{q_i}{T} \right) - \frac{1}{T} \rho_0 r = - \frac{q_i}{T^2} \frac{\partial T}{\partial X_i} + \frac{1}{T} \jmath_i \mathcal{E}_i + \frac{1}{T} {}^{\mathrm{d}}\sigma_{ji} \frac{\partial v_i}{\partial X_j} \ , \\ \rho_0 \frac{\partial \eta}{\partial t} + \frac{1}{T} \frac{\partial q_i}{\partial X_i} - \frac{1}{T} \rho_0 r = \frac{1}{T} \jmath_i \mathcal{E}_i + \frac{1}{T} {}^{\mathrm{d}}\sigma_{ji} \frac{\partial v_i}{\partial X_j} \ . \end{aligned} \tag{IV.59}$$

We assume that the deformation is purely elastic, ${}^{\mathrm{d}}\sigma_{ji} = 0$. Hence, the weak form for temperature reads in the unit of energy

$$\begin{aligned} \mathrm{F}_T = \int_\Omega \Big(\rho_0(\eta - \eta^0)\delta T - \Delta t q_i \Big(\frac{\delta T}{T}\Big)_{,i} - \frac{\Delta t}{T}\rho_0 r \delta T - \\ - \frac{\Delta t}{T} \jmath_i \mathcal{E}_i \delta T \Big) \,\mathrm{d}V + \int_{\partial\Omega} \frac{\Delta t}{T} h (T - T_{\text{ref.}}) \delta T \,\mathrm{d}A \ , \end{aligned} \tag{IV.60}$$

where for boundaries we readily applied the natural boundary condition, $q_i N_i = h(T - T_{\text{ref.}})$, with an ambient temperature as equal as the reference and initial temperature. The nonlinear weak form is the sum of all forms above:

$$\text{Form} = \mathrm{F}_\phi + \mathrm{F}_{\boldsymbol{A}} + \mathrm{F}_{\boldsymbol{u}} + \mathrm{F}_T \ , \tag{IV.61}$$

with the following constitutive equations:

$$\begin{gathered} \jmath_i = \varsigma\pi \frac{\partial T}{\partial x_i} + \varsigma \mathcal{E}_i \ , \quad D_i = \varepsilon_0 E_i \ , \quad H_i = \frac{1}{\mu_0} B_i \ , \quad \sigma_{ij} = {}^{\mathrm{e}}\sigma_{ij} + {}^{\mathrm{d}}\sigma_{ij} \ , \\ {}^{\mathrm{e}}\sigma_{ij} = C_{ijkl}\big(\varepsilon_{kl} - \alpha_{kl}(T - T_{\text{ref.}})\big) \ , \quad {}^{\mathrm{d}}\sigma_{ij} = 0 \ , \\ \eta = c \ln\Big(\frac{T}{T_{\text{ref.}}}\Big) + C_{ijkl}\alpha_{kl} v \varepsilon_{ij} \ , \quad q_i = -\kappa \frac{\partial T}{\partial x_i} + \varsigma\pi T \mathcal{E}_i \ , \end{gathered} \tag{IV.62}$$

and

$$\mathcal{E}_i = E_i + \epsilon_{ijk} v_j B_k \ , \quad E_i = -\phi_{,i} - \frac{A_i - A_i^0}{\Delta t} \ , \quad B_i = \epsilon_{ijk} A_{k,j} \ . \tag{IV.63}$$

The material parameters, C_{ijkl}, α_{ij}, κ, c, π, and ς are constant. For an isotropic material the stiffness tensor and coefficients of thermal expansion read

$$C_{ijkl} = \lambda \delta_{ij}\delta_{kl} + \mu \delta_{ik}\delta_{jl} + \mu \delta_{il}\delta_{jk} \ , \quad \alpha_{ij} = \alpha \delta_{ij} \ , \tag{IV.64}$$

by reducing to three materials parameters, viz., the LAME parameters, λ, μ, and the coefficient of thermal expansion, α.

The beam is made out of chromel, which is a nickel and chromium alloy with a relatively large thermoelectric coupling such that it is used as a thermocouple. The temperatures at both ends of the beam are given by DIRICHLET boundary conditions. The beam possesses $T_{\text{ref.}}$ on one end and a linearly increasing temperature on the other end. The temperature difference induces in addition to a thermal flux also an electric flux, i.e., the electric conduction current $\jmath_i$ since $\pi \neq 0$ for chromel material. Therefore, an electric potential difference occurs, see Figs. IV.1. After 30 s the temperature is almost in steady state and the potential difference is approximately 0.3 mV. The magnetic (vector) potential is directed in the same direction (no curl exists) such that magnetic flux vanishes. By measuring the potential difference we can estimate the temperature difference in a real application. Moreover, the body is

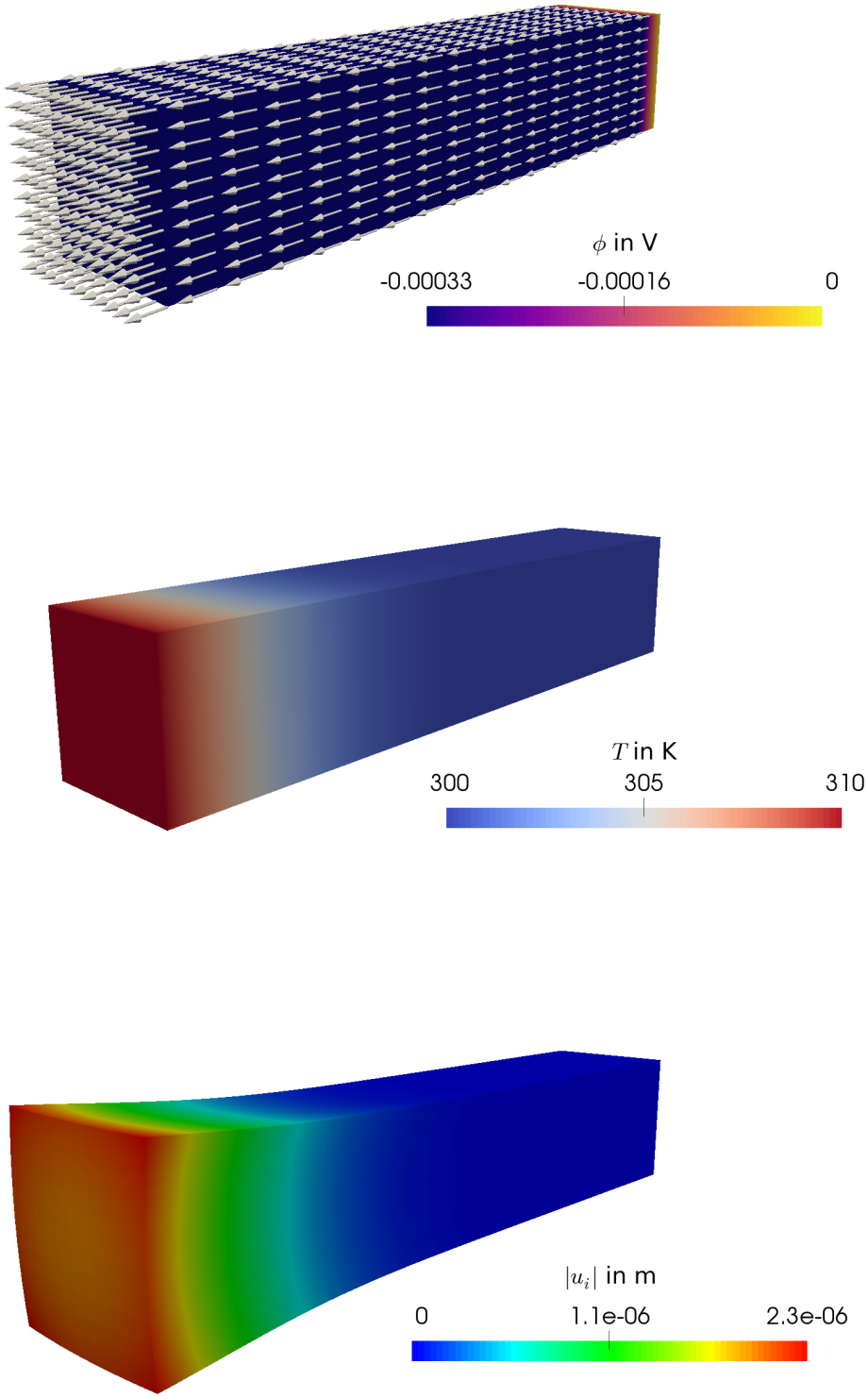

Figure IV.1.: Electric potential, temperature, and displacements after 30 s due to the temperature difference at both ends. Displacements are 2000 times enlarged for a better visualization. Arrows denote the magnetic potential.

a conductor such that in an electric circuit the potential difference implies an electric current. Hence, by using a PELTIER element we can light a bulb due to a temperature difference, however, it is quite inefficient. A PELTIER element is mainly used for measuring the temperature accurately or for tuning the temperature precisely by pumping heat flux in or out of the system. In many devices performing material tests, the control of temperature is established by using PELTIER elements. The following code has been used for the simulation of nonlinear and coupled field equations, where all primitive variables, ϕ, A_i, u_i, T, are solved at once.

```
"""Computational reality 17, thermoelectric coupling"""
__author__ = "B. Emek Abali"
__license__  = "GNU GPL Version 3.0 or later"
#This code underlies the GNU General Public License, http://
    ↪ www.gnu.org/licenses/gpl-3.0.en.html

from fenics import *
import numpy
set_log_level(ERROR)
#units: m, kg, s, A, V, K
delta = Identity(3)
levicivita2 = as_matrix([ (0,1,-1) , (-1,0,1) , (1,-1,0) ])
levicivita3 = as_tensor([ ( (0,0,0),(0,0,1),(0,-1,0) ) , (
    ↪ (0,0,-1),(0,0,0),(1,0,0) ) , ( (0,1,0),(-1,0,0),(0,0,0) ) ])
epsilon = levicivita3

#thermocouple of type E is made of
#chromel (nickel-chromium alloy) and
#is non-magnetic in reality, we also
#assume that it is non-polarizable
resistivity = 0.706E-6 #in Ohm m
varsigma = 1./resistivity #0.625 #in S/m
pi = 68E-6 #V/K
kappa = 19.0 #in W/(m K)
capacity = 390. #in J / (kg K)
alpha = 12.8E-6 #in 1/K
EModul = 186E+9 #in Pa
nu = 0.32
h = 10. #in J / (s m^2 K)

eps_0 = 8.85E-12 #in A s/(V m)
mu_0 = 12.6E-7 #in V s/(A m)

rho0 = 8500. #in kg / m^3
T_ref = 300.0 # K

tMax = 30.0
Dt = 1.0
```

```
37 t = 0.0
38
39 mesh = BoxMesh(Point(-0.05,-0.01,-0.01), Point(0.05,0.01,0.01),
       ↪ 50,10,10)
40 N = FacetNormal(mesh)
41
42 Scalar = FunctionSpace(mesh, 'P', 1)
43 Vector = VectorFunctionSpace(mesh, 'P', 1)
44 Tensor = TensorFunctionSpace(mesh, 'P', 1)
45 #phi, A, u, T
46 Space = MixedFunctionSpace([Scalar,Vector, Vector, Scalar])
47
48 cells = CellFunction('size_t', mesh)
49 facets = FacetFunction('size_t', mesh)
50 dV = Measure('dx', domain=mesh, subdomain_data=cells)
51 dA = Measure('ds', domain=mesh, subdomain_data=facets)
52
53 cells.set_all(0)
54 facets.set_all(0)
55 left = CompiledSubDomain('near(x[0],-0.05) && on_boundary')
56 right = CompiledSubDomain('near(x[0],0.05) && on_boundary')
57 boundaries = CompiledSubDomain('on_boundary')
58
59 #phi, A, u, T
60 bc_T = Expression('T_r + 1.0*time', T_r=T_ref,time=0.)
61 bc01=DirichletBC(Space.sub(0), 0.0, right)
62 bc02=DirichletBC(Space.sub(2), Constant((0.,0.,0.)), right)
63 bc03=DirichletBC(Space.sub(3), T_ref, right)
64 bc04=DirichletBC(Space.sub(3), bc_T, left)
65
66 bc = [bc01,bc02,bc03,bc04]
67
68 dunkn = TrialFunction(Space)
69 test = TestFunction(Space)
70 unkn = Function(Space)
71 unkn0 = Function(Space)
72 unkn00 = Function(Space)
73
74 unkn_init = Expression(('0.','0.','0.','0.','0.','0.','0.','T_r'),
       ↪ T_r=T_ref)
75 unkn00 = interpolate(unkn_init,Space)
76 unkn0.assign(unkn00)
77 unkn.assign(unkn0)
78
79 del_phi,del_A,del_u,del_T = split(test)
80 phi,A,u,T = split(unkn)
81 phi0,A0,u0,T0 = split(unkn0)
```

```
82  phi00,A00,u00,T00 = split(unkn00)
83
84  i, j, k, l = indices(4)
85  delta = Identity(3)
86
87  lam = EModul * nu / (1.+nu) / (1.-2.*nu)
88  mu = 0.5 * EModul / (1.+nu)
89  C = as_tensor(lam*delta[i,j]*delta[k,l] + mu*delta[i,k]*delta[j,l]
        ↪  + mu*delta[i,l]*delta[j,k], (i,j,k,l))
90  alfa = alpha*delta
91
92  eps = sym(grad(u))
93  eps0 = sym(grad(u0))
94  v = as_tensor( (u-u0)[i]/Dt, (i,))
95  E = as_tensor(-phi.dx(i)-(A-A0)[i]/Dt, (i,))
96  E0 = as_tensor(-phi0.dx(i)-(A0-A00)[i]/Dt, (i,))
97  B = as_tensor(epsilon[i,j,k]*A[k].dx(j), (i,))
98  EE = as_tensor(E[i]+epsilon[i,j,k]*v[j]*B[k], (i,))
99
100 D = eps_0*E
101 D0 = eps_0*E0
102 H = 1./mu_0*B
103 JJ = as_tensor( varsigma*pi*T.dx(i) + varsigma*EE[i], (i,))
104 J = as_tensor( JJ[i] + D[j].dx(j)*v[i], (i,))
105 sigma = as_tensor( C[i,j,k,l]*(eps[k,l]-alfa[k,l]*(T-T_ref)), (i,j
        ↪ ))
106 eta = as_tensor( capacity*ln(T/T_ref) + C[i,j,k,l]*alfa[k,l]/rho0*
        ↪ eps[i,j], ())
107 eta0 = as_tensor( capacity*ln(T0/T_ref) + C[i,j,k,l]*alfa[k,l]/
        ↪ rho0*eps0[i,j], ())
108 q = as_tensor(-kappa*T.dx(i)+varsigma*pi*T*EE[i], (i,))
109 FF = as_tensor(D[j].dx(j)*E[i] + epsilon[i,j,k]*J[j]*B[k], (i,))
110 f = Constant((0.,0.,0.))
111 r = Constant(0.0)
112
113 F_phi = (-(D-D0)[i]*del_phi.dx(i) - Dt*J[i]*del_phi.dx(i) )*dV +
        ↪ Dt*J[i]*del_phi*N[i]*dA
114 F_A = (eps_0*(A-2.*A0+A00)[i]/Dt/Dt*del_A[i] + 1./mu_0*A[i].dx(j)*
        ↪ del_A[i].dx(j) - J[i]*del_A[i] )*dV
115 F_u = (rho0*(u-2.*u0+u00)[i]/Dt/Dt*del_u[i] + sigma[j,i]*del_u[i].
        ↪ dx(j) - rho0*f[i]*del_u[i] - FF[i]*del_u[i])*dV
116 F_T = (rho0*(eta-eta0)*del_T - Dt*q[i]*(del_T/T).dx(i) - Dt/T*rho0
        ↪ *r*del_T - Dt/T*JJ[i]*EE[i]*del_T )*dV + Dt/T*h*(T-T_ref)*
        ↪ del_T*dA
117
118 Form = F_phi + F_A + F_u + F_T
119 Gain = derivative(Form, unkn, dunkn)
```

```
120
121 pwd='/calcul/CR17/'
122 file_phi = File(pwd+'phi.pvd')
123 file_A = File(pwd+'A.pvd')
124 file_E = File(pwd+'E.pvd')
125 file_B = File(pwd+'B.pvd')
126 file_u = File(pwd+'u.pvd')
127 file_T = File(pwd+'T.pvd')
128
129 phi_ = Function(Scalar, name='$\phi$')
130 A_ = Function(Vector, name='$A_i$')
131 u_ = Function(Vector, name='$u_i$')
132 T_ = Function(Scalar, name='$T$')
133 E_ = Function(Vector, name='$E_i$')
134 B_ = Function(Vector, name='$B_i$')
135
136 while t < tMax:
137     print 'time: ',t
138     if t <= 10.: bc_T.time = t
139     solve(Form==0, unkn, bc, J=Gain, \
140         solver_parameters={"newton_solver":{"linear_solver": "
            ↪ mumps", "relative_tolerance": 1e-5} }, \
141         form_compiler_parameters={"cpp_optimize": True, "
            ↪ representation": "quadrature", "quadrature_degree":
            ↪ 2}  )
142
143     phi_.assign(unkn.split(deepcopy=True)[0])
144     A_.assign(unkn.split(deepcopy=True)[1])
145     u_.assign(unkn.split(deepcopy=True)[2])
146     T_.assign(unkn.split(deepcopy=True)[3])
147     E_.assign(project(E,Vector))
148     B_.assign(project(B,Vector))
149
150     print '    max. electric potential: ',max(phi_.vector()), ' V'
151     print '    min. electric potential: ',min(phi_.vector()), ' V'
152
153     file_phi << (phi_, t)
154     file_A << (A_, t)
155     file_E << (E_,t)
156     file_B << (B_,t)
157     file_u << (u_, t)
158     file_T << (T_, t)
159
160     unkn00.assign(unkn0)
161     unkn0.assign(unkn)
162     t += Dt
```

To-do

Thermoelectric coupling is discussed and implemented.

- Which equation needs to be changed, if we want to include the polarization?
- Inspect the boundary conditions. Repeat and list the physical meanings of the applied boundary conditions.
- Search for such computations in the literature. Try to find a coupled monolithic solution by using a staggered scheme or by solving all unknowns at once as above.
- Perform a web-based search in order to grasp the different types of PELTIER elements. Find out the crystallographic defects for an n-type and p-type PELTIER element.

References

Abali, B. E. (2017). *Computational Reality, Solving Nonlinear and Coupled Problems in Continuum Mechanics*. Vol. 55. Advanced Structured Materials. Springer. ISBN: 978-981-10-2443-6.

Modeling of power transmission and stress grading for corona protection

The post-print version of the published manuscript:
Zohdi, T. I. & Abali, B. E. (2018). Modeling of power transmission and stress grading for corona protection. Computational Mechanics, 62(3), 411–420.

The final publication is available at Springer via
https://doi.org/10.1007/s00466-017-1504-2

Abstract

Electrical high voltage (HV) machines are prone to corona discharges leading to power losses as well as damage of the insulating layer. Many different techniques are applied as corona protection and computational methods aid to select the best design. In this paper we develop a reduced-order model in 1D estimating electric field and temperature distribution of a conductor wrapped with different layers, as usual for HV-machines. Many assumptions and simplifications are undertaken for this 1D model, therefore, we compare its results to a direct numerical simulation in 3D quantitatively. Both models are transient and nonlinear, giving a possibility to quickly estimate in 1D or fully compute in 3D by a computational cost. Such tools enable understanding, evaluation, and optimization of corona shielding systems for multilayered coils.

1. Introduction

With the invention of power transformer in 1880s, the feasibility of power transmission was greatly increased. Growing demand in electric power motivates researchers for further optimization in power transmission. High voltage (HV) machines generate electric current transported in specially designed cables as alternate current (AC)

or direct current (DC). These HVAC or HVDC transmission mediums have several inefficiencies leading to losses and leakage, which imply an active research and development, see Meah and Ula, 2007, Planas et al., 2015, Chen et al., 2015. Two important issues for HVAC as well HVDC are: high amount of heat produced by the electric current and power loss due to a corona discharge. These phenomena are also related to each other, since the produced heat increases the temperature of the surrounding air, which enhances the ionization leading to corona. The cables are insulated, for example with resin like polypropylene or with a high-dense Kraft paper, and along the surface of this insulation the electric potential varies. If the potential gradient exceeds a material specific threshold value, coronas break down the surface of insulating layer. Therefore, an extra layer is used as corona protection by equalizing the potential gradient.

Corona protection is realized by using a partially-insulating layer wrapped around the insulating layer surrounding the conducting core (copper). Silicon carbide filled resin or inorganic fiber reinforced composite material is used as a semiconductor around the insulator, see Kelen and Virsberg, 1962, Klaussner et al., 2004, Brockschmidt et al., 2013 and the references in T. Zohdi, 2017. Such a material is more efficient as a thermal conductor and also its electrical resistivity increases with an increasing applied electric field (voltage stress), $\boldsymbol{E}$. This corona protection layer can be applied as a lacquer (paint, spray) or tape (band). As outer corona protection or shielding (OCP or OCS), a slightly different coating is used than as end corona protection or shielding (ECP or ECS) along the wire. These different materials used for corona protection are called *stress grading* materials—we use the wording *electric field* instead of *voltage stress*. Such materials are semiconductors; hence, the resistivity depends on temperature as well as on electric field, see Donzel, Greuter, and Christen, 2011, Wheeler et al., 2007.

Different proposals have been used for simulating the system response of power transmission. Maxwell's equations coupled with the balance of energy need to be solved in order to obtain distribution of electromagnetic fields and temperature in the system. With system specific assumptions and simplifications, numerical solutions are presented by several researchers, see Egiziano et al., 1999, Sima et al., 2004, Stefanini et al., 2010, Sharifi, Jayaram, and Cherney, 2010, Weida, Böhmelt, and Clemens, 2010, C. Staubach, Wulff, and Jenau, 2012, Schmidt, Litinsky, and A. Staubach, 2015, Gatzsche et al., 2017.

In this work we propose an efficient reduced-order model in 1D and test its accuracy by using a transient solution of coupled field equations based on finite element method (FEM) in 3D. As a model we use 10 cm×3 cm copper block of 50 cm length, covered with a resin of 1 cm thickness. We decompose it into 3 sections of 10-30-10 cm and use

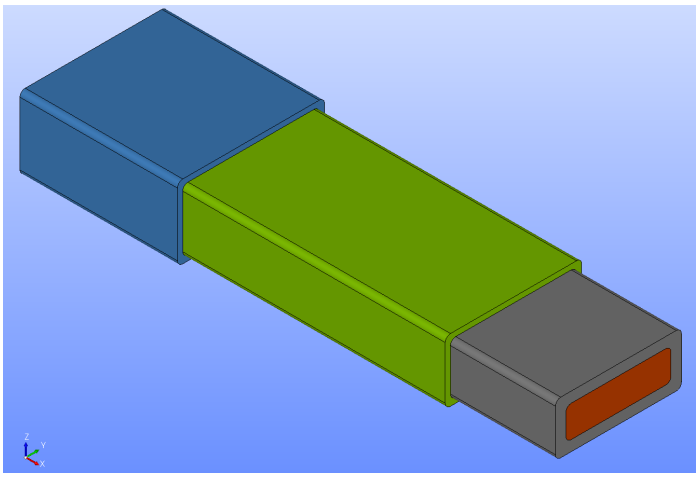

Figure V.1.: Power transmission cable model, copper as core (orange), resin as insulator (gray), OCP (green), and ECP (blue).

at first and second sections OCP and at first section ECP, both 0.5 cm of thickness. All corners are filled with 0.5 cm of radius. The geometry can be depicted in Fig. V.1.

2. Field equations for 1D model problem

The continuum body is modeled as a rigid, unpolarized, and conductive system. Therefore, we need to solve two coupled field equations for computing the electric potential V and the temperature θ. We explain for the one-dimensional system under consideration, a simple but reliable semi-analytic method in order to determine V and θ quickly.

2.1. Current flow

Signal propagation is fast with respect to the motion of electric charge. Hence it is appropriate to assume that at the time an electric charge enters a control volume, another electric charge leaves the control volume such that the total amount of charge remains conserved. It reads

$$+\,(JA)^{-} - (JA)^{+} = 0 \tag{V.1}$$

along Δx and if $\Delta x \to 0$, by using Ohm's law, $J = \sigma E$, we obtain

$$\frac{\mathrm{d}(JA)}{\mathrm{d}x} = \frac{\mathrm{d}(\sigma E A)}{\mathrm{d}x} = 0\ , \tag{V.2}$$

where $A(x)$ is the cross-sectional area, which changes section by section as seen in Fig. V.1. The flow of current can be rewritten by using, $E = -\,\mathrm{d}V/\,\mathrm{d}x$ as follows

$$\frac{\mathrm{d}(JA)}{\mathrm{d}x} = \frac{\mathrm{d}(\sigma E A)}{\mathrm{d}x} = -\frac{\mathrm{d}}{\mathrm{d}x}\Big(\sigma \frac{\mathrm{d}V}{\mathrm{d}x} A\Big) = 0 \ , \tag{V.3}$$

where the voltage is controlled at the ends $V(x=0) = V_0$ and $V(x=L) = V_L$. Hence Eq, V.3 is solved as

$$\begin{aligned} \sigma \frac{\mathrm{d}V}{\mathrm{d}x} A &= c_1 \ , \\ V - V_0 &= c_1 \int_0^x \frac{\mathrm{d}\bar{x}}{\sigma(\bar{x},t)A(\bar{x})} \ , \\ V(x,t) &= V_0 + \frac{V_L - V_0}{\displaystyle\int_0^L \frac{\mathrm{d}\bar{x}}{\sigma(\bar{x},t)A(\bar{x})}} \int_0^x \frac{\mathrm{d}\bar{x}}{\sigma(\bar{x},t)A(\bar{x})} \ . \end{aligned} \tag{V.4}$$

We can simply evaluate for every x by providing the conductivity σ as well as the cross-sectional area A for every section. Concretely, for a beam of 3 sections with lengths L^{I}, L^{II}, L^{III}, such that $L = L^{\mathrm{I}} + L^{\mathrm{II}} + L^{\mathrm{III}}$ we have

$$\int_0^L \frac{\mathrm{d}\bar{x}}{\sigma(\bar{x},t)A(\bar{x})} = \frac{L^{\mathrm{I}}}{\sigma^{\mathrm{I}}A^{\mathrm{I}}} + \frac{L^{\mathrm{II}}}{\sigma^{\mathrm{II}}A^{\mathrm{II}}} + \frac{L^{\mathrm{III}}}{\sigma^{\mathrm{III}}A^{\mathrm{III}}},$$

$$\int_0^x \frac{\mathrm{d}\bar{x}}{\sigma(\bar{x},t)A(\bar{x})} = \begin{cases} \dfrac{x}{\sigma^{\mathrm{I}}A^{\mathrm{I}}} & \text{if } x < L^{\mathrm{I}} \\ \dfrac{L^{\mathrm{I}}}{\sigma^{\mathrm{I}}A^{\mathrm{I}}} + \dfrac{x - L^{\mathrm{I}}}{\sigma^{\mathrm{II}}A^{\mathrm{II}}} & \text{if } x \geq L^{\mathrm{I}} \text{ and } x < L^{\mathrm{I}} + L^{\mathrm{II}} \\ \dfrac{L^{\mathrm{I}}}{\sigma^{\mathrm{I}}A^{\mathrm{I}}} + \dfrac{L^{\mathrm{II}}}{\sigma^{\mathrm{II}}A^{\mathrm{II}}} + \dfrac{x - (L^{\mathrm{I}} + L^{\mathrm{II}})}{\sigma^{\mathrm{III}}A^{\mathrm{III}}} & \text{if } x \geq L^{\mathrm{I}} + L^{\mathrm{II}} \end{cases} \tag{V.5}$$

Every section consists of different layers. The copper core is framed with different layers such as insulator, ECP, OCP. For a section $\alpha \in \{\mathrm{I}, \mathrm{II}, \mathrm{III}\}$ suppose there are $n \in \{1, 2, 3, 4, \dots\}$ layers of different materials. Every layer has an electrical conductivity σ_n and a corresponding cross-section area A_n. Since the electric field is assumed uniform at each cross-section (at a fixed location x), the electric current area density, $\sigma(x,t)E$, over the whole cross-section reads

$$\frac{1}{A(x)} \int_{A(x)} J \ \mathrm{d}A = \frac{1}{A(x)} \sum_{i=1}^{n} J_i A_i = \frac{1}{A(x)} \sum_{i=1}^{n} \sigma_i E A_i \ . \tag{V.6}$$

Thus, we obtain

$$\sigma(x,t) = \frac{1}{A(x)} \sum_{i=1}^{n} \sigma_i A_i \ . \tag{V.7}$$

The effective conductivity of a cross-section is the sum of the individual conductivities multiplied by their share of the cross-sectional area. In each section we have

$$\sigma^\alpha = \frac{1}{A^\alpha}\sum_{i=1}^{n}\sigma_i^\alpha A_i^\alpha \ , \ A^\alpha = \sum_{i=1}^{n} A_i^\alpha \ . \tag{V.8}$$

In each section, the number of layers may vary, $n = n(\alpha)$, which we have omitted in the notation for the sake of brevity.

2.2. Temperature evolution

Analogously, we use the energy conservation within a control volume

$$\rho c\frac{\partial\theta}{\partial t}\Delta V = +(qA)^- - (qA)^+ + aJE\Delta V \ , \tag{V.9}$$

where the volume is $\Delta V = A\Delta x$, c denotes the (constant in each section) specific heat capacity, $q = -\kappa\partial\theta/\partial x$ is the heat flux, and a system specific parameter a models possible losses from the control volume, we set $a = 1$. Dividing both sides by $\rho c\Delta V$ yields

$$\frac{\partial\theta}{\partial t} = \underbrace{\frac{1}{\rho c}\frac{\partial}{\partial x}\Big(\kappa\frac{\partial\theta}{\partial x}\Big) + \frac{JE}{\rho c}}_{\mathcal{F}(x,t)} \ . \tag{V.10}$$

Approximating the time derivative of θ at x and t as

$$\frac{\partial\theta}{\partial t} \approx \frac{\theta(x,t+\Delta t) - \theta(x,t)}{\Delta t} \tag{V.11}$$

we obtain

$$\theta(x,t+\Delta t) = \theta(x,t) + \Delta t\mathcal{F}(x,t) \ . \tag{V.12}$$

For the derivative term inside of $\mathcal{F}$, we approximate

$$\begin{aligned}\frac{\partial}{\partial x}\Big(\kappa\frac{\partial\theta}{\partial x}\Big) &= \frac{\partial}{\partial x}\left(\frac{\kappa(x)}{\Delta x}\left(\theta\Big(x+\frac{\Delta x}{2}\Big) - \theta\Big(x-\frac{\Delta x}{2}\Big)\right)\right)\\ &= \frac{1}{(\Delta x)^2}\left(\kappa\Big(x+\frac{\Delta x}{2}\Big)\Big(\theta(x+\Delta x) - \theta(x)\Big) - \kappa\Big(x-\frac{\Delta x}{2}\Big)\Big(\theta(x) - \theta(x-\Delta x)\Big)\right) \ .\end{aligned} \tag{V.13}$$

2.3. Algorithm

The solution algorithm for the reduced-order model works in 1D. The geometry consists of different parts (layers) such as copper, resin, ECP, and OCP. These layers

have different material properties used for calculating the effective conductivity. In the 1D model we compute electric potential and temperature only within the copper core; however, we present the results on a 3D mesh for the sake of a better visualization.

A line mesh is generated and along that line the electric potential is computed with Eq. (V.4) by using the temperature field from the last time step. Since we have neglected polarization, the electric potential is identical for different layers. Therefore, we can solve for the whole body with one reduced 1D model. After the computation of the electric potential, the temperature distribution is computed with Eq. (V.12) by using the current electric potential. Since JOULE's heat depends on the material coefficient (electrical conductivity), for each of the layer we need to determine the temperature separately as another 1D model. So in each time step we follow the steps:

- Compute the electric potential V along x by using the temperature from the last time step θ^0 (or initial condition),
- Compute J and E with the current value of σ in each layer,
- Compute $\theta(x, t + \Delta t)$ at each node in system,
- Compute $\sigma^*(x, t + \Delta t)$, go to the next time step and repeat.

We solve two 1D equations: one for electric potential and another for temperature. Then we derive electric field and electric current from the solution and combine them in a 3D mesh for a better visualization. The computation is fast; but it may be error prone effected by the various assumptions. First, we assume rigid bodies and neglect dielectric properties of the materials (no polarization). Second, we use a weak coupling in the sense that the temperature and the electric field affect each other with a delay of one time step. Third, we neglect the magnetic potential completely. Fourth, the heat flux is only along x_1 and we ignore a heat exchange with the environment (no losses). These assumptions might lead to inaccuracies. In order to estimate the accuracy of this reduced model, we implement a direct numerical computation in 3D and compare the results of 1D to the results in 3D.

3. Direct numerical FEM calculations

Consider a rigid, polarized continuum body, within which we want to compute the electric potential ϕ, the magnetic potential $\boldsymbol{A}$, and the temperature T as a function

in space $\boldsymbol{x}$ and in time t. We call the list unknowns $\{\phi, \boldsymbol{A}, T\}$ as the primitive variables. The solution of primitive variables has to fulfill the governing equations motivated by balance equations. We very briefly sum up this motivation and present the governing equations, for details we refer to Abali, 2017a, Chap. 3. All fields are expressed in Cartesian coordinates, we apply Einstein's summation convention over repeated indices, and we understand a derivative with respect to x_i by the comma notation $(\cdot)_{,i}$ as a lower index.

The continuum body has an electric charge composed of free and bound charges. Their characteristics differ since the free charges move in macroscopic distances, whereas the bound charges displace in microscopic lengths. We start with the balance of electric charge as well as balance of magnetic flux such that four Maxwell equations are derived. Two of them can be solved by means of the following *ansatz* functions

$$E_i = -\phi_{,i} - \frac{\partial A_i}{\partial t} \ , \quad B_i = \epsilon_{ijk} A_{k,j} \ , \tag{V.14}$$

between electromagnetic fields E_i, B_i and electromagnetic potentials ϕ, A_i up to an arbitrary gauge—because of numerical reasons, we apply the Lorenz gauge. By starting with the balance of electric charge and inserting Maxwell's equations, we obtain

$$\frac{\partial \mathfrak{D}_{i,i}}{\partial t} + \left(J_i^{\text{fr.}} + \epsilon_{ijk} \mathcal{M}_{k,j} \right)_{,i} = 0 \ , \tag{V.15}$$

where the charge potential $\mathfrak{D}_i$ (also called the dielectric displacement) is created by the free electric charges, $J_i^{\text{fr.}}$ denotes the electric current due to the motion of the free electric charges, ϵ_{ijk} is the Levi-Civita symbol being equal to the permutation symbol in Cartesian coordinates, and the magnetic polarization $\mathcal{M}_i$ is the magnetization effected by the bound electric charges. In the case of a rigid body, for $\mathfrak{D}_i$, $J_i^{\text{fr.}}$, and $\mathcal{M}_i$ we apply following constitutive equations:

$$\begin{aligned} &\mathfrak{D}_i = D_i + P_i \ , \quad D_i = \varepsilon_0 E_i \ , \quad P_i = \varepsilon_0 \chi^{\text{el.}} E_i \ , \\ &J_i^{\text{fr.}} = \sigma \pi T_{,i} + \sigma E_i \ , \quad \mathcal{M}_i = \frac{\chi^{\text{mag.}}}{\mu_0 (1 + \chi^{\text{mag.}})} B_i \ , \end{aligned} \tag{V.16}$$

giving the connection to the electric field E_i, the magnetic flux B_i, and the temperature T by means of the universal constants ε_0 and μ_0, as well as the material specific coefficients, namely the electrical conductivity σ, thermoelectric or Peltier's constant π, electric susceptibility $\chi^{\text{el.}}$, and magnetic susceptibility $\chi^{\text{mag.}}$. Electric polarization P_i is due to the bound electric charges. Herein we neglect the magnetoelectric effect such that electric polarization depends only on the electric field, analogously, magnetic polarization depends only on the magnetic flux. For computing the magnetic potential, A_i, we utilize Maxwell's equation and after inserting the Lorenz

gauge, we acquire

$$\varepsilon_0 \frac{\partial^2 A_i}{\partial t^2} - \frac{1}{\mu_0} A_{i,jj} = J_i^{\text{fr.}} + \frac{\partial P_i}{\partial t} + \epsilon_{ijk} \mathcal{M}_{k,j} \ . \tag{V.17}$$

For computing the temperature T, we use the balance of entropy

$$\rho \frac{\partial \eta}{\partial t} + \Phi_{i,i} - \rho \frac{r}{T} = \Sigma \ , \tag{V.18}$$

where the supply term r vanishes in our application, the specific (per mass) entropy η and its flux Φ_i as constitutive equations and the production term Σ read

$$\eta = c \ln\left(\frac{T}{T_{\text{ref.}}}\right) \ , \quad \Phi_i = \frac{q_i}{T} \ , \quad q_i = -\kappa T_{,i} + \sigma \pi T E_i \ , \quad \Sigma = -\frac{q_i}{T^2} T_{,i} + \frac{1}{T} E_i J_i^{\text{fr.}} \ , \tag{V.19}$$

for rigid, polarized, thermal bodies under the assumption that irreversible polarization effects (such as hysteresis) are neglected. The additional material coefficients—specific heat capacity c, thermal conductivity κ—need to be determined for every different material by means of experiments.

The governing Eqs. (V.15), (V.17), (V.18) are coupled and nonlinear. In order to solve them we use finite element method in space and finite difference method in time. For the space discretization we follow the standard variational formulation, namely multiply the governing equations with appropriate test functions and integrate by parts for weakening the continuity condition. The 5 primitive variables $\boldsymbol{p} = \{\phi, A_1, A_2, A_3, T\}$ are approximated as a class C^n function in 5-dimensional Hilbert space,

$$\mathcal{V} = \left\{ \boldsymbol{p} \in [\mathcal{H}^n(\Omega)]^5 : \boldsymbol{p}\big|_{\partial\Omega} = \text{given} \right\} \ , \tag{V.20}$$

where the differentiability properties are included such that it is a Sobolev space. For the sake of simplicity, we omit to emphasize the discrete representations of the analytic functions and use the same symbols henceforth. Furthermore, we use the Galerkin approach and choose test functions from the same space as the primitive variables, whereas the test functions vanish on the Dirichlet boundaries. For the time discretization, we choose the Euler backwards schema. After space and time discretization, we acquire the following weak forms:

$$\begin{aligned}
F_\phi &= \int_\Omega \Big(-(\mathfrak{D}_i - \mathfrak{D}_i^0)\delta\phi_{,i} - \Delta t J_i^{\text{fr.}} \delta\phi_{,i} - \Delta t \epsilon_{ijk} \mathcal{M}_{k,j} \delta\phi_{,i} \Big) \,\mathrm{d}v + \int_{\partial\Omega} n_i \Delta t \epsilon_{ijk} [\![\mathcal{M}_{k,j}]\!] \delta\phi \,\mathrm{d}a \ , \\
F_{\boldsymbol{A}} &= \int_\Omega \left(\varepsilon_0 \frac{A_i - 2A_i^0 + A^{00}}{\Delta t^2} \delta A_i + \frac{1}{\mu_0} A_{i,j} \delta A_{i,j} - J_i^{\text{fr.}} \delta A_i - \frac{P_i - P_i^0}{\Delta t} \delta A_i + \epsilon_{ijk} \mathcal{M}_k \delta A_{i,j} \right) \mathrm{d}v \ , \\
F_T &= \int_\Omega \left(\rho(\eta - \eta^0)\delta T - \Delta t \Phi_i \delta T_{,i} - \Delta t \rho \frac{r}{T} \delta T - \Delta t \Sigma \delta T \right) \mathrm{d}v + \int_{\partial\Omega} \Delta t [\![\Phi_i]\!] \delta T n_i \,\mathrm{d}a \ .
\end{aligned} \tag{V.21}$$

We solve in discrete time steps. Terms with an upper index of zero, $(\cdot)^0$, denote the numerical values from the last time step. The jump brackets, $[\![(\cdot)]\!]$, indicate the difference on a surface between the values determined by the shape functions of adjacent (neighboring) finite elements. The solution fields, namely ϕ, A_i, and T are continuous over the element boundaries; however, the constitutive equations may have jumps across the interface between two different materials. We already applied the well-known jump conditions over the element boundaries by assuming that no surface charges and currents are existing and assuming that the electric current is continuous (along the normal direction n_i), see Abali and Reich, 2017 for details. Assembly over the whole domain give the nonlinear and coupled weak form

$$\text{Form} = F_\phi + F_{\boldsymbol{A}} + F_T \ , \tag{V.22}$$

which is solved after an automatic linearization at the partial differential level by using the novel collection of packages developed under the FEniCS project Logg, Mardal, and Wells, 2012, Logg, Mardal, and Wells, 2011. It is important to distinguish the method used herein from the rich literature for computation of electromagnetism. We use standard finite elements of order one, which is not used for electromagnetism. Starting with Raviart and Thomas, 1977 and Nédélec, 1980, solution of Maxwell's equation are obtained by using mixed elements, for different proposals and implementations, see Bossavit, 1988, Ciarlet Jr and Zou, 1999, Demkowicz, 2006, Sect. 17, Li, 2009, Gillette, Rand, and Bajaj, 2016. Nowadays, there exist several element types, see Arnold and Logg, 2014. Roughly, the overall idea relies on solving electromagnetic fields, E_i and B_i, by satisfying all Maxwell equations. Of course, this strategy is fine; however, by using electromagnetic potentials, ϕ and A_i, it is possible to solve the system by means of standard finite elements, as presented in Abali, 2017a, Chap. 3, Abali and Reich, 2017, Abali, 2017b with various examples. We use the same element type, namely $\mathcal{P}_1$ continuous Lagrange elements of order one for each primitive variable.

4. Material properties

As electrical conductor, nearly always, copper is used, which is a homogeneous and isotropic material at least in the millimeter length-scale. The copper core is surrounded by an insulator in order to avoid arcing. A polymeric type of resin will be modeled. ECP and OCP are particle-functionalized or fiber reinforced composite materials. Owing to the nature of composite character, we need to introduce estimates on the material properties. For every constitutive equation for OCP and ECP, we

use "effective" material constants

$$\begin{aligned}
\langle P_i\rangle_\Omega &= \varepsilon_0\chi^*_{\text{el.}}\langle E_i\rangle_\Omega \ , \\
\langle \mathcal{M}_i\rangle_\Omega &= \frac{\chi_{\text{mag.}}}{\mu_0(1+\chi^*_{\text{mag.}})}\langle B_i\rangle_\Omega \ , \\
\langle J_i^{\text{fr.}}\rangle_\Omega &= -\sigma^*\pi^*\langle T_{,i}\rangle_\Omega + \sigma^*\langle E_i\rangle_\Omega \ , \\
\langle q_i\rangle_\Omega &= -\kappa^*\langle T_{,i}\rangle_\Omega + \sigma^*\pi^*\langle T\rangle_\Omega\langle E_i\rangle_\Omega \ ,
\end{aligned} \tag{V.23}$$

where $(\cdot)^*$ is the effective material parameter of the composite material, $\langle\cdot\rangle_\Omega$ is the volume averaged field with the averaging operator:

$$\langle\cdot\rangle_\Omega \overset{\text{def}}{=} \frac{1}{|\Omega|}\int_\Omega (\cdot)\,\mathrm{d}\Omega \tag{V.24}$$

over a statistically representative volume element with domain Ω. In the following we briefly present how to estimate the effective parameters based on T. Zohdi, 2008, T. I. Zohdi, 2012.

4.1. Determining the effective material parameters

In order to make estimates of the overall properties of the composite, we consider the widely used Hashin–Shtrikman bounds for isotropic materials with isotropic effective responses. These estimates provide one with upper and lower bounds on the overall response of the material. For two isotropic materials with an overall isotropic response, we utilize the following estimates:

$$\underbrace{\sigma_1 + \frac{v_2}{\frac{1}{\sigma_2-\sigma_1} + \frac{1-v_2}{3\sigma_1}}}_{\sigma^{*,-}} \leq \sigma^* \leq \underbrace{\sigma_2 + \frac{1-v_2}{\frac{1}{\sigma_1-\sigma_2} + \frac{v_2}{3\sigma_2}}}_{\sigma^{*,+}}, \tag{V.25}$$

where the conductivity of phase 2 (with volume fraction v_2) is larger than phase 1 ($\sigma_2 \geq \sigma_1$). Usually, v_2 corresponds to the particle material, although there can be applications where the matrix is more conductive than the particles. In that case, v_2 would correspond to the matrix material. Provided that the volume fractions and constituent conductivities are the only known information about the microstructure, the expressions are the tightest bounds for the overall isotropic effective responses for two phase media, where the constituents are both isotropic. A critical observation is that the lower bound is more accurate when the material is composed of high conductivity particles that are surrounded by a low conductivity matrix (denoted case 1) and the upper bound is more accurate for a high conductivity matrix surrounding low conductivity particles (denoted case 2).

This can be explained by considering two cases of material combinations, one with

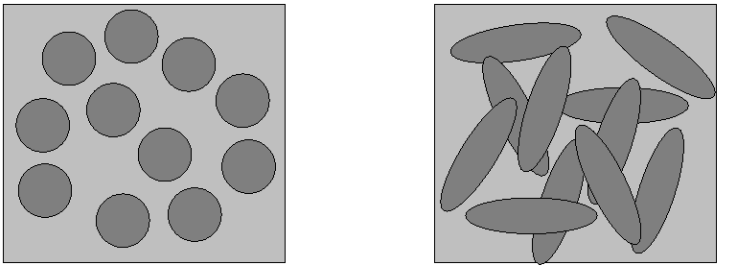

Figure V.2.: Comparing microstructures with the same volume fractions. Flakes touch more, and thus need a higher value of Ψ.

50% low conductivity material and 50% high conductivity material. A material with a continuous low conductivity (fine-scale powder) binder (50%) will isolate the high conductivity particles ((50%), and the overall system will not conduct electricity well (this is case 1 and the lower bound is more accurate), while a material formed by a continuous high conductivity (fine-scale powder) binder (50%) surrounding low conductivity particles (50%, case 2) will, in an overall sense, conduct electricity better than case 1. Thus, case 2 is more closely approximated by the upper bound and case 1 is closer to the lower bound. Since the true effective property lies between the upper and lower bounds, one can construct the following approximation

$$\sigma^* \approx \Psi\sigma^{*,+} + (1-\Psi)\sigma^{*,-}, \tag{V.26}$$

where $0 \leq \Psi \leq 1$ depends on the microstructure and must be calibrated. For high conductivity spherical particles, at low volume fractions, under 15%, where the particles are not in contact, the lower bound is more accurate. Thus, one would pick $\Psi = \Psi^s \leq 0.5$ to bias the estimate to the lower bound. However, using the same setup but replacing the spherical particles with flakes, there is a greater likelihood of connecting flakes, thus producing high-conductivity pathways. Their overall conductivity will be higher than those of sphere at the same volume fraction. Thus, one would pick $\Psi = \Psi^f > \Psi^s$. One can calibrate Ψ by comparing it to different experiments as already done in T. Zohdi, Monteiro, and Lamour, 2002. Essentially, more particle interaction makes the upper bound more relevant. The general trends are (a) for cases where the upper bound is more accurate, $\Psi > \frac{1}{2}$ and (b) for cases when the lower bound is more accurate, $\Psi < \frac{1}{2}$. The parameter Ψ indicates the degree of interaction of the particulate constituents. Analogously, the thermal conductivity has the following bounds:

$$\underbrace{\kappa_1 + \frac{v_2}{\frac{1}{\kappa_2-\kappa_1} + \frac{1-v_2}{3\kappa_1}}}_{\kappa^{*,-}} \leq \kappa^* \leq \underbrace{\kappa_2 + \frac{1-v_2}{\frac{1}{\kappa_1-\kappa_2} + \frac{v_2}{3\kappa_2}}}_{\kappa^{*,+}}. \tag{V.27}$$

such that the effective parameter reads

$$\kappa^* \approx \Psi\kappa^{*,+} + (1-\Psi)\kappa^{*,-} \ . \tag{V.28}$$

In case of other material specific parameters, namely the mass density, the heat capacity, the susceptibilities, we use the volumetric fraction such that the microstructure effect is excluded

$$\begin{aligned} \rho^* &= (1-v_2)\rho_1 + v_2\rho_2 \ , \\ c^* &= (1-v_2)c_1 + v_2c_2 \ , \\ \chi^* &= (1-v_2)\chi_1 + v_2\chi_2. \end{aligned} \tag{V.29}$$

4.2. Nonlinearity due to the material parameters

As pointed out in the Introduction, the heat and electrical conductive material properties of all the materials depend on temperature and electric field. We assume for this dependence the following functional form:

$$\begin{aligned} \sigma &= \sigma_o \exp\Big(-C_1\frac{T-T_{\text{ref.}}}{T_{\text{ref.}}}\Big)\exp\Big(-C_2\frac{\|\boldsymbol{E}\|-E_{\text{ref.}}}{E_{\text{ref.}}}\Big) \ , \\ \kappa &= \kappa_o \exp\Big(-C_3\frac{T-T_{\text{ref.}}}{T_{\text{ref.}}}\Big)\exp\Big(-C_4\frac{\|\boldsymbol{E}\|-E_{\text{ref.}}}{E_{\text{ref.}}}\Big) \ , \end{aligned} \tag{V.30}$$

where $C_\times$ are material constants and $T_{\text{ref.}}$, $E_{\text{ref.}}$ are reference values. For $T_{\text{ref.}}$ we can choose the initial temperature, where no flux or stress arise. For $E_{\text{ref.}}$ we can choose the electric field at the breakdown voltage, at which the insulator becomes partially conductive. The constant σ_o, κ_o is the value at the reference temperature and electric field. For the sake of simplicity we will use $C_3 = C_4 = 0$ providing a constant thermal conductivity.

5. Results and comparison

By using the reduced model and FEM implementation, we solve the system shown in Fig. V.1 out of four different materials for the equal set of boundary conditions. Since the conductivity of copper is high, there is a significant amount of production of entropy due to JOULE's loss, increasing the temperature of the system. For the reduced model we only solve in 1D and visualize in 3D by using the material coefficients compiled in Table V.1.

In the case of FEM implementation, we embed the geometry in air as shown in Fig. V.3. This 3D geometry allows us to set homogeneous far field boundaries, i.e.,

Table V.1.: Material coefficients for the reduced model.

Material	Coefficient	Unit
Copper	$\rho = 8960$	$\mathrm{kg/m^3}$
	$\sigma_o = 5.8 \cdot 10^7$	$\mathrm{S/m}$
	$C_1 = 1$	-
	$C_2 = 0$	-
	$\kappa = 400$	$\mathrm{W/(m\,K)}$
	$c = 390$	$\mathrm{J/(kg\,K)}$
Epoxy resin	$\rho = 1000$	$\mathrm{kg/m^3}$
	$\sigma_o = 1 \cdot 10^{-13}$	$\mathrm{S/m}$
	$C_1 = 0$	-
	$C_2 = 10$	-
	$\kappa = 1.5$	$\mathrm{W/(m\,K)}$
	$c = 800$	$\mathrm{J/(kg\,K)}$
	$E_{\mathrm{ref.}} = 500 \cdot 10^6$	$\mathrm{V/m}$
OCP	$\rho^* = 1100$	$\mathrm{kg/m^3}$
	$\sigma_o^* = 10$	$\mathrm{S/m}$
	$C_1 = 10$	-
	$C_2 = 10$	-
	$\kappa^* = 1$	$\mathrm{W/(m\,K)}$
	$c^* = 1000$	$\mathrm{J/(kg\,K)}$
	$E_{\mathrm{ref.}} = 20 \cdot 10^6$	$\mathrm{V/m}$
ECP	$\rho^* = 3000$	$\mathrm{kg/m^3}$
	$\sigma_o^* = 10^3$	$\mathrm{S/m}$
	$C_1 = 10$	-
	$C_2 = 0$	-
	$\kappa^* = 10$	$\mathrm{W/(m\,K)}$
	$c^* = 700$	$\mathrm{J/(kg\,K)}$

electromagnetic potentials vanish at the outer shell. In addition to Table V.1, we use the material parameters from Table V.2. All material constants are approximate but realistic values. The intention in this work is to test the proposed 1D model against 3D model quantitatively. In the 1D approach we obtain quick results because of several simplifications. One time step lasts approximately 1.5 s on a single core,[83]

[83] Intel Core i7-2600 at 3.4 GHz running on Ubuntu server with Linux 4.4.0-64-generic

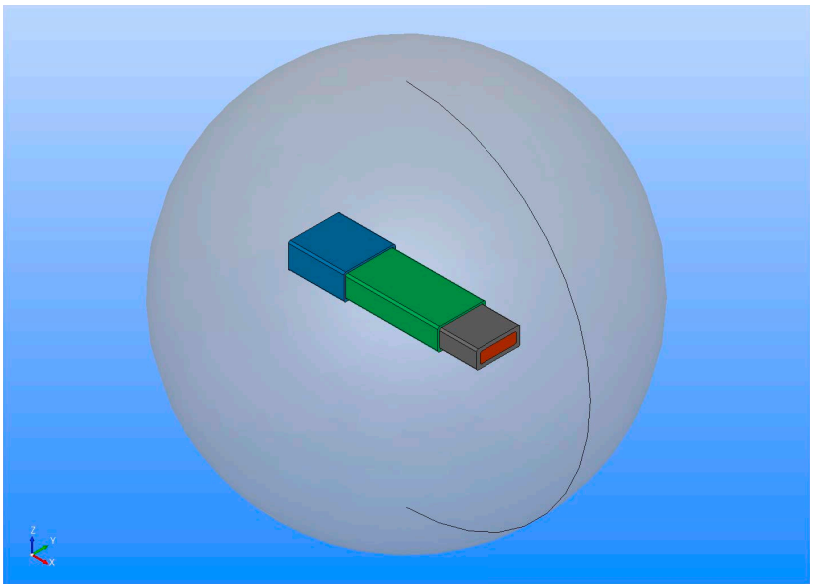

Figure V.3.: Power transmission cable model, copper as core (orange), resin as insulator (gray), OCP (green), and ECP (blue), all embedded in air (transparent).

where most of the computation time is used for projecting on a 3D mesh for the sake of a better visualization. In the 3D model we involve many coupling effects and assume that the result is more accurate than the 1D approach. As expected, 3D modeling takes longer, for a time step approximately 17 min on 6 cores with the same machine. We perform a test example with both approaches and compare them in the following.

Consider a power station of $P = 0.5\,\mathrm{MW}$ where at the beginning of transmission the electric potential is converted to (a relatively low potential difference) $V = 30\,\mathrm{kV}$ at a standard frequency of 50 Hz. The conductor copper possesses the resistance $R = V^2/P$ and the resistivity $r = RA/L$, where the cross-section $A = A^{\mathrm{I}}$ and the total length $L = L^{\mathrm{I}} + L^{\mathrm{II}} + L^{\mathrm{III}}$ are given. The electrical conductivity of copper is exchanged with $\sigma_o = 1/r$ in order to model this phenomenon. In reality, there is an additional resistor restricting the electric current for the circuit. By applying the electric potential of 30 kV sinusoidally on one end and grounding the other end, we compute the electric potential and temperature directly, out of which the electric field and current are derived.

Since the loading is sinusoidal, we present in Fig. V.4 the distribution of potential and electric field at the quarter of a cycle, where the amplitude 30 kV is reached. The complete solution of electromagnetic potentials results in the expected characteristic closed (equipotential) lines. Within the conductor, the magnitude remains nearly constant and a comparison with the reduced model in Fig. V.5 convinces us that

Table V.2.: Additional material coefficients for the FEM model.

Material	Coefficient	Unit
Copper	$\chi^{\text{el.}} = 0$	-
	$\chi^{\text{mag.}} = -1 \cdot 10^{-5}$	-
	$\pi = 68 \cdot 10^{-6}$	V/K
Resin	$\chi^{\text{el.}} = 2$	-
	$\chi^{\text{mag.}} = 0$	-
	$\pi = 0$	V/K
OCP	$\chi^{*}_{\text{el.}} = 5$	-
	$\chi^{*}_{\text{mag.}} = 0$	-
	$\pi^{*} = 0$	V/K
ECP	$\chi^{*}_{\text{el.}} = 10$	-
	$\chi^{*}_{\text{mag.}} = 0$	-
	$\pi^{*} = 0$	V/K
Air	$\rho = 1.2$	kg/m^3
	$\sigma_o = 3 \cdot 10^{-15}$	S/m
	$C_1 = 0$	-
	$C_2 = 0$	-
	$\kappa = 0.0257$	W/(m K)
	$c = 1005$	J/(kg K)
	$\chi_{\text{el.}} = 0$	-
	$\chi_{\text{mag.}} = 0$	-
	$\pi = 0$	V/K

the approximation of 1D model within the conductor has an error up to 4%. It is important to recall that we use an effective conductivity in 1D model introduced in Eq. (V.7). For this specific example the approximation is accurate leading to a precise estimation of the electric current, too. Distribution of electric current and its comparison can be depicted in Fig. V.6. Since the electric potential is computed by using linear finite elements, its derivative leading to electric field and electric current is constant within each elements. In the post-processing, however, the visualization smoothes the fields such that apparent spikes are seen.

The electric conductivity depends on the temperature, which is non-constant in 3D and constant in 1D across the cross-section. Therefore, there is a significant discrep-

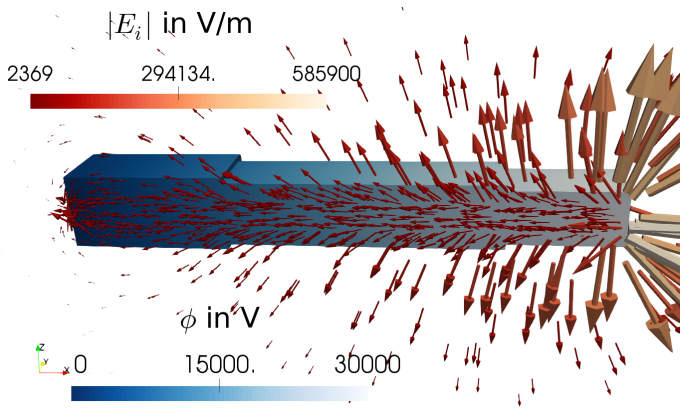

Figure V.4.: At the quarter of a cycle, $t = 0.005\,\mathrm{s}$, distribution of electric potential (colors) and electric field (scaled arrows with colors) are shown.

ancy between the computed magnitude—white arrows represent 3D computation, black arrow is the constant current from 1D model. However, the mean value of 3D solution matches the 1D electric current such that JOULE's heat over the cross-section is nearly identical resulting to a similar temperature evolution, as seen in Fig. V.7 at the end of a period.

We use discontinuous elements for presenting the 1D temperature solution such that the value has a sharp jump across the interface. In 3D model we use continuous elements and hence the interface is modeled depending on the mesh size. This phenomenon is indicated by using a cut on the element boundaries on yz-plane. The temperature difference to initial $T_{\mathrm{ref.}} = 300\,\mathrm{K}$ is accurate within 1% error such that 1D model can be declared as verified for this specific application. In other words, the taken assumptions are admissible for the presented case. Polarization can be spared since the effective conductivity is approximating the electric potential distribution accurately. The weak coupling between the temperature and electric field is appropriate, because the instantaneous evolution of the electric field generates the same amount of heat over the whole conductor. Temperature conduction over the cross-section can be omitted as long as the cooling over the boundary becomes important for the application. In other words, we miss the effect of heat exchange with the environment. For studying the consequences, we perform another simulation only with the 1D model for 1000 cycles and present the electric field for the first 5 cycles and temperature over time in Fig. V.8. Even after 1000 cycles meaning 20 s, the temperature fails to reach a steady state. This phenomenon is indeed due to the lack of heat exchange in 1D model. Owing to the computational cost, 3D modeling is not feasible. For a concrete application, a correction factor to JOULE's heat—the system specific parameter a in Eq. (V.9)—can be introduced amending the temperature rise over time by simulating once with 3D model. For encouraging further studies, we make all codes publicly available in Abali, 2013 to be used under the GNU Public

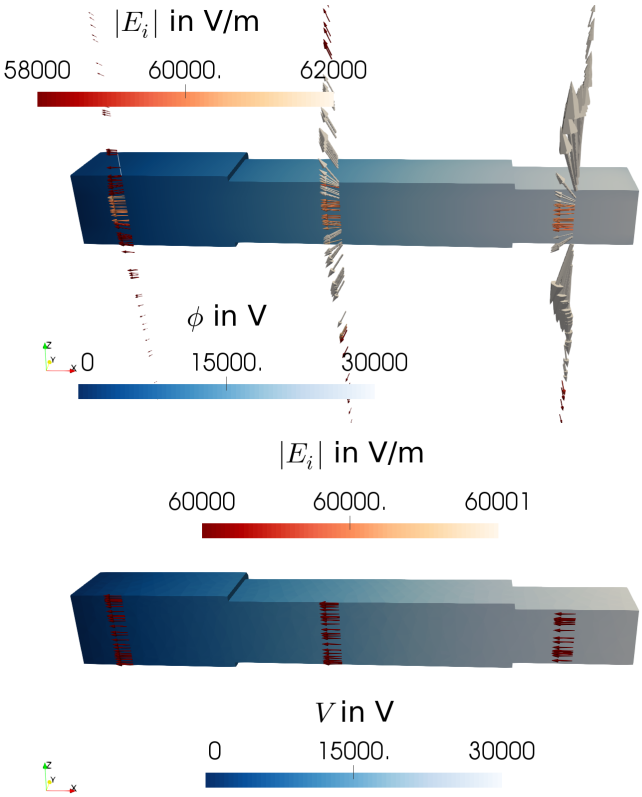

Figure V.5.: At the quarter cycle, $t = 0.005\,\mathrm{s}$, electric potential distribution (colors), electric field from 3D model (top) as well as from 1D (bottom) with scaled and colored arrows on different slices are shown.

license as written in Gnu GPL, 2007.

6. Conclusion

In HV machines, corona discharge is seen as one of the main reasons of power losses. Efficient corona protection is of paramount importance and computational methods help to propose a new design or to amend existing designs. An electromagnetic simulation of part of a transmission is possible in 3D with all electrodynamics and coupling phenomena. However, such an analysis is computationally costly such that reduced-order models are used in the industry. We have developed a 1D model under several assumptions and verified their admissibility through a single run of a 3D model. The computed variables (electric potential and temperature) are compared, as well as the derived variables such as electric field, electric current are studied. The reduced-order model involving material nonlinearities performs an excellent estimation of the transient simulation for a very specific but realistic design. One deficiency and a possible

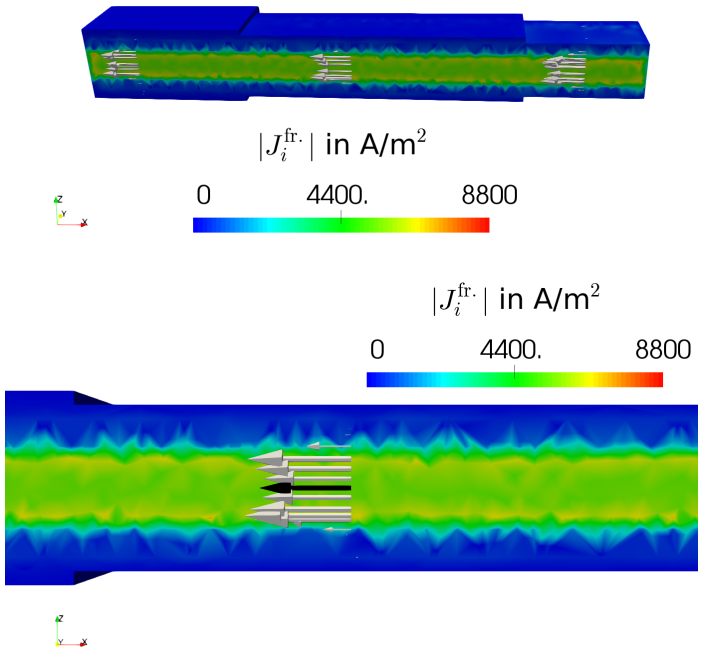

Figure V.6.: At the quarter cycle, $t = 0.005\,\text{s}$, electric current is shown. Top: magnitude in colors and scaled arrows in white from 3D model. Bottom: additionally 1D solution as black arrow (equally scaled) as representing the constant current along the cross-section.

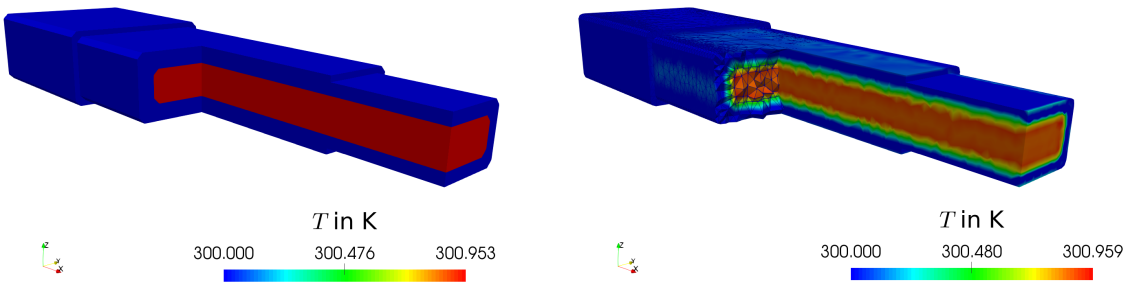

Figure V.7.: Temperature distribution obtained from 1D (left) and 3D (right) solutions, shown at the end of a loading cycle at 50 Hz, i.e., $t = 0.02\,\text{s}$.

correction is discussed. Codes are made publicly available for continuation of similar efforts for concrete geometries and conditions.

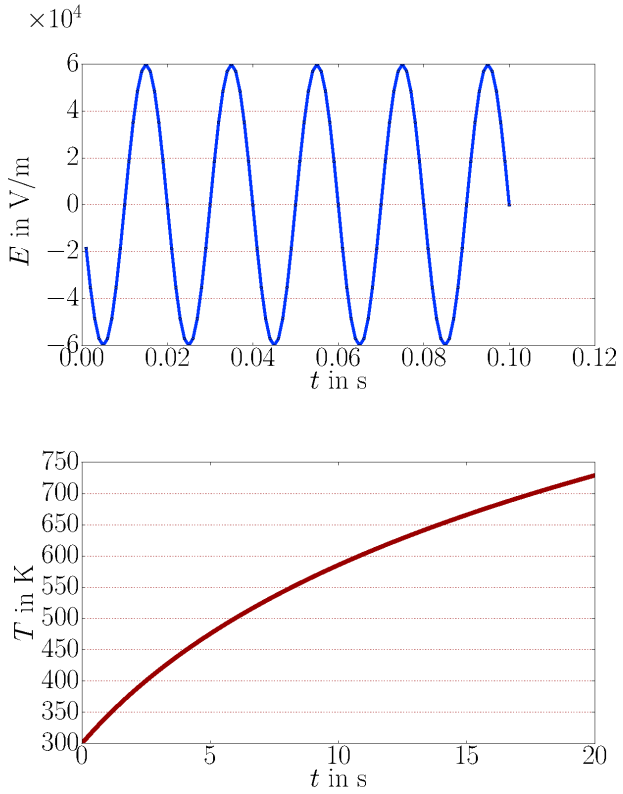

Figure V.8.: Temperature and electric field change over time under the excitation at 50 Hz. Top: electric field in 5 cycles. Bottom: temperature in 1000 cycles.

Acknowledgements

T. Zohdi gratefully acknowledges the generous support of the Siemens corporation during the course of this research. B. E. Abali's work was supported by a grant from the Max Kade Foundation to the University of California, Berkeley.

References

Abali, B. E. (2013). *Supply code, Computational Reality, Technical University of Berlin, Institute of Mechanics, Chair of Continuum Mechanics and Material Theory*. http://www.lkm.tu-berlin.de/ComputationalReality/.

Abali, B. E. (2017a). *Computational Reality, Solving Nonlinear and Coupled Problems in Continuum Mechanics*. Vol. 55. Advanced Structured Materials. Springer. ISBN: 978-981-10-2443-6.

Abali, B. E. and Reich, F. A. (2017). „Thermodynamically consistent derivation and computation of electro-thermo-mechanical systems for solid bodies.“ In: *Computer Methods in Applied Mechanics and Engineering* 319, pp. 567–595. ISSN: 0045-7825.

Abali, B. E. (2017b). „Computational study for reliability improvement of a circuit board.“ In: *Mechanics of Advanced Materials and Modern Processes* 3.1, p. 11.

Arnold, D. N. and Logg, A. (2014). „Periodic table of the finite elements.“ In: *SIAM News* 47.9.

Bossavit, A. (1988). „Whitney forms: A class of finite elements for three-dimensional computations in electromagnetism.“ In: *IEE Proceedings A (Physical Science, Measurement and Instrumentation, Management and Education, Reviews)* 135.8, pp. 493–500.

Brockschmidt, M., Gröppel, P., Pohlmann, F., Rohr, C., and Röding, R. (2013). *Material for insulation system, insulation system, external corona shield and an electric machine*. US Patent App. 14/386,261.

Chen, G., Hao, M., Xu, Z., Vaughan, A., Cao, J., and Wang, H. (2015). „Review of high voltage direct current cables.“ In: *CSEE Journal of Power and Energy Systems* 1.2, pp. 9–21.

Ciarlet Jr, P. and Zou, J. (1999). „Fully discrete finite element approaches for time-dependent Maxwell's equations.“ In: *Numerische Mathematik* 82.2, pp. 193–219.

Demkowicz, L. (2006). *Computing with hp-adaptive finite elements: volume 1 one and two dimensional elliptic and Maxwell problems*. CRC Press.

Donzel, L., Greuter, F., and Christen, T. (2011). „Nonlinear resistive electric field grading Part 2: Materials and applications.“ In: *IEEE Electrical Insulation Magazine* 27.2.

Egiziano, L., Tucci, V., Petrarca, C., and Vitelli, M. (1999). „A Galerkin model to study the field distribution in electrical components employing nonlinear stress grading materials.“ In: *IEEE Transactions on dielectrics and electrical insulation* 6.6, pp. 765–773.

Gatzsche, M., Lücke, N., Großmann, S., Kufner, T., and Freudiger, G. (2017). „Evaluation of Electric–Thermal Performance of High-Power Contact Systems With the Voltage–Temperature Relation.“ In: *IEEE Transactions on Components, Packaging and Manufacturing Technology* 7.3, pp. 317–328.

Gillette, A., Rand, A., and Bajaj, C. (2016). „Construction of scalar and vector finite element families on polygonal and polyhedral meshes.“ In: *Computational Methods in Applied Mathematics* 16.4, pp. 667–683.

Gnu GPL (2007). *Gnu Gpl—the GNU General Public License*. http://www.gnu.org/copyleft/gpl.html.

Kelen, A. and Virsberg, L.-G. (1962). *Coating for equalizing the potential gradient along the surface of an electric insulation.* US Patent 3,066,180.

Klaussner, B., Meyer, C., Muhrer, V., Maurer, A., Russel, C., and Schafer, K. (2004). *Corona shield, and method of making a corona shield.* US Patent App. 11/014,631.

Li, J. (2009). „Numerical convergence and physical fidelity analysis for Maxwell's equations in metamaterials." In: *Computer Methods in Applied Mechanics and Engineering* 198.37, pp. 3161–3172.

Logg, A., Mardal, K. A., and Wells, G. N. (2011). *Automated Solution of Differential Equations by the Finite Element Method, The FEniCS Book.* Vol. 84. Lecture Notes in Computational Science and Engineering. Springer.

Logg, A., Mardal, K. A., and Wells, G. N. (2012). *Automated solution of differential equations by the finite element method, the FEniCS book.* Vol. 84. Lecture Notes in Computational Science and Engineering. Springer. ISBN: 978-3-642-23098-1.

Meah, K. and Ula, S. (2007). „Comparative evaluation of HVDC and HVAC transmission systems." In: *Power Engineering Society General Meeting, 2007. IEEE.* IEEE, pp. 1–5.

Nédélec, J.-C. (1980). „Mixed finite elements in $\mathbb{R}^3$." In: *Numerische Mathematik* 35.3, pp. 315–341.

Planas, E., Andreu, J., Gárate, J. I., Alegría, I. M. de, and Ibarra, E. (2015). „AC and DC technology in microgrids: A review." In: *Renewable and Sustainable Energy Reviews* 43, pp. 726–749.

Raviart, P.-A. and Thomas, J.-M. (1977). „A mixed finite element method for 2-nd order elliptic problems." In: *Mathematical aspects of finite element methods.* Springer, pp. 292–315.

Schmidt, G., Litinsky, A., and Staubach, A. (2015). „Enhanced calculation and dimensioning of outer corona protection systems in large rotating machines." In: *International Symposium on High Voltage Engineering.*

Sharifi, E., Jayaram, S., and Cherney, E. (2010). „A coupled electro-thermal study of the stress grading system of medium voltage motor coils when energized by repetitive fast pulses." In: *Electrical Insulation (ISEI), Conference Record of the 2010 IEEE International Symposium on.* IEEE, pp. 1–4.

Sima, W., Espino-Cortes, F. P., Cherney, E. A., and Jayaram, S. H. (2004). „Optimization of corona ring design for long-rod insulators using FEM based computational analysis." In: *Electrical Insulation, 2004. Conference Record of the 2004 IEEE International Symposium on.* IEEE, pp. 480–483.

Staubach, C., Wulff, J., and Jenau, F. (2012). „Particle swarm based simplex optimization implemented in a nonlinear, multiple-coupled finite-element-model for stress

grading in generator end windings.“ In: *Optimization of Electrical and Electronic Equipment (OPTIM), 2012 13th International Conference on*. IEEE, pp. 482–488.

Stefanini, D., Seifert, J., Clemens, M., and Weida, D. (2010). „Three dimensional FEM electrical field calculations for EHV composite insulator strings.“ In: *Power Modulator and High Voltage Conference (IPMHVC), 2010 IEEE International*. IEEE, pp. 238–242.

Weida, D., Böhmelt, S., and Clemens, M. (2010). „Design of ZnO microvaristor end corona protection for electrical machines.“ In: *Electrical Insulation (ISEI), Conference Record of the 2010 IEEE International Symposium on*. IEEE, pp. 1–4.

Wheeler, J., Gully, A., Baker, A., and Perrot, F. (2007). „Thermal performance of stress grading systems for converter-fed motors.“ In: *IEEE Electrical Insulation Magazine* 23.2, pp. 5–11.

Zohdi, T. I. (2012). *Electromagnetic properties of multiphase dielectrics: a primer on modeling, theory and computation*. Vol. 64. Springer Science & Business Media.

Zohdi, T. (2008). „On the computation of the coupled thermo-electromagnetic response of continua with particulate microstructure.“ In: *International journal for numerical methods in engineering* 76.8, pp. 1250–1279.

Zohdi, T. (2017). „Modeling and rapid simulation of the propagation and multiple branching of electrical discharges in gaseous atmospheres.“ In: *Computational Mechanics*, pp. 1–11.

Zohdi, T., Monteiro, P., and Lamour, V. (2002). „Extraction of elastic moduli from granular compacts.“ In: *International journal of fracture* 115.3, pp. 49–54.

Kapitel VI

Computational study for reliability improvement of a circuit board

The post-print version of the published manuscript:
Abali, B. E. (2017). Computational study for reliability improvement of a circuit board. Mechanics of Advanced Materials and Modern Processes, 3(1), 11.

The final publication is available at Springer via https://doi.org/10.1186/s40759-017-0024-2

Abstract

An electronic device consists of electronic components attached on a circuit board. Reliability of such a device is limited to fatigue properties of the components as well as of the board. Printed circuit board (PCB) consists of conducting traces and vertical interconnect access (via) out of copper embedded in a composite material. Usually the composite material is fiber reinforced laminate out of glass fibers and polyimid matrix. Different reasons play a role by choosing the components of the laminate for the board, one of them is its structural strength and fatigue properties. An improvement of board's lifetime can be proposed by using computational mechanics. In this work we present the theory and computation of a simplified one layer circuit board conducting electrical signals along its copper via, producing heat that leads to thermal stresses. Such stresses are high enough to perform a plastic deformation. Although the plastic deformation is small, subsequent use of the electronic device causes accumulating plastic deformation, which ends the lifetime effected by a fatigue failure in the copper via. Computer simulations provide a convenient method for understanding the nature of this phenomenon as well as predicting the lifetime. We present a coupled and monolithic way for solving the multiphysics problem of this electro-thermo-mechanical system, numerically, by using finite element method in space and finite difference method in time.

1. Introduction

Materials fail due to different phenomena, in general, we can distinguish a monotonic loading from a cyclic loading. The first type of failure is caused by a monotonic loading, where the forces trespass the ultimate strength of the material. This failure is determined by utilizing a uniaxial tensile test. The ultimate strength value is a material specific threshold such that any design remaining below that threshold can be verified as being "safe." The second failure mechanism appears under a cyclic loading. Although the amplitude of the loading is small enough that the design shall be "safe," the material fails due to fatigue. The determination of a material specific threshold value in the case of fatigue is challenging. Often, experiments are used to find a lifetime for one single design and this threshold is assumed to hold for small design changes tested by means of computations. Prediction of lifetime for printed circuit boards (PCBs) is discussed heavily in the literature, see for example Solomon, 1991; Ridout and Bailey, 2007; Roellig et al., 2007; Atli-Veltin et al., 2012; Abali, Reich, and Müller, 2014; Abali, Lofink, and Müller, 2014; Kpobie et al., 2016.

Considering electronic devices, the fatigue failure occurs more frequently under cyclic loadings. In a daily use of an electronic device, we switch some transistors on and off such that heat is produced on the component and traces as well as vias (wires conducting electric signals). This heat increases the temperature of the circuit board. As a consequence, copper and the composite material try to expand differently—regarding their coefficients of thermal expansion—so-called thermal stresses occur. Unfortunately, such stresses are higher than the yield stress such that plastic deformation is induced. Since the produced heat escapes the device by an active or passive cooling, the electronic device tries to shrink or expand to its original shape. Due to the plastic deformation, this shape change generates stresses again. Hence a cyclic loading implies a plastic deformation in each cycle. The plastic deformation is irreversible and in each cycle the amount of plastic deformation accumulates. Sooner or later, there appear cracks caused by fatigue. In order to prevent these cracks, we may try to match the constants of thermal expansion of wire and composite material. Therefore, a possible improvement of fatigue properties in a circuit board relies on the choice of the composite material. In this study we investigate a non-conventional composite material and its effect to the reliability of the circuit board by using computation of thermo-electro-mechanical simulations.

Reliability tests of PCBs are performed in the design process. In order to accelerate the tests, electronic devices are placed in an oven and temperature in the oven is changed periodically by a given frequency and amplitude. Since the board is thin and metal components have a high thermal conductivity, a nearly homogeneous temperature distribution occurs. There is a significant amount of know-how for thermal

reliability tests and manufacturers are using their own calibrated tests, i.e., choice of frequency and amplitude. In order to obtain results as quick as possible, the oven achieves more than 100 K in less than a minute, which is not only technologically challenging; but also costly. Another method is much more easier and is sometimes called an *active* reliability test. An electric potential difference is applied such that an electric current produces JOULE's heat leading to the temperature change. According to the free or forced convection, the necessary temperature differences in similar frequencies can be achieved. There are still some drawbacks and a lack of a comprehensive analysis of active tests. Computational methods can be fruitful for getting a better understanding and suggesting newer methods or design amendments. In this work we present the method of solving a coupled thermo-electro-mechanical system with open-source packages developed under the FEniCS project, see Logg, Mardal, and Wells, 2012; Logg, Mardal, and Wells, 2011. Coupled and nonlinear partial differential equations can be solved monolithically by using research codes, for example FEniCS. Commercial programs are not capable to perform such tasks, at least at the time when this work was established. In order to demonstrate the strength of such computation, we perform an active reliability test for different laminate materials and compare then. We deliver the codes applied on a single thru hole via on PCB with different materials used for the board. Different materials as well as geometries can easily be applied by using the code in Abali, 2013 under the GNU Public license Gnu GPL, 2007.

2. Methods

We follow closely Abali, 2017, Sect. 3.4 and outline herein the theory as well as the method of computation very briefly. The objective is to simulate an unpopulated circuit board consisting of one thru hole via. Copper via is a conductor and is embedded in the composite, which is an insulator. In order to set the ideas, consider Fig. VI.1. The board is clamped on the four chamfer faces. As in a real experiment, we can set the electric potential, ϕ in V(olt), on the ends of the via at front and back faces (on yz-planes) of the board. The electric potential difference creates an electric field, E_i in V/m(eter), leading to an electric current, $\jmath_i$ in A(mpere)/m^2, measured on the material frame. In other words, this current is the effective motion of charges with respect to the continuum body. Independently, the body can have a motion such as deformation, too. A deformation of the material is observed with respect to the laboratory frame. The electric current in the laboratory frame is given by

$$J_i = \jmath_i + v_i \rho z \ , \tag{VI.1}$$

where ρ denotes the mass density in k(ilo)g(ram)/m^3, z the specific charge in C(oulomb)/kg, and v_i the velocity of the continuum body as rate of displacement,

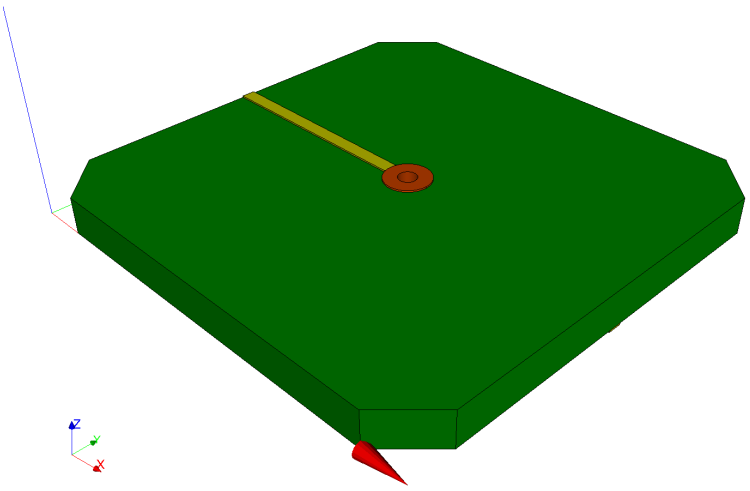

Figure VI.1.: *CAD model of a single via on a circuit board.* Composite board (green) embeds a copper trace (yellow) and a thru hole via (brown).

$v_i = u_i^{\bullet}$. Strictly speaking, the formulation is in the reference placement; however, by assuming small deformations we refrain from distinguishing between reference and current placement. Since the formulation is in the reference placement, the time rate $(\cdot)^{\bullet}$ is simply the partial time derivative. We search for the displacement, u_i, effected by the electric potential set on each end of the via. Concretely, we set one end zero (grounded); on the other end we apply a harmonic excitation with a relatively low frequency, thus, it is appropriate to presuppose that the magnetic potential is negligibly small, $A_i = 0$, no magnetic flux emerges. Then the electric field is given by the electric potential

$$E_i = -\phi_{,i} \ . \tag{VI.2}$$

A comma denotes a partial differentiation in space. The electric potential ϕ needs to satisfy the balance of electric charge:

$$\frac{\partial \rho z}{\partial t} + J_{i,i} = 0 \ , \tag{VI.3}$$

where and throughout the paper we understand the Einstein summation convention over doubly repeated indices. We can reformulate the balance of electric charge. By using Maxwell's equation:

$$\rho z = D_{i,i} \ , \tag{VI.4}$$

with the charge potential (electric displacement) D_i in $\mathrm{C/m^2}$, we acquire

$$\frac{\partial D_{i,i}}{\partial t} + J_{i,i} = 0 \ . \tag{VI.5}$$

This governing equation will be used to compute the electric potential. Copper is a conductor so we can neglect its electric polarization. Composite board may exhibit

an electric polarization, for the sake of brevity, we neglect this, too. We assume that both materials for the printed circuit board are unpolarized. We will discuss the connection between charge potential, electric charge, and electric potential for unpolarized materials in the next section.

The electric current—flowing along the conducting trace and via—produces energy that alters temperature. Temperature distribution will be computed by satisfying the balance of entropy:

$$\rho\eta^{\bullet} + \Phi_{i,i} - \rho\frac{r}{T} = \Sigma \ , \tag{VI.6}$$

where the specific (per mass) entropy, η, its flux term, Φ_i, and its production term, Σ, needs to be defined. The entropy supply is given by the so-called radiant heat r, which is known. It is the term changing the temperature volumetrically, for example, in a microwave oven or in the case of a laser beam, r is the irradiated power of the oven or laser. For the printed circuit board, such a term is not supplied, $r = 0$. After a careful study for unpolarized materials in Abali, 2017, Sect. 3.3, we know that we may select the entropy flux and define the entropy production as

$$\Phi_i = \frac{q_i}{T} \ , \quad \Sigma = -\frac{q_i}{T^2}T_{,i} + \frac{1}{T}\jmath_i E_i + \frac{1}{T}\sigma_{ij}\,{}^{\mathrm{p}}\varepsilon^{\bullet}_{ij} \ . \tag{VI.7}$$

Heat flux, q_i, and stress, σ_{ij}, will be defined in the next section. The plastic strain ${}^{\mathrm{p}}\varepsilon_{ij}$ comes from the small deformation plasticity, where the the total strain is decomposed additively into a reversible as well as irreversible (plastic) part

$$\varepsilon_{ij} = {}^{\mathrm{r}}\varepsilon_{ij} + {}^{\mathrm{p}}\varepsilon_{ij} \ . \tag{VI.8}$$

By assuming small strains we can use the linear strain measure:

$$\varepsilon_{ij} = \frac{1}{2}(u_{i,j} + u_{j,i}) \ , \tag{VI.9}$$

where u_i denotes the displacement field to be computed. Definition of the plastic strain will be given in the next section. Now we have found out the governing equation for the temperature,

$$\rho\frac{\partial\eta}{\partial t} + \left(\frac{q_i}{T}\right)_{,i} = \Sigma \ . \tag{VI.10}$$

Initially the temperature is set at the so-called *reference* temperature of 300 K. Any deviation from the reference temperature induces a stress, which will be implemented via constitutive equations in the next section.

Induced stress causes a deformation. We search for displacements leading to that deformation. The stress, σ_{ji}, is the momentum flux in the balance of linear momen-

tum:

$$\rho v_i^{\bullet} - \sigma_{ji,j} - \rho f_i = \mathcal{F}_i \ , \tag{VI.11}$$

where the specific body force f_i is given—gravitational acceleration is a specific body force—and the production term $\mathcal{F}_i$ defines the interaction with the electromagnetic forces. For the application that we want to study, the gravitational forces have a negligible effect, so we simplify the system by setting $f_i = 0$. For unpolarized systems, the production term is the LORENTZ force density:

$$\mathcal{F}_i = \rho z E_i + (\boldsymbol{J} \times \boldsymbol{B})_i = D_{j,j} E_i \ , \tag{VI.12}$$

since we have assumed that the magnetic flux vanishes, $B_i = 0$. The displacement has to fulfill the governing equation:

$$\rho \frac{\partial^2 u_i}{\partial t^2} - \sigma_{ji,j} - D_{j,j} E_i = 0 \ . \tag{VI.13}$$

We can compute ϕ, T, and u_i from Eqs. (VII.39), (VII.46), (VII.45), respectively, after having defined D_i, $\mathcal{J}_i$, q_i, η, σ_{ij}, ${}^{\mathrm{p}}\varepsilon_{ij}^{\bullet}$ by means of ϕ, u_i, T.

2.1. Constitutive equations

We aim at defining the charge potential D_i, the electric current $\mathcal{J}_i$, the heat flux q_i, the specific entropy η, the stress σ_{ij}, and the rate of plastic strain ${}^{\mathrm{p}}\varepsilon_{ij}^{\bullet}$. They are called constitutive or material equations closing the governing equations leading to partial differential equations of the electric potential ϕ, the displacement u_i, and the temperature T.

The necessary connection for the charge potential is given by the so-called MAXWELL–LORENTZ aether relation:

$$D_i = \varepsilon_0 E_i \ , \tag{VI.14}$$

with the universal constant $\varepsilon_0 = 8.85 \cdot 10^{-12}\,\mathrm{C/(V\,m)}$. For the electric current we use OHM's law:

$$\mathcal{J}_i = \varsigma E_i \ , \tag{VI.15}$$

where the electrical conductivity, ς, is a material dependent parameter. For the heat flux we use FOURIER's law:

$$q_i = -\kappa T_{,i} \ , \tag{VI.16}$$

with the material parameter κ called the thermal conductivity. The material parameters may depend on the temperature as well as electric field. Usually they are given as constants since such measurements are challenging. In order to define stress and entropy, we restrict the materials being simple such that their material parameters

are constants. Then we can acquire for the entropy

$$\eta = c \ln\left(\frac{T}{T_{\text{ref.}}}\right) + \frac{1}{\rho}\alpha_{ij}\sigma_{ij} \ , \tag{VI.17}$$

and for the stress HOOKE's law with DUHAMEL–NEUMANN extension:

$$\sigma_{ij} = C_{ijkl}(\varepsilon_{kl} - {}^{\text{p}}\varepsilon_{kl} - {}^{\text{th}}\varepsilon_{kl}) \ , \tag{VI.18}$$

where the thermal strain reads

$${}^{\text{th}}\varepsilon_{ij} = \alpha_{ij}(T - T_{\text{ref.}}) \ . \tag{VI.19}$$

The heat capacity c, coefficients of thermal expansion α_{ij}, components of stiffness tensor C_{ijkl} are assumed to be constant, otherwise the above material equations are not valid, for a thermodynamical derivation of all aforementioned constitutive equations, see Abali, 2017, Sect. 3.3.

In time the solution will be in a discrete fashion, where Δt represents the time step. In order to calculate current (unknown) plastic strain, ${}^{\text{p}}\varepsilon_{ij}$, by using the (known) plastic strain from the last time step, ${}^{\text{p}}\varepsilon^{0}_{ij}$, incrementally,

$${}^{\text{p}}\varepsilon_{ij} = {}^{\text{p}}\varepsilon^{0}_{ij} + \Delta t \, {}^{\text{p}}\dot{\varepsilon}_{ij} \ , \tag{VI.20}$$

we use PRANDTL–REUSS theory with kinematic hardening

$${}^{\text{p}}\dot{\varepsilon}_{mn} = \langle\gamma\rangle \frac{\left(\sigma^{0}_{|ij|} - \beta^{0}_{ij}\right) C_{ijkl}(\dot{\varepsilon}_{kl} - {}^{\text{th}}\dot{\varepsilon}_{kl})}{\frac{4}{9}h\sigma^{2}_{\text{Y}} + \left(\sigma^{0}_{|ij|} - \beta^{0}_{ij}\right) C_{ijkl}\left(\sigma^{0}_{|kl|} - \beta^{0}_{kl}\right)} (\sigma^{0}_{|mn|} - \beta^{0}_{mn}) \ , \tag{VI.21}$$

where the material parameters h and σ_{Y} are determined from a uniaxial tensile testing. The yield stress σ_{Y} represents the threshold for plastic deformation. The slope of stress versus plastic strain is given by h. The so-called MACAULAY brackets as in $\langle\gamma\rangle$ defines a conditional parameter as being 1 or 0 depending on the VON MISES equivalent stress, σ_{eq}, defined by the deviatoric stress, $\sigma_{|ij|}$, as follows

$$\sigma_{\text{eq}} = \sqrt{\frac{2}{3}\sigma_{|ij|}\sigma_{|ij|}} \ , \quad \sigma_{|ij|} = \sigma_{ij} - \frac{1}{3}\sigma_{kk}\delta_{ij} \ , \tag{VI.22}$$

such that it becomes

$$\langle\gamma\rangle = \begin{cases} 1 & \text{if } \sigma_{\text{eq}} \geq \sigma_{\text{Y}} \\ 0 & \text{otherwise} \end{cases} \ . \tag{VI.23}$$

The so-called back stress, β_{ij}, evolves with the plastic stress, again incrementally,

$$\beta_{ij} = \beta^{0}_{ij} + \Delta t \dot{\beta}_{ij} \ , \quad \dot{\beta}_{ij} = \bar{c} \, {}^{\text{p}}\dot{\varepsilon}_{ij} \ , \tag{VI.24}$$

where we are going to choose $\bar{c} = 2h/3$ in the simulations. A circuit board consist of copper traces and via embedded in a composite material. Since we want to detect the failure in the copper, we model the copper deforming elasto-plastically. Copper is a cubic material. In a circuit board copper has the thickness of 20–40 µm whereas its grain size is only 0.5 µm, see Song et al., 2013. Hence we may assume that a polycristalline structure is present and the expected materials response is isotropic in this geometric scale. As a consequence of miniaturization this assumption may be critical in the near future. Hence we implement herein copper as a cubic material. For presenting the difference between isotropic and cubic materials, consider an isotropic material with the following material parameter tensors

$$C_{ijkl} = \lambda\delta_{ij}\delta_{kl} + \mu(\delta_{ik}\delta_{jl} + \delta_{il}\delta_{jk}) \ , \quad \alpha_{ij} = \alpha\delta_{ij} \ , \tag{VI.25}$$

where the LAME constants, λ, μ, and the thermal expansion constant α are the necessary material parameters. The parameters, λ, μ, read from the engineering constants, E, ν, G, which can be measured directly:

$$\lambda = \frac{E\nu}{(1+\nu)(1-2\nu)} = \frac{2G\nu}{(1-2\nu)} \ , \quad \mu = \frac{E}{2(1+\nu)} = G \ . \tag{VI.26}$$

YOUNG's modulus, E, POISSON's ratio, ν, and shear modulus, G, are coupled for isotropic materials as follows

$$G = \frac{E}{2(1+\nu)} \ . \tag{VI.27}$$

In the case of a cubic material the latter relation fails to hold such that the material possesses three independent parameters, namely E, G, and ν need to be measured independently. We can write the stiffness tensor in a matrix notation

$$C_{IJ} = \begin{pmatrix} C_{1111} & C_{1122} & C_{1133} & C_{1123} & C_{1113} & C_{1112} \\ C_{2211} & C_{2222} & C_{2233} & C_{2223} & C_{2213} & C_{2212} \\ C_{3311} & C_{3322} & C_{3333} & C_{3323} & C_{3313} & C_{3312} \\ C_{2311} & C_{2322} & C_{2333} & C_{2323} & C_{2313} & C_{2312} \\ C_{1311} & C_{1322} & C_{1333} & C_{1323} & C_{1313} & C_{1312} \\ C_{1211} & C_{1222} & C_{1233} & C_{1223} & C_{1213} & C_{1212} \end{pmatrix} \ , \tag{VI.28}$$

called the VOIGT notation and calculate it as the inverse of the compliance matrix,

$$C_{IJ} = (S_{JI})^{-1} \ , \quad S_{IJ} = \begin{pmatrix} \frac{1}{E} & -\frac{\nu}{E} & -\frac{\nu}{E} & 0 & 0 & 0 \\ & \frac{1}{E} & -\frac{\nu}{E} & 0 & 0 & 0 \\ & & \frac{1}{E} & 0 & 0 & 0 \\ & & & \frac{1}{G} & 0 & 0 \\ & \text{sym.} & & & \frac{1}{G} & 0 \\ & & & & & \frac{1}{G} \end{pmatrix} \ . \tag{VI.29}$$

Analogously for the coefficients of thermal expansion

$$\alpha_{ij} = \begin{pmatrix} \alpha_x & 0 & 0 \\ & \alpha_y & 0 \\ \text{sym.} & & \alpha_z \end{pmatrix} , \tag{VI.30}$$

we need to determine three independent coefficients for a cubic material. Necessary values for copper are taken from Ledbetter and Naimon, 1974, Table 10, Deutsches Kupferinstitut, 2014; Srikanth et al., 2007 as follows

$$\begin{aligned} C_{IJ}^{\mathrm{Cu}} &= \begin{pmatrix} 169.1 & 122.2 & 122.2 & 0 & 0 & 0 \\ & 169.1 & 122.2 & 0 & 0 & 0 \\ & & 169.1 & 0 & 0 & 0 \\ & & & 75.42 & 0 & 0 \\ & \text{sym.} & & & 75.42 & 0 \\ & & & & & 75.42 \end{pmatrix} \cdot 10^9\,\mathrm{Pa} , \\ \alpha_{ij}^{\mathrm{Cu}} &= \begin{pmatrix} 17 & 0 & 0 \\ 0 & 17 & 0 \\ 0 & 0 & 17 \end{pmatrix} \cdot 10^{-6}\,\mathrm{K}^{-1} , \end{aligned} \tag{VI.31}$$

$$\sigma_{\mathrm{Y}}^{\mathrm{Cu}} = 100 \cdot 10^6\,\mathrm{Pa} , \quad h^{\mathrm{Cu}} = 615 \cdot 10^6\,\mathrm{Pa} , \quad \rho^{\mathrm{Cu}} = 8.94 \cdot 10^3\,\mathrm{kg/m^3} ,$$
$$c^{\mathrm{Cu}} = 390\,\mathrm{J/(kg\ K)} , \quad \kappa^{\mathrm{Cu}} = 385\,\mathrm{W/(K\,m)} , \quad \varsigma^{\mathrm{Cu}} = 5.8 \cdot 10^7\,\mathrm{S/m} .$$

The composite material for the board is a fiber-reinforced laminate structure. Fibers are placed orthogonal in a woven structure such that the board material is orthotropic. For an orthotropic material, the compliance matrix in the VOIGT notation reads

$$S_{IJ}^{\mathrm{orth.}} = \begin{pmatrix} \frac{1}{E_x} & -\frac{\nu_{xy}}{E_y} & -\frac{\nu_{xz}}{E_z} & 0 & 0 & 0 \\ & \frac{1}{E_y} & -\frac{\nu_{yz}}{E_z} & 0 & 0 & 0 \\ & & \frac{1}{E_z} & 0 & 0 & 0 \\ & & & \frac{1}{G_{yz}} & 0 & 0 \\ & \text{sym.} & & & \frac{1}{G_{zx}} & 0 \\ & & & & & \frac{1}{G_{xy}} \end{pmatrix} . \tag{VI.32}$$

All of 9 parameters need to be measured independently. Such a measurement is cumbersome. Instead, we can calculate the so-called *homogenized* parameters for the composite material. Consider different unidirectional plies stacked upon each other in such a way that we obtain an orthotropic material. In each unidirectional ply the material parameters can be calculated as a "weighted sum." A ply consists of fiber and matrix—parameters of fiber and matrix are easier to obtain separately. Therefore, first we determine the materials data of each unidirectional ply. Secondly, we sum the properties by considering a particular orientation leading to the orthotropic board.

A unidirectional ply is transverse-isotropic. In order to identify material parameters, we choose a coordinate system, (x_1, x_2, x_3), where the first direction, x_1, is along the fibers in the ply. With respect to this so-called *local* coordinate system, we obtain the following compliance matrix in the VOIGT notation:

$$S_{IJ}^{\text{ply}} = \begin{pmatrix} \frac{1}{E_{11}} & -\frac{\nu_{21}}{E_{11}} & -\frac{\nu_{21}}{E_{11}} & 0 & 0 & 0 \\ & \frac{1}{E_{22}} & -\frac{\nu_{23}}{E_{22}} & 0 & 0 & 0 \\ & & \frac{1}{E_{22}} & 0 & 0 & 0 \\ & & & \frac{2(1+\nu_{23})}{E_{22}} & 0 & 0 \\ & \text{sym.} & & & \frac{1}{G_{12}} & 0 \\ & & & & & \frac{1}{G_{12}} \end{pmatrix} . \tag{VI.33}$$

These 5 parameters, E_{11}, E_{22}, ν_{21}, ν_{23}, and G_{12} can be calculated from the parameters of matrix and fiber by using micromechanical rules, see Schürmann, 2005, §8. These rules are simple models based on the linear elasticity. The most important assumption is that matrix and fiber be connected perfectly, in other words, no voids or cracks are existing such that the length change of matrix and fiber are identical. Then we can combine the materials data of fiber and matrix; and we can calculate from them the parameters in a ply consisting of φ–fiber and $(1-\varphi)$–matrix as follows

$$\begin{aligned} E_{11} = \varphi E_{11}^{\text{f.}} + (1-\varphi) E_{11}^{\text{m.}} \ , \quad E_{22} &= \frac{E_{22}^{\text{m.}} E_{22}^{\text{f.}}}{\varphi E_{22}^{\text{m.}} + (1-\varphi) E_{22}^{\text{f.}}} \ , \\ \nu_{21} &= \varphi \nu_{21}^{\text{f.}} + (1-\varphi) \nu_{21}^{\text{m.}} \ , \\ \nu_{23} = \varphi \nu_{23}^{\text{f.}} + (1-\varphi) \nu_{23}^{\text{m.}} &\left(\frac{1 + \nu_{23}^{\text{m.}} - \nu_{21}^{\text{f.}} \frac{E_{11}^{\text{m.}}}{E_{11}^{\text{f.}}}}{1 - (\nu_{23}^{\text{m.}})^2 + \nu_{23}^{\text{m.}} \nu_{21}^{\text{f.}} \frac{E_{11}^{\text{m.}}}{E_{11}^{\text{f.}}}} \right) \ , \\ G_{12} &= \frac{G_{12}^{\text{m.}} G_{12}^{\text{f.}}}{\varphi G_{12}^{\text{m.}} + (1-\varphi) G_{12}^{\text{f.}}} \ , \end{aligned} \tag{VI.34}$$

and

$$\begin{aligned} \alpha_{11} &= \frac{(1-\varphi)\alpha_{11}^{\text{m.}} E_{11}^{\text{m.}} + \varphi \alpha_{11}^{\text{f.}} E_{11}^{\text{f.}}}{(1-\varphi) E_{11}^{\text{m.}} + \varphi E_{11}^{\text{f.}}} \ , \\ \alpha_{22} = \varphi \alpha_{22}^{\text{f.}} + (1-\varphi) \alpha_{22}^{\text{m.}} \ , \quad \alpha_{33} &= \varphi \alpha_{33}^{\text{f.}} + (1-\varphi) \alpha_{33}^{\text{m.}} \ . \end{aligned} \tag{VI.35}$$

The upper $(\cdot)^{\text{m.}}$ and $(\cdot)^{\text{f.}}$ denote the materials data of matrix and fiber, respectively. The materials data for s-glass, e-glass, and aramid are taken from A JPS Industries Inc. Company JPS Composite Materials, n.d.; Suter Kunststoffe AG, n.d. The data of the epoxy matrix are found in Soden, Hinton, and Kaddour, 1998. By using Eq. (VI.34), parameters in Eq. (VI.33) are calculated. All used and calculated parameters are compiled in Table VI.1. After having determined the parameters for a unidirectional ply, we can simply construct a laminate of several plies by stacking them orthogonally. The result is an orthotropic material. Owing to the linear constitutive equations, we can superpose each ply's material tensors as transformed to the

Table VI.1.: Materials data of s-glass (I), e-glass (II), and aramid (III) fibers and epoxy matrix. Parameters marked with * are approximated values. Calculated unidirectional plies with s-glass, e-glass, and aramid are denoted by Ply I, II, and III, respectively.

	S-glass (I)	E-glass (II)	Aramid (III)	Epoxy	Ply I	Ply II	Ply III
E_{11} in GPa	85	65	100	4.2	53	41	62
E_{22} in GPa	85	65	5.4	4.2	9.8	9.6	4.9
ν_{21}	0.23	0.20	0.37*	0.34	0.27	0.26	0.36
ν_{23}	0.4*	0.4*	0.4*	0.34	0.44	0.44	0.44
G_{12} in GPa	33	28	1.5*	1.6	3.7	3.6	1.5
α_{11} in µm/(m K)	1.5	4	-3	45	2.9	5.7	-2.2
α_{22} in µm/(m K)	1.5	4	17	45	18.9	20.4	28.2
α_{33} in µm/(m K)	1.5	4	17	45	18.9	20.4	28.2

global coordinate system. All necessary materials data are compiled in Table VI.2. In

Table VI.2.: Materials data of Lam. I (s-glass and epoxy), Lam. II (e-glass and epoxy), and Lam. III (aramid and epoxy) in the global coordinate system.

	Lam. I	Lam. II	Lam. III
E_x in GPa	32	25	34
E_y in GPa	32	25	34
E_z in GPa	11	11	6
ν_{xy}	0.09	0.10	0.05
ν_{xz}	0.14	0.16	0.08
ν_{yz}	0.14	0.16	0.08
G_{yz} in GPa	3.5	3.5	1.6
G_{zx} in GPa	3.5	3.5	1.6
G_{xy} in GPa	3.7	3.6	1.5
α_x in µm/(m K)	10.9	13.1	13.0
α_y in µm/(m K)	10.9	13.1	13.0
α_z in µm/(m K)	18.9	20.4	28.2

addition to the aforementioned materials parameter, we use for laminate the following

data:

$$\rho^{\text{lam.}} = 2500\,\text{kg/m}^3\ ,\quad c^{\text{lam.}} = 800\,\text{J/(kg K)}\ ,\quad \kappa^{\text{lam.}} = 1.3\,\text{W/(m K)}\ ,\quad \varsigma^{\text{lam.}} = 0\ . \tag{VI.36}$$

2.2. Weak form

The primitive variables, ϕ, u_i, T, are continuous functions in space and time. We want to compute them by satisfying Eqs. (VII.39), (VII.45), (VII.46) augmented by the constitutive equations introduced in the last section. We will approximate space by means of finite element method (FEM) and time by using finite difference method (FDM). Time discretization is quite intuitive, as a list of subsequent time steps, whereas for simplicity in programming we choose identical time steps

$$t = \{0, \Delta t, 2\Delta t, \dots\}\ . \tag{VI.37}$$

Instead of a partial time derivative, we write the following difference equations:

$$\frac{\partial(\cdot)}{\partial t} = \frac{(\cdot) - (\cdot)^0}{\Delta t}\ ,\quad \frac{\partial^2(\cdot)}{\partial t^2} = \frac{(\cdot) - 2(\cdot)^0 + (\cdot)^{00}}{\Delta t \Delta t}\ , \tag{VI.38}$$

where $(\cdot)^0$ and $(\cdot)^{00}$ indicate the computed values from the last and second last time steps, respectively. In order to approximate the functions in a discretized space, we multiply the governing equations by appropriate test functions and obtain a variational form for each primitive variable,

$$\begin{aligned} \mathrm{F}_\phi &= \int_{\Omega^e} \Big(\frac{D_{i,i} - D^0_{i,i}}{\Delta t} + J_{i,i} \Big) \delta\phi \,\mathrm{d}V = 0\ , \\ \mathrm{F}_{\boldsymbol{u}} &= \int_{\Omega^e} \Big(\rho \frac{u_i - 2u^0_i + u^{00}_i}{\Delta t \Delta t} - \sigma_{ji,j} - D_{j,j} E_i \Big) \delta u_i \,\mathrm{d}V = 0\ , \\ \mathrm{F}_T &= \int_{\Omega^e} \Big(\rho \frac{\eta - \eta^0}{\Delta t} + \Phi_{i,i} - \Sigma \Big) \delta T \,\mathrm{d}V = 0\ , \end{aligned} \tag{VI.39}$$

integrated over a finite element Ω^e. The forms F_ϕ and F_T are in the unit of power, whereas $\mathrm{F}_{\boldsymbol{u}}$ is in the unit of energy. By multiplying F_ϕ and F_T by Δt, we obtain all forms in the same unit. The following terms: D_i, J_i, σ_{ji}, Φ_i consist of (space) derivatives of primitive variables. In the variational forms another derivative is addressed. Hence, the primitive variables have to be (at least) two times differentiable. This condition can be weakened by integrating by parts such that one of the derivatives is

shifted to the corresponding test function, as follows

$$\begin{aligned}
\mathrm{F}_\phi &= -\int_{\Omega^e} \big(D_i - D_i^0 + \Delta t J_i\big)\delta\phi_{,i}\,\mathrm{d}V + \int_{\partial\Omega^e} \big(D_i - D_i^0 + \Delta t J_i\big)\delta\phi N_i\,\mathrm{d}A\ , \\
\mathrm{F}_{\boldsymbol{u}} &= \int_{\Omega^e} \Big(\rho\frac{u_i - 2u_i^0 + u_i^{00}}{\Delta t\Delta t}\delta u_i + \sigma_{ji}\delta u_{i,j} - D_{j,j}E_i\delta u_i\Big)\,\mathrm{d}V - \int_{\partial\Omega^e}\sigma_{ji}\delta u_i N_j\,\mathrm{d}A\ , \\
\mathrm{F}_T &= \int_{\Omega^e} \big(\rho(\eta - \eta^0)\delta T - \Delta t\Phi_i\delta T_{,i} - \Delta t\Sigma\delta T\big)\,\mathrm{d}V + \int_{\partial\Omega^e}\Delta t\Phi_i\delta T N_i\,\mathrm{d}A\ ,
\end{aligned} \tag{VI.40}$$

with N_i being the plane normal pointing outward from Ω^e. The latter integral forms are called the weak forms. The whole computational domain, Ω, consists of two different materials, each material is divided by finite elements satisfying $\mathrm{F} = 0$ with

$$\mathrm{F} = \mathrm{F}_\phi + \mathrm{F}_{\boldsymbol{u}} + \mathrm{F}_T\ . \tag{VI.41}$$

We can assembly by summing over all elements. An element with its plane normal N_i and its adjacent element with its opposing plane normal eliminate the boundary terms within a material. All primitive variables are continuous. Over the interface, $\partial\Omega^I$, between different materials, there may occur jumps since the material parameters have different values. The weak forms read

$$\begin{aligned}
\mathrm{F}_\phi = -\int_{\Omega} \big(D_i - D_i^0 + \Delta t J_i\big)\delta\phi_{,i}\,\mathrm{d}V + \int_{\partial\Omega^I} \big[\!\big[D_i - D_i^0 + \Delta t J_i\big]\!\big]\delta\phi N_i\,\mathrm{d}A + \\
+ \int_{\partial\Omega} \big(D_i - D_i^0 + \Delta t J_i\big)\delta\phi N_i\,\mathrm{d}A\ , \\
\mathrm{F}_{\boldsymbol{u}} = \int_{\Omega} \Big(\rho\frac{u_i - 2u_i^0 + u_i^{00}}{\Delta t\Delta t}\delta u_i + \sigma_{ji}\delta u_{i,j} - D_{j,j}E_i\delta u_i\Big)\,\mathrm{d}V - \\
- \int_{\partial\Omega^I} [\![\sigma_{ji}]\!]\delta u_i N_j\,\mathrm{d}A - \int_{\partial\Omega}\sigma_{ji}\delta u_i N_j\,\mathrm{d}A\ , \\
\mathrm{F}_T = \int_{\Omega} \big(\rho(\eta - \eta^0)\delta T - \Delta t\Phi_i\delta T_{,i} - \Delta t\Sigma\delta T\big)\,\mathrm{d}V + \\
+ \int_{\partial\Omega^I}\Delta t[\![\Phi_i]\!]\delta T N_i\,\mathrm{d}A + \int_{\partial\Omega}\Delta t\Phi_i\delta T N_i\,\mathrm{d}A\ .
\end{aligned} \tag{VI.42}$$

On the interface, i.e., between two different materials, since ϕ is continuous, D_i is continuous, too. No electric current is allowed along the normal direction, since copper is surrounded by the insulating board or air. According Newton's lemma—action is equal to reaction—we expect that traction vectors $t_i = N_j\sigma_{ji}$ are also continuous. On the boundary, $\partial\Omega$, the traction vector $\hat{t}_i$ is given. In our example, we have free surfaces such that $\hat{t}_i = 0$ on $\partial\Omega$ or clamped faces where the displacement is given (as zero). On boundaries where the solution is given, we apply a Dirichlet boundary condition and the test function vanishes. Temperature at the boundary can be modeled by using mixed boundary condition such that a deviation from the reference temperature causes a heat flux, $q_i N_i = \bar{h}(T - T_{\text{ref.}})$, depending on the convective heat transfer

coefficient $\bar{h}$ in $\mathrm{J}/(\mathrm{s\,m^2\,K})$. Finally, we acquire the weak form to be implemented

$$\begin{aligned}\mathrm{F} = \int_\Omega \Big(&- (D_i - D_i^0)\delta\phi_{,i} - \Delta t J_i \delta\phi_{,i} + \rho\frac{u_i - 2u_i^0 + u_i^{00}}{\Delta t \Delta t}\delta u_i + \sigma_{ji}\delta u_{i,j} - \\ &- D_{j,j}E_i\delta u_i + \rho(\eta - \eta^0)\delta T - \Delta t \Phi_i \delta T_{,i} - \Delta t \Sigma \delta T\Big)\,\mathrm{d}V + \\ &+ \int_{\partial\Omega^I} \Delta t [\![\Phi_i]\!]\delta T N_i\,\mathrm{d}A + \int_{\partial\Omega} \Delta t \bar{h}(T - T_{\mathrm{ref.}})\frac{\delta T}{T}\,\mathrm{d}A\ .\end{aligned} \tag{VI.43}$$

We exploit the open-source packages developed under the FEniCS project and solve the coupled and nonlinear weak form for the simulations demonstrated in the next sections.

2.3. Lifetime prediction

Under a cyclic loading, copper traces and via deform plastically and material fails after a number of cycles, $N_{\mathrm{f.}}$. Since plastic deformation is irreversible, in each cycle, plastic deformation accumulates. By means of computation we can determine the accumulated plastic strain in one cycle and use this as a measure of lifetime. The plastic strain rate, ${}^{\mathrm{p}}\dot{\varepsilon}_{ij}$, is deviatoric, thus, the equivalent strain rate reads

$${}^{\mathrm{p}}\dot{\varepsilon}_{\mathrm{eq.}} = \sqrt{\frac{3}{2}\,{}^{\mathrm{p}}\dot{\varepsilon}_{ij}\,{}^{\mathrm{p}}\dot{\varepsilon}_{ij}}\ . \tag{VI.44}$$

The plastic strain accumulates in a cycle with the latter rate of equivalent strain,

$${}^{\mathrm{p}}\varepsilon_{\mathrm{acc.}} = \int_{\mathrm{cycle}} {}^{\mathrm{p}}\dot{\varepsilon}_{\mathrm{eq.}}\,\mathrm{d}t\ . \tag{VI.45}$$

This accumulated strain is a distribution in the copper wire. Its mean value can be determined by averaging over a chosen volume V

$$\left\langle {}^{\mathrm{p}}\varepsilon \right\rangle = \frac{\displaystyle\int_V {}^{\mathrm{p}}\varepsilon_{\mathrm{acc.}}\,\mathrm{d}V}{\displaystyle\int_V \mathrm{d}V} \tag{VI.46}$$

This measure for a lifetime prediction, $\left\langle {}^{\mathrm{p}}\varepsilon \right\rangle$, is computed by using the aforementioned approach. In order to establish a connection between the measure, $\left\langle {}^{\mathrm{p}}\varepsilon \right\rangle$, and the number of cycles to failure, $N_{\mathrm{f.}}$, there are various suggestions. They are mostly empirical such as computations and experiments need to be conducted and fitted. A theoretical analysis in Manson, 1968 provides the following relation

$$\left\langle {}^{\mathrm{p}}\varepsilon \right\rangle = D^{0.6} N_{\mathrm{f.}}^{-0.6}\ , \tag{VI.47}$$

for metallic compounds such as copper used in traces and via. The material specific constant, D, reads from the reduction of cross section, R, in a tensile test,

$$D = \ln\left(\frac{100}{100 - R}\right) . \tag{VI.48}$$

Cross section reduction, R, is in percentage and we take it as $R = 60$ for the electrodeposited copper material, see Valiev et al., 2002. It is important to recall that the parameter D can be obtained from a tensile testing. By employing computation we obtain $\langle {}^{\mathrm{p}}\varepsilon \rangle$ and estimate the lifetime

$$N_{\mathrm{f.}} = D \langle {}^{\mathrm{p}}\varepsilon \rangle^{-5/3} . \tag{VI.49}$$

This lifetime estimation is for the case of an accelerated test. It is challenging to determine a specific amount of months or years for the underlying electronic device. For comparing several designs, it is a helpful measure. A design with a longer lifetime is expected to be chosen from the point of mechanics.

3. Results and discussion

For analyzing the multiphysics and estimating the number of failure on a simplified unpopulated—so-called *bare*-board—we choose realistic geometric dimensions used in the industry. As shown in Fig. VI.2, the CAD geometry is prepared and preprocessed in Salome v7.5 Salome, 2016 by using NETGEN algorithms Schöberl, 1997. We have

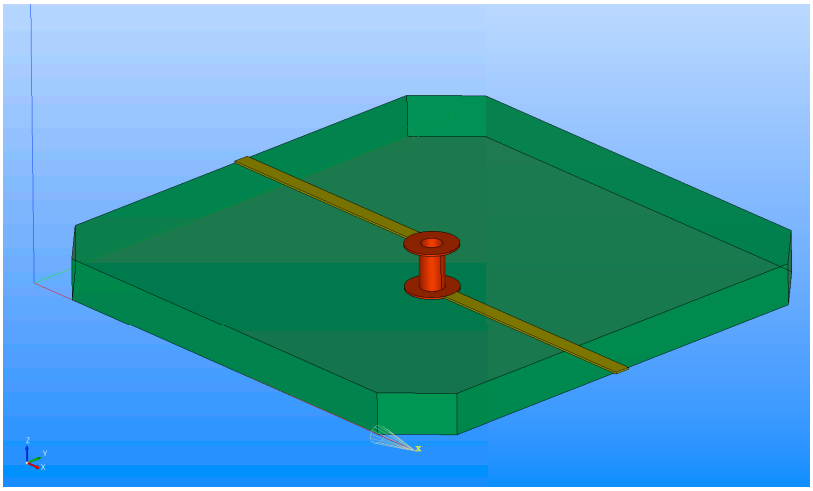

Figure VI.2.: *Simulation model of the one layer circuit board.* Composite board (green, transparent) embeds a copper trace (yellow) and a thru hole via (brown).

chosen a board of dimensions $10 \times 10 \times 0.8\,\mathrm{mm}$. Although all material parameters are given in SI units, we have converted them into mm, Mg (tonne), s, mA, K for

the simulation such that the geometry is captured accurately (up to the machine precision) in mm. The conducting wire is called *trace* and *via*, both from the same material, namely 5N copper. We use a standard 1 oz. copper modeled with 35 µm of thickness. Starting from the back side of the board, a trace along x-axis is placed on top of the board. The trace has a width of 300 µm and is connected by the annular ring (pad) of 500 µm radius to the thru hole via. Trace and annular ring are produced by masking and etching. Actually the profile of the trace and ring is trapezoidal due to the etching process; however, we model it as rectangular. After ring and trace are plated, a hole with 200 µm radius is drilled and the via is electroplated with a given thickness. Herein we model the wall thickness of the via also as 35 µm. There are no standards for this thickness and the simulation results would be different by variating this thickness. Via connects the trace on top to the trace on bottom that runs until the front side of the board. Especially around traces and via, several refinements of the mesh are applied; the final finite element mesh can be seen in Fig. VI.3.

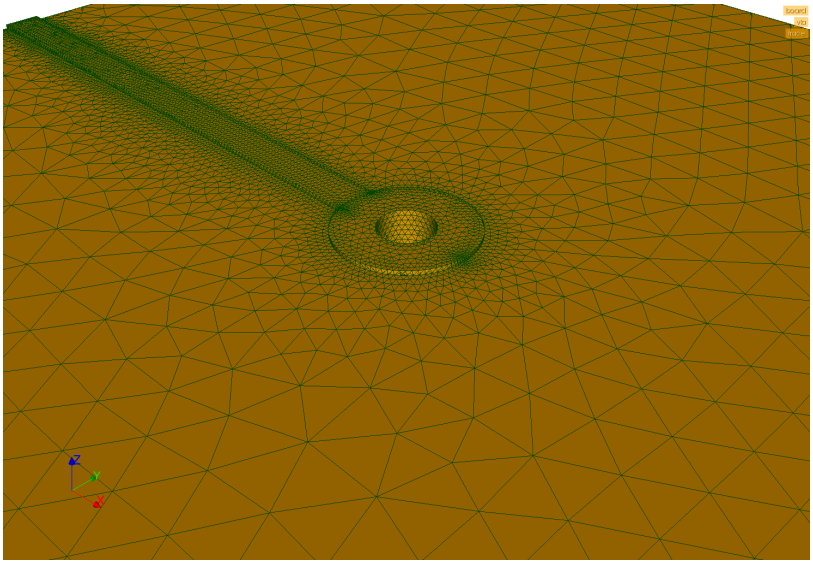

Figure VI.3.: *Mesh of the simulation model.* Tetrahedron first order continuous LAGRANGEan elements are generated in Salome by using NETGEN algorithm, zoomed to the via and annular ring for the sake of better visibility, approximately 20,000 nodes in the whole model.

We present simulations of a possible measurement. All boundary conditions are selected as it would be the case in reality. Board is usually fastened by bolts on four holes near to the edges. In order to hold the board on four edges, we model chamfers on the edges and hold on these four chamfer faces as being clamped in all directions. We simply set the deformation zero as a DIRICHLET boundary condition. The conducting copper is driven by an electric potential difference. At the endings of traces on back and front faces, the electric potential is set as a DIRICHLET boundary

condition. One end is grounded and the other is given harmonically,

$$\hat{\phi} = \phi_{\text{amp.}} \sin(2\pi\nu t) \ . \tag{VI.50}$$

For all simulations we have selected the period of 10 s leading to the frequency $\nu = 0.1\,\text{Hz}$ and an amplitude as $\phi_{\text{amp.}} = 0.2\,\text{V}$ in order to reach high enough temperatures leading to significant plastic strains. Since we have only a highly conductive copper wire, even such a small potential difference lead to high electric currents and dissipated heat, JOULE's loss. This setting is also configured in an accelerated fatigue test; but in an electronic device such conditions are not valid. Normally, there is a component like a resistor or capacitor connected to the circuit such that the electrical conductivity is lowered, leading to a smaller current, thus, a lower temperature increase. The computational model mimics a possible accelerated active fatigue experiment. In order to simulate an existing test; geometry and boundary conditions need to be accurately determined and applied.

The weak form in Eq. (VII.88) is nonlinear. By using FEniCS packages the linearization is handled automatically at the level of the partial differential level, before the assembly. Solution is searched by a standard NEWTON–RAPHSON algorithm after assembly operation. Every time step lasts approximately 8 min on one (3 min on two) Intel Xeon Processors (i7-2600) running on Ubuntu 16.04.

In order to comprehend the complicated multiphysics bearing electro-thermo-mechanical coupling, we present several results on one board at the quarter of one period, $t = 2.5\,\text{s}$. The results with other laminates are qualitatively the same. The potential difference generates an electric current. It is in equal amount in ampere along the trace and via. The current density, $\jmath_i$, is the amount per cross section. Since we have chosen the trace as well as via of the same thickness and the circumference of the via is longer than the width of the trace, the current density is greater along the trace than through the via. The electric potential and current density can be seen in Fig. VI.4. Greater electric current density implies a greater JOULE's heat, $\jmath_i E_i$, directly responsible for the temperature increase. Hence, the temperature increase is more on the trace than on the via. The temperature distribution again at the quarter period can be depicted in Fig. VI.5. For another wall thickness, this result would be different.

It is of importance to recall that the temperature distribution is not homogeneous, which is indeed the case in reality. This fact is overseen in an accelerated fatigue test performed in an oven. Temperature is changed quickly in the chamber, as a consequence, a homogeneous temperature distribution emerges, since the board is thin and copper is a good conductor. In this configuration the damage occurs in

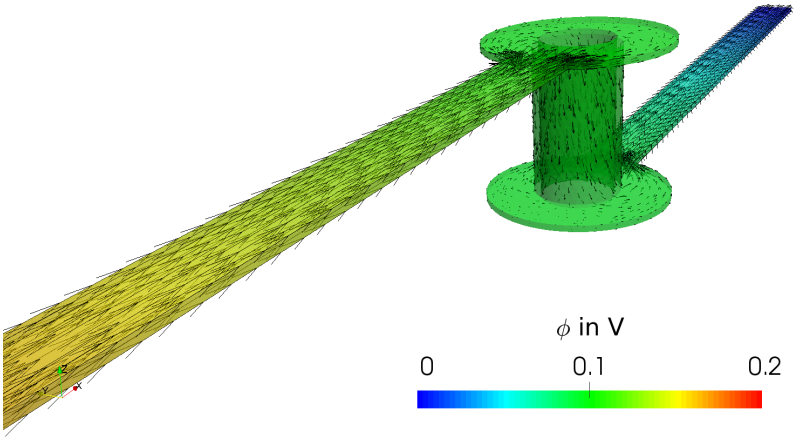

Figure VI.4.: *Simulation results at $t = 2.5\,s$, electric potential and current density.* For the sake of visibility, electric potential ϕ and electric current density $\jmath_i$ are presented on the transparent copper conductor. Color distribution denotes the electric potential. Arrows indicates the current density.

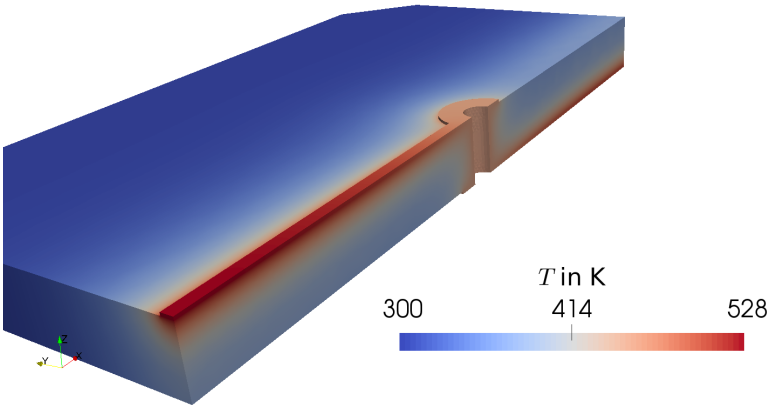

Figure VI.5.: *Simulation results at $t = 2.5\,s$, temperature distribution.* Temperature distribution, T, is shown as colors on the sliced model, the other half has a mirror symmetry.

the via. In an active test, however, we realize that the temperature distribution is heterogeneous that lead to another deformation mode in each cycle. In order to visualize the deformation, see Fig. VI.6. It is interesting to see that the middle part of the via is not moving; however, the variation of the displacement along the hole still induces a strain.

Approximately more than 20 K deviation from the reference temperature $T_{\text{ref.}} = 300\,\text{K}$ results stresses higher than the yield stress and plastic deformation starts accumulating. Simultaneously, heat escapes to the ambient, in the simulation we use the same convective heat transfer coefficients for the board as well as via, $\bar{h} = 10\,\text{J}/(\text{s}\,\text{m}^2\,\text{K})$,

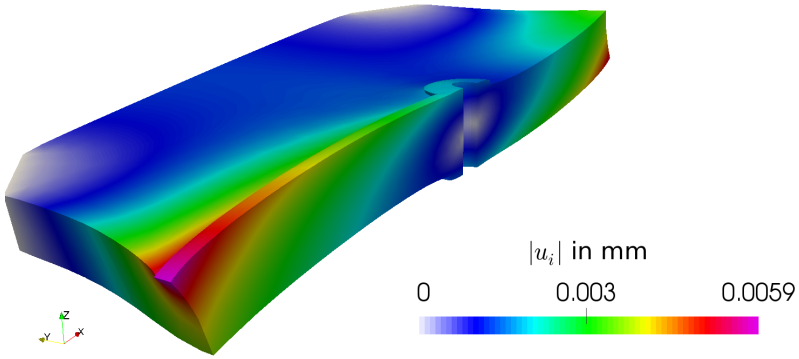

Figure VI.6.: *Simulation results at $t = 2.5\,s$, displacement.* Deformation is visualized with a scaling of 150. Colors denote the magnitude of displacement, u_i, on the sliced model, the other half has a mirror symmetry.

modeling a relatively slow free convection. This parameter is very difficult to measure accurately such that we choose a value and use the same for all simulations.

Temperature is produced within the conductor and exchanged over its boundary at the same time. Change across the boundary is greater when the temperature on the boundary increases. However, since we model free convection, this rate is small compared to the heat production. Depending on the excitation frequency of the given electric potential and depending on the convective heat transfer coefficient, the temperature increases until the heat exchange rate and production are equal in their absolute values. This steady-state condition is difficult to reach in the simulation, at least for the first 5 cycles the steady-state is not reached, see Fig. VI.7. We realize that a real experiment with the aforementioned setting might be difficult since within one minute the melting temperature of the board would be reached. Either a forced convection (using a fan) or a resistor connected to the circuit decreases the temperature increase. Although the increase is high, the total difference between the maximum and minimum temperature remains approximately the same in every cycle.

The fatigue failure occurs mostly because of the plastic strain accumulation. At the end of the first cycle, see the equivalent plastic strains in Fig. VI.8. The heterogeneous temperature distribution and the presented deformation lead to high plastic strains in the trace as well as in the via. This result is different compared to a fatigue experiment in an oven, where the most of the plastic strain accumulates within the via. Herein, in an active testing, we observe especially at the middle height of the via higher values than within the trace. For a better comparison we determine the mean values in two different volumes: over the traces and over the

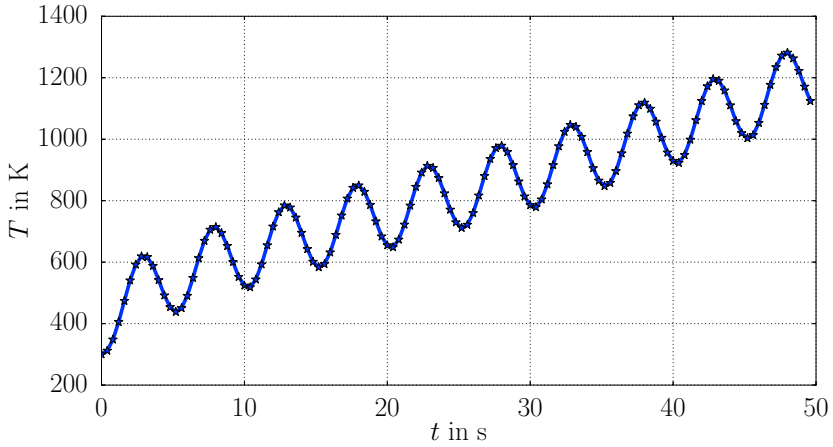

Figure VI.7.: *Temperature increase.* Maximum temperature is presented over time for 5 cycles.

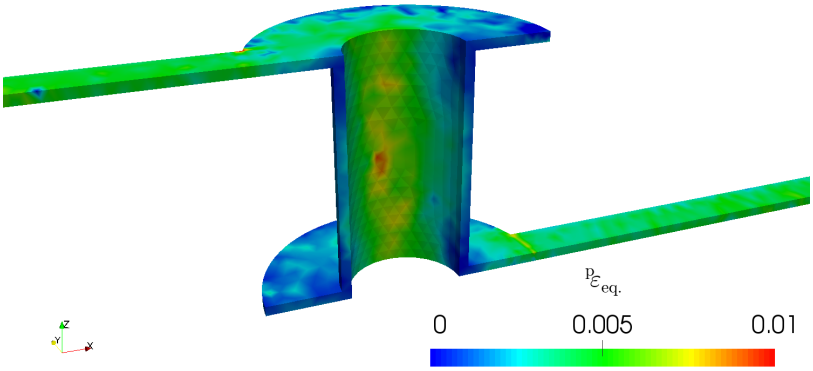

Figure VI.8.: *Simulation results at $t = 10\,s$, equivalent plastic strain.* Equivalent plastic strain is shown as a color distribution on the copper at the end of one cycle.

via. The accumulation of the mean value of the plastic strain averaged over these two regions can be seen in Fig. VI.9. Due to the irreversible character, the plastic strain accumulates whenever the temperature is increasing and remains the same at the moment when the temperature is decreasing. In every cycle the amount of the newly accumulated plastic strain is compiled in Table VI.3. A steady-state cannot be reached before the temperature variation gets stabilized.

Results in all laminates are qualitatively similar. They do differ quantitatively in terms of the plastic strain. In order to compare different laminates and their effects to the fatigue behavior, we conduct three simulations and compute the mean accu-

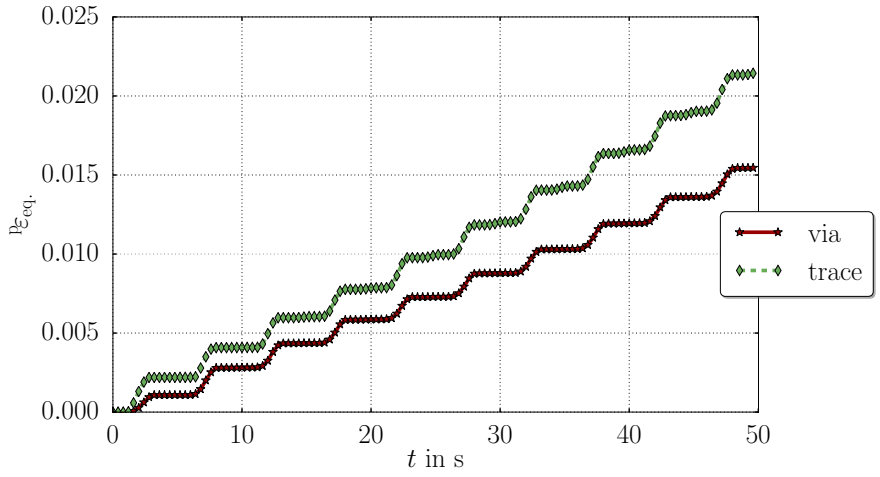

Figure VI.9.: *Accumulated plastic strains.* Accumulation of the plastic strains. Mean value over traces and via are presented for 5 cycles.

Table VI.3.: Mean accumulated plastic strain in each cycle for the laminate I.

	$\langle {}^{p}\varepsilon \rangle$ in %	
cycle	trace	via
1	0.409	0.282
2	0.377	0.305
3	0.417	0.293
4	0.455	0.315
4	0.497	0.352

mulated plastic strain at the end of one cycle. Again the aforementioned two volumes are used for averaging. The choice of the averaging volume is somehow heuristic and challenging; however, for a comparison between three laminates, the choice fails to be relevant. The values are compiled in Table VI.4.

By considering the fatigue as the sole criterion, it is fair to claim that the laminate III—aramid reinforced epoxy composite material—performs better than glass fiber reinforced epoxy materials. Since the governing equations are coupled and nonlinear, such a conclusion is challenging to predict based on the material parameters. Laminate III has the highest thermal expansion coefficient along the plate thickness, so the mismatch between expansion coefficients is higher. Hence, it is intuitive to guess that it would lead to greater plastic strains. As we see from

Table VI.4.: Number of failure calculated by the accumulated plastic strain in each cycle for three different laminates.

	Lam. I		Lam. II		Lam. III	
	trace	via	trace	via	trace	via
$\langle {}^{\mathrm{p}}\varepsilon \rangle$ in %	0.409	0.282	0.318	0.236	0.262	0.204
$N_{\mathrm{f.}}$	8 760	16 279	13 325	21 903	18 402	27 924

the deformation mode, the boundary conditions lead to a more shearing deformation that is the real reason of a plastic deformation. Expansion along the board thickness reduces shearing deformation leading to smaller plastic strains. Based on only one of the material parameters, we might prejudge the outcome differently than the observation by means of computations as presented herein. There are many coupling effects acting simultaneously, the only prediction shall be based on simulations with the least number of assumptions. Herein we present a robust method for computing an electro-thermo-mechanical system. In order to verify the code, we need to simulate existing experiments by correctly choosing boundary conditions as well as the geometry. According to the demonstrated comparison, a different choice for the laminate composition might increase the fatigue strength. There is a growing attention to find out variations of FR4 PCBs out of e-glass and epoxy. Stablcor Technology Inc. has patented its own PCF consisting of carbon fibers. Thermount is a registered trademark by DuPont and it uses aramid fibers.

Coupled computations is of importance to obtain a detailed investigation guiding toward newer insight into multiphysics. Herein we have neglected magnetic potential and thermoelectric effects. Often more assumptions are undertaken in order to simplify or decouple the governing equations leading to a fast simulation. With today's technological possibilities, we can perform computations as presented herein by using a laptop. Hence, we can get a detailed understanding of the phenomenon and even suggest design changes. In order to enable a scientific exchange, we deliver our codes in Abali, 2013 to be used under the GNU Public license Gnu GPL, 2007.

4. Conclusions

Using rational continuum mechanics, all necessary governing equations and constitutive equations are presented for a electro-thermo-mechanical system. We have directly attacked an application from electronics industry, namely a phenomenon called fatigue in copper vias. Accelerated experiments are generally conducted in an oven so

the temperature is controlled globally. In the recent years, more sophisticated experiments started to emerge, where the electric potential is controlled that leads to a local heating. This multiphysics problem is challenging to compute numerically, since the governing equations are nonlinear and coupled. We have presented an approach for computing coupled and nonlinear governing equations by means of open-source packages and simulated the electro-thermo-mechanical system monolithically. The results seem to be promising, a verification with experimental results is left to future research.

List of abbreviations

PCB–Printed Circuit Board
FEM–Finite Element Method
FDM–Finite Difference Method

Availability of data and materials

All codes used for simulations are publicly available in Abali, 2013 licensed under the GNU Public license Gnu GPL, 2007.

Competing interests

The author declares that they has no competing interests.

Funding

This work was completed while B. E. Abali was supported by a grant from the Max Kade Foundation to the University of California, Berkeley.

Acknowledgements

This work was completed while B. E. Abali was supported by a grant from the Max Kade Foundation to the University of California, Berkeley.

References

A JPS Industries Inc. Company JPS Composite Materials. http://jpsglass.com/jps_databook.pdf.

Abali, B. E. (2013). *Supply code, Computational Reality, Technical University of Berlin, Institute of Mechanics, Chair of Continuum Mechanics and Material Theory*. http://www.lkm.tu-berlin.de/ComputationalReality/.

Abali, B. E. (2017). *Computational Reality, Solving Nonlinear and Coupled Problems in Continuum Mechanics*. Vol. 55. Advanced Structured Materials. Springer. ISBN: 978-981-10-2443-6.

Abali, B. E., Reich, F. A., and Müller, W. H. (2014). „Fatigue analysis of anisotropic copper-vias in a circuit board." In: *GMM, Mikro-Nano-Integration, VDE Verlag, Berlin*, pp. 92–95.

Abali, B. E., Lofink, P., and Müller, W. H. (2014). „Variation of plastic materials data of copper and its impact on the durability of Cu-via interconnects." In: *Microelectronic packaging in the 21st century*. Ed. by R. Aschenbrenner and M. Schneider-Ramelow. Fraunhofer Verlag. Chap. 7.2, pp. 305–308. ISBN: 978-3-8396-0826-5.

Atli-Veltin, B., Ling, H., Zhao, S., Noijen, S., Caers, J., Weifeng, L., Feng, G., and Yuming, Y. (2012). „Thermo-mechanical investigation of the reliability of embedded components in PCBs during processing and under bending loading." In: *Thermal, Mechanical and Multi-Physics Simulation and Experiments in Microelectronics and Microsystems (EuroSimE), 2012 13th International Conference on*. IEEE, pp. 1–4.

Deutsches Kupferinstitut (2014). *Kupfer in der Elektrotechnik – Kabel und Leitungen*. www.kupferinstitut.de.

Gnu GPL (2007). *Gnu Gpl—the GNU General Public License*. http://www.gnu.org/copyleft/gpl.html.

Kpobie, W., Martiny, M., Mercier, S., Lechleiter, F., Bodin, L., Etangs-Levallois, A. L. des, and Brizoux, M. (2016). „Thermo-mechanical simulation of PCB with embedded components." In: *Microelectronics Reliability* 65, pp. 108–130.

Ledbetter, H. and Naimon, E. (1974). „Elastic properties of metals and alloys. II. Copper." In: *Journal of physical and chemical reference data* 3.4, pp. 897–935.

Logg, A., Mardal, K. A., and Wells, G. N. (2011). *Automated Solution of Differential Equations by the Finite Element Method, The FEniCS Book*. Vol. 84. Lecture Notes in Computational Science and Engineering. Springer.

Logg, A., Mardal, K. A., and Wells, G. N. (2012). *Automated solution of differential equations by the finite element method, the FEniCS book*. Vol. 84. Lecture Notes in Computational Science and Engineering. Springer. ISBN: 978-3-642-23098-1.

Manson, S. (1968). „A simple procedure for estimating high-temperature low-cycle fatigue." In: *Experimental Mechanics* 8.8, pp. 349–355.

Ridout, S. and Bailey, C. (2007). „Review of methods to predict solder joint reliability under thermo-mechanical cycling." In: *Fatigue & Fracture of Engineering Materials & Structures* 30.5, pp. 400–412.

Roellig, M., Dudek, R., Wiese, S., Boehme, B., Wunderle, B., Wolter, K.-J., and Michel, B. (2007). „Fatigue analysis of miniaturized lead-free solder contacts based on a novel test concept." In: *Microelectronics Reliability* 47.2, pp. 187–195.

Salome (2016). *The Open Source Integration Platform for Numerical Simulation, 1993–2016*. http://salome-platform.org.

Schöberl, J. (1997). „NETGEN an advancing front 2d/3d-mesh generator based on abstract rules." In: *Computing and visualization in science* 1.1, pp. 41–52.

Schürmann, H. (2005). *Konstruieren mit Faser-Kunststoff-Verbunden*. Springer.

Soden, P., Hinton, M., and Kaddour, A. (1998). „Lamina properties, lay-up configurations and loading conditions for a range of fibre-reinforced composite laminates." In: *Composites Science and Technology* 58.7, pp. 1011–1022.

Solomon, H. D. (1991). „Predicting thermal and mechanical fatigue lives from isothermal low cycle data." In: *Solder Joint Reliability*. Springer, pp. 406–454.

Song, J.-M., Wang, D.-S., Yeh, C.-H., Lu, W.-C., Tsou, Y.-S., and Lin, S.-C. (2013). „Texture and temperature dependence on the mechanical characteristics of copper electrodeposits." In: *Materials Science and Engineering: A* 559, pp. 655–664.

Srikanth, N., Premkumar, J., Sivakumar, M., Wong, Y., and Vath, C. (2007). „Effect of wire purity on copper wire bonding." In: *Electronics Packaging Technology Conference, 2007. EPTC 2007. 9th*. IEEE, pp. 755–759.

Suter Kunststoffe AG. http://www.swiss-composite.ch/pdf/i-Werkstoffdaten.pdf.

Valiev, R., Alexandrov, I., Zhu, Y., and Lowe, T. (2002). „Paradox of strength and ductility in metals processed bysevere plastic deformation.“ In: *Journal of Materials Research* 17.01, pp. 5–8.

Thermodynamically consistent derivation and computation of electro-thermo-mechanical systems for solid bodies

The post-print version of the published manuscript:
Abali, B. E. & Reich, F. A. (2017). Thermodynamically consistent derivation and computation of electro-thermo-mechanical systems for solid bodies. Computer Methods in Applied Mechanics and Engineering, 319, 567–595.

The final publication is available at Elsevier via
https://doi.org/10.1016/j.cma.2017.03.016

Abstract

For electro-thermo-mechanical systems such as a piezoceramic transducer, pyroelectric energy harvester, or a magnetic sensor using a magnetoelectric coupling, there are various formulations in continuum mechanics. The consensus of a well-established formulation is still missing. In this work we try to shed light to varying formulations and develop a thermodynamically consistent derivation of field equations for electro-thermo-mechanical systems. In order to justify their feasibility and verify their strength of modeling a physical system, we present simulations of engineering applications by exploiting open-source packages and solving problems monolithically with finite difference method in time and finite element method in space.

1. Introduction

In the last four decades many numerical studies have been proposed regarding the behavior of systems with electromagnetic interactions in solid bodies. In piezoelectric materials mechanical motion is coupled to the electric field. This coupling is examined by several authors by means of finite element simulations, for detailed reviews, see Benjeddou, 2000; Hachkevych and Terlets'kyi, 2004; Vidal et al., 2011. Mostly the formulation is restricted to the quasi-static case in order to employ HAMILTON's principle for obtaining a variational formulation as in Yi et al., 1999, or by using the principle of virtual work as in Ahmad, Upadhyay, and Venkatesan, 2006. Recently, a nearly complete dynamical description of such systems has been presented in Queiruga and Zohdi, 2016.

Difficulties arise in the formulation, especially if dynamics of electromagnetic interactions are involved. One of the main issues lies in the different representations of MAXWELL's equations, cf. Pao and Hutter, 1975 and Chu, Haus, and Penfield Jr, 1966, §II. There are methodologies to circumvent and solve this issue. Probably the most frequently used solution is the assumption of a quasi-static process so that time may be considered as a load parameter as in McMeeking, Landis, and Jimenez, 2007. Another possible solution is to introduce a magnetic scalar potential from which the magnetic field is derivable, similar to the derivation of the electric field from an electric scalar potential, cf. Kuczmann, 2009. However, such a definition is possible when the free electric conduction current vanishes. Another difficulty arises by introducing the balance equations with electromagnetic interactions in matter; there are different approaches in the literature, see Truesdell and Toupin, 1960, §286. Yet another drawback occurs by including temperature distribution in a polarized system. A non-isothermal theory has to be thermodynamically consistent. There exist a few theories for polarized deformable media, for example see Groot and Mazur, 1984, § XIII, Müller, 1985, Chap. 9, Kovetz, 2000, Brechet and Ansermet, 2014, and Abali, 2017, Chap. 3. They follow different thermodynamical approaches such that they cannot be compared with each other. However, we can point out one important difference between these approaches: they all define the balance of total energy differently, see Ericksen, 2007 for a more comprehensive comparison. We postulate that the total energy is a conserved quantity, start with an undefined and general balance equation, out of which the balance of internal energy is deduced. We follow mainly the approach called non-equilibrium thermodynamics.

Because of the aforementioned differences in the formulation and for the sake of clarity, we outline very briefly the theory introduced in Abali, 2017, Chap. 3 and compute the *primitive* variables for solids, viz., temperature T, displacement $\boldsymbol{u}$, and electromagnetic potentials ϕ, $\boldsymbol{A}$. We formulate all variables by means of a reference

frame, where $\boldsymbol{X}$ denotes the reference position of a massive particle. As the reference position we choose the initial position, which is known. Since particles occupy non-congruent positions, this formulation includes the same particles for all times, thus, it is a *material system*. All primitive variables are functions in space $\boldsymbol{X}$ and in time t. In order to compute the primitive variables, we need governing equations.

For calculating temperature T and displacement $\boldsymbol{u}$ we employ the balance of internal energy and the balance of linear momentum, respectively. For calculating the electric potential ϕ and the magnetic potential $\boldsymbol{A}$, we utilize MAXWELL's equations. In order to close these equations we need constitutive equations, which are derived in a thermodynamically consistent fashion by neglecting geometric nonlinearities. After inserting them in the governing equations, we obtain the *field* equations. This field equations are coupled, nonlinear partial differential equations and can only be solved numerically. Hence we generate a weak form out of the field equations and solve it with the aid of the novel collection of open-source packages provided by the FEniCS project, see Logg, Mardal, and Wells, 2012; Logg, Mardal, and Wells, 2011. We present some examples and publish their codes in Abali, 2013 under the GNU Public license Gnu GPL, 2007, in order to encourage further studies.

2. Governing equations

Consider a continuum body, $\mathfrak{b}$, consisting of particles with mass and electric charge. Their initial positions are denoted by $\boldsymbol{X}$ and their current positions read $\boldsymbol{x}$. The solid body is deforming under electric, thermal, and mechanical loadings. We aim at computing the primitive fields: displacement $\boldsymbol{u} = \boldsymbol{x} - \boldsymbol{X}$ in m(eter), temperature T in K(elvin), electric potential ϕ in V(olt), and magnetic potential $\boldsymbol{A}$ in T(esla) m. The initial frame is equipped with a Cartesian coordinate system and we use the standard continuum mechanical notations as well as the EINSTEIN summation convention over repeated indices. We start off with a balance of electromagnetic momentum:

$$\frac{\partial \mathcal{G}_i}{\partial t} = \frac{\partial m_{ji}}{\partial x_j} - \mathcal{F}_i \ , \tag{VII.1}$$

where the relation is defined between the electromagnetic momentum density, $\mathcal{G}_i$, the electromagnetic stress tensor, m_{ji}, and the electromagnetic supply term, $\mathcal{F}_i$. The definition of m_{ji} depends on the definition of $\mathcal{F}_i$, i.e., their definitions are in some sense arbitrary. However, their definitions have to be such that the relation in Eq. (VII.1) holds, see Groot and Mazur, 1984, Chap. XIV. First we need to define $\mathcal{G}_i$, then, we can determine some m_{ji} and $\mathcal{F}_i$ satisfying the restriction in Eq. (VII.1). Unfortunately, the consensus for a unique definition of the electromagnetic momentum $\mathcal{G}_i$ is still missing.

This issue is discussed heavily in the literature, see for example Obukhov, 2008; Mansuripur, 2010; Griffiths, 2012; Bethune-Waddell and Chau, 2015. By following Barnett, 2010 we underline that different choices of an electromagnetic momentum are admissible. The most prominent variants for the electromagnetic momentum are: the POYNTING vector,

$$\mathcal{G}_i^{\mathrm{P}} = (\boldsymbol{D} \times \boldsymbol{B})_i \ , \tag{VII.2}$$

where the charge potential (dielectric displacement due to the *total* charge) is denoted by $\boldsymbol{D}$ and the magnetic flux (area) density by $\boldsymbol{B}$; MINKOWSKI's choice,

$$\mathcal{G}_i^{\mathrm{M}} = (\mathfrak{D} \times \boldsymbol{B})_i \ , \tag{VII.3}$$

where the free charge potential (electric displacement because of *free* charges) is given by $\mathfrak{D}$; and ABRAHAM's proposal,

$$\mathcal{G}_i^{\mathrm{A}} = \frac{1}{c^2}(\boldsymbol{E} \times \mathfrak{H})_i \ , \tag{VII.4}$$

where the electric field is denoted by $\boldsymbol{E}$ and the free current potential (magnetic field created by *free* charges) by $\mathfrak{H}$. One of the fundamental assumptions in electromagnetic interactions with matter relies on the decomposition of the electric charge since it is an extensive quantity. Total specific charge (electric charge per mass) z is additively separated into *free* specific charge $z^{\mathrm{fr.}}$ and *bound* specific charge $z^{\mathrm{bo.}}$ as follows

$$z = z^{\mathrm{fr.}} + z^{\mathrm{bo.}} \ . \tag{VII.5}$$

Analogously, we can separate the total charge potential D_i and the total current potential H_i in order to obtain

$$D_i = \mathfrak{D}_i - P_i \ , \quad H_i = \mathfrak{H}_i + M_i + (\boldsymbol{P} \times \boldsymbol{v})_i = \mathfrak{H}_i + \mathcal{M}_i \ , \tag{VII.6}$$

where the free charge potential $\mathfrak{D}_i$ and the free current potential $\mathfrak{H}_i$ are effected by free charges; and the electric polarization[84] P_i as well as the magnetic polarization M_i are caused by bound charges. Experimentally, distinguishing between a magnetic polarization and a moving electric polarization is not possible. We therefore add the term, $\boldsymbol{P} \times \boldsymbol{v}$, in order to ensure consistency with experiments.[85]

If we choose ABRAHAM's proposal as electromagnetic momentum we can rewrite this term by using the universal constants ε_0 and μ_0 with $c^2 = (\varepsilon_0 \mu_0)^{-1}$ and the

[84] Historically, the electric polarization is defined in the direction of an electric field. Therefore, a (positively) charged particle converges towards the electric polarization such that $-\frac{\partial P_i}{\partial x_i} = \rho z^{\mathrm{bo.}}$ holds. Hence, in front of the electric polarization, we see a minus sign owing to this convention.

[85] Actually, by using tensor rules one can show that $\mathcal{M}_i$ is objective and M_i is not such that $\mathcal{M}_i$ is the appropriate choice.

Maxwell–Lorentz aether relations:

$$D_i = \varepsilon_0 E_i \ , \quad H_i = \frac{1}{\mu_0} B_i \ , \tag{VII.7}$$

as follows

$$\mathcal{G}_i^{\mathrm{A}} = \varepsilon_0 \mu_0 \epsilon_{ijk} E_j \mathfrak{H}_k = \epsilon_{ijk} D_j (B_k - \mu_0 \mathcal{M}_k) = \mathcal{G}_i^{\mathrm{P}} - \mu_0 (\boldsymbol{D} \times \boldsymbol{\mathcal{M}})_i \ . \tag{VII.8}$$

Analogously, for Minkowki's choice, we obtain

$$\mathcal{G}_i^{\mathrm{M}} = \mathcal{G}_i^{\mathrm{P}} + (\boldsymbol{P} \times \boldsymbol{B})_i \ . \tag{VII.9}$$

Hence, in a system without polarization, all choices are identical. For a polarized system, the choice is arbitrary. As shown in Pfeifer et al., 2007 we can use Minkowski's or Abraham's momentum definition without any hesitation since both are valid and correct. The choice, however, leads to different electromagnetic stress and supply terms.

2.1. Electromagnetic stress and supply

For a material without polarization, we rewrite $\mathcal{G}_i^{\mathrm{P}}$ in Eq. (VII.1) by using the following Maxwell equations expressed in fixed Cartesian coordinates

$$-\frac{\partial D_i}{\partial t} + \epsilon_{ijk} \frac{\partial H_k}{\partial x_j} = J_i \ , \quad \frac{\partial B_i}{\partial t} + \epsilon_{ijk} \frac{\partial E_k}{\partial x_j} = 0 \ , \tag{VII.10}$$

where the Levi-Civita symbol, ϵ_{ijk}, is the permutation symbol in Cartesian coordinates. Electric current, J_i, is introduced and will be defined later. Moreover, we use as the Maxwell–Lorentz aether relations as in Eq. (VII.7) and the following Maxwell equations:

$$\frac{\partial B_i}{\partial x_i} = 0 \ , \quad \frac{\partial D_i}{\partial x_i} = \rho z \ , \tag{VII.11}$$

in order to acquire the so-called Poynting equation:

$$\begin{aligned} \frac{\partial}{\partial t}(\boldsymbol{D} \times \boldsymbol{B})_i = \frac{\partial \mathcal{G}_i^{\mathrm{P}}}{\partial t} = \frac{\partial}{\partial x_j}\Big(-\frac{1}{2}\delta_{ji}(H_k B_k + D_k E_k) + H_i B_j + D_j E_i \Big) - \\ -\rho z E_i - (\boldsymbol{J} \times \boldsymbol{B})_i \ , \end{aligned} \tag{VII.12}$$

as the balance of electromagnetic momentum. We refer to Appendix A for detailed derivation of the latter.

By a simple comparison of the latter with the general form as in Eq. (VII.1), we determine the electromagnetic stress tensor, called Maxwell's stress, for an unpolarized

system

$$m_{ji} = -\frac{1}{2}\delta_{ji}(H_k B_k + D_k E_k) + H_i B_j + D_j E_i \ , \tag{VII.13}$$

and the supply term, known as LORENTZ's force density:

$$\mathcal{F}_i = \rho z E_i + \epsilon_{ijk} J_j B_k \ . \tag{VII.14}$$

For a polarized system we may choose $\mathcal{G}_i^{\mathrm{M}}$ or $\mathcal{G}_i^{\mathrm{A}}$. A thermodynamical formulation for the choice of $\mathcal{G}_i^{\mathrm{A}}$ can be found in Groot and Mazur, 1984, Ch. XIV, §2. We choose $\mathcal{G}_i^{\mathrm{M}}$ in the following. First the balance of electromagnetic momentum changes slightly, since MINKOWSKI's definition has an additional term: $\mathcal{G}_i^{\mathrm{M}} = \mathcal{G}_i^{\mathrm{P}} + \epsilon_{ijk} P_j B_k$. The simplest change is to add the rate of these terms to the supply term in order to acquire

$$\begin{aligned} m_{ji} &= -\frac{1}{2}\delta_{ji}(H_k B_k + D_k E_k) + H_i B_j + D_j E_i \ , \\ \mathcal{F}_i &= \rho z E_i + \epsilon_{ijk} J_j B_k - \epsilon_{ijk} \frac{\partial P_j}{\partial t} B_k - \epsilon_{ijk} P_j \frac{\partial B_k}{\partial t} \ . \end{aligned} \tag{VII.15}$$

2.2. Balance equations with the electromagnetic interaction

Total (linear) momentum is axiomatically postulated as being a conserved quantity. It is beneficial to separate the total momentum density into a part due to the electromagnetism, momentum of field, $\mathcal{G}_i$, and into another part caused by the (macroscopic) motion of the mass, momentum of matter, ρv_i. A conserved quantity is described by a balance equation without a production term

$$\frac{\partial}{\partial t}\big(\rho v_i + \mathcal{G}_i\big) - \frac{\partial}{\partial x_j}\big(- v_j \rho v_i + \sigma_{ji} + m_{ji}\big) - \rho f_i = 0 \ , \tag{VII.16}$$

where the flux term of momentum of matter, σ_{ji}, is referred to as CAUCHY's stress and the specific supply term, f_i, is a body force derived from a potential alike gravitational forces. Momentum of matter can be convected by massive particles as indicated with the first term in the divergence. However, momentum of field is independent of the underlying material. In other words, electromagnetic fields propagate even in vacuum (without any medium like massive particles). Mass is a conserved quantity, too. The balance of mass reads

$$\frac{\partial \rho}{\partial t} - \frac{\partial}{\partial x_j}\big(- v_j \rho\big) = 0 \ . \tag{VII.17}$$

By introducing

$$\frac{\mathrm{d}}{\mathrm{d}t} = \frac{\partial}{\partial t} + v_j \frac{\partial}{\partial x_j} \ , \tag{VII.18}$$

we can rewrite the balance of mass:

$$\frac{\mathrm{d}\rho}{\mathrm{d}t} + \rho \frac{\partial v_j}{\partial x_j} = 0 \ . \tag{VII.19}$$

The balance of the total momentum can be rewritten by inserting the balance of electromagnetic momentum as in Eq. (VII.1) and then using the balance of mass, as follows

$$\begin{aligned} \frac{\partial \rho v_i}{\partial t} - \frac{\partial}{\partial x_j}\big(- v_j \rho v_i + \sigma_{ji}\big) - \rho f_i = \mathcal{F}_i \ , \\ \rho \frac{\mathrm{d} v_i}{\mathrm{d} t} - \frac{\partial \sigma_{ji}}{\partial x_j} - \rho f_i = \mathcal{F}_i \ . \end{aligned} \tag{VII.20}$$

By referring to Appendix B, we reformulate the balance of momentum after multiplying by velocity

$$\frac{\partial}{\partial t}\Big(\frac{1}{2}\rho v_i v_i\Big) - \frac{\partial}{\partial x_j}\Big(- v_j \frac{1}{2}\rho v_i v_i + \sigma_{ji} v_i\Big) - \rho f_i v_i = -\sigma_{ji}\frac{\partial v_i}{\partial x_j} + \mathcal{F}_i v_i \ , \tag{VII.21}$$

where the right-hand side is a production term. The second production term of the kinetic energy, $\mathcal{F}_i v_i$, can be rewritten in order to gain appropriate equations for a thermodynamical formulation

$$\begin{aligned} \mathcal{F}_i v_i = \frac{\partial}{\partial x_j}\Big((-P_j E_i + \mathcal{M}_i B_j) v_i + \big(\mathfrak{H} \times \boldsymbol{E}\big)_j\Big) + \\ + \frac{\partial}{\partial t}\Big(B_i \mathcal{M}_i - P_j E_j - \frac{1}{2} D_j E_j - \frac{1}{2} B_i H_i\Big) - (-P_j E_i + \mathcal{M}_i B_j)\frac{\partial v_i}{\partial x_j} - \\ - \mathcal{E}_i \mathcal{J}_i^{\mathrm{fr.}} + P_i \frac{\mathrm{d} E_i}{\mathrm{d} t} - B_i \frac{\mathrm{d} \mathcal{M}_i}{\mathrm{d} t} \ , \end{aligned} \tag{VII.22}$$

where we refer to Abali, 2017, Chap. 3 for the derivation. The formulation is is universal, i.e., it holds for every material, since during the reformulation only Maxwell's equations and the Maxwell–Lorentz aether relations are used. The electromotive force $\mathcal{E}_i = E_i + (\boldsymbol{v} \times \boldsymbol{B})_i$ is the electric field measured on the moving particles and generates an effective electric current $\mathcal{J}_i^{\mathrm{fr.}}$ yet to be defined. Now we can introduce the energy density due to matter, $\rho e^{\mathrm{m.}}$, the energy density caused by polarization, $e^{\mathrm{p.}}$, as well as the energy density effected by the field, $e^{\mathrm{f.}}$, as follows

$$\begin{aligned} \rho e^{\mathrm{m.}} = \frac{1}{2}\rho v_i v_i \ , \quad e^{\mathrm{p.}} = -B_i \mathcal{M}_i + P_j E_j \ , \quad e^{\mathrm{f.}} = \frac{1}{2}\big(D_j E_j + B_i H_i\big) \ , \\ \rho e^{\mathrm{kin.}} = \rho e^{\mathrm{m.}} + e^{\mathrm{p.}} + e^{\mathrm{f.}} \ . \end{aligned} \tag{VII.23}$$

The balance of kinetic energy can be rewritten by using the latter relations as

$$\begin{aligned} \frac{\partial \rho e^{\mathrm{kin.}}}{\partial t} - \frac{\partial}{\partial x_j}\Big(- v_j(\rho e^{\mathrm{kin.}} - e^{\mathrm{p.}} - e^{\mathrm{f.}}) - \big(\boldsymbol{E} \times \mathfrak{H}\big)_j + \big(\sigma_{ji} - P_j E_i + \mathcal{M}_i B_j\big) v_i\Big) - \\ - \rho f_i v_i = -\big(\sigma_{ji} - P_j E_i + \mathcal{M}_i B_j\big)\frac{\partial v_i}{\partial x_j} - \mathcal{E}_i \mathcal{J}_i^{\mathrm{fr.}} + P_i \frac{\mathrm{d} E_i}{\mathrm{d} t} - B_i \frac{\mathrm{d} \mathcal{M}_i}{\mathrm{d} t} \ . \end{aligned} \tag{VII.24}$$

The *total* energy is a conserved quantity. Since it is a conserved quantity, no production terms arise and the balance of total energy reads

$$\frac{\partial \rho e}{\partial t} - \frac{\partial}{\partial x_j}\big(- v_j \rho e + F_j\big) - \rho s = 0 \ , \tag{VII.25}$$

where the specific total energy, e, its flux term, F_j, and its specific supply term, s, are all undefined for the moment. We start with the specific total energy e and define it as a sum of the specific kinetic energy $e^{\text{kin.}}$ and specific internal energy u as follows

$$e = e^{\text{kin.}} + u \ . \tag{VII.26}$$

Thus, we subtract the balance of kinetic energy from the balance of total energy and obtain the balance of internal energy

$$\frac{\partial \rho u}{\partial t} - \frac{\partial}{\partial x_j}\big(- v_j \rho u - q_j\big) - \rho r = \Gamma \ , \tag{VII.27}$$

where the internal energy's flux term $-q_j$, its specific supply term r, and its production term Γ read

$$\begin{aligned} -q_j &= -v_j(e^{\text{p.}} + e^{\text{f.}}) + F_j + \big(\boldsymbol{E} \times \boldsymbol{\mathfrak{H}}\big)_j - \big(\sigma_{ji} - P_j E_i + \mathcal{M}_i B_j\big) v_i \ , \\ r &= s - f_i v_i \ , \\ \Gamma &= \big(\sigma_{ji} - P_j E_i + \mathcal{M}_i B_j\big) \frac{\partial v_i}{\partial x_j} + \mathcal{E}_i \mathcal{J}_i^{\text{fr.}} - P_i \frac{\mathrm{d}E_i}{\mathrm{d}t} + B_i \frac{\mathrm{d}\mathcal{M}_i}{\mathrm{d}t} \ . \end{aligned} \tag{VII.28}$$

After using the balance of mass once more, the balance of internal energy reads

$$\rho \frac{\mathrm{d}u}{\mathrm{d}t} + \frac{\partial q_j}{\partial x_j} - \rho r = \Gamma \ . \tag{VII.29}$$

The flux of internal energy, $-q_i$, is called the *heat flux* and it has a minus sign. Historically, the balance of internal energy was seen as an evolution equation for temperature by associating the internal energy only with the heat energy. This assumption is true for an ideal gas. The first machines were converting heat to mechanical work, hence the heat flux into the system had been seen as a positive quantity leading to the minus sign in front of the heat flux. We will define this term with respect to all of primitive variables. The supply term, r, is referred to as *radiant heating*. A typical example is a laser beam or microwave oven heating up the system volumetrically. This term is given. The production term, Γ, includes σ_{ji}, P_i, $\mathcal{M}_i$, and $\mathcal{J}_i^{\text{fr.}}$, they all will be defined later.

2.3. Field equations

The primitive variables for a solid body are electric field E_i, magnetic flux density B_i, displacement u_i, and temperature T. The formulation will be done in the initial frame by neglecting geometric nonlinearities. In other words, we approximate the deformation gradient as being the identity such as the deformation is small with respect to the geometric dimensions of the continuum body. We start with the following Maxwell equations:

$$\frac{\partial B_i}{\partial x_i} = 0 \ , \quad \frac{\partial B_i}{\partial t} + \epsilon_{ijk}\frac{\partial E_k}{\partial x_j} = 0 \ , \tag{VII.30}$$

and transform these onto the initial frame X_i by neglecting the geometric nonlinearities

$$\frac{\partial B_i}{\partial X_i} = 0 \ , \quad \frac{\partial B_i}{\partial t} + \epsilon_{ijk}\frac{\partial E_k}{\partial X_j} = 0 \ , \tag{VII.31}$$

and solve them by using the following *ansatz* functions:

$$E_i = -\frac{\partial \phi}{\partial X_i} - \frac{\partial A_i}{\partial t} \ , \quad B_i = \epsilon_{ijk}\frac{\partial A_k}{\partial X_j} \ . \tag{VII.32}$$

Now we aim for computing the electric potential ϕ in V and the magnetic potential A_i in T m. Of course, the six components of E_i and B_i cannot be defined uniquely by the four components of ϕ and A_i in three-dimensional space. We have to restrict them using so-called gauge freedom by stating fixing the functions $\partial\phi/\partial t$ and $\partial A_i/\partial X_i$. The simplest choice is to set them zero, known as Gauss's gauge. Numerically, Gauss's gauge yields problems in solving the equations, see Baumanns, Clemens, and Schops, 2013. We propose to use Lorenz's gauge:

$$\frac{\partial \phi}{\partial t} = -c^2\frac{\partial A_i}{\partial X_i} \ , \tag{VII.33}$$

which is adequate for a numerical solving procedure. The following Maxwell equations:

$$\rho z = \frac{\partial D_i}{\partial x_i} \ , \quad -\frac{\partial D_i}{\partial t} + \epsilon_{ijk}\frac{\partial H_k}{\partial x_j} = J_i \ , \tag{VII.34}$$

can be rewritten in the initial frame by neglecting the geometric nonlinearities

$$\rho z = \frac{\partial D_i}{\partial X_i} \ , \quad -\frac{\partial D_i}{\partial t} + \epsilon_{ijk}\frac{\partial H_k}{\partial X_j} = J_i \ . \tag{VII.35}$$

Furthermore, they can be combined and rewritten as follows

$$\frac{\partial \rho z}{\partial t} + \frac{\partial J_i}{\partial X_i} = 0 \ , \quad -\frac{\partial D_i}{\partial t} + \epsilon_{ijk}\frac{\partial H_k}{\partial X_j} = J_i \ , \tag{VII.36}$$

where the former is known as the balance of electric charge. As introduced in Eq. (VII.6) we can use electric polarization P_i and magnetic polarization $\mathcal{M}_i$ in Eq. (VII.36)$_2$ such that we obtain

$$-\frac{\partial \mathfrak{D}_i}{\partial t} + \epsilon_{ijk}\frac{\partial \mathfrak{H}_k}{\partial X_j} = J_i - \frac{\partial P_i}{\partial t} - \epsilon_{ijk}\frac{\partial \mathcal{M}_k}{\partial X_j} = J_i^{\text{fr.}} \ , \tag{VII.37}$$

where $J_i^{\text{fr.}} = \mathcal{J}_i^{\text{fr.}} + v_i \rho z^{\text{fr.}}$ is the conduction current due to the free charges in the material. Especially $\mathcal{J}_i^{\text{fr.}}$ is the effective current we use in our daily-lives. Using Maxwell's equation we acquire

$$\rho z = \rho z^{\text{fr.}} + \rho z^{\text{bo.}} \ , \quad \frac{\partial D_i}{\partial X_i} = \frac{\partial \mathfrak{D}_i}{\partial X_i} - \frac{\partial P_i}{\partial X_i} \ . \tag{VII.38}$$

The balance of electric charge in Eq. (VII.37)$_1$ can be rewritten with the latter,

$$\begin{aligned} \frac{\partial^2 D_i}{\partial t \partial X_i} + \frac{\partial^2 P_i}{\partial X_i \partial t} + \frac{\partial}{\partial X_i}\Big(J_i^{\text{fr.}} + \epsilon_{ijk}\frac{\partial \mathcal{M}_k}{\partial X_j}\Big) = 0 \ , \\ \frac{\partial^2 \mathfrak{D}_i}{\partial t \partial X_i} + \frac{\partial}{\partial X_i}\Big(\mathcal{J}_i^{\text{fr.}} + v_i \frac{\partial \mathfrak{D}_j}{\partial X_j} + \epsilon_{ijk}\frac{\partial \mathcal{M}_k}{\partial X_j}\Big) = 0 \ , \end{aligned} \tag{VII.39}$$

which will be used for computing the electric potential ϕ. It is important to notice that we have interchanged space and time derivation, which is allowed as long as P_i is continuous.

Equation (VII.36)$_2$ can be rewritten once more by using the Maxwell–Lorentz aether relations as in Eq. (VII.7) as follows

$$\begin{aligned} -\frac{\partial \varepsilon_0 E_i}{\partial t} + \epsilon_{ijk}\frac{\partial}{\partial X_j}\Big(\frac{1}{\mu_0}B_k\Big) = J_i \ , \\ \varepsilon_0 \frac{\partial}{\partial t}\Big(\frac{\partial \phi}{\partial X_i} + \frac{\partial A_i}{\partial t}\Big) + \frac{1}{\mu_0}\epsilon_{ijk}\epsilon_{kmn}\frac{\partial^2 A_n}{\partial X_j \partial X_m} = J_i \ , \\ \frac{\partial}{\partial X_i}\Big(\varepsilon_0 \frac{\partial \phi}{\partial t} + \frac{1}{\mu_0}\frac{\partial A_j}{\partial X_j}\Big) + \varepsilon_0 \frac{\partial^2 A_i}{\partial t^2} - \frac{1}{\mu_0}\frac{\partial^2 A_i}{\partial X_j \partial X_j} = J_i \ , \end{aligned} \tag{VII.40}$$

where $\epsilon_{ijk}\epsilon_{kmn} = \delta_{im}\delta_{jn} - \delta_{in}\delta_{jm}$ has been used. By inserting Lorenz's gauge into the latter, the first term vanishes and we obtain the governing equation for calculating the magnetic potential

$$\varepsilon_0 \frac{\partial^2 A_i}{\partial t^2} - \frac{1}{\mu_0}\frac{\partial^2 A_i}{\partial X_j \partial X_j} = J_i \ . \tag{VII.41}$$

The balance of total momentum in Eq. (VII.20)$_2$ reads after inserting the balance of

electromagnetic momentum

$$\rho\frac{\mathrm{d}v_i}{\mathrm{d}t}+\frac{\partial(\mathfrak{D}\times\boldsymbol{B})_i}{\partial t}-\frac{\partial(\sigma_{ji}+m_{ji})}{\partial x_j}-\rho f_i=0\ . \tag{VII.42}$$

The displacement, u_i, is given by

$$u_i=x_i-X_i\ , \tag{VII.43}$$

with the use of the current position, x_i, and the initial position, X_i, of the same particle. Since the initial position, X_i, remains the same,

$$v_i=\frac{\mathrm{d}x_i}{\mathrm{d}t}=\frac{\mathrm{d}u_i}{\mathrm{d}t} \tag{VII.44}$$

holds. By using the latter and neglecting the geometric nonlinearities we obtain the governing equation for the displacement in the initial frame

$$\rho_0\frac{\mathrm{d}^2u_i}{\mathrm{d}t^2}+\frac{\partial(\mathfrak{D}\times\boldsymbol{B})_i}{\partial t}-\frac{\partial(\sigma_{ji}+m_{ji})}{\partial X_j}-\rho f_i=0\ . \tag{VII.45}$$

The balance of internal energy reads in the LAGRANGEan frame without geometric nonlinearities

$$\rho_0\frac{\mathrm{d}u}{\mathrm{d}t}+\frac{\partial q_j}{\partial X_j}-\rho r=\left(\sigma_{ji}-P_jE_i+\mathcal{M}_iB_j\right)\frac{\partial v_i}{\partial X_j}+\mathcal{E}_i\mathcal{J}_i^{\mathrm{fr.}}-P_i\frac{\mathrm{d}E_i}{\mathrm{d}t}+B_i\frac{\mathrm{d}\mathcal{M}_i}{\mathrm{d}t}\ , \tag{VII.46}$$

which can be used as the governing equation for the temperature T.

We have neglected the geometric nonlinearities in the formulation, for a discussion of a more generic formulation we refer to Hutter, 1975. In order to solve all governing equations we need to define *constitutive equations* for P_i, $\mathcal{M}_i$, $\mathcal{J}_i^{\mathrm{fr.}}$, σ_{ij}, u, and q_i.

3. Constitutive equations

The balance of internal energy holds in thermodynamic equilibrium as well as in non-equilibrium. We will separately investigate these cases. In the case of a thermodynamic equilibrium the 1st law of thermodynamics and in the case of non-equilibrium the 2nd law of thermodynamics are going to be used such that all constitutive equations will be derived. The primitive variables are temperature T, displacement u_i, electric potential ϕ, and magnetic potential A_i.

3.1. At equilibrium

Stress, electric and magnetic polarizations are the unknowns. By following the thermodynamics of non-equilibrium processes, we decompose stress and polarization tensors into reversible and a dissipative terms as follows

$$\sigma_{ij} = {}^{\mathrm{r}}\sigma_{ij} + {}^{\mathrm{d}}\sigma_{ij} \ , \quad P_i = {}^{\mathrm{r}}P_i + {}^{\mathrm{d}}P_i \ , \quad \mathcal{M}_i = {}^{\mathrm{r}}\mathcal{M}_i + {}^{\mathrm{d}}\mathcal{M}_i \ . \tag{VII.47}$$

Instead of searching for three tensors, now we search for six tensors. The idea is that in case of equilibrium the dissipative terms vanish. For example the stress tensor has only elasticity in its reversible part. Any viscous effect or plasticity related term belongs to the dissipative term. For the heat flux the decomposition reads according to Groot and Mazur, 1984, Ch. XIV, §2, as follows

$$-\left.\frac{\partial q_i}{\partial X_i}\right|_{\mathrm{eq.}} = \frac{\mathrm{d}Q}{\mathrm{d}t} \ , \quad \frac{1}{T}\frac{\mathrm{d}Q}{\mathrm{d}t} = \rho_0 \frac{\mathrm{d}\eta}{\mathrm{d}t} \ , \tag{VII.48}$$

where the specific entropy, η, has been introduced. We need a constitutive equation for the entropy that adopts the role of the heat flux in the case of equilibrium.

At equilibrium, a supply term is not allowed. By supplying energy into system by means of radiant heating, r, we cannot expect to reach an equilibrium. A conducting current prohibits an electromagnetic equilibrium such that $\mathcal{J}_i^{\mathrm{fr.}}$ has to vanish in the case of equilibrium. Therefore, at equilibrium the balance of internal energy reduces to

$$\rho_0 \frac{\mathrm{d}u}{\mathrm{d}t} - \rho_0 T \frac{\mathrm{d}\eta}{\mathrm{d}t} = {}^{\mathrm{r}}\sigma_{ji}\frac{\mathrm{d}\varepsilon_{ij}}{\mathrm{d}t} - {}^{\mathrm{r}}P_i \frac{\mathrm{d}E_i}{\mathrm{d}t} + B_i \frac{\mathrm{d}\,{}^{\mathrm{r}}\mathcal{M}_i}{\mathrm{d}t} \ , \tag{VII.49}$$

with reversible parts of stress and polarization tensors. According to the 1st law of thermodynamics there exists a total differential for the internal energy, see Pauli, 1973. Hence, the latter can be rewritten

$$\mathrm{d}u = T\,\mathrm{d}\eta + {}^{\mathrm{r}}\sigma_{ji} v\,\mathrm{d}\varepsilon_{ij} - {}^{\mathrm{r}}P_i v\,\mathrm{d}E_i + B_i v\,\mathrm{d}\,{}^{\mathrm{r}}\mathcal{M}_i \ , \tag{VII.50}$$

where we have utilized the specific volume, $v = 1/\rho_0$, which is constant (in time) in the LAGRANGEan frame. The latter equation may be called GIBBS's equation. By integrating the latter we can define the specific internal energy, after having defined η, ${}^{\mathrm{r}}\sigma_{ji}$, ${}^{\mathrm{r}}P_i$, and ${}^{\mathrm{r}}\mathcal{M}_i$. The objective is to express all quantities by means of the primitive variables $\{T, u_i, \phi, A_i\}$. We name $\{T, \varepsilon_{ij}, E_i, B_i\}$ as primary or state variables and we search for the dual variables $\{\eta, {}^{\mathrm{r}}\sigma_{ji}, {}^{\mathrm{r}}P_i, {}^{\mathrm{r}}\mathcal{M}_i\}$. For their detailed derivation, we refer

to Appendix C and write the general relations for the dual variables

$$\begin{aligned}
\mathrm{d}\eta &= \tilde{c}\,\mathrm{d}T + vC_{ijkl}\alpha_{kl}\,\mathrm{d}\varepsilon_{ij} - v\tilde{T}_{ijk}\alpha_{jk}\,\mathrm{d}E_i - v\tilde{S}_{ijk}\alpha_{jk}\,\mathrm{d}B_i\ ,\\
\mathrm{d}^{\mathrm{r}}\sigma_{ij} &= -C_{ijkl}\alpha_{kl}\,\mathrm{d}T + C_{ijkl}\,\mathrm{d}\varepsilon_{kl} - \tilde{T}_{kij}\,\mathrm{d}E_k + \tilde{S}_{kji}\,\mathrm{d}B_k\ ,\\
\mathrm{d}^{\mathrm{r}}P_i &= -\tilde{T}_{ijk}\alpha_{jk}\,\mathrm{d}T + \tilde{T}_{ijk}\,\mathrm{d}\varepsilon_{jk} + \tilde{\chi}^{\mathrm{el.}}_{ij}\,\mathrm{d}E_j + \tilde{R}_{ji}\,\mathrm{d}B_j\ ,\\
\mathrm{d}^{\mathrm{r}}\mathcal{M}_i &= -\tilde{S}_{ijk}\alpha_{jk}\,\mathrm{d}T + \tilde{S}_{ijk}\,\mathrm{d}\varepsilon_{jk} + \tilde{R}_{ij}\,\mathrm{d}E_j + \tilde{\chi}^{\mathrm{mag.}}_{ij}\,\mathrm{d}B_j\ .
\end{aligned} \tag{VII.51}$$

Experiments are necessary in order to determine the coefficients, namely $\tilde{c}$, C_{ijkl}, α_{ij}, $\tilde{T}_{ijk}$, $\tilde{S}_{ijk}$, $\tilde{\chi}^{\mathrm{el.}}_{ij}$, $\tilde{R}_{ij}$, $\tilde{\chi}^{\mathrm{mag.}}_{ij}$. These experiments are established by varying a primary variable while holding the other primary variables fixed and measuring the corresponding dual variables. The stiffness tensor, C_{ijkl}, is measured for fixed temperature, $\mathrm{d}T = 0$, fixed electric field, $\mathrm{d}E_i = 0$, fixed magnetic intensity, $\mathrm{d}B_i = 0$, by varying strain, $\mathrm{d}\varepsilon_{ij}$, and measuring stress, $\mathrm{d}\sigma_{ij}$. The parameter $\tilde{\chi}^{\mathrm{el.}}_{ij}$ is measured analogously by varying $\mathrm{d}E_i$ and measuring $\mathrm{d}^{\mathrm{r}}P_i$. Often the susceptibility is measured by varying the charge potential and measuring the polarization such that we write $\tilde{\chi}^{\mathrm{el.}}_{ij} = \varepsilon_0\chi^{\mathrm{el.}}_{ij}$ with the vacuum permittivity ε_0 and the electric susceptibility $\chi^{\mathrm{el.}}_{ij}$ of the material. The parameter $\tilde{\chi}^{\mathrm{mag.}}_{ij}$ is measured by varying $\mathrm{d}B_i$ and measuring $\mathrm{d}^{\mathrm{r}}\mathcal{M}_i$. It is often the case that the charge potential is varied and polarization is measured, so we write $\tilde{\chi}^{\mathrm{mag.}}_{ij} = (\boldsymbol{\mu}^{-1}_{\mathrm{mag.}})_{ik}\chi^{\mathrm{mag.}}_{kj}$ with the magnetic susceptibility $\chi^{\mathrm{mag.}}_{ij}$ and permeability $\mu_{\mathrm{mag.}}$ of the material. We cannot measure entropy directly but the heat energy $\delta Q = T\rho_0\,\mathrm{d}\eta$ can be measured by varying temperature $\delta Q = T\rho_0\tilde{c}\,\mathrm{d}T$. The relation between heat energy and temperature is referred to as the specific heat capacity $c = T\tilde{c}$. If we would write Eq. (VII.51) in a matrix form, all direct coefficients would be on the diagonal. Diagonal coefficients for many engineering materials can be found in the literature. The off-diagonal terms are called coupling coefficients. Magnetoelectric coupling, $\tilde{R}_i$, piezoelectric tensor, $\tilde{T}_{ijk}$, piezomagnetic tensor, $\tilde{S}_{ijk}$, and thermal expansion coefficients, α_{ij} are to be determined in an analogous fashion. Their experiments are more challenging. By varying magnetic flux and measuring electric polarization, we can obtain the coefficients of magnetoelectric coupling. By varying strains and measuring electric or magnetic polarization, piezoelectric or piezomagnetic tensor is determined. Strain variation leading to temperature change gives the coefficients of thermal expansion. All coefficients can be a function of primary variables.

For a simple and linear material, where material parameters are constants in the primary variables,[86] we can obtain the dual variables simply by integrating from the

[86] For heterogeneous materials the material parameters depend on X_i.

ground or reference state, $T = T_{\text{ref.}}$, $\varepsilon_{ij} = 0$, $E_i = 0$, $B_i = 0$, to the present state

$$\begin{aligned}
\eta &= c \ln\left(\frac{T}{T_{\text{ref.}}}\right) + v C_{ijkl}\alpha_{kl}\varepsilon_{ij} - v\tilde{T}_{ijk}\alpha_{jk}E_i - v\tilde{S}_{ijk}\alpha_{jk}B_i \ , \\
{}^{\text{r}}\sigma_{ij} &= -C_{ijkl}\alpha_{kl}(T - T_{\text{ref.}}) + C_{ijkl}\varepsilon_{kl} - \tilde{T}_{kij}E_k + \tilde{S}_{kji}B_k \ , \\
{}^{\text{r}}P_i &= -\tilde{T}_{ijk}\alpha_{jk}(T - T_{\text{ref.}}) + \tilde{T}_{ijk}\varepsilon_{jk} + \varepsilon_0\chi^{\text{el.}}_{ij}E_j + \tilde{R}_{ji}B_j \ , \\
{}^{\text{r}}\mathcal{M}_i &= -\tilde{S}_{ijk}\alpha_{jk}(T - T_{\text{ref.}}) + \tilde{S}_{ijk}\varepsilon_{jk} + \tilde{R}_{ij}E_j + (\boldsymbol{\mu}^{-1}_{\text{mag.}})_{ik}\chi^{\text{mag.}}_{kj}B_j \ .
\end{aligned} \tag{VII.52}$$

By defining all dual variables, we have completely defined the internal energy necessary for Eq. (VII.49). Furthermore, we assume that the same relation holds at non-equilibrium, in other words, we suppose that the internal energy is fully recoverable by following Pauli, 1973. Since we have used a kinetic energy depending on the velocity (rate of displacement), the presented theory is capable of describing systems, where rate of temperature and electromagnetic potentials are sufficiently small such that they do not contribute to the total energy.

3.2. At non-equilibrium

Now, even in the case of non-equilibrium, the balance of internal energy can be rewritten by inserting Eq. (VII.50) as follows

$$\begin{aligned}
\rho_0 T\frac{\mathrm{d}\eta}{\mathrm{d}t} + \frac{\partial q_j}{\partial X_j} - \rho_0 r = \big({}^{\text{d}}\sigma_{ji} - P_j E_i + \mathcal{M}_i B_j\big)\frac{\partial v_i}{\partial X_j} + \\
+ \mathcal{E}_i \mathcal{J}^{\text{fr.}}_i - \frac{1}{T}\,{}^{\text{d}}P_i\frac{\mathrm{d}E_i}{\mathrm{d}t} + \frac{1}{T}B_i\frac{\mathrm{d}\,{}^{\text{d}}\mathcal{M}_i}{\mathrm{d}t} \ ,
\end{aligned} \tag{VII.53}$$

thus,

$$\begin{aligned}
\rho_0\frac{\mathrm{d}\eta}{\mathrm{d}t} + \frac{\partial}{\partial X_j}\left(\frac{q_j}{T}\right) - \rho_0\frac{r}{T} = q_j\frac{\partial}{\partial X_j}\left(\frac{1}{T}\right) + \frac{1}{T}\big({}^{\text{d}}\sigma_{ji} - P_j E_i + \mathcal{M}_i B_j\big)\frac{\partial v_i}{\partial X_j} + \\
+ \frac{1}{T}\mathcal{E}_i \mathcal{J}^{\text{fr.}}_i - \frac{1}{T}\,{}^{\text{d}}P_i\frac{\mathrm{d}E_i}{\mathrm{d}t} + \frac{1}{T}B_i\frac{\mathrm{d}\,{}^{\text{d}}\mathcal{M}_i}{\mathrm{d}t} \ ,
\end{aligned} \tag{VII.54}$$

such that the latter equation is the balance of entropy:

$$\rho_0\frac{\mathrm{d}\eta}{\mathrm{d}t} + \frac{\partial\Phi_j}{\partial X_j} - \rho_0\frac{r}{T} = \Sigma \ , \tag{VII.55}$$

with a flux term, Φ, and a production term, Σ, as follows

$$\begin{aligned} \Phi_j &= \frac{q_j}{T} \ , \\ \Sigma &= -\frac{q_j}{T^2}\frac{\partial T}{\partial X_j} + \frac{1}{T}\big({}^{\mathrm{d}}\sigma_{ji} - P_j E_i + \mathcal{M}_i B_j\big)\frac{\partial v_i}{\partial X_j} + \\ &\quad + \frac{1}{T}\mathcal{E}_i \mathcal{J}_i^{\mathrm{fr.}} - \frac{1}{T}\,{}^{\mathrm{d}}P_i \frac{\mathrm{d}E_i}{\mathrm{d}t} + \frac{1}{T}B_i \frac{\mathrm{d}\,{}^{\mathrm{d}}\mathcal{M}_i}{\mathrm{d}t} \ . \end{aligned} \tag{VII.56}$$

The entropy flux can differ from this formulation if the energy flux in Eq. $(\text{VII.28})_2$ is defined differently. For example, we could include the term $\boldsymbol{E} \times \boldsymbol{\mathfrak{H}}$ into the heat flux. Then the entropy flux and production would have an additional term in the heat flux similar to a Hall effect. For its interpretation see Müller, 1985, §9.9.4. We continue by using the chosen definition. Moreover, we restrict our formalism and neglect any irreversible polarization terms, ${}^{\mathrm{d}}P_i = 0$, ${}^{\mathrm{d}}\mathcal{M}_i = 0$, and thus

$$P_i = {}^{\mathrm{r}}P_i \ , \quad \mathcal{M}_i = {}^{\mathrm{r}}\mathcal{M}_i \ . \tag{VII.57}$$

This assumption is based on the experimental observation that a piezoelectric material performs no irreversible work in action. In its own jargon one says that the piezoelectric transducers work in *zero energy*. This condition leads to the following entropy production:

$$\Sigma = -\frac{q_j}{T^2}\frac{\partial T}{\partial X_j} + \frac{1}{T}\big({}^{\mathrm{d}}\sigma_{ji} - P_j E_i + \mathcal{M}_i B_j\big)\frac{\partial v_i}{\partial X_j} + \frac{1}{T}\mathcal{E}_i \mathcal{J}_i^{\mathrm{fr.}} \ . \tag{VII.58}$$

According to the 2nd law of thermodynamics the production of entropy is zero for reversible processes (at equilibrium) and greater than zero for irreversible processes (at non-equilibrium), $\Sigma \geq 0$. Moreover, tensors of rank two can be decomposed into the spherical, symmetric deviatoric, and antisymmetric terms. For example, a generic tensor of rank two, A_{ij}, can be decomposed as follows

$$\begin{aligned} A_{ji} &= A_{(ji)} + A_{[ji]} = A_{|(ji)|} + \frac{1}{3}A_{kk}\delta_{ji} + A_{[ji]} \ , \\ A_{(ji)} &= \frac{1}{2}\big(A_{ji} + A_{ij}\big) \ , \quad A_{|(ji)|} = A_{(ji)} - \frac{1}{3}A_{kk}\delta_{ji} \ , \quad A_{[ji]} = \frac{1}{2}\big(A_{ji} - A_{ij}\big) \ . \end{aligned} \tag{VII.59}$$

Hence we can introduce a new term for brevity and apply the decomposition

$$\begin{aligned} {}^{\mathrm{d}}\sigma_{ji} - P_j E_i + \mathcal{M}_i B_j &= \Xi_{ji} \ , \\ \frac{1}{T}\Xi_{ji}\frac{\partial v_i}{\partial X_j} &= \frac{1}{T}\Xi_{|(ji)|}\frac{\partial v_{|(i}}{\partial X_{j)|}} + \frac{1}{3T}\Xi_{ii}\frac{\partial v_j}{\partial X_j} + \frac{1}{T}\Xi_{[ji]}\frac{\partial v_{[i}}{\partial X_{j]}} \ . \end{aligned} \tag{VII.60}$$

Moreover, we can rewrite the production of entropy by introducing two lists:

$$\begin{aligned}\mathcal{K}^\alpha &= \left\{ \frac{1}{T^2}\frac{\partial T}{\partial X_j} \ , \quad \frac{1}{T}\frac{\partial v_{|(i}}{\partial X_{j)|}} \ , \quad \frac{1}{3T}\frac{\partial v_j}{\partial X_j} \ , \quad \frac{1}{T}\frac{\partial v_{[i}}{\partial X_{j]}} \ , \quad \frac{1}{T}\mathcal{E}_i \right\} \ , \\ \mathcal{F}^\alpha &= \left\{ -q_j \ , \quad \Xi_{|(ji)|} \ , \quad \Xi_{ii} \ , \quad \Xi_{[ji]} \ , \quad \mathcal{J}_i^{\text{fr.}} \right\} \ ,\end{aligned} \tag{VII.61}$$

where the so-called *thermodynamical forces*, $\mathcal{K}^\alpha$, are derived from the primitive variables; the *thermodynamical fluxes*, $\mathcal{F}^\alpha$, shall be defined depending on the thermodynamical forces. The production of entropy reads

$$\Sigma = \mathcal{K}^\alpha \cdot \mathcal{F}^\alpha \geq 0 \ , \quad \alpha = 1, 2, \dots 5 \ , \tag{VII.62}$$

where the summation convention is used over α. In principle, the thermodynamical fluxes may depend on all thermodynamical forces. However, their multiplication has to be a scalar. Therefore, there occurs an important restriction that the thermodynamical fluxes may depend only on the thermodynamical forces of the same type. This restriction is due to the different transformation properties of tensors of different types and referred to as the Curie principle. Tensors of different ranks are of different types. The symmetric and antisymmetric tensors are of different types. Since the dependency is limited we can readily propose the constitutive equations by applying representation theorems. The thermodynamical flux of rank zero reads

$$\Xi_{ii} = \bar{A}\frac{1}{3T}\frac{\partial v_j}{\partial X_j} \ . \tag{VII.63}$$

Analogously, the thermodynamical fluxes of rank one become

$$-q_j = \bar{a}\frac{1}{T^2}\frac{\partial T}{\partial X_j} + \bar{b}\frac{1}{T}\mathcal{E}_j \ , \quad \mathcal{J}_i^{\text{fr.}} = \bar{B}\frac{1}{T^2}\frac{\partial T}{\partial X_j} + \bar{c}\frac{1}{T}\mathcal{E}_j \ . \tag{VII.64}$$

The thermodynamical fluxes of rank two reads

$$\Xi_{|(ji)|} = \bar{d}_1\frac{1}{T}\frac{\partial v_{|(i}}{\partial X_{j)|}} + \bar{d}_2\frac{1}{T}\frac{\partial v_{|(i}}{\partial X_{k)|}}\frac{\partial v_{|(k}}{\partial X_{j)|}} \ , \quad \Xi_{[ji]} = \bar{e}_1\frac{1}{T}\frac{\partial v_{[i}}{\partial X_{j]}} + \bar{e}_2\frac{1}{T}\frac{\partial v_{[i}}{\partial X_{k]}}\frac{\partial v_{[k}}{\partial X_{j]}} \ . \tag{VII.65}$$

In order to fulfill the 2nd law of thermodynamics we acquire

$$\begin{aligned}\Sigma = \frac{\bar{A}}{9T^2}\frac{\partial v_i}{\partial X_i}\frac{\partial v_j}{\partial X_j} + \frac{\bar{a}}{T^4}\frac{\partial T}{\partial X_j}\frac{\partial T}{\partial X_j} + \frac{1}{T^3}\frac{\partial T}{\partial X_j}\mathcal{E}_j(\bar{b}+\bar{B}) + \bar{c}\frac{1}{T^2}\mathcal{E}_i\mathcal{E}_i + \\ + \frac{\bar{d}_1}{T^2}\frac{\partial v_{|(i}}{\partial X_{j)|}}\frac{\partial v_{|(i}}{\partial X_{j)|}} + \frac{\bar{d}_2}{T^2}\frac{\partial v_{|(i}}{\partial X_{k)|}}\frac{\partial v_{|(k}}{\partial X_{j)|}}\frac{\partial v_{|(i}}{\partial X_{j)|}} + \\ + \frac{\bar{e}_1}{T^2}\frac{\partial v_{[i}}{\partial X_{j]}}\frac{\partial v_{[i}}{\partial X_{j]}} + \frac{\bar{e}_2}{T^2}\frac{\partial v_{[i}}{\partial X_{k]}}\frac{\partial v_{[k}}{\partial X_{j]}}\frac{\partial v_{[i}}{\partial X_{j]}} \geq 0 \ .\end{aligned} \tag{VII.66}$$

For any process $\Sigma \geq 0$ has to hold. Since the quadratic terms are positive, we realize that $\bar{A} > 0$, $\bar{a} > 0$, $\bar{c} > 0$, $\bar{d}_1 > 0$, and $\bar{e}_1 > 0$ have to hold. In some processes the cubic terms can be positive, too. However, in order to fulfill the 2nd law in all processes, we coerce the parameters into $\bar{d}_2 = 0$ and $\bar{e}_2 = 0$. Analogously, for the coupling constants we have to obtain $\bar{b} + \bar{B} = 0$ in order to inhibit a negative entropy production. These interpretations are based only on the 2nd law; although $\bar{b} = -\bar{B}$ is also referred to as ONSAGER's relation, which is motivated differently and allowing only for linear relations between thermodynamical fluxe and forces. It is of paramount importance to state that the approach herein has no such a restriction: the material parameters are scalar functions of the corresponding thermodynamical forces. This scalar functions can be nonlinear equations depending on (the invariants of) thermodynamical forces. Since determination of material parameters for nonlinear models is challenging in experiments, often, linear models are chosen for simulations.

For showing the relevance to well-established phenomenological equations, we rename the material parameters

$$\kappa = \frac{\bar{a}}{T^2} \ , \quad \varsigma = \frac{\bar{c}}{T} \ , \quad \varsigma\pi = -\frac{\bar{b}}{T^2} \ , \tag{VII.67}$$

and obtain the following constitutive equations:

$$q_i = -\kappa \frac{\partial T}{\partial X_i} + \varsigma\pi T \mathcal{E}_i \ , \quad \mathcal{J}_i^{\text{fr.}} = \varsigma\pi \frac{\partial T}{\partial X_i} + \varsigma \mathcal{E}_i \ . \tag{VII.68}$$

The heat conduction coefficient, κ, electrical conductivity, ς, and the thermoelectric coupling coefficient, π, need to be determined experimentally. The thermoelectric coupling is constant for many engineering materials and called the PELTIER constant. Actually every conducting material possesses a PELTIER constant; however, it might be so small that we can neglect it. For the case of $\kappa = \text{const.}$ and $\pi = 0$ the constitutive equation for the heat flux is referred to as FOURIER's law. For the case of $\varsigma = \text{const.}$ and $\pi = 0$ the constitutive equation for the electric current is called OHM's law.

For all applications in this work, the deformation remains in the elastic regime such that we exclude viscoelasticity and plasticity by setting $\bar{A} = 0$, $\bar{d}_1 = 0$, and $\bar{e}_1 = 0$.

The dissipative stress tensor becomes

$$\begin{gathered}\Xi_{ii} = 0 \ , \quad \Xi_{|(ij)|} = 0 \ , \quad \Xi_{[ij]} = 0 \ , \\ {}^{\mathrm{d}}\sigma_{ii} = P_i E_i - \mathcal{M}_i B_i \ , \quad {}^{\mathrm{d}}\sigma_{|(ji)|} = P_{|j} E_{i)|} - \mathcal{M}_{|(i} B_{j)|} \ , \quad {}^{\mathrm{d}}\sigma_{[ji]} = P_{[j} E_{i]} - \mathcal{M}_{[i} B_{j]} \ , \\ {}^{\mathrm{d}}\sigma_{ji} = \frac{1}{3}\,{}^{\mathrm{d}}\sigma_{kk}\delta_{ji} + {}^{\mathrm{d}}\sigma_{|(ji)|} + {}^{\mathrm{d}}\sigma_{[ji]} = P_j E_i - \mathcal{M}_i B_j \ .\end{gathered} \tag{VII.69}$$

We have deduced all necessary constitutive equations (VII.52), (VII.68), (VII.69) by using thermodynamics. The material parameters c, C_{ijkl}, $\tilde{T}_{ijk}$, $\tilde{S}_{ijk}$, α_{ij}, $\chi^{\mathrm{el.}}_{ij}$, $\tilde{R}_{ij}$, $\chi^{\mathrm{mag.}}_{ij}$ in Eqs. (VII.52) and the parameters κ, ς, π in Eqs. (VII.68) are all constants such that the material is *linear*. For nonlinear materials the dependency has to be determined by experiments such that the integration leading to Eqs. (VII.52) can be established. All necessary constitutive equations are defined, so the governing equations are now closed and can be solved. Since we have acquired many different coupling terms, the governing equations are coupled. Even in the case of linear materials, due to the production term in the balance of energy and effected by the coupling terms, the governing equations are nonlinear.

4. Computational approach

We want to demonstrate engineering applications, where the primitive variables, ϕ, A_i, u_i, T, are computed as functions of space X_i and time t. Since X_i is constant in time, the time rate is simply the partial time derivative. We introduce $(\cdot)_{,i}$, for the partial derivative in X_i and recall the governing equations from Eqs. (VII.39), (VII.41), (VII.45), (VII.46) in the LAGRANGEan frame:

$$\begin{gathered}\frac{\partial \mathfrak{D}_{i,i}}{\partial t} + \left(\jmath^{\mathrm{fr.}}_i + v_i \mathfrak{D}_{j,j} + \epsilon_{ijk}\mathcal{M}_{k,j}\right)_{,i} = 0 \ , \\ \varepsilon_0 \frac{\partial^2 A_i}{\partial t^2} - \frac{1}{\mu_0}\frac{\partial^2 A_i}{\partial X_j \partial X_j} = \jmath^{\mathrm{fr.}}_i + v_i \mathfrak{D}_{j,j} + \frac{\partial P_i}{\partial t} + \epsilon_{ijk}\mathcal{M}_{k,j} \ , \\ \rho_0 \frac{\partial^2 u_i}{\partial t^2} + \epsilon_{ijk}\frac{\partial \mathfrak{D}_j B_k}{\partial t} - (\sigma_{ji} + m_{ji})_{,j} - \rho_0 f_i = 0 \ , \\ \rho_0 \frac{\partial \eta}{\partial t} + \Phi_{j,j} - \rho_0 \frac{r}{T} = \Sigma \ ,\end{gathered} \tag{VII.70}$$

in order to compute the primitive variables ϕ, A_i, u_i, T, respectively. We generate the so-called *weak form* by applying the following three steps:

1. Discretization in time by using the finite difference method and applying the variational formulation.

2. Linearization at the partial differential level with the Newton–Raphson method.

3. Discretization in space by using the finite element method.

This weak form leads to a monolithic computation of primitive variables. The order of the aforementioned steps is of importance. First, the time discretization will be discussed and applied. Secondly, the linearization will be performed. The linearization is at the level of partial differential equations. Thirdly, the space discretization will be applied. Therefore, the linearization is independent of the chosen type of space discretization, which is a great benefit. Especially in a nonlinear and coupled set of equations this feature eliminates numerical problems implied by the choice of element type and quality. Moreover, any type of nonlinearity can be solved by using aforementioned steps.

An important difference to the existing literature needs to be recalled in the computational approach that we implement. Galerkin method suggests to use the same type of elements for the primitive as well as their test functions. Standard finite elements are of order one within the element and continuous across elements. These continuous piecewise polynomials are often called $\mathcal{P}_1$ elements. For mechanics and thermodynamics, it is typical to use this element type. Starting with Raviart and Thomas, 1977 and Nédélec, 1980, solution of Maxwell's equation by using finite element method has emerged by using mixed elements. Various techniques are introduced, among others, see for example Bossavit, 1988, Ciarlet Jr and Zou, 1999, Demkowicz, 2006, Sect. 17, J. Li, 2009, Gillette, Rand, and Bajaj, 2016. Nowadays, there are many different element types, see Arnold and Logg, 2014. The general idea in computation of electromagnetism relies on solving electromagnetic fields, namely E_i and B_i, directly by satisfying all Maxwell equations. Although, from a theoretical point of view, this method is correct, we have seen in the formulation that the introduction of electromagnetic potentials ϕ and A_i simplified the procedure. We solve electromagnetic potentials instead of electromagnetic fields. Furthermore, the special elements have the correct representation of electromagnetic fields satisfying jump conditions. We will naturally implement the jump conditions in this section such that we do not need to use any special finite element. All simulations are accomplished by using the same, standard, namely $\mathcal{P}_1$ elements for each primitive variable ϕ, A_i, u_i, and T.

For the time discretization we employ the finite difference method

$$\frac{\partial(\cdot)}{\partial t} \approx \frac{(\cdot) - (\cdot)^0}{\Delta t} \,. \tag{VII.71}$$

The time interval Δt is kept constant throughout the simulation, whereas a sufficiently small interval leads to a converged solution. In Eq. (VII.71) the symbols $(\cdot)$ denote the numerical values in the current time, in other words, they are the unknowns. The previously computed values $(\cdot)^0$ one time step before are known. We use this time discretization for all partial time derivatives in Eqs. (VII.70). This method is stable for every real valued problems, since the evaluation of the time derivative is accomplished at the current time.

In order to generate the weak form, we multiply the governing equations with the corresponding test functions, $\delta\phi$, δA_i, δu_i, δT, and integrate over a computational domain Ω^*, where all constitutive equations are continuous. We assume that primitive variables and their derivatives are continuous in the whole domain. Therefore, the primary variables are continuous. If we only employ one material in the computation, then the dual variables are continuous, too. However, if there are several materials in the domain, then due to the jump of the material parameters on the interface between two adjacent materials, the dual variables are not continuous. Consider $\Omega = \Omega_1 \cup \Omega_2$, where $\Omega_\times$ denotes the domain of a material. On the adjacent faces there is an interface Ω^I, which is a singular surface for the dual variable possessing a jump over this interface. By using an integration by parts in each finite sized element, we obtain a boundary term. After adding up all elements compiling the computational domain, the adjacent boundaries belonging to the same material vanish. This fact is owing to the opposite boundary normals N_i on boundaries of adjacent elements and because of the identical value of the integrand within one material. If, however, the boundary is an interface then there is a jump, which we explicitly write in the following. We start with Eqs. $(\text{VII.70})_{1,2}$ and obtain the following weak forms in the unit of energy:

$$\begin{aligned}\mathrm{F}_\phi = \int_\Omega \big(&- (\mathfrak{D}_i - \mathfrak{D}_i^0)\delta\phi_{,i} - \Delta t \mathfrak{J}_i^{\mathrm{fr.}}\delta\phi_{,i} - (u_i - u_i^0)\mathfrak{D}_{j,j}\delta\phi_{,i} - \Delta t \epsilon_{ijk}\mathcal{M}_{k,j}\delta\phi_{,i}\big)\,\mathrm{d}V + \\ &+ \int_{\partial\Omega^I} N_i \Big[\!\Big[\mathfrak{D}_i - \mathfrak{D}_i^0 + \Delta t \mathfrak{J}_i^{\mathrm{fr.}} + (u_i - u_i^0)\mathfrak{D}_{j,j} + \Delta t \epsilon_{ijk}\mathcal{M}_{k,j} \Big]\!\Big] \delta\phi \,\mathrm{d}A + \\ &+ \int_{\partial\Omega} N_i \Big(\mathfrak{D}_i - \mathfrak{D}_i^0 + \Delta t \mathfrak{J}_i^{\mathrm{fr.}} + (u_i - u_i^0)\mathfrak{D}_{j,j} + \Delta t \epsilon_{ijk}\mathcal{M}_{k,j} \Big) \delta\phi \,\mathrm{d}A \ ,\end{aligned} \tag{VII.72}$$

for the electic potential as well as

$$\begin{aligned}\mathrm{F}_{\boldsymbol{A}} = \int_\Omega \Big(&\varepsilon_0 \frac{A_i - 2A_i^0 + A_i^{00}}{\Delta t \Delta t}\delta A_i + \frac{1}{\mu_0} A_{i,j}\delta A_{i,j} - \mathfrak{J}_i^{\mathrm{fr.}}\delta A_i - \frac{u_i - u_i^0}{\Delta t}\mathfrak{D}_{j,j}\delta A_i - \\ &- \frac{P_i - P_i^0}{\Delta t}\delta A_i + \epsilon_{ijk}\mathcal{M}_k \delta A_{i,j} \Big)\,\mathrm{d}V - \int_{\partial\Omega^I} \Big[\!\Big[\frac{1}{\mu_0} A_{i,j} + \epsilon_{ijk}\mathcal{M}_k \Big]\!\Big] \delta A_i N_j \,\mathrm{d}A - \\ &- \int_{\partial\Omega} \Big(\frac{1}{\mu_0} A_{i,j} + \epsilon_{ijk}\mathcal{M}_k \Big) \delta A_i N_j \,\mathrm{d}A \ ,\end{aligned} \tag{VII.73}$$

for the magnetic potential. The jump brackets $[\![\dots]\!]$ denotes the difference between the values of the integrand as calculated from Ω_1 and from Ω_2. For the sake of brevity we skip a lengthy derivation of balance equations on singular surfaces and assume that the singular surface is just an interface between two materials, it is a fictitious separation without its own mass. Then the balance equations on a singular surface—moving with velocity $\boldsymbol{w}$—read

$$\boldsymbol{N} \cdot [\![\boldsymbol{\mathfrak{D}}]\!] = q^{\text{fr.}} \ , \quad \boldsymbol{N} \cdot \boldsymbol{w}[\![\boldsymbol{\mathfrak{D}}]\!] + \boldsymbol{N} \times [\![\boldsymbol{\mathfrak{H}}]\!] = \boldsymbol{j}^{\text{fr.}} \ , \tag{VII.74}$$

where $q^{\text{fr.}}$ denotes surface charge and $\boldsymbol{j}^{\text{fr.}}$ surface current, see for example Reich, Stahn, and Müller, 2015, Table 1. We identify the singular surface with the interface. The interface does not move with respect to the initial frame, $w_i = 0$. Moreover, we assume that surface charge and current can be neglected for the selected applications of solid bodies. They would be important in applications of mixtures where adhesive forces alter the motion. Under these conditions the balance equations on singular surfaces read

$$N_i[\![\mathfrak{D}_i]\!] = 0 \ , \quad \epsilon_{ijk} N_j [\![\mathfrak{H}_k]\!] = 0 \ , \tag{VII.75}$$

The first equation can be used directly in Eq. (VII.72). By neglecting surface current and by using the first equation, we can imply that the jump of electric current in normal direction is zero, $N_i[\![\mathcal{J}_i^{\text{fr.}}]\!] = 0$. The second equation in Eq. (VII.75) needs to be rewritten. By using $+$ for the material within Ω_1 and $-$ for the adjacent material within Ω_2 we can rewrite the latter equations:

$$\begin{aligned} \epsilon_{ijk} N_j [\![H_k - \mathcal{M}_k]\!] = 0 \ , \\ \epsilon_{ijk} N_j [\![H_k]\!] = \epsilon_{ijk} N_j [\![\mathcal{M}_k]\!] \ , \\ \epsilon_{ijk} N_j \frac{1}{\mu_0} \epsilon_{klm} [\![A_{m,l}]\!] = \epsilon_{ijk} N_j [\![\mathcal{M}_k]\!] \ . \end{aligned} \tag{VII.76}$$

Since the primitive variables and their derivatives are continuous, we conclude that the right-hand side has to vanish. We will model the application to be surrounding with air and set the electromagnetic potentials zero on the boundaries $\partial\Omega$. Hence, the test functions $\delta\phi$, δA_i vanish on $\partial\Omega$. By inserting the results from the singular balance equations the weak forms read

$$\begin{aligned} \mathrm{F}_\phi = \int_\Omega \big(&- (\mathfrak{D}_i - \mathfrak{D}_i^0)\delta\phi_{,i} - \Delta t \mathcal{J}_i^{\text{fr.}} \delta\phi_{,i} - (u_i - u_i^0)\mathfrak{D}_{j,j}\delta\phi_{,i} - \\ &- \Delta t \epsilon_{ijk} \mathcal{M}_{k,j} \delta\phi_{,i} \big) \, \mathrm{d}V + \int_{\partial\Omega^I} N_i \Delta t \epsilon_{ijk} [\![\mathcal{M}_{k,j}]\!] \delta\phi \, \mathrm{d}A \end{aligned} \tag{VII.77}$$

and

$$\begin{aligned} \mathrm{F}_{\boldsymbol{A}} = \int_\Omega \Big(&\varepsilon_0 \frac{A_i - 2A_i^0 + A_i^{00}}{\Delta t \Delta t} \delta A_i + \frac{1}{\mu_0} A_{i,j} \delta A_{i,j} - \mathcal{J}_i^{\text{fr.}} \delta A_i - \\ &- \frac{u_i - u_i^0}{\Delta t} \mathfrak{D}_{j,j} \delta A_i - \frac{P_i - P_i^0}{\Delta t} \delta A_i + \epsilon_{ijk} \mathcal{M}_k \delta A_{i,j} \Big) \, \mathrm{d}V \ , \end{aligned} \tag{VII.78}$$

with the following constitutive equations

$$\begin{aligned} \mathcal{J}_i^{\text{fr.}} &= \varsigma\pi T_{,i} + \varsigma\mathcal{E}_i \ , \\ P_i &= -\tilde{T}_{ijk}\alpha_{jk}(T - T_{\text{ref.}}) + \tilde{T}_{ijk}\varepsilon_{jk} + \varepsilon_0\chi_{ij}^{\text{el.}}E_j + \tilde{R}_{ji}B_j \ , \\ \mathcal{M}_i &= -\tilde{S}_{ijk}\alpha_{jk}(T - T_{\text{ref.}}) + \tilde{S}_{ijk}\varepsilon_{jk} + \tilde{R}_{ij}E_j + (\boldsymbol{\mu}_{\text{mag.}}^{-1})_{ik}\chi_{kj}^{\text{mag.}}B_j \ , \end{aligned} \tag{VII.79}$$

and the following complementary relations

$$\begin{aligned} \mathfrak{D}_i = D_i + P_i \ , \quad \mathcal{E}_i = E_i + \epsilon_{ijk}\frac{u_j - u_j^0}{\Delta t}B_k \ , \\ E_i = -\phi_{,i} - \frac{A_i - A_i^0}{\Delta t} \ , \quad B_i = \epsilon_{ijk}A_{k,j} \ . \end{aligned} \tag{VII.80}$$

For computing the displacement we acquire a weak form from Eq. (VII.70)$_3$. We combine Cauchy's and Maxwell's stress

$$\begin{aligned} \sigma_{ji} = {}^{\text{d}}\sigma_{ji} + {}^{\text{r}}\sigma_{ji} = P_jE_i - \mathcal{M}_iB_j - C_{jikl}\alpha_{kl}(T - T_{\text{ref.}}) + C_{jikl}\varepsilon_{kl} - \\ -\tilde{T}_{kji}E_k + \tilde{S}_{kji}B_k \ , \\ m_{ji} = -\frac{1}{2}\delta_{ji}(H_kB_k + D_kE_k) + H_iB_j + D_jE_i \ , \\ \sigma_{ji}^{\text{tot.}} = m_{ji} + \sigma_{ji} = -\frac{1}{2}\delta_{ji}(H_kB_k + D_kE_k) + \mathfrak{H}_iB_j + \mathfrak{D}_jE_i - \\ -C_{jikl}\alpha_{kl}(T - T_{\text{ref.}}) + C_{jikl}\varepsilon_{kl} - \tilde{T}_{kji}E_k + \tilde{S}_{kji}B_k \ . \end{aligned} \tag{VII.81}$$

We integrate by parts only the terms in the stress tensor including a derivative of the primitive variables. First we decompose the total stress

$$\sigma_{ji}^{\text{tot.}} = \bar{\sigma}_{ji} + \tau_{ji} \ , \tag{VII.82}$$

into a term, τ_{ji}, involving derivatives of ϕ, A_i, u_i, T and into another term, $\bar{\sigma}_{ji}$, involving only primitive variables but no derivatives

$$\begin{aligned} \tau_{ji} = -\frac{1}{2}\delta_{ji}(H_kB_k + D_kE_k) + \mathfrak{H}_iB_j + \mathfrak{D}_jE_i + C_{jikl}\varepsilon_{kl} - \tilde{T}_{kji}E_k + \tilde{S}_{kji}B_k \ , \\ \bar{\sigma}_{ji} = -C_{jikl}\alpha_{kl}(T - T_{\text{ref.}}) \ . \end{aligned} \tag{VII.83}$$

Then we acquire the weak form after integrating by parts and summing up over the whole domain as follows

$$\begin{aligned} \mathrm{F}_{\boldsymbol{u}} = \int_\Omega \Bigg(\rho_0\frac{u_i - 2u_i^0 + u_i^{00}}{\Delta t\Delta t}\delta u_i + \epsilon_{ijk}\frac{\mathfrak{D}_jB_k - \mathfrak{D}_j^0B_k^0}{\Delta t}\delta u_i - \bar{\sigma}_{ji,j}\delta u_i + \tau_{ji}\delta u_{i,j} - \\ -\rho_0 f_i\delta u_i \Bigg) \,\mathrm{d}V - \int_{\partial\Omega^I} N_j[\![\sigma_{ji}^{\text{tot.}} - \bar{\sigma}_{ji}]\!]\delta u_i \,\mathrm{d}A - \int_{\partial\Omega} N_j(\sigma_{ji}^{\text{tot.}} - \bar{\sigma}_{ji})\delta u_i \,\mathrm{d}A \ . \end{aligned} \tag{VII.84}$$

For a singular surface without mass—here the interface $\partial\Omega^I$—the balance of momentum reduces to $N_j[\![\sigma_{ji}^{\text{tot.}}]\!] = 0$. Again the modeling will be accomplished by embedding the structure in air, and the displacements at the boundary of the computational domain can be chosen as zero, $u_i\big|_{\partial\Omega} = 0$, such that the test function for displacement vanishes on the boundary. We obtain

$$\mathrm{F}_{\boldsymbol{u}} = \int_\Omega \left(\rho_0 \frac{u_i - 2u_i^0 + u_i^{00}}{\Delta t \Delta t} \delta u_i + \epsilon_{ijk} \frac{\mathfrak{D}_j B_k - \mathfrak{D}_j^0 B_k^0}{\Delta t} \delta u_i - \bar{\sigma}_{ji,j} \delta u_i + \tau_{ji} \delta u_{i,j} - \right. \\ \left. - \rho_0 f_i \delta u_i \right) \mathrm{d}V + \int_{\partial\Omega^I} N_j [\![\bar{\sigma}_{ji}]\!] \delta u_i \, \mathrm{d}A \ . \tag{VII.85}$$

This weak form is in the unit of energy. The deformation is caused by a traction vector separated into mechanical and electromagnetic terms depending on the values of the material parameters in the constitutive equations.

For computing the temperature distribution, we acquire the weak form from the balance of entropy as given in Eq. (VII.70)$_4$. After integrating by part and multiplying by Δt, we obtain the weak form in the unit of energy as follows

$$\mathrm{F}_T = \int_\Omega \left(\rho_0 (\eta - \eta^0) \delta T - \Delta t \Phi_i \delta T_{,i} - \Delta t \rho_0 \frac{r}{T} \delta T - \Delta t \Sigma \delta T \right) \mathrm{d}V + \\ + \int_{\partial\Omega^I} \Delta t [\![\Phi_i]\!] N_i \delta T \, \mathrm{d}A \ . \tag{VII.86}$$

On the boundary the temperature is given as being equal to the reference temperature such that the test function vanishes. The entropy flux and production are already determined

$$\Sigma = -\frac{q_i}{T^2} T_{,i} + \frac{1}{T} \mathcal{E}_i \jmath_i^{\text{fr.}} \ , \quad \Phi_i = \frac{q_i}{T} \ , \quad q_i = -\kappa T_{,i} + \varsigma \pi T \mathcal{E}_i \ . \tag{VII.87}$$

We have obtained weak forms in Eqs. (VII.77), (VII.78), (VII.85), (VII.86) in the same unit such that we can sum them up

$$\text{Form} = \mathrm{F}_\phi + \mathrm{F}_{\boldsymbol{A}} + \mathrm{F}_{\boldsymbol{u}} + \mathrm{F}_T \ . \tag{VII.88}$$

The weak form is coupled and nonlinear in the primitive variables. We perform an abstract linearization using Newton's method at the partial differential level by following the ideas in Logg, Mardal, and Wells, 2012, Part I, §2.2.3. We gather all primitive variables and their variations together

$$\begin{aligned} \boldsymbol{p} &= \{\phi, A_1, A_2, A_3, u_1, u_2, u_3, T\} \ , \\ \delta\boldsymbol{p} &= \{\delta\phi, \delta A_1, \delta A_2, \delta A_3, \delta u_1, \delta u_2, \delta u_3, \delta T\} \ . \end{aligned} \tag{VII.89}$$

The weak form is a functional of $\boldsymbol{p}$ and $\delta\boldsymbol{p}$, we write it as Form $= F(\boldsymbol{p}, \delta\boldsymbol{p})$. At the initial time instant, t_0, the form is fulfilled since we set the initial conditions at the beginning. Then we search for the next time instant, $t = \Delta t + t_0$, by considering the known values, $\boldsymbol{p}^0$. For every subsequent time step exactly the same approach holds by knowing the (computed) values from the last time instant. We can formulate the aim:

$$\begin{aligned} \text{given: } & \boldsymbol{p}(t) \text{ for } \boldsymbol{x} \ , \\ \text{find: } & \boldsymbol{p}(t + \Delta t) \text{ at } \boldsymbol{x} \ , \\ \text{satisfying: } & F(\boldsymbol{p}(t + \Delta t), \delta\boldsymbol{p}) = 0 \ . \end{aligned} \tag{VII.90}$$

Instead of searching for $\boldsymbol{p}(t + \Delta t)$ we might search for the deviation from the known values:

$$\boldsymbol{p}(t + \Delta t) = \boldsymbol{p}(t) + \Delta\boldsymbol{p}(t) \ . \tag{VII.91}$$

If Δt is sufficiently small, then the solution is so close to the known solution such that we can utilize a Taylor expansion up to the order one around the known values, $\boldsymbol{p}(t)$, as follows

$$F(\boldsymbol{p} + \Delta\boldsymbol{p}, \delta\boldsymbol{p}) = F(\boldsymbol{p}, \delta\boldsymbol{p}) + \nabla_{\boldsymbol{p}} F(\boldsymbol{p} + \Delta\boldsymbol{p}, \delta\boldsymbol{p}) \cdot \Delta\boldsymbol{p} \ , \tag{VII.92}$$

where we have suppressed the time argument for the sake of a simplified notation. The formulation is in polynomial degree one, in other words, we have neglected the quadratic terms in the expansion. The same condition holds for the differentiation operator, $\nabla_{\boldsymbol{p}}$, applied on the functional $F(\boldsymbol{p} + \epsilon\Delta\boldsymbol{p}, \delta\boldsymbol{p})$. We introduce the directed or Gateaux derivative:

$$\nabla_{\boldsymbol{p}} F(\boldsymbol{p} + \Delta\boldsymbol{p}, \delta\boldsymbol{p}) \cdot \Delta\boldsymbol{p} = \boldsymbol{J}(\boldsymbol{p}, \delta\boldsymbol{p}) \cdot \Delta\boldsymbol{p} = \lim_{\epsilon \to 0} \frac{\mathrm{d}}{\mathrm{d}\epsilon} F(\boldsymbol{p} + \epsilon\Delta\boldsymbol{p}, \delta\boldsymbol{p}) \ , \tag{VII.93}$$

where the differentiation allows only linear terms in ϵ. The newly introduced notation $\boldsymbol{J}$ denotes the derivative or Jacobian of the system. Now we can reformulate the aim:

$$\begin{aligned} \text{given: } & \boldsymbol{p} \text{ for } \boldsymbol{x} \ , \\ \text{find: } & \Delta\boldsymbol{p} \text{ at } \boldsymbol{x} \ , \\ \text{satisfying: } & F(\boldsymbol{p}, \delta\boldsymbol{p}) + \boldsymbol{J}(\boldsymbol{p}, \delta\boldsymbol{p}) \cdot \Delta\boldsymbol{p} = 0 \ . \end{aligned} \tag{VII.94}$$

Since now the governing function is linear in $\Delta\boldsymbol{p}$ we can solve it. By applying this iteratively we acquire

$$\boldsymbol{p} := \boldsymbol{p} + \Delta\boldsymbol{p} \ , \tag{VII.95}$$

where ":=" is an assign operator in computational algebra. The algorithm for this approach reads

$$\begin{aligned} &\text{while } |\Delta\boldsymbol{p}| > \text{TOL.} \\ &\quad \text{solve } \Delta\boldsymbol{p}, \text{ where } F(\boldsymbol{p}, \delta\boldsymbol{p}) + \boldsymbol{J}(\boldsymbol{p}, \delta\boldsymbol{p}) \cdot \Delta\boldsymbol{p} = 0 \\ &\quad \boldsymbol{p} := \boldsymbol{p} + \Delta\boldsymbol{p} \end{aligned} \tag{VII.96}$$

The term $\boldsymbol{J} \cdot \Delta\boldsymbol{p}$ can be computed automatically. This symbolic computation is realized by SyFi in the FEniCS project, see Alnaes and Mardal, 2010; Alnaes and Mardal, 2012. Moreover, this linearization occurs before the space discretization avoiding any numerical problems regarding element quality.

After the linearization step, the third step can be applied in order to discretize in space. Consider a triangulation of the continuum body to discrete finite sized elements. The totality of the elements represents the discrete body. We use tetragonal elements with form functions of degree $n = 1$ such that every element in 3D consists of four nodes. The primitive variables are represented with their nodal values interpolated using the form functions. This is the discrete representation of primitive variables. We omit to distinguish between the discrete and continuous representations as they never appear together. Concretely, 8 primitive variables in three-dimensional space, $\boldsymbol{p}$, belong to

$$\mathcal{V} = \left\{ \boldsymbol{p} \in [\mathcal{H}^n(\Omega)]^8 : \boldsymbol{p}|_{\partial\Omega} = \text{given} \right\} , \tag{VII.97}$$

where $[\mathcal{H}^n]^8$ is a 8-dimensional Hilbert space as defined in Hilbert, 1902. It is of class C^n and includes the differentiability properties, i.e., it is technically a Sobolev space. The test functions, $\delta\boldsymbol{p}$, stem from the same space, according to Galerkin's procedure:

$$\hat{\mathcal{V}} = \left\{ \delta\boldsymbol{p} \in [\mathcal{H}^n(\Omega)]^8 : \delta\boldsymbol{p}|_{\partial\Omega} = \text{given} \right\} . \tag{VII.98}$$

Since the test functions are arbitrary we choose them zero on the Dirichlet boundaries where the primitive variables are given.

For the computation of the engineering examples following in the next sections, we wrote a code in Python, see Oliphant, 2007 and compiled using Dolfin packages, cf., Logg and Wells, 2010 and for FEniCS project see Logg, Mardal, and Wells, 2012 and Logg, Mardal, and Wells, 2011. In order to encourage further studies we publish the code under Gnu GPL, 2007, see the website in Abali, 2013.

5. Applications

In order to present the strength of simulations with the proposed method, we consider various multiphysics engineering applications presenting coupling effects and interaction between primitive variables.

5.1. Piezoelectric transducer and pyroelectric energy harvester

Piezo- and pyroelectric materials are used as sensors and actuators in many technological applications, for example, in accelerometers, sonar projectors, and medical imaging. Especially piezoelectric materials are used as pressure sensors for more than five decades. In recent years, by using different fabrications techniques, their sensitivities became greatly increased, see Park and Hackenberger, 2002 for single crystals and Persano et al., 2013 for polymers.

For the sake of simplicity we use same a similar system for presenting two different engineering applications. First we show a transducer, where electric energy is transformed into mechanical energy. Secondly, we present an energy harvester, where a thermal fluctuation is used to generate and store energy.

Consider a simple plate made of epoxy that is clamped on one end. The geometric dimensions are in millimeter length scale. Near to the clamped end, a thin piezoelectric layer is glued onto the epoxy plate. This piezoelement is loaded with the help of an electric circuit (which is not included in the model). By a harmonic input of voltage on the piezoelement, a shear strain is induced on the plate resulting in a bending motion in nearly the same periodicity as the input, since we model epoxy as an elastic material. This system can be used as a cooling fan in electronic devices as patented multiple times in the last three decades, see for example Yamada, Fujimoto, and Inoue, 1988; Losinski, 1999; Sauciuc and Chrysler, 2006; Tanida, Sunaga, and Wada, 2013. The plate with the attached piezoelement made of PZT[87] is embedded in air, the model geometry can be seen in Fig. VII.1. The non-vanishing material coefficients for epoxy are approximated as follows

$$\begin{aligned} \rho_0 = 2500\,\mathrm{kg/m^3}\ , \quad E = 20\cdot 10^9\,\mathrm{Pa}\ , \quad G = 6\cdot 10^9\,\mathrm{Pa}\ , \\ \lambda = \frac{(E-2G)G}{3G-E}\ , \quad \mu = G\ , \quad \bar{\varepsilon}^{\mathrm{el.}} = 1\ , \quad \bar{\mu}^{\mathrm{mag.}} = 1\ , \\ c = 800\,\mathrm{J/(kg\,K)}\ , \quad \kappa = 1.3\,\mathrm{W/(m\,K)}\ , \quad \alpha = 13\cdot 10^{-6}\,1/\mathrm{K}\ , \end{aligned} \tag{VII.99}$$

such that the stiffness matrix in the VOIGT notation, electric and magnetic suscepti-

[87] PZT is a given name for lead-zirconate-titanate. The common compositions are $Pb_{1.1}Zr_{0.3}Ti_{0.7}O_3$ and $PbZr_{0.52}Ti_{0.48}O_3$.

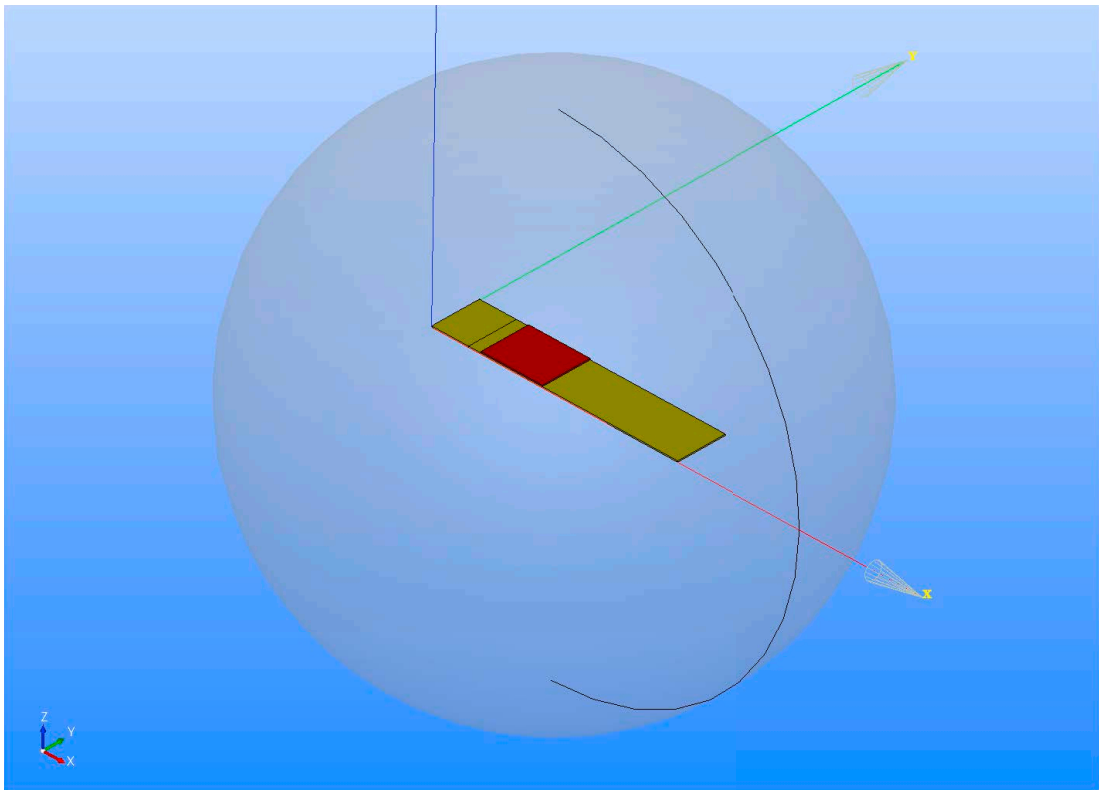

Figure VII.1.: Simulation model of the piezoelectric fan, created in Salome-Platform. Inside a 100 mm sphere of air (transparent gray) an epoxy cantilever (yellow) of $100 \times 20 \times 0.5$ mm is clamped on $x = 0$. On top of the epoxy plate, a piezoelectric sheet (red) of $25 \times 20 \times 0.5$ mm is attached.

bilities, coefficients of thermal expansions read

$$C_{IJ} = \begin{pmatrix} \lambda+2\mu & \lambda & \lambda & 0 & 0 & 0 \\ \lambda & \lambda+2\mu & \lambda & 0 & 0 & 0 \\ \lambda & \lambda & \lambda+2\mu & 0 & 0 & 0 \\ 0 & 0 & 0 & \mu & 0 & 0 \\ 0 & 0 & 0 & 0 & \mu & 0 \\ 0 & 0 & 0 & 0 & 0 & \mu \end{pmatrix} , \tag{VII.100}$$

$$\chi_{ij}^{\text{el.}} = \bar{\varepsilon}^{\text{el.}}\delta_{ij} - \delta_{ij} = 0 \ , \quad \chi_{ij}^{\text{mag.}} = \bar{\mu}^{\text{mag.}}\delta_{ij} - \delta_{ij} = 0 \ , \quad \alpha_{ij} = \alpha\delta_{ij} \ ,$$

respectively. We obtain from data sheets[88] of PZT-5H the following values for the

[88] All parameters are compiled from internet sources as PI, 2016; Boston Piezo-Optics, 2016; efunda, 2016

non-zero coefficients:

$$\begin{gathered}\rho_0 = 7500\,\mathrm{kg/m^3}\ ,\\ S_{11} = 16.5\cdot10^{-12}\,\mathrm{m^2/N}\ ,\quad S_{12} = -4.78\cdot10^{-12}\,\mathrm{m^2/N}\ ,\quad S_{13} = -8.45\cdot10^{-12}\,\mathrm{m^2/N}\ ,\\ S_{33} = 20.7\cdot10^{-12}\,\mathrm{m^2/N}\ ,\quad S_{44} = 43.5\cdot10^{-12}\,\mathrm{m^2/N}\ ,\quad S_{66} = 42.65\cdot10^{-12}\,\mathrm{m^2/N}\ ,\\ \tilde{d}_{33} = 585\cdot10^{-12}\,\mathrm{m/V}\ ,\quad \tilde{d}_{31} = -265\cdot10^{-12}\,\mathrm{m/V}\ ,\quad \tilde{d}_{15} = 730\cdot10^{-12}\,\mathrm{m/V}\ ,\\ \bar{\varepsilon}^{\mathrm{el.}}_{33} = 3400\ ,\quad \bar{\varepsilon}^{\mathrm{el.}}_{11} = 3130\ ,\quad \bar{\mu}^{\mathrm{mag.}} = 1\ ,\\ c = 350\,\mathrm{J/(kg\,K)}\ ,\quad \kappa = 1.1\,\mathrm{W/(m\,K)}\ ,\\ \alpha_{33} = -4\cdot10^{-6}\,\mathrm{1/K}\ ,\quad \alpha_{11} = 6\cdot10^{-6}\,\mathrm{1/K}\ .\end{gathered} \tag{VII.101}$$

The compliance matrix in VOIGT notation reads

$$S_{IJ} = \begin{pmatrix} S_{11} & S_{12} & S_{13} & 0 & 0 & 0\\ S_{12} & S_{11} & S_{13} & 0 & 0 & 0\\ S_{13} & S_{13} & S_{33} & 0 & 0 & 0\\ 0 & 0 & 0 & S_{44} & 0 & 0\\ 0 & 0 & 0 & 0 & S_{44} & 0\\ 0 & 0 & 0 & 0 & 0 & S_{66} \end{pmatrix}\ , \tag{VII.102}$$

and the stiffness matrix in VOIGT notation is obtained by computing the inverse

$$(S_{JI})^{-1} = C_{IJ} = \begin{pmatrix} C_{1111} & C_{1122} & C_{1133} & C_{1123} & C_{1113} & C_{1112}\\ C_{2211} & C_{2222} & C_{2233} & C_{2223} & C_{2213} & C_{2212}\\ C_{3311} & C_{3322} & C_{3333} & C_{3323} & C_{3313} & C_{3312}\\ C_{2311} & C_{2322} & C_{2333} & C_{2323} & C_{2313} & C_{2312}\\ C_{1311} & C_{1322} & C_{1333} & C_{1323} & C_{1313} & C_{1312}\\ C_{1211} & C_{1222} & C_{1233} & C_{1223} & C_{1213} & C_{1212} \end{pmatrix}\ . \tag{VII.103}$$

Analogously, we have the piezoelectric constants in the VOIGT notation:

$$\tilde{d}_{iJ} = \begin{pmatrix} \tilde{d}_{111} & \tilde{d}_{122} & \tilde{d}_{133} & \tilde{d}_{123} & \tilde{d}_{131} & \tilde{d}_{112}\\ \tilde{d}_{211} & \tilde{d}_{222} & \tilde{d}_{233} & \tilde{d}_{223} & \tilde{d}_{231} & \tilde{d}_{212}\\ \tilde{d}_{311} & \tilde{d}_{322} & \tilde{d}_{333} & \tilde{d}_{323} & \tilde{d}_{331} & \tilde{d}_{312} \end{pmatrix} = \begin{pmatrix} 0 & 0 & 0 & 0 & \tilde{d}_{15} & 0\\ 0 & 0 & 0 & \tilde{d}_{15} & 0 & 0\\ \tilde{d}_{31} & \tilde{d}_{31} & \tilde{d}_{33} & 0 & 0 & 0 \end{pmatrix}\ , \tag{VII.104}$$

where the indices belonging to strain are written in the VOIGT notation, since we have only 6 independent coefficients owing to symmetric strain. The necessary coefficients for the computation read

$$\tilde{T}_{mij} = C_{ijkl}\tilde{d}_{mkl}\ . \tag{VII.105}$$

The susceptibilities and thermal expansion coefficients are

$$\chi_{ij}^{\text{el.}} = \begin{pmatrix} \bar{\varepsilon}_{11}^{\text{el.}} & 0 & 0 \\ 0 & \bar{\varepsilon}_{11}^{\text{el.}} & 0 \\ 0 & 0 & \bar{\varepsilon}_{33}^{\text{el.}} \end{pmatrix} - \delta_{ij} \ , \quad \chi_{ij}^{\text{mag.}} = \begin{pmatrix} \bar{\varepsilon}_{11}^{\text{mag.}} & 0 & 0 \\ 0 & \bar{\varepsilon}_{11}^{\text{el.}} & 0 \\ 0 & 0 & \bar{\varepsilon}_{33}^{\text{el.}} \end{pmatrix} - \delta_{ij} \ , \\ \alpha_{ij} = \begin{pmatrix} \alpha_{11} & 0 & 0 \\ 0 & \alpha_{11} & 0 \\ 0 & 0 & \alpha_{33} \end{pmatrix} \ . \tag{VII.106}$$

We excite the piezoelectric fan by grounding one side of the piezoelement and actuating the other side by a standard (in Europe) potential supplied from a wall plug as follows

$$\phi_{\text{act.}} = A \sin(2\pi\nu t) \ , \quad A = 240\,\text{V} \ , \quad \nu = 50\,\text{Hz} \ . \tag{VII.107}$$

Since the piezoelement is attached to the epoxy plate, the piezoelectric deformation of the single PZT sheet bends the plate in nearly same phase as we have modeled the plate as elastic. Effected by the inertia a small phase delay can be seen. At the first and third quarter of the period, the maximum deflection is nearly reached, see Fig. VII.2. No significant change is observed in the temperature distribution.

Another useful application of the same material—PZT-5H—is based on its pyroelectric properties given by $\tilde{L}_i = -\tilde{T}_{ijk}\alpha_{jk}$. Temperature change from the reference temperature creates piezolectricity. Rate of piezoelectricity creates an electric current and by designing an electric circuit with a pyroelectric element in it, we can generate energy as a consequence of temperature change. Recently, different energy harvesters are proposed, see for example Sebald, Pruvost, and Guyomar, 2007; Cuadras, Gasulla, and Ferrari, 2010; Bowen et al., 2014. The main idea is to use a pyroelectric element between two conductors connected as a supply in a circuit. We present a simple $50 \times 50\,\text{mm}$ energy harvester of three layers. A PZT-plate is placed between a top and bottom brass plate, forming a sandwich structure. All is embedded in air, as shown in Fig. VII.3.

Suppose that we install the plate in a place in the world, where the ambient temperature varies $\pm 5\,\text{K}$ throughout the day—we may model it as a sinusoidal alteration,

$$T_{\text{amb.}} = T_{\text{ref.}} + T_{\text{amp.}} \sin(2\pi\nu t) \ , \\ T_{\text{ref.}} = 300\,\text{K} \ , \quad T_{\text{amp.}} = 5\,\text{K} \ , \quad \nu = \frac{1}{24 \times 60 \times 60}\,\text{Hz} \ . \tag{VII.108}$$

We set this temperature on the boundary of the whole computational domain. Therefore, heat is transferred through air up to the top and bottom surfaces of the plate. The computed potential difference between top and bottom surfaces is plotted in Fig. VII.4. In each time step, the potential on one surface is found by averaging over the whole surface, i.e., by integrating over the surface and dividing by the

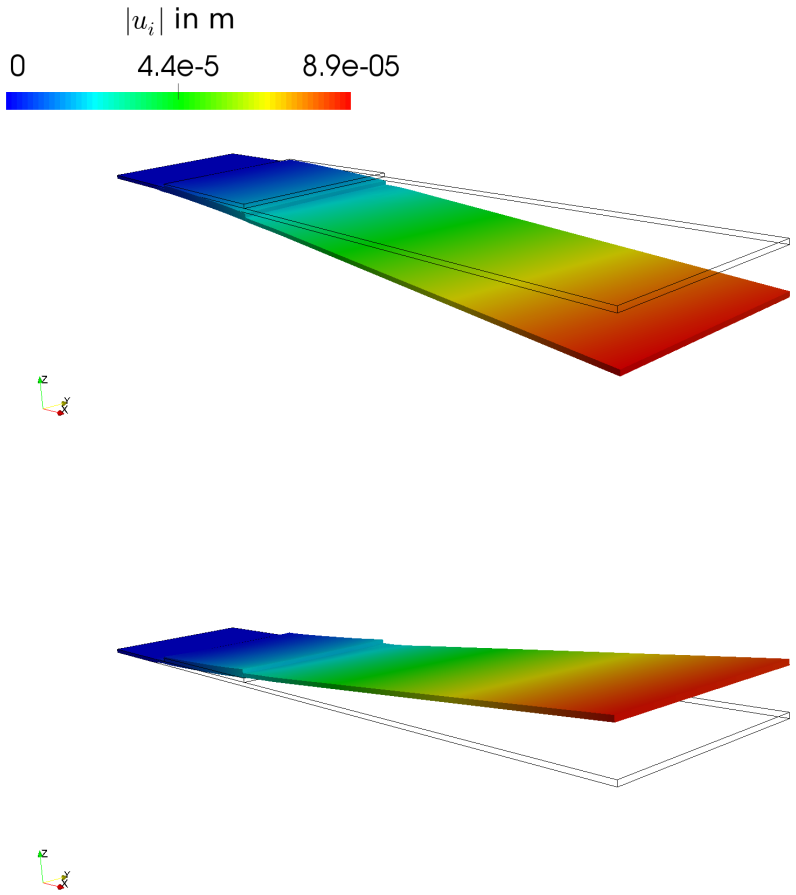

Figure VII.2.: Displacements with a scale factor of 50 are shown on the piezoelement and epoxy plate at 1/4 of a period (top) and 3/4 of a period (bottom).

surface area. Since brass is a good conductor, the distribution is nearly constant as expected.

After a full cycle, the potential difference goes back to zero indicating that the process within the energy harvester is reversible. Indeed, the entropy production becomes zero since in the piezoelectric material no electric current is flowing, its deformation is elastic, and the heat flux over the thickness is zero since the temperature values on the top and bottom surfaces change simultaneously. Therefore, such an energy harvester can be used for many times without any losses. By using a simple circuit, a small amount of energy can be stored by using a relatively cheap piezoceramic sheet. Such a design for energy scavenging could be useful for self-powered devices in desert areas or on Mars where the temperature differences become high and energy supply is costly.

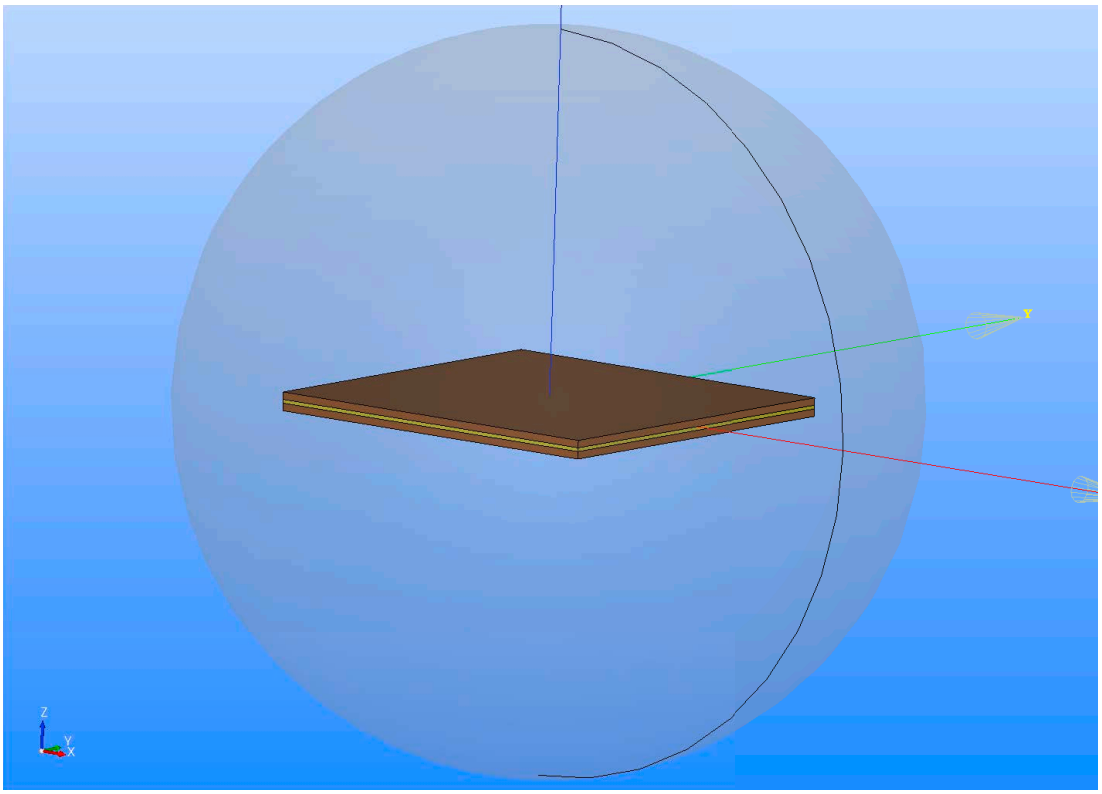

Figure VII.3.: Simulation model of the pyroelectric energy harvester crafted in Salome-Platform. Inside a 50 mm sphere of air (transparent gray) a PZT-plate (yellow) of 50 × 50 × 1 mm is sandwiched between two brass plates (brown) of 50 × 50 × 0.5 mm. The three layer plate is hold on the below surface; the top and below surfaces possess the ambient temperature $T_{\text{amb.}}$, which alters during a day.

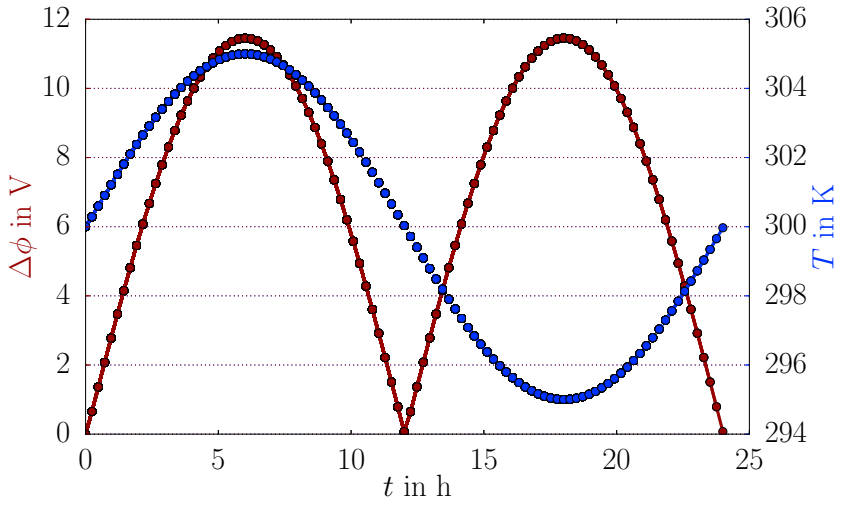

Figure VII.4.: Obtained potential difference effected by the temperature change during a day.

5.2. Magnetostriction on an inductor

Most ferromagnetic materials change their shape effected by a magnetic field. This so-called magnetostriction is modeled by $\tilde{S}_{ijk}$ coefficients in Eq. (VII.52)$_{2,4}$ and causes the humming of a core in a transformer or more simply in an inductor. Moreover, it is responsible for an energy loss, see Weiser, Pfutzner, and Anger, 2000 for a discussion of transformer losses and the role of magnetostriction. Magnetostriction is often measured as λ which indicates the length change $\Delta\ell/\ell$ subject to a magnetic flux in tesla. Two different components of λ are given, one parallel to the applied field and one perpendicular. Consider the inductor consisting of coil and a core parallel to z-axis as shown in Fig. VII.5. Coil and core are embedded in epoxy, which is held fixed

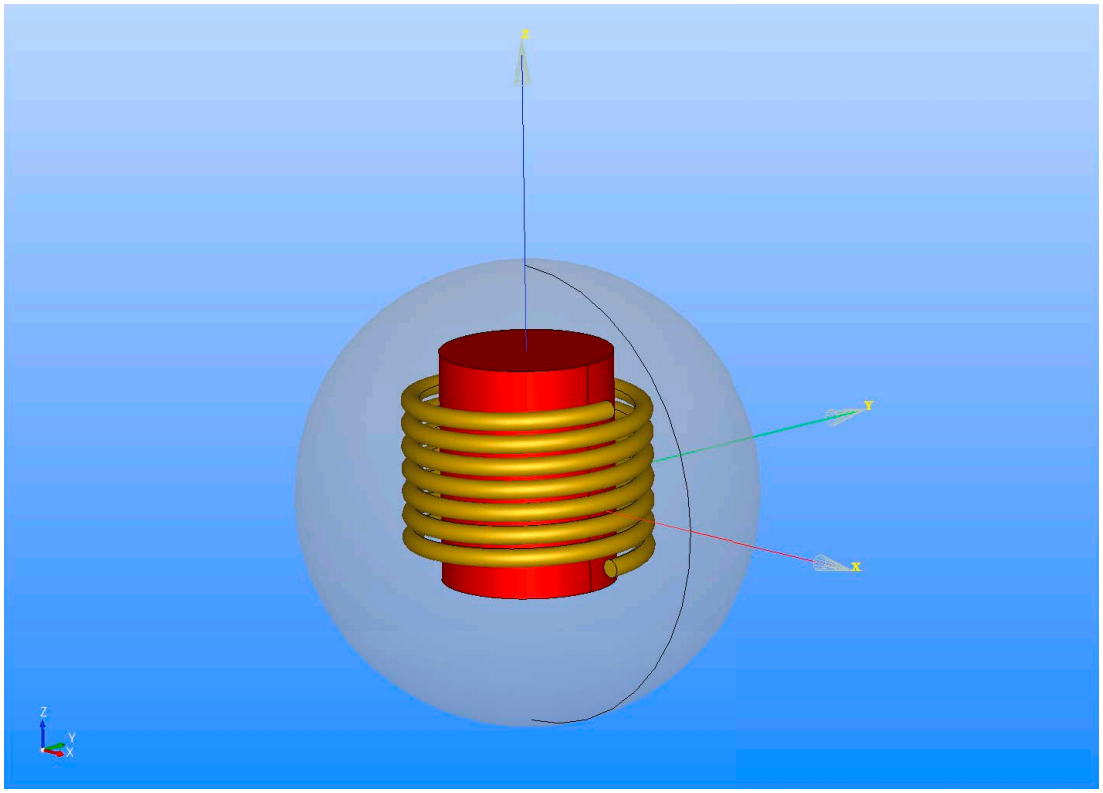

Figure VII.5.: Simulation model of the inductor constructed in Salome-Platform. The winding is a copper coil (yellow) around an oriented electric steel (red) core, embedded in a spherical epoxy (transparent gray) of 40 mm radius.

on its boundaries. By using electric steel we will have a piezomagnetic effect causing a deformation of the core. The coil is not polarized; however, the electromagnetic supply, i.e. the LORENTZ force, may induce a deformation. We use the data in Somkun, Moses, and Anderson, 2016, Fig. 4(b) for estimating λ as magnetostriction constant and approximate the relation as linear (below 1.3 T). Since magnetic flux per permeability gives the magnetic field, slope in Somkun, Moses, and Anderson, 2016, Fig. 4(b) per permeability reads $\tilde{S}_{33}$ in rolling direction (RD) and $\tilde{S}_{31} = \tilde{S}_{32}$ in

traverse direction (TD) such that we acquire

$$\tilde{S}_{31} = 5.2 \cdot 10^6\,\mathrm{A/m}\ , \quad \tilde{S}_{33} = -3.7 \cdot 10^6\,\mathrm{A/m}\ , \tag{VII.109}$$

as we could not find any measurement for shear strain we set, $\tilde{S}_{15} = 0$, and we obtain the following piezomagnetic tensor:

$$\tilde{S}_{iJ} = \begin{pmatrix} 0 & 0 & 0 & 0 & \tilde{S}_{15} & 0 \\ 0 & 0 & 0 & \tilde{S}_{15} & 0 & 0 \\ \tilde{S}_{31} & \tilde{S}_{31} & \tilde{S}_{33} & 0 & 0 & 0 \end{pmatrix}\ , \tag{VII.110}$$

in the VOIGT notation. The magnetostriction is mathematically quite analogous to piezoelectricity. This fact is obvious by calling the material properties piezomagnetic properties instead of magnetostrictive.

As in reality, the system is excited by electric current. We set the electric potential on one end of the coil to zero (grounded) and on the other end as follows

$$\phi = \phi_{\mathrm{amp.}} \sin(2\pi\nu t)\ , \quad \phi_{\mathrm{amp.}} = 240\,\mathrm{V}\ , \quad \nu = 50\,\mathrm{Hz}\ . \tag{VII.111}$$

Potential difference in the wire generates an electric current, such a current induces a magnetic field creating a magnetic polarization in the core. The magnetic polarization implies strain due to the piezomagnetic constants. In addition to the aforementioned piezomagnetic constants, we use the following properties for the grain oriented electric steel used herein as a core,

$$\begin{aligned} \rho_0 = 7850\,\mathrm{kg/m^3}\ , \quad E = 210 \cdot 10^9\,\mathrm{Pa}\ , \quad G = 80 \cdot 10^9\,\mathrm{Pa}\ , \\ \bar{\varepsilon}^{\mathrm{el.}} = 1\ , \quad \bar{\mu}^{\mathrm{mag.}} = 20\,000\ , \quad c = 430\,\mathrm{J/(kg\,K)}\ , \\ \kappa = 57\,\mathrm{W/(m\,K)}\ , \quad \alpha = 12.2 \cdot 10^{-6}\,\mathrm{1/K}\ , \quad \varsigma = 2.2 \cdot 10^6\,\mathrm{S/m}\ . \end{aligned} \tag{VII.112}$$

For the epoxy housing we use the same material properties as in the last application. For the copper coils we use the following material parameters:

$$\begin{aligned} \rho_0 = 8450\,\mathrm{kg/m^3}\ , \quad E = 105 \cdot 10^9\,\mathrm{Pa}\ , \quad G = 36 \cdot 10^9\,\mathrm{Pa}\ , \\ \bar{\varepsilon}^{\mathrm{el.}} = 1\ , \quad \bar{\mu}^{\mathrm{mag.}} = 1\ , \quad c = 380\,\mathrm{J/(kg\,K)}\ , \quad \pi = 68 \cdot 10^{-6}\,\mathrm{V/K}\ , \\ \kappa = 109\,\mathrm{W/(m\,K)}\ , \quad \alpha = 19 \cdot 10^{-6}\,\mathrm{1/K}\ , \quad \varsigma = 0.6\,\mathrm{S/m}\ , \end{aligned} \tag{VII.113}$$

by assuming the coil as a part of a circuit such that ς is an approximate value of the whole circuit, which is not modeled. The current rate as well as its direction alter in time such that the magnetic field varies and sets the core in motion. We have fixed the coil and let the core freely move as embedded in the epoxy. Two different simulations have been established. First simulation is isothermal and second simulation is by computing the temperature, both only for two periods at 50 Hz. The temperature rise is less than 1 K in such that one might claim that an isothermal

simulation is accurate enough. Interestingly, even in this application this is not the case. In Fig. VII.6 we present the deformation for both simulations. The deformation

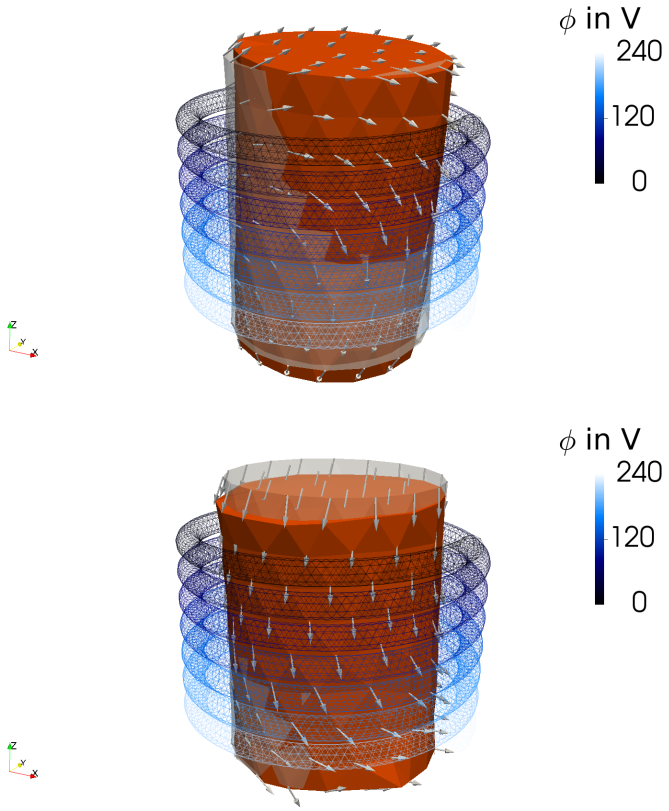

Figure VII.6.: Inductor simulations results. Coil as wireframe and core in its initial shape (transparent gray) are shown. Top: the scaled displacement (orange) with unscaled arrows is shown for the isothermal case. Bottom: the scaled displacement (orange) with unscaled arrows is shown for the non-isothermal case.

in both cases is different. In the isothermal case, the core is tilted and in the non-isothermal case the core is stretched more than tilted. For visualization purposes we have scaled the deformation differently, in the non-isothermal case the deformation is greater than the isothermal case. For getting a better insight, we compute the equivalent VON MISES stress

$$\sigma_{\text{eq.}}^{\text{tot.}} = \sqrt{\frac{3}{2}\sigma_{|ij|}^{\text{tot.}}\sigma_{|ij|}^{\text{tot.}}} \ , \quad \sigma_{|ij|}^{\text{tot.}} = \sigma_{ij}^{\text{tot.}} - \frac{1}{3}\sigma_{kk}^{\text{tot.}}\delta_{ij} \ , \tag{VII.114}$$

averaged over the boundaries of the core and plot it for both cases in Fig. VII.7. Equivalent stress indicates that the deformation is increasing. For just two periods, its value is negligibly small. Depending on the heat exchange rate with the environment, this increase will converge to a value. It is important to observe the effect of the temperature, although the temperature itself is small, its effect is even bigger than the magnetostriction. In the case of a study of the deformation of a core, assumption

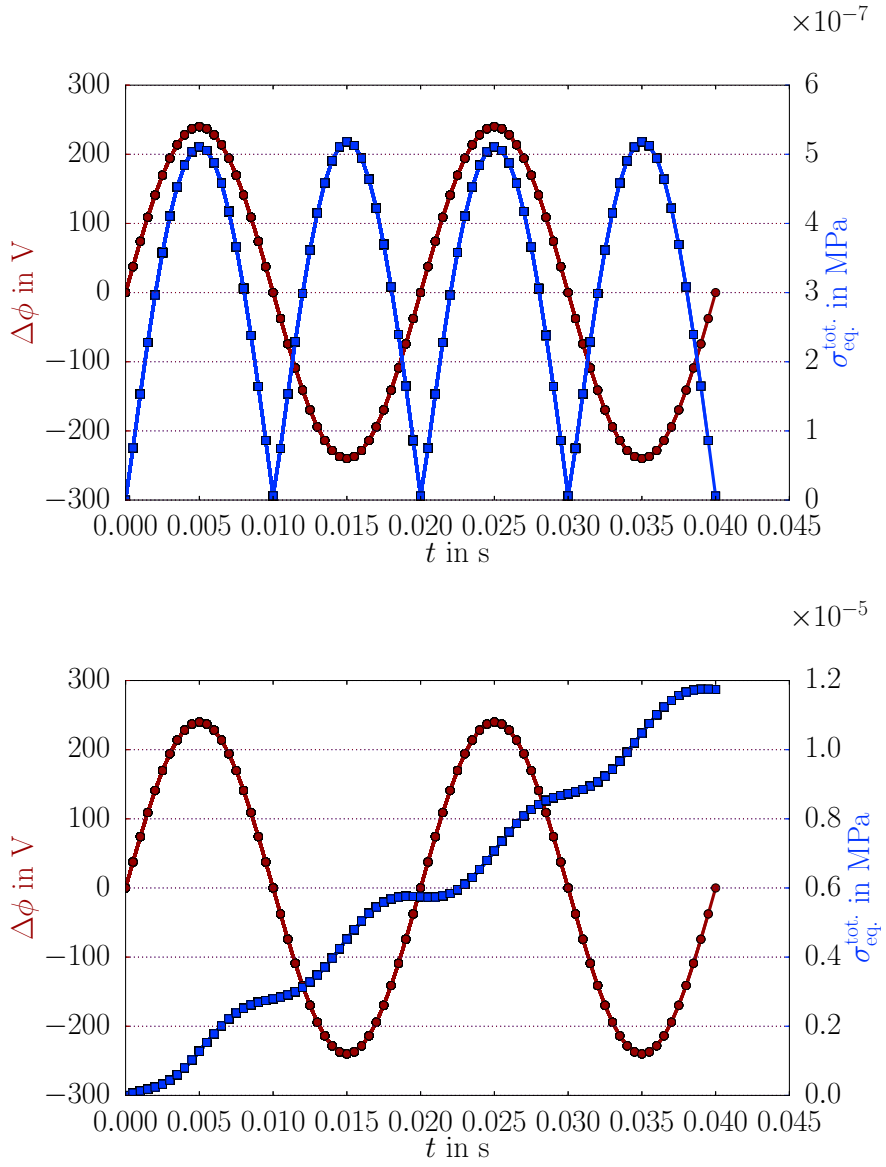

Figure VII.7.: For inductor simulations, electric potential and equivalent stress over time. Top: for the isothermal case. Bottom: for the non-isothermal case.

of isotherm state seems to be wrong. For a study of the humming noise, it has no effect. The frequency does not change since we model all materials without viscosity. The motion creates a sound, in our example in the frequency of 50 Hz, which is audible and can be disturbing if the geometry has its eigenfrequency near 50 Hz.

5.3. Sensor based on magnetoelectric coupling

Started in 1970s a direct magnetoelectric coupling has been measured in non-centrosymmetric crystals, see Schmid, 1994 for an overview and Eerenstein, Mathur,

and Scott, 2006 for this coupling in single-phase materials. This coupling term emerged as $\tilde{R}_{ij}$ in Eq. (VII.52)$_{3,4}$. A magnetic flux leads to an electric polarization, as well as an electric field causes a magnetic polarization. This coupling term is quite challenging to measure and there are various proposals in the literature, see for example Ryu et al., 2002; Vopsaroiu et al., 2008; Mathe, Srinivasan, and Balbashov, 2008; Chaudhuri and Mandal, 2015. Unfortunately, there are only few known materials showing a direct coupling effect, see Hill, 2000 for a discussion and a partial reasoning in the atomistic scale. The magnetoelectric coupling is quite useful, for example in magnetic sensors. Hence, there is increasing focus on devices with such a coupling. An outstanding idea is to produce composites of piezoelectric and magnetoelastic layers such that a magnetoelectric coupling is generated in an indirect manner. A magnetic flux deforms a magnetoelastic layer. Since it is adhered to a piezoelectric layer, the co-deformation of the piezoelectric layer induces an electric polarization. Such an indirect coupling effect allows a measurement of a magnetic flux. There are several design ideas to construct sensors with even higher sensitivity than superconducting quantum interference devices (SQUID) and giant magnetoresistances (GMR), see for example Zhai et al., 2006; Marauska et al., 2012; Shen, 2014. Magnetic sensors exploiting electromagnetic coupling are understood as a promising alternative to already available commercial magnetic sensors. Currently, they are not in use.

Terfenol-D 0-3 composite is a highly magnetostrictive material. Usually the composite consists of a polymer matrix (often epoxy) dispersed with Terfenol-D particles.[89] As in the preceding section, we obtain the piezomagnetic parameters by using λ over magnetic flux data in Sandlund et al., 1994, Fig. 2 or in Or, T. Li, and Chan, 2005 with a volume fraction of 0.5, and approximate the other piezomagnetic parameters by means of the determined constant. We use in the simulation the following properties:

$$\begin{gathered} \mu_r^{\text{mag.}} = 2.8 \ , \quad E = 13\,\text{GPa} \ , \\ \tilde{S}_{11} = 322.6 \cdot 10^6\,\text{A/m} \ , \quad \tilde{S}_{12} = -\frac{1}{2}\tilde{S}_{11} \ , \quad \tilde{S}_{26} = \frac{1}{2}\tilde{S}_{11} \ . \end{gathered} \tag{VII.115}$$

Therefore, the piezomagnetic tensor in the Voigt notation becomes

$$\tilde{S}_{iJ} = \begin{pmatrix} \tilde{S}_{11} & \tilde{S}_{12} & \tilde{S}_{12} & 0 & 0 & 0 \\ 0 & 0 & 0 & 0 & 0 & \tilde{S}_{26} \\ 0 & 0 & 0 & 0 & \tilde{S}_{26} & 0 \end{pmatrix} \ , \tag{VII.116}$$

such that a magnetic field in x-axis induces a normal strain on the plane directed along x-axis. Moreover, it generates (half in size) normal strains in the perpendicular directions. Since we lack measurements of the epoxy-Terfenol-D composite, we use

[89] Terfenol-D is an alloy of Terbium (Ter), Iron (fe), Dysprosium (-D) made in Naval Ordnance Lab (nol), its chemical structure reads $\text{Tb}_{0.27-0.30}\text{Dy}_{0.73-0.70}\text{Fe}_{1.90-1.95}$

the same properties as of epoxy in addition to the aforementioned properties,

$$\begin{aligned} \rho_0 = 2500\,\mathrm{kg/m^3}\ , \quad G = 5\cdot 10^9\,\mathrm{Pa}\ , \\ c = 800\,\mathrm{J/(kg\,K)}\ , \quad \kappa = 1.3\,\mathrm{W/(m\,K)}\ , \quad \alpha = 13\cdot 10^{-6}\,1/\mathrm{K}\ , \quad \varepsilon^{\mathrm{el.}} = 1\ . \end{aligned} \tag{VII.117}$$

For simulating a simple magnetic sensor, we use a multiferroic laminate consisting of three layers. A multiferroic material shows ferroelectric and ferromagnetic properties together, in other words, the material is piezoelectric and piezomagnetic at the same time. Of course, the material herein is a laminate consisting different layers with piezoelectric or piezomagnetic property. The first and third layers are a Terfenol-D composite and the middle layer is made of PZT-5H. We use the same material properties for PZT-5H as given in the former sections. The important design detail is the poling directions of piezoelectric and piezomagnetic layers. The Terfenol-D layers are responsive to the x-axis as given by Eq. (VII.116) and the piezoelectric PZT layer is poled along z-axis as given by Eq. (VII.104). The stacking of the layers are ordered in such a way that it operates in a longitudinally magnetized and transversely polarized mode, since this increases the magnetoelectric effect, see Yang et al., 2006.

Consider a coil creating magnetic flux in air. The magnetoelectric sensor is positioned in the middle and its one face on xy-plane is clamped, see Fig. VII.8. Magnetic flux

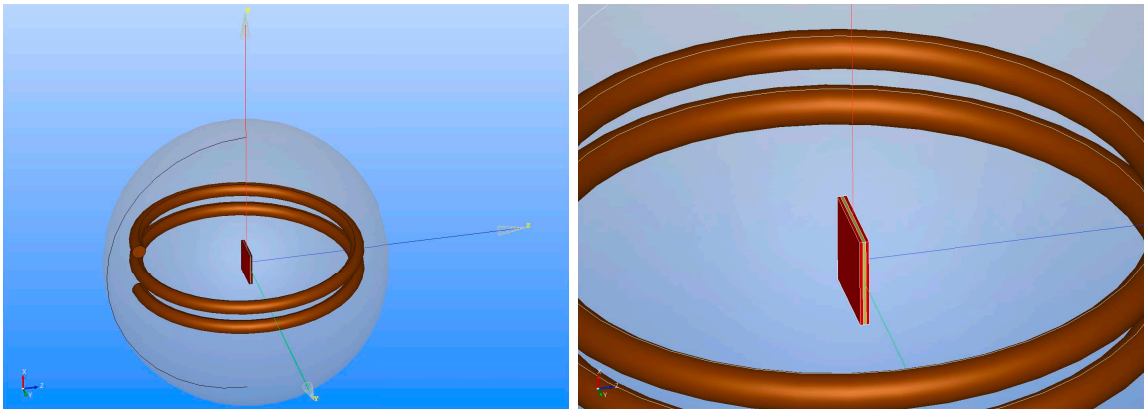

Figure VII.8.: Simulation model of the magnetic sensor designed in Salome-Platform. Left: Inside a 40 mm sphere of air (transparent gray) a copper coil is placed (brown) for generating a magnetic flux. Right: In the middle of the coil three layers of each $3 \times 3 \times 0.1$ mm model the sensor. The outer layers (red) are of Terfenol-D composite and the middle layer (yellow) is of PZT-5H.

generated by the coil will be directed toward x-axis in the middle of the core. The magnetoelectric sensor is sensitive along x-axis and it lies in such a way that the magnetic flux occurs on its wider face. By setting the potential of one end of the coil as $\phi = 220\sin(2\pi 50t)\,\mathrm{V}$ and the other end grounded, we create a magnetic flux as shown in Fig. VII.9. The magnetic field is nearly homogeneous on the sensor. It

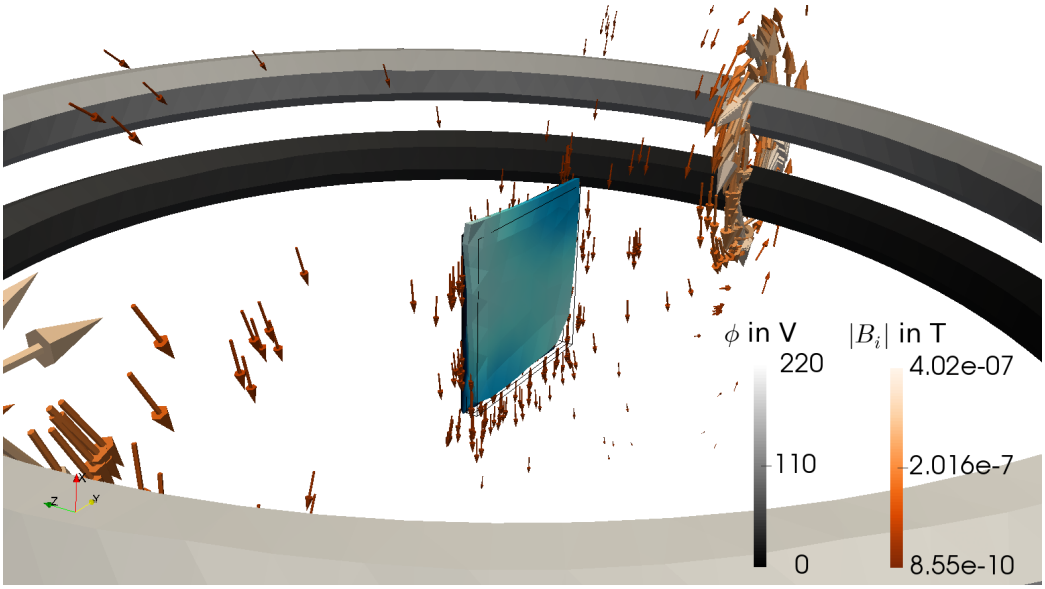

Figure VII.9.: The distribution of the electric potential in the coil at the quarter of a period. The magnetic flux is visualized as stream lines on a slice. Sensor is held on one side and it is deformed as being sheared.

is along x-axis such that normal strain on x occurs at maximum, whereas normal strains on y and z planes exist, too. We present the scaled deformation and also the undeformed sensor with black lines in the figure. The deformation is qualitatively in picometer length scale, hence, this configuration is only a numerical toy example. In reality the sensor might not be sensing such a small magnetic field. By using many layers, a configuration can be proposed by using the provided computation. Even though it is difficult to see in the figure, the sensor gets sheared such that the piezoelectric layer creates a distribution of ϕ within the sensor. By computing the voltages on top and bottom of the piezoelectric layer and recording the difference as $\Delta\phi$ we obtain Fig. VII.10. After a simple calibration, such a sensor can be used to detect magnetic field. The coupling effect is reversible such that the accuracy of the sensor does not sag with usage. Moreover, no mechanism has been used, we only exploit materials response such that the proposed measurements are highly sensitive. As seen here, even magnetic fluxes in nT region can be detected as long as one has an experimental facility capable of detecting electric potential in µV scale.

6. Conclusion

We have presented a complete theory of continuum mechanics with electromagnetic interaction in solid bodies under small deformations. Balance equations for mechanical, thermal, and electromagnetic fields have been discussed and all necessary consti-

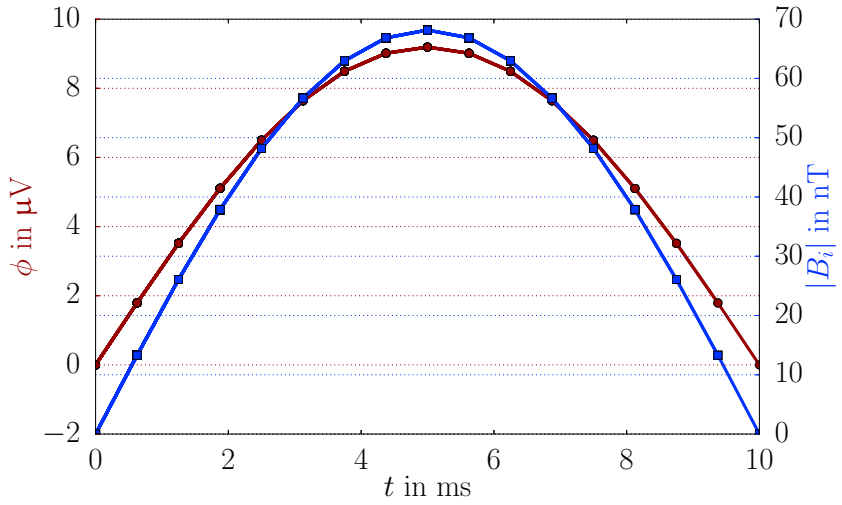

Figure VII.10.: Magnetic flux and electric potential difference between the top and bottom of the piezoelectric layer over time.

tutive equations have been derived with thermodynamical principles. The governing equations—even in the case of linear constitutive equations—are coupled and nonlinear. Their decoupling might be possible for some specific systems. However, in order to present a general approach we have applied a strategy for solving these coupled and nonlinear field equations, numerically. By exploiting open-source packages developed in the FEniCS project, we have achieved to implement and solve simplified engineering problems in order to show coupling phenomena between mechanics, thermodynamics, and electromagnetism. For encouraging further achievements, we share all written codes for the applications as well as the used geometry in Abali, 2013 to be used under the GNU Public license as in Gnu GPL, 2007. Implementing nonlinear constitutive equations is possible but left for future studies due to the fact that we have been unable to find material parameters and specific engineering applications for such purposes.

Acknowledgements

This work was completed while B. E. Abali was supported by a grant from the Max Kade Foundation to the University of California, Berkeley.

Appendix

A. Poynting equation

We insert the MAXWELL equations in Eq. (VII.10) into the balance electromagnetic momentum as in Eq. (VII.1) in order to obtain

$$\begin{aligned}\frac{\partial}{\partial t}(\boldsymbol{D}\times\boldsymbol{B})_i &= \epsilon_{ijk}\frac{\partial D_j B_k}{\partial t} = \epsilon_{ijk}\frac{\partial D_j}{\partial t}B_k + \epsilon_{ijk}D_j\frac{\partial B_k}{\partial t} = \\ &= \epsilon_{ijk}\left(\epsilon_{jlm}\frac{\partial H_m}{\partial x_l} - J_j\right)B_k - \epsilon_{ijk}D_j\epsilon_{klm}\frac{\partial E_m}{\partial x_l} = \\ &= -\frac{\partial H_k}{\partial x_i}B_k + \frac{\partial H_i}{\partial x_k}B_k - (\boldsymbol{J}\times\boldsymbol{B})_i - D_j\frac{\partial E_j}{\partial x_i} + D_j\frac{\partial E_i}{\partial x_j}\ ,\end{aligned} \tag{VII.118}$$

where $\epsilon_{ijk} = -\epsilon_{ikj}$ and $\epsilon_{ijk}\epsilon_{klm} = \delta_{il}\delta_{jm} - \delta_{im}\delta_{jl}$ has been used with the KRONECKER delta, δ_{ij}. Once more we can use the MAXWELL–LORENTZ aether relations and rewrite first and fourth terms from the latter

$$\begin{aligned}-\frac{\partial H_k}{\partial x_i}B_k - D_j\frac{\partial E_j}{\partial x_i} &= -\frac{1}{\mu_0}\frac{\partial B_k}{\partial x_i}B_k - \varepsilon_0 E_k\frac{\partial E_k}{\partial x_i} = \\ &= -\frac{1}{2\mu_0}\frac{\partial}{\partial x_j}(B_k B_k\delta_{ji}) - \frac{\varepsilon_0}{2}\frac{\partial}{\partial x_j}(E_k E_k\delta_{ji}) = \\ &= -\frac{\partial}{\partial x_j}\left(\frac{1}{2}\delta_{ji}(H_k B_k + D_k E_k)\right)\ .\end{aligned} \tag{VII.119}$$

Next, we employ the following MAXWELL equations:

$$\frac{\partial B_i}{\partial x_i} = 0\ ,\quad \frac{\partial D_i}{\partial x_i} = \rho z\ , \tag{VII.120}$$

and reformulate the second and fifth terms in Eq. (VII.118)

$$\frac{\partial H_i}{\partial x_j}B_j + D_j\frac{\partial E_i}{\partial x_j} = \frac{\partial}{\partial x_j}(H_i B_j + D_j E_i) - E_i\rho z\ . \tag{VII.121}$$

Hence we obtain the so-called POYNTING equation:

$$\begin{aligned}\frac{\partial}{\partial t}(\boldsymbol{D}\times\boldsymbol{B})_i = \frac{\partial\mathcal{G}_i^{\mathrm{P}}}{\partial t} = \frac{\partial}{\partial x_j}\Big(-\frac{1}{2}\delta_{ji}(H_k B_k + D_k E_k) + H_i B_j + D_j E_i\Big) - \\ -\rho z E_i - (\boldsymbol{J}\times\boldsymbol{B})_i\ ,\end{aligned} \tag{VII.122}$$

B. Reformulation of the momentum balance

The balance of mass kinetic energy can then be obtained by multiplying the balance of momentum with the velocity, v_i, and by reformulating

$$\rho\frac{\mathrm{d}}{\mathrm{d}t}\Big(\frac{1}{2}v_iv_i\Big) - \frac{\partial\sigma_{ji}v_i}{\partial x_j} - \rho f_iv_i = -\sigma_{ji}\frac{\partial v_i}{\partial x_j} + \mathcal{F}_iv_i \ . \tag{VII.123}$$

The first term can be rewritten by using the balance of mass once again

$$\begin{aligned}\rho\frac{\mathrm{d}}{\mathrm{d}t}\Big(\frac{1}{2}v_iv_i\Big) &= \rho\frac{\partial}{\partial t}\Big(\frac{1}{2}v_iv_i\Big) + \rho v_j\frac{\partial}{\partial x_j}\Big(\frac{1}{2}v_iv_i\Big) = \\ &= \rho\frac{\partial}{\partial t}\Big(\frac{1}{2}v_iv_i\Big) + \frac{\partial}{\partial x_j}\Big(\rho v_j\frac{1}{2}v_iv_i\Big) - \frac{\partial\rho v_j}{\partial x_j}\frac{1}{2}v_iv_i = \\ &= \frac{\partial}{\partial t}\Big(\frac{1}{2}\rho v_iv_i\Big) + \frac{\partial}{\partial x_j}\Big(\rho v_j\frac{1}{2}v_iv_i\Big) \ .\end{aligned} \tag{VII.124}$$

Hence, the balance of mass kinetic energy reads

$$\frac{\partial}{\partial t}\Big(\frac{1}{2}\rho v_iv_i\Big) - \frac{\partial}{\partial x_j}\Big(-v_j\frac{1}{2}\rho v_iv_i + \sigma_{ji}v_i\Big) - \rho f_iv_i = -\sigma_{ji}\frac{\partial v_i}{\partial x_j} + \mathcal{F}_iv_i \ . \tag{VII.125}$$

C. Constitutive equations in equilibrium

From the total differential

$$\mathrm{d}u = T\,\mathrm{d}\eta + {}^{\mathrm{r}}\sigma_{ji}v\,\mathrm{d}\varepsilon_{ij} - {}^{\mathrm{r}}P_iv\,\mathrm{d}E_i + B_iv\,\mathrm{d}\,{}^{\mathrm{r}}\mathcal{M}_i \ , \tag{VII.126}$$

we realize that the specific internal energy depends on these variables: η, ε_{ij}, E_i, and ${}^{\mathrm{r}}\mathcal{M}_i$. It is more beneficial to obtain an energy depending on T, ε_{ij}, E_i, and B_i since we know their relation to the primitive variables $\{T, u_i, \phi, A_i\}$. We name $\{T, \varepsilon_{ij}, E_i, B_i\}$ as primary or state variables and want to obtain an energy related solely to the primary variables. For this purpose we introduce a free energy:

$$\psi = u - T\eta - B_iv\,{}^{\mathrm{r}}\mathcal{M}_i \ , \tag{VII.127}$$

and by taking its total differential we obtain

$$\begin{aligned}\mathrm{d}\psi &= \mathrm{d}u - \eta\,\mathrm{d}T - T\,\mathrm{d}\eta - B_iv\,\mathrm{d}\,{}^{\mathrm{r}}\mathcal{M}_i - {}^{\mathrm{r}}\mathcal{M}_iv\,\mathrm{d}B_i = \\ &= -\eta\,\mathrm{d}T + {}^{\mathrm{r}}\sigma_{ji}v\,\mathrm{d}\varepsilon_{ij} - {}^{\mathrm{r}}P_iv\,\mathrm{d}E_i - {}^{\mathrm{r}}\mathcal{M}_iv\,\mathrm{d}B_i \ ,\end{aligned} \tag{VII.128}$$

after inserting Gibbs's Eq. (VII.126). The specific free energy depends on the primary variables and we need to find relations defining dual variables, $\{\eta, {}^{\mathrm{r}}\sigma_{ij}, {}^{\mathrm{r}}P_i, {}^{\mathrm{r}}\mathcal{M}_i\}$. We assume that the free energy has a first integral such that its differential form $\mathrm{d}\psi$ is

exact (perfect) leading to

$$\frac{\partial\psi}{\partial T} = -\eta \ , \quad \frac{\partial\psi}{\partial\varepsilon_{ij}} = {}^{\mathrm{r}}\sigma_{ji}v \ , \quad \frac{\partial\psi}{\partial E_i} = -{}^{\mathrm{r}}P_i v \ , \quad \frac{\partial\psi}{\partial B_i} = -{}^{\mathrm{r}}\mathcal{M}_i v \ , \tag{VII.129}$$

we realize that the dual variables depend on the same set of arguments as the energy, which is often called the equipresence principle, see Truesdell and Toupin, 1960, §293.η. Since dual variables depend on primary variables, we acquire

$$\begin{aligned}
\mathrm{d}\eta &= \tilde{c}\,\mathrm{d}T + \tilde{p}_{ij}\,\mathrm{d}\varepsilon_{ij} + \tilde{\ell}_i\,\mathrm{d}E_i + \tilde{o}_i\,\mathrm{d}B_i \ , \\
\mathrm{d}\,{}^{\mathrm{r}}\sigma_{ij} &= \tilde{P}_{ij}\,\mathrm{d}T + C_{ijkl}\,\mathrm{d}\varepsilon_{kl} + \tilde{t}_{kij}\,\mathrm{d}E_k + \tilde{s}_{ijk}B_k \ , \\
\mathrm{d}\,{}^{\mathrm{r}}P_i &= \tilde{L}_i\,\mathrm{d}T + \tilde{T}_{ijk}\,\mathrm{d}\varepsilon_{jk} + \tilde{\chi}^{\mathrm{el.}}_{ij}\,\mathrm{d}E_j + \tilde{r}_{ij}B_j \ , \\
\mathrm{d}\,{}^{\mathrm{r}}\mathcal{M}_i &= \tilde{O}_i\,\mathrm{d}T + \tilde{S}_{ijk}\,\mathrm{d}\varepsilon_{jk} + \tilde{R}_{ij}\,\mathrm{d}E_j + \tilde{\chi}^{\mathrm{mag.}}_{ij}B_j \ .
\end{aligned} \tag{VII.130}$$

All material parameters, $\tilde{c}$, $\tilde{p}_{ij}$, $\tilde{\ell}_i$, $\tilde{o}_i$, $\tilde{P}_{ij}$, C_{ijkl}, $\tilde{t}_{kij}$, $\tilde{s}_{ijk}$, $\tilde{L}_i$, $\tilde{T}_{ijk}$, $\tilde{\chi}^{\mathrm{el.}}_{ij}$, $\tilde{r}_{ij}$, $\tilde{O}_i$, $\tilde{S}_{ijk}$, $\tilde{R}_{ij}$, $\tilde{\chi}^{\mathrm{mag.}}_{ij}$ shall be determined experimentally. By using the so-called Maxwell symmetry relations:

$$\begin{aligned}
\tilde{P}_{ij} = \frac{\partial\,{}^{\mathrm{r}}\sigma_{ij}}{\partial T} = \rho_0\frac{\partial\,{}^{\mathrm{r}}\sigma_{ij}v}{\partial T} = \rho_0\frac{\partial^2\psi}{\partial T\partial\varepsilon_{ij}} = \rho_0\frac{\partial^2\psi}{\partial\varepsilon_{ij}\partial T} = -\rho_0\frac{\partial\eta}{\partial\varepsilon_{ij}} = -\rho_0\tilde{p}_{ij} \\
\Rightarrow \tilde{p}_{ij} = -v\tilde{P}_{ij} \ , \\
\tilde{L}_i = \frac{\partial\,{}^{\mathrm{r}}P_i}{\partial T} = \rho_0\frac{\partial\,{}^{\mathrm{r}}P_i v}{\partial T} = -\rho_0\frac{\partial^2\psi}{\partial T\partial E_i} = -\rho_0\frac{\partial^2\psi}{\partial E_i\partial T} = \rho_0\frac{\partial\eta}{\partial E_i} = \rho_0\tilde{\ell}_i \\
\Rightarrow \tilde{\ell}_i = v\tilde{L}_i \ , \\
\tilde{O}_i = \frac{\partial\,{}^{\mathrm{r}}\mathcal{M}_i}{\partial T} = \rho_0\frac{\partial\,{}^{\mathrm{r}}\mathcal{M}_i v}{\partial T} = -\rho_0\frac{\partial^2\psi}{\partial T\partial B_i} = -\rho_0\frac{\partial^2\psi}{\partial B_i\partial T} = \rho_0\frac{\partial\eta}{\partial B_i} = \rho_0\tilde{o}_i \\
\Rightarrow \tilde{o}_i = v\tilde{O}_i \ ,
\end{aligned} \tag{VII.131}$$

as well as

$$\begin{aligned}
\tilde{T}_{ijk} = \frac{\partial\,{}^{\mathrm{r}}P_i}{\partial\varepsilon_{jk}} = \rho_0\frac{\partial\,{}^{\mathrm{r}}P_i v}{\partial\varepsilon_{jk}} = -\rho_0\frac{\partial^2\psi}{\partial\varepsilon_{jk}\partial E_i} = -\rho_0\frac{\partial^2\psi}{\partial E_i\partial\varepsilon_{jk}} = -\rho_0\frac{\partial\,{}^{\mathrm{r}}\sigma_{jk}v}{\partial E_i} = -\tilde{t}_{ijk} \\
\Rightarrow \tilde{t}_{kij} = -\tilde{T}_{kij} \ , \\
\tilde{S}_{ijk} = \frac{\partial\,{}^{\mathrm{r}}\mathcal{M}_i}{\partial\varepsilon_{jk}} = \rho_0\frac{\partial\,{}^{\mathrm{r}}\mathcal{M}_i v}{\partial\varepsilon_{jk}} = -\rho_0\frac{\partial^2\psi}{\partial\varepsilon_{jk}\partial B_i} = -\rho_0\frac{\partial^2\psi}{\partial B_i\partial\varepsilon_{jk}} = -\frac{\partial\,{}^{\mathrm{r}}\sigma_{kj}}{\partial B_i} = -\tilde{s}_{kji} \\
\Rightarrow \tilde{s}_{ijk} = \tilde{S}_{kji} \ , \\
\tilde{R}_{ij} = \frac{\partial\,{}^{\mathrm{r}}\mathcal{M}_i}{\partial E_j} = \rho_0\frac{\partial\,{}^{\mathrm{r}}\mathcal{M}_i v}{\partial E_j} = -\rho_0\frac{\partial^2\psi}{\partial E_j\partial B_i} = -\rho_0\frac{\partial^2\psi}{\partial B_i\partial E_j} = \frac{\partial\,{}^{\mathrm{r}}P_j}{\partial B_i} = \tilde{r}_{ji} \\
\Rightarrow \tilde{r}_{ij} = \tilde{R}_{ji} \ ,
\end{aligned} \tag{VII.132}$$

we can reduce the necessary amount of measurements for determining materials parameter. For the coupling terms, viz., thermal pressure, $\tilde{P}_{ij}$, pyroelectric tensor, $\tilde{L}_i$, magnetoelectric coupling, $\tilde{R}_i$, piezoelectric tensor, $\tilde{T}_{ijk}$, and piezomagnetic tensor, $\tilde{S}_{ijk}$, we will make a reformulation since they are difficult to find in the literature. Hence we introduce coefficients of thermal expansion α_{ij}, which is measured by varying temperature and measuring strains

$$\mathrm{d}\varepsilon_{ij} = \alpha_{ij}\,\mathrm{d}T \ , \tag{VII.133}$$

by holding the other variables fixed. From Eq. (VII.130) we obtain for fixed ${}^{\mathrm{r}}\sigma_{ij}$, E_i, B_i,

$$0 = \tilde{P}_{ij}\,\mathrm{d}T + C_{ijkl}\,\mathrm{d}\varepsilon_{kl} = \tilde{P}_{ij}\,\mathrm{d}T + C_{ijkl}\alpha_{kl}\,\mathrm{d}T \Rightarrow -\tilde{P}_{ij} = C_{ijkl}\alpha_{kl} \ . \tag{VII.134}$$

Analogously we acquire

$$-\tilde{L}_i = \tilde{T}_{ijk}\alpha_{jk} \ , \quad -\tilde{O}_i = \tilde{S}_{ijk}\alpha_{jk} \ . \tag{VII.135}$$

Now after using the latter relations in Eq. (VII.130) we obtain

$$\begin{aligned}
\mathrm{d}\eta &= \tilde{c}\,\mathrm{d}T + vC_{ijkl}\alpha_{kl}\,\mathrm{d}\varepsilon_{ij} - v\tilde{T}_{ijk}\alpha_{jk}\,\mathrm{d}E_i - v\tilde{S}_{ijk}\alpha_{jk}\,\mathrm{d}B_i \ , \\
\mathrm{d}\,{}^{\mathrm{r}}\sigma_{ij} &= -C_{ijkl}\alpha_{kl}\,\mathrm{d}T + C_{ijkl}\,\mathrm{d}\varepsilon_{kl} - \tilde{T}_{kij}\,\mathrm{d}E_k + \tilde{S}_{kji}B_k \ , \\
\mathrm{d}\,{}^{\mathrm{r}}P_i &= -\tilde{T}_{ijk}\alpha_{jk}\,\mathrm{d}T + \tilde{T}_{ijk}\,\mathrm{d}\varepsilon_{jk} + \tilde{\chi}^{\mathrm{el.}}_{ij}\,\mathrm{d}E_j + \tilde{R}_{ji}B_j \ , \\
\mathrm{d}\,{}^{\mathrm{r}}\mathcal{M}_i &= -\tilde{S}_{ijk}\alpha_{jk}\,\mathrm{d}T + \tilde{S}_{ijk}\,\mathrm{d}\varepsilon_{jk} + \tilde{R}_{ij}\,\mathrm{d}E_j + \tilde{\chi}^{\mathrm{mag.}}_{ij}B_j \ .
\end{aligned} \tag{VII.136}$$

References

Abali, B. E. (2013). *Supply code, Computational Reality, Technical University of Berlin, Institute of Mechanics, Chair of Continuum Mechanics and Material Theory*. http://www.lkm.tu-berlin.de/ComputationalReality/.

Abali, B. E. (2017). *Computational Reality, Solving Nonlinear and Coupled Problems in Continuum Mechanics*. Vol. 55. Advanced Structured Materials. Springer. ISBN: 978-981-10-2443-6.

Ahmad, S. N., Upadhyay, C., and Venkatesan, C. (2006). „Electro-thermo-elastic formulation for the analysis of smart structures.“ In: *Smart materials and structures* 15.2, p. 401.

Alnaes, M. S. and Mardal, K. A. (2010). „On the Efficiency of Symbolic Computations Combined With Code Generation for Finite Element Methods.“ In: *ACM Transactions on Mathematical Software* 37.1.

Alnaes, M. S. and Mardal, K. A. (2012). „Automated solution of differential equations by the finite element method, the FEniCS book.“ In: *Automated Solution of Differential Equations by the Finite Element Method*. Ed. by A. Logg, K.-A. Mardal, and G. N. Wells. Vol. 84. Lecture Notes in Computational Science and Engineering. Springer. Chap. 15 Syfi and sfc: symbolic finite elements and form compilation.

Arnold, D. N. and Logg, A. (2014). „Periodic table of the finite elements.“ In: *SIAM News* 47.9.

Barnett, S. M. (2010). „Resolution of the Abraham–Minkowski dilemma.“ In: *Physical Review Letters* 104.7, p. 070401.

Baumanns, S., Clemens, M., and Schops, S. (2013). „Structural aspects of regularized full Maxwell electrodynamic potential formulations using FIT.“ In: *Electromagnetic Theory (EMTS), Proceedings of 2013 URSI International Symposium on*. IEEE, pp. 1007–1010.

Benjeddou, A. (2000). „Advances in piezoelectric finite element modeling of adaptive structural elements: a survey.“ In: *Computers & Structures* 76.1, pp. 347–363.

Bethune-Waddell, M. and Chau, K. J. (2015). „Simulations of radiation pressure experiments narrow down the energy and momentum of light in matter.“ In: *Reports on Progress in Physics* 78.12, p. 122401.

Bossavit, A. (1988). „Whitney forms: A class of finite elements for three-dimensional computations in electromagnetism.“ In: *IEE Proceedings A (Physical Science, Measurement and Instrumentation, Management and Education, Reviews)* 135.8, pp. 493–500.

Boston Piezo-Optics (2016). *Inc.*

Bowen, C., Taylor, J., LeBoulbar, E., Zabek, D., Chauhan, A., and Vaish, R. (2014). „Pyroelectric materials and devices for energy harvesting applications.“ In: *Energy & Environmental Science* 7.12, pp. 3836–3856.

Brechet, S. D. and Ansermet, J.-P. (2014). „Thermodynamics of continuous media with intrinsic rotation and magnetoelectric coupling.“ In: *Continuum Mechanics and Thermodynamics* 26.2, pp. 115–142.

Chaudhuri, A. and Mandal, K. (2015). „Large magnetoelectric properties in CoFe 2 O 4: BaTiO 3 core–shell nanocomposites.“ In: *Journal of Magnetism and Magnetic Materials* 377, pp. 441–445.

Chu, L. J., Haus, H. A., and Penfield Jr, P. (1966). „The force density in polarizable and magnetizable fluids.“ In: *Proceedings of the IEEE* 54.7, pp. 920–935.

Ciarlet Jr, P. and Zou, J. (1999). „Fully discrete finite element approaches for time-dependent Maxwell's equations.“ In: *Numerische Mathematik* 82.2, pp. 193–219.

Cuadras, A., Gasulla, M., and Ferrari, V. (2010). „Thermal energy harvesting through pyroelectricity.“ In: *Sensors and Actuators A: Physical* 158.1, pp. 132–139.

Demkowicz, L. (2006). *Computing with hp-adaptive finite elements: volume 1 one and two dimensional elliptic and Maxwell problems*. CRC Press.

Eerenstein, W., Mathur, N., and Scott, J. F. (2006). „Multiferroic and magnetoelectric materials.“ In: *nature* 442.7104, pp. 759–765.

efunda (2016). *engineering Fundamentals*.

Ericksen, J. (2007). „On formulating and assessing continuum theories of electromagnetic fields in elastic materials.“ In: *Journal of Elasticity* 87.2-3, pp. 95–108.

Gillette, A., Rand, A., and Bajaj, C. (2016). „Construction of scalar and vector finite element families on polygonal and polyhedral meshes.“ In: *Computational Methods in Applied Mathematics* 16.4, pp. 667–683.

Gnu GPL (2007). *Gnu Gpl—the GNU General Public License*. http://www.gnu.org/copyleft/gpl.html.

Griffiths, D. J. (2012). „Resource letter EM-1: electromagnetic momentum.“ In: *American Journal of Physics* 80.1, pp. 7–18.

Groot, S. R. de and Mazur, P. (1984). *Non-equilibrium thermodynamics*. Dover Publications, New York.

Hachkevych, O. R. and Terlets'kyi, R. F. (2004). „Models of thermomechanics of magnetizable and polarizable conducting deformable solids.“ In: *Materials Science* 40.3, pp. 320–336.

Hilbert, D. (1902). „The Foundations of Geometry (Transl. by Townsend, E. J.)“ In: *The Open Court Publishing Co.*

Hill, N. A. (2000). „Why are there so few magnetic ferroelectrics?“ In: *The Journal of Physical Chemistry B* 104.29, pp. 6694–6709.

Hutter, K. (1975). „On thermodynamics and thermostatics of viscous thermoelastic solids in the electromagnetic fields. A Lagrangian formulation.“ English. In: *Arch. Ration. Mech. Anal.* 58, pp. 339–368.

Kovetz, A. (2000). *Electromagnetic theory*. Oxford University Press Oxford.

Kuczmann, M. (2009). *Potential Formulations in Magnetics applying the Finite Element Method*. Széchenyi István University, Laboratory of Electromagnetic Field.

Li, J. (2009). „Numerical convergence and physical fidelity analysis for Maxwell's equations in metamaterials.“ In: *Computer Methods in Applied Mechanics and Engineering* 198.37, pp. 3161–3172.

Logg, A., Mardal, K. A., and Wells, G. N. (2011). *Automated Solution of Differential Equations by the Finite Element Method, The FEniCS Book*. Vol. 84. Lecture Notes in Computational Science and Engineering. Springer.

Logg, A., Mardal, K. A., and Wells, G. N. (2012). *Automated solution of differential equations by the finite element method, the FEniCS book*. Vol. 84. Lecture Notes in Computational Science and Engineering. Springer. ISBN: 978-3-642-23098-1.

Logg, A. and Wells, G. N. (2010). „DOLFIN: Automated finite element computing." In: *ACM Trans. Math. Softw.* 37.2, 20:1–20:28. ISSN: 0098-3500.

Losinski, A. (1999). *Low-profile axial-flow single-blade piezoelectric fan*. US Patent 5,861,703.

Mansuripur, M. (2010). „Resolution of the Abraham–Minkowski controversy." In: *Optics Communications* 283.10, pp. 1997–2005.

Marauska, S., Jahns, R., Greve, H., Quandt, E., Knöchel, R., and Wagner, B. (2012). „MEMS magnetic field sensor based on magnetoelectric composites." In: *Journal of Micromechanics and Microengineering* 22.6, p. 065024.

Mathe, V., Srinivasan, G., and Balbashov, A. (2008). „Magnetoelectric effects in bilayers of lead zirconate titanate and single crystal hexaferrites." In: *Applied Physics Letters* 92.12, p. 122505.

McMeeking, R. M., Landis, C. M., and Jimenez, S. (2007). „A principle of virtual work for combined electrostatic and mechanical loading of materials." In: *International Journal of Non-Linear Mechanics* 42.6, pp. 831–838.

Müller, I. (1985). *Thermodynamics*. Pitman Publishing, London.

Nédélec, J.-C. (1980). „Mixed finite elements in $\mathbb{R}^3$." In: *Numerische Mathematik* 35.3, pp. 315–341.

Obukhov, Y. N. (2008). „Electromagnetic energy and momentum in moving media." In: *Annalen der Physik* 17.9-10, pp. 830–851.

Oliphant, T. E. (2007). „Python for Scientific Computing." In: *Computing in Science & Engineering* 9.3, pp. 10–20.

Or, D., Li, T., and Chan, H. L. W. (2005). „Dynamic magnetomechanical properties of Terfenol-D/epoxy pseudo 1-3 composites." In: *Journal of applied physics*.

Pao, Y.-H. and Hutter, K. (1975). „Electrodynamics for moving elastic solids and viscous fluids." In: *Proceedings of the IEEE* 63.7, pp. 1011–1021.

Park, S.-E. E. and Hackenberger, W. (2002). „High performance single crystal piezoelectrics: applications and issues." In: *Current Opinion in Solid State and Materials Science* 6.1, pp. 11–18.

Pauli, W. (1973). *Pauli lectures on Physics, vol.3, Thermodynamics and the kinetic theory of gases*. Dover (2000) repub. of MIT Press, Cambridge, Massachusetts.

Persano, L., Dagdeviren, C., Su, Y., Zhang, Y., Girardo, S., Pisignano, D., Huang, Y., and Rogers, J. A. (2013). „High performance piezoelectric devices based on aligned arrays of nanofibers of poly (vinylidenefluoride-co-trifluoroethylene)." In: *Nature communications* 4, p. 1633.

Pfeifer, R. N., Nieminen, T. A., Heckenberg, N. R., and Rubinsztein-Dunlop, H. (2007). „Colloquium: Momentum of an electromagnetic wave in dielectric media." In: *Reviews of Modern Physics* 79.4, p. 1197.

PI (2016). *Piezo Technology*.

Queiruga, A. F. and Zohdi, T. I. (2016). „Formulation and numerical analysis of a fully-coupled dynamically deforming electromagnetic wire." In: *Computer Methods in Applied Mechanics and Engineering* 305, pp. 292–315.

Raviart, P.-A. and Thomas, J.-M. (1977). „A mixed finite element method for 2-nd order elliptic problems." In: *Mathematical aspects of finite element methods*. Springer, pp. 292–315.

Reich, F. A., Stahn, O., and Müller, W. H. (2015). „A review of electrodynamics and its coupling with classical balance equations." In: *Advanced Problems in Mechanics, International Summer School–Conference Proceedings*. Institute for Problems in Mechanical Engineering, 22 June 2015 - 27 June 2015. St. Petersburg, Russia, pp. 367–376.

Ryu, J., Priya, S., Uchino, K., and Kim, H.-E. (2002). „Magnetoelectric effect in composites of magnetostrictive and piezoelectric materials." In: *Journal of electroceramics* 8.2, pp. 107–119.

Sandlund, L., Fahlander, M., Cedell, T., Clark, A., Restorff, J., and Wun-Fogle, M. (1994). „Magnetostriction, elastic moduli, and coupling factors of composite Terfenol-D." In: *Journal of Applied Physics* 75.10, pp. 5656–5658.

Sauciuc, I. and Chrysler, G. M. (2006). *Electronic thermal management*. US Patent 7,031,155.

Schmid, H. (1994). „Introduction to the proceedings of the 2nd international conference on magnetoelectric interaction phenomena in crystals, MEIPIC-2." In: *Ferroelectrics* 161.1, pp. 1–28.

Sebald, G., Pruvost, S., and Guyomar, D. (2007). „Energy harvesting based on Ericsson pyroelectric cycles in a relaxor ferroelectric ceramic." In: *Smart Materials and Structures* 17.1, p. 015012.

Shen, Y. (2014). „Applications of Magnetoelectric Sensors." PhD thesis. Virginia Polytechnic Institute and State University.

Somkun, S., Moses, A. J., and Anderson, P. I. (2016). „Magnetostriction in grain-oriented electrical steels under AC magnetisation at angles to the rolling direction.“ In: *IET Electric Power Applications* 10.9, pp. 932–938.

Tanida, M., Sunaga, M., and Wada, H. (2013). *Piezoelectric fan and air cooling apparatus using the piezoelectric fan.* US Patent App. 13/370,341.

Truesdell, C. and Toupin, R. A. (1960). *Principles of classical mechanics and field theory, Handbuch der Physik Vol. III/1 (Ed. by Flügge, S.)* Ed. by S. Flügge. Springer, Berlin Heidelberg.

Vidal, P., D'Ottavio, M., Thaïer, M. B., and Polit, O. (2011). „An Efficient Finite Shell Element for the Static Response of Piezoelectric Laminates.“ In: *Journal of Intelligent Material Systems and Structures* 22.7, pp. 671–690.

Vopsaroiu, M., Stewart, M., Hegarty, T., Muniz-Piniella, A., McCartney, N., Cain, M., and Srinivasan, G. (2008). „Experimental determination of the magnetoelectric coupling coefficient via piezoelectric measurements.“ In: *Measurement Science and Technology* 19.4, p. 045106.

Weiser, B., Pfutzner, H., and Anger, J. (2000). „Relevance of magnetostriction and forces for the generation of audible noise of transformer cores.“ In: *IEEE Transactions on Magnetics* 36.5, pp. 3759–3777.

Yamada, Y., Fujimoto, K., and Inoue, J. (1988). *Piezoelectric fan.* US Patent 4,780,062.

Yang, P., Zhao, K., Yin, Y., Wan, J., and Zhu, J. (2006). „Magnetoelectric effect in magnetostrictive/piezoelectric laminate composite Terfenol-D/LiNbO3 [(zxtw)-129/30].“ In: *Applied physics letters* 88.17, p. 2903.

Yi, S., Ling, S. F., Ying, M., Hilton, H. H., and Vinson, J. R. (1999). „Finite element formulation for anisotropic coupled piezoelectro-hygro-thermo-viscoelastodynamic problems.“ In: *International journal for numerical methods in engineering* 45.11, pp. 1531–1546.

Zhai, J., Xing, Z., Dong, S., Li, J.-F., and Viehland, D. (2006). „Detection of pico-Tesla magnetic fields using magneto-electric sensors at room temperature.“ In: *Applied physics letters* 88.6, p. 062510.